LOWER HYBRID CURRENT DRIVE EXPERIMENTS ON THE ENCORE TOKAMAK

Thesis by

Lawrence Sverdrup

In Partial Fulfillment of the Requirements

for the Degree of

Doctor of Philosophy

California Institute of Technology

Pasadena, California

2002

(Defended July 18, 2001)

ACKNOWLEDGEMENTS

I would like to thank my thesis advisor, Dr. Paul Bellan, for his support and guidance over the course of this work. I would also like to thank my advisor for his patience. My broad curiosity and interest in science demonstrations has occasionally led me to significant diversions. Plasma experiments are complicated due to the fact that so many things are going on simultaneously, involving diverse branches of physics. Focusing in on a portion of this physics while wearing blinders to the rest of the world in order to get something accomplished is perhaps my most valuable lesson. Dr. Bellan found most of the LHCD density limit data from experiments other than on Encore.

I am indebted to Frank Cosso for his considerable effort in the construction and debugging of the four channel, 40 kW, 450 MHz power supply utilized in these experiments. The occasional fireball spewing out of a blown kapton bypass capacitor did not deter him.

Elmer Szombathy in the mechanical engineering machine shop gave me considerable guidance as I milled, bent and soldered parts of the various plasma wave antennas while listening to KBIG, the last super mellow radio channel in Los Angeles. Elmer once asked me whether the wave-guide channels were intended to guide air or water. He simply shook his head when I explained that they were to guide electromagnetic waves.

The efforts of Eric Fredrickson in construction and maintenance of laboratory hardware and programming of the data acquisition computer in pursuit of his own thesis were in turn invaluable in the completion of this work.

I enjoyed many interesting conversations with Glenn Greene, Eric Fredrickson, Jon McChesney, Stewart Zweben, Noel Corngold and the rest of the Caltech plasma physics group.

The support of my wife Mirian during completion of the manuscript was invaluable.

ABSTRACT

The work of this thesis concerns a technological aspect of a tokamak fusion power reactor. A toroidal current in tokamaks is necessary for plasma equilibrium. Ohmic heated tokamaks are inherently pulsed devices since the toroidal plasma current is essentially a single turn secondary of a transformer. A pulsed power reactor is undesirable for a number of reasons including thermal fatigue to material structures and other mechanical cycling effects. Various means to drive a continuous current have been studied. One of the more successful schemes has been to inject unidirectional lower hybrid plasma waves into a tokamak. The plasma waves Landau damp on the high velocity tail of the electron distribution, delivering wave momentum to electrons and generating plasma current.

The results of early experiments produced two plasma physics problems. First, the current drive effect disappeared above a certain plasma density that depended in some way on the particulars of the experiment. This effect became known as the 'density limit' problem. Secondly, the phase velocities of the launched lower hybrid plasma waves in most experiments turned out to be so high that essentially no electrons in the high velocity tail of the electron distribution were available to interact with the plasma waves. Despite this, large currents were indeed driven in most of the experiments. Somehow the 'spectral gap' between the launch phase velocity of the wave and the Landau damping phase velocity was being bridged.

Experiments at Caltech on the Encore tokamak failed to produce the large driven currents seen in other experiments. The reason for this and simultaneously the cause of the density limit seen in the other experiments was explained by a relatively simple and appealing theory.

Small driven currents were observed. Initially puzzling was the result that currents could be driven in the same toroidal direction regardless of the directionality of the launched lower hybrid waves. The Encore tokamak had a handedness. The cause of this handedness turned out to be a radial, horizontal, magnetic error field associated with the toroidal magnetic field which led to a horizontal spiraling of the toroidal field lines.

TABLE OF CONTENTS

LIST OF SYMBOLS

a	tokamak minor radius
A_{ϕ}	vector potential in the toroidal direction
B	magnetic field
B_{θ}	poloidal magnetic field component
B_{ϕ}	toroidal magnetic field component
c	speed of light
D	Stix off-diagonal component of the cold plasma dielectric tensor
$D(\mathbf{k},,\mathbf{r})$	plasma dispersion function
E	energy; electric field
$E_{\parallel}$	electric field parallel to the local toroidal magnetic field
$E_{\perp}$	electric field perpendicular to the local toroidal magnetic field
f	frequency
f_{LH}	lower hybrid frequency
f_{pe}	electron plasma frequency
f_{ce}	electron cyclotron frequency
H	Hamiltonian; magnetic induction
I_p	plasma current
I_p^{RF}	plasma current driven by rf plasma waves
I_p^{ohmic}	plasma current driven by the tokamak ohmic heating supply
J	current density
$\mathbf{k}$	wave vector of plasma wave
k	Boltzmann's constant
$k_{\parallel}$	wave vector component in the toroidal direction
$k_{\perp}$	wave vector component perpendicular to the toroidal direction
k_r	wave vector component in the radial direction
L	Lagrangian
LH	lower hybrid

LHCD	lower hybrid current drive
m	poloidal mode number
m_i	ion atomic mass
m_e	electron mass
n	plasma density, or toroidal mode number
N	speed of light divided by plasma wave phase velocity
$N_{\|\|}$	speed of light divided by wave phase velocity in the toroidal direction
$N_{\|\|a}$	accessibility limit
$N_\perp$	speed of light divided by wave phase velocity perpendicular to B_ϕ
P	Stix diagonal component of the cold plasma dielectric tensor
P_{RF}	microwave power
P_ϕ	momentum conjugate to ϕ
q	tokamak rotational transform
R	position in major radius; electrical resistance
R_o	tokamak major radius
S	Stix diagonal component of the cold plasma dielectric tensor
T_e	electron temperature
T_i	ion temperature
v	velocity
$v_{thermal}$	thermal velocity
$v_{\|\|}$	velocity parallel to the local toroidal magnetic field
$v_\perp$	velocity perpendicular to the local toroidal magnetic field
V_{loop}	voltage induced across the gap in the tokamak vacuum chamber
w	ratio of plasma wave speed in the toroidal direction to thermal velocity
$W_{\|\|}$	energy due to motion parallel to the local toroidal magnetic field
$W_\perp$	energy due to motion perpendicular to the local toroidal magnetic field
Z_i	whole number specifying the ion charge state
β	ratio of plasma pressure to magnetic pressure
ε	ratio of minor radius to major radius (toricity)
ε_o	permittivity of vacuum

$\boldsymbol{\varepsilon}$, $\boldsymbol{\varepsilon}_r$	plasma dielectric tensor
$\boldsymbol{\varepsilon}_{th}$	thermal component of the plasma dielectric tensor
$\boldsymbol{\varepsilon}_{\perp}$	perpendicular component of the plasma dielectric tensor
$\boldsymbol{\varepsilon}_{\parallel}$	parallel component of the plasma dielectric tensor
ϕ	toroidal direction (long way around in toroidal geometry)
$\lambda_{\parallel}$	wavelength of plasma wave along the toroidal direction
$\lambda_{\perp}$	wavelength of plasma wave perpendicular to the magnetic field
$\boldsymbol{\mu}$	plasma permeability tensor
μ_m	magnetic moment
μ_o	permeability of vacuum
ν	plasma collision frequency
θ	poloidal direction (short way around in toroidal geometry)
ω	angular frequency of electromagnetic or plasma wave
ω_{ce}	electron cyclotron angular frequency
ω_{ci}	ion cyclotron angular frequency
ω_{pe}	electron plasma angular frequency
ω_{pi}	ion plasma angular frequency
Λ	collision impact parameter

1 Introduction

A major issue for the tokamak approach to fusion energy involves the difficulties involved in heating plasmas. Plasma resistivity decreases with temperature. At plasma temperatures corresponding to particle energies of 10 keV, the resistivity of a hydrogen plasma is less than 10^{-7} ohm-cm, about one-tenth that of copper at ordinary temperatures.[1] This effect makes it difficult to heat plasmas to the temperatures desired in a fusion reactor solely with ohmic heating from plasma currents. Essentially, unreasonably large ohmic currents would have to be employed. The effective impedance of the current source would have to be unreasonably small. For this reason, plasma heating via other means has been an extensively studied area. One very promising approach has been to launch various plasma waves into the plasmas. These waves decay, converting wave energy into plasma thermal energy.

Another major problem associated with the tokamak approach to a fusion reactor is that such a reactor is necessarily a pulsed device if it relies upon ohmic currents to produce the plasma equilibrium. Essentially an ohmic heated tokamak is a single-turn secondary of a transformer. When the allowable volt-seconds of flux swing is limited by core saturation or primary current limitations, the tokamak must be turned off, and the transformer reset. This is very undesirable for a fusion reactor since a continuous, uninterrupted flow of power is required by the utilities, and thermal storage systems are expensive. The differential expansion and contraction of materials inherent in a thermally cycled system leads to material damage due to thermal fatigue. Materials suffering such damage will not be easy to replace in a tokamak reactor environment.[2] Consequently, many alternate schemes to drive continuous currents in plasmas have been proposed.

One very promising scheme is a natural outgrowth of the aforementioned plasma wave heating experiments. The idea is to launch plasma waves to subsequently produce net plasma current by any of a number of processes. Since the plasma waves can be launched continuously, any driven current would also be produced continuously. In the case of lower hybrid current drive (LHCD), directionally launched lower hybrid waves Landau damp on the plasma electrons. Wave momentum is delivered to the electrons and the velocity space distribution of the electrons is modified to a non-symmetric form yielding net plasma current. Some of the first major experiments in this area worked beautifully. When the switch was flipped energizing the microwave antennas launching the plasma waves, large plasma currents were induced.[3]

Certain unexplained features rapidly became evident, however. The phase velocities of the launched plasma waves were in retrospect seen to be far too high to interact with the electron distribution, although experimentally interaction was clearly observed. Somehow the "spectral gap" between launch phase-velocity and electron distribution tail velocity was being bridged. Another feature was the unexplained loss of current drive at a critical plasma density that varied from experiment to experiment. This phenomenological "density limit" was observed in virtually every LHCD experiment. Since the number of major LHCD experiments across the world numbered in the dozens, these problems received a considerable amount of attention.

Funding was received to study LHCD on the ENCORE tokamak at Caltech, where lower hybrid waves have been extensively studied in the past. A low power antenna for launching directional lower hybrid waves was built and a 40 kW RF power source was designed, and construction initiated. At this point the project was handed to the author of this thesis. This thesis is the story of the construction and testing of three high power antennas for launching lower hybrid waves, and the experiments performed with the apparatus.

Unlike the experiments at Princeton and elsewhere, when the switch was flipped at Caltech nothing much happened! Actually a small but definite amount of current drive was observed under certain conditions and the study of these currents proved fascinating. Initially baffling was the discovery that these currents were independent of the antenna phasing which controls plasma wave directionality. Thus the driven plasma currents could be found oriented opposite to the direction predicted by LHCD theory. It turned out that plasma currents were driven in both directions since it was experimentally impossible to launch purely unidirectional plasma waves. The current driven in one direction spiraled outward in a horizontal plane and was attenuated at the chamber wall. Current driven in the other direction spiraled into the interior of the plasma chamber contributing to the net current. Horizontal magnetic "error" fields in the tokamak chamber turned out to play the major role in net current production.

The efficiency for LHCD in ENCORE measured in amps-per-watt was unusually small compared to experiments in other tokamaks. This is true even allowing for the magnetic error field effects in ENCORE. After much thought on the reasons why LHCD experiments in ENCORE were producing so little current drive, a theory was proposed. The theory noted that at a high enough plasma density, lower hybrid waves in the "spectral gap" between launch phase velocity and electron tail velocity would suffer a mode conversion to another type of plasma wave which is heavily damped. Essentially the theory purported to explain the density limit to lower hybrid current drive, and proposed that the ENCORE experiments took place in a part of parameter space beyond the density limit. Proof of the theory came when it was noted that every density limit seen in numerous LHCD experiments across the world could be adequately explained by this theory.

---

[1] S. Glasstone and R. Lovberg, Controlled Thermonuclear Reactions, Robert E. Krieger Publishing Co. 1975, p. 103

[2] D. A. Ehst et al., "A comparison of pulsed and steady-state tokamak reactor burn cycles," Part I: thermal effects and lifetime limitations, p. 305; Part II: magnet fatique, power supplies and cost analysis, p. 319, Nuc. Eng and Design, **2**, (1985)

[3] R. Motley et al., Bulletin of the American Physical Society, **28**, No. 8, Oct. 1983, p. 1092

2 Overview of Current Drive Theory

It is not the purpose of this section to give an exhaustive rendering of the theory of current drive in plasmas. Instead certain key concepts underlying the theory are to be highlighted. For a more in depth review see the references.[1, 2] The expected lower hybrid current drive efficiency in the Encore tokamak will be estimated. It will be shown that the experimentally obtained efficiency is anomalous, being too low.

A current can be produced without net momentum. With ions traveling in a direction opposite to the electrons, but at a slower speed, it can be arranged so that the net momentum is zero. Nevertheless many current drive schemes including lower hybrid current drive (LHCD) depend upon selectively depositing momentum in either the electrons or ions. A unidirectional plasma wave is launched which pushes on only the electrons or ions via resonant absorption. Plasma wave momentum is converted into the momentum of charged particles. This newly created particle momentum represents an electrical current since only one species of charge has been accelerated. Since all plasma waves with non-vanishing wave-number carry momentum, all are candidates for current drive. There are many issues affecting the attractiveness of the various plasma waves for current drive, however.

Following Fisch and Boozer[3] consider the effect of incremental changes in electron velocity. Imagine that an electron in the plasma with velocity $\mathbf{v}_1$ absorbs energy from a plasma wave changing velocity by an amount $\Delta\mathbf{v} = \mathbf{v}_2 - \mathbf{v}_1$. The amount of energy absorbed by the electron is

$$\Delta E \cong \Delta\mathbf{v} \cdot \frac{\partial E}{\partial \mathbf{v}} , \tag{2.1}$$

provided that $\Delta\mathbf{v} << \mathbf{v}_1$. The electron kinetic energy is $E = (mv^2)/2$. Collisions in the plasma will cause the perturbation to relax. It is assumed for these calculations that most of the electrons in the distribution function are unaffected so that the collision frequencies are only a function of the electron speed. Thus a transient current density parallel to the magnetic field will be generated whose time dependence is given by

$$\Delta J_{\parallel}(t) = -e\,n\left[v_{\parallel 2}e^{-\nu_2 t} - v_{\parallel 1}e^{-\nu_1 t}\right]. \tag{2.2}$$

A factor representing the density of such accelerated charges has been suppressed. The first term on the right-hand side of equation (2.2) is due to the newly created electron at velocity $\mathbf{v}_2$. The second term is due to the absence of an electron at velocity $\mathbf{v}_1$. The momentum destruction frequency ν is assumed to be solely a function of the magnitude of the electron velocity. If a continuous stream of electrons is given a kick in velocity space, each kick separated by time ΔT that is long compared to ν^{-1}, a steady production of current results. The time average of this current is given by integrating (2.2) divided by ΔT to obtain

$$\langle \mathbf{J}_{\parallel}\rangle \equiv \frac{1}{\Delta T}\int_0^{\Delta T} J(t)\,dt = \frac{-e}{\Delta T}\left(\frac{v_{\parallel 1}}{\nu_1} - \frac{v_{\parallel 2}}{\nu_2}\right) \cong \frac{-e}{\Delta T}\Delta\mathbf{v}\cdot\frac{\partial}{\partial\mathbf{v}}\frac{v_{\parallel}}{\nu(v)}. \tag{2.3}$$

This current can be rewritten by expanding the derivative as

$$\langle J_{\parallel}\rangle = \frac{-e}{\Delta T}\left[\frac{\Delta v_{\parallel}}{\nu} - \frac{v_{\parallel}\Delta v}{\nu^2}\frac{\partial\nu}{\partial v}\right]. \tag{2.4}$$

Note that the second term in equation (2.4) produces a current even when $\Delta v_{\parallel} = 0$. Thus, even when momentum is not delivered by the plasma wave, current drive is still possible. This effect depends upon the lower rate of collisions suffered by faster electrons. Damping of electron cyclotron waves with little parallel momentum increases the velocity of resonant electrons in the direction perpendicular to the magnetic field. Calculations indicate that cyclotron damping current drive can be almost as efficient as Landau damping current drive for a given parallel phase velocity spectrum.[4] The ratio of the two efficiencies (J/P) is 4/3 according to linear theory. Nonlinear theories indicate an enhancement of the current drive efficiency over the linear result by as much as a factor of two.

In electron-cyclotron perpendicular-heating current drive, the frequency of the driven plasma wave is comparable to the electron-cyclotron frequency in the plasma. In existing machines as well as in anticipated tokamak fusion reactors, the electron cyclotron frequency is well over 10 GHz. The Alcator-C tokamak with a toroidal magnetic field of 100 kG has an electron cyclotron frequency of 280 GHz. There are no readily available high power microwave sources in this frequency range. Consequently, electron cyclotron current drive has seen less experimental effort than LHCD for which there are many adequate high power RF sources.

The power required to produce the current in equation (2.3) is

$$\mathrm{P} = \frac{\Delta E}{\Delta T} = \frac{\Delta \mathbf{v}}{\Delta T} \cdot \frac{\partial E}{\partial \mathbf{v}}. \tag{2.5}$$

The efficiency of current generation is given by the ratio of (2.3) and (2.5) and is given by

$$\frac{\mathrm{J}}{\mathrm{P}} = -e \frac{\hat{\mathbf{s}} \cdot \dfrac{\partial}{\partial \mathbf{v}} \dfrac{\mathrm{v}_{\parallel}}{\nu(\mathrm{v})}}{\hat{\mathbf{s}} \cdot \dfrac{\partial E}{\partial \mathbf{v}}}. \tag{2.6}$$

In equation (2.6) $\hat{\mathrm{s}}$ is a unit vector in the direction of $\Delta\mathbf{v}$. There are two important limits in regard to equation (2.6).

J/P is large when the denominator of (2.6) is small. This occurs when the velocity of the resonant electron in the direction of $\Delta\mathbf{v}$ is small. The energy required to produce a given $\Delta\mathrm{v}$ is less if $\mathrm{v}_1 \cdot \Delta\mathrm{v}$ is less. Note that this does not necessarily require that $\mathbf{v}_1$ be small. Basically less energy is required to produce a given velocity increase at lower velocities due to the quadratic dependence of kinetic energy on velocity.

J/P is also large when the numerator of (2.6) is large. This occurs when the velocity of the resonant electrons is very large. Assuming that the momentum destruction frequency scales like the self collision frequency,

$$\nu(\mathrm{v}) \approx \mathrm{constant} \cdot \frac{1}{\mathrm{v}^3}, \tag{2.7}$$

the numerator of (2.6) is larger the larger the total velocity. Relativistic effects that have been neglected eventually limit this effect. Basically fast electrons are relatively collisionless and currents generated by them tend to persist longer.

Thus there are two regimes of efficient current drive involving either very fast or very slow electrons. Since resonant absorption is being considered the plasma wave must satisfy the phase matching criterion

$$\mathrm{v} \approx \frac{\omega}{\mathrm{k}}. \tag{2.8}$$

The energy and momentum of a plasma-wave scale as ω and k respectively. The phase velocity of a wave is a measure of its energy to momentum ratio. Current drive involving fast electrons requires plasma waves with high phase velocity and large ratio of energy to momentum. LHCD falls into this category. Current drive involving slow electrons requires plasma waves with low phase velocity and large ratio of momentum to energy.

It is believed that slow electron current drive in tokamaks would suffer from the trapping of slow electrons in magnetic wells. The toroidal magnetic field of a tokamak falls off inversely with the major radius ($B_T \approx 1/R$), being weaker at the outer edge of the torus than at the inner edge. Due to the poloidal magnetic field the net magnetic field lines spiral around the toroidal axis. Charged particles gyrating around and following the net magnetic field lines are thus continually entering regions of strengthening and lessening magnetic field. The magnetic moment μ_m of a gyrating particle is an adiabatic invariant[5]

$$\mu_m = \frac{W_\perp}{B} \approx \text{constant}. \tag{2.9}$$

Here $W_\perp$ is the kinetic energy of the particle perpendicular to the magnetic field. Total kinetic energy is also conserved,

$$W_\perp + W_\parallel = \text{constant}. \tag{2.10}$$

From (2.9) as B increases, so must $W_\perp$ increase. Equation (2.10) then predicts that $W_\parallel$ must decrease. If $W_\parallel$ is sufficiently small to start with, it will go to zero as B increases and the particle will be reflected. Slow electron current drive has seen much less experimental work than fast electron current drive.

Current drive operating with the advantages of both the slow and fast electron regimes may be possible.[6] An electron cyclotron wave with parallel phase velocity much less than the electron thermal velocity can deposit momentum in supra-thermal electrons by resonating with electrons with small $v_{||}$ and large $v_{\perp}$. The large $v_{\perp}$ insures that the resonant electrons are relatively collisionless. The small $v_{||}$ means that relatively small amounts of energy are required to produce increases in parallel velocity. The very fact that $\omega/k_{||}$ is small indicates that this kind of plasma wave has a large amount of parallel momentum per unit energy. Wave induced diffusion will significantly increase the parallel velocity of the resonant electrons eliminating trapping as an obstacle. It can be shown, however, that such plasma waves require large values of $k_{||}$, with parallel wavelengths less than a millimeter in a tokamak with toroidal field of 100 kG.[7] Launching such waves at high power presents serious difficulties. The launching structure would have to consist of a series of extremely small phased antennas. An evanescent layer at the plasma edge of the order of $\lambda_{||}$ would make efficient coupling to the plasma difficult. Until these problems are solved this potential current drive candidate cannot receive experimental attention.

An additional point is evident from equation (2.6). Since the collision frequency increases with the density of potential scattering particles, the numerator of (2.6) will get smaller as the density increases. Virtually all current-drive schemes suffer decreases in the current drive efficiency parameter J/P as plasma density increases. Since collision frequencies are proportional to the density, equation (2.6) predicts that J/P varies inversely with plasma density and experiments with LHCD confirm this scaling.[8]

Fisch and Boozer[9] have argued that the appropriate collision frequency to use in equation (2.6) is

$$\nu = \frac{\omega_p^4 \ln(\Lambda)(5+Z_i)}{4\pi \, \mathrm{n_o} \mathrm{v}^3}. \qquad (2.11)$$

A version of equation (2.6) appropriate for LHCD is obtained by employing (2.11) and setting $\hat{s}$ equal to a unit vector in the parallel direction (along the magnetic field)

$$\frac{J}{P} = \frac{-e\,4\pi\, n_o}{m\omega_p^4 \ln(\Lambda)(5+Z_i)}\left(\frac{v^3}{v_\parallel} + 3v_\parallel v\right). \tag{2.12}$$

Setting $Z_i = 1$ and assuming $v_\parallel >> v_\perp$ in (2.12) obtains

$$\frac{J}{P} = \frac{-e\,8\pi\, n_o v_\parallel^2}{3m\omega_p^4 \ln(\Lambda)}. \tag{2.13}$$

Define the parameter w as

$$w = \frac{v_\parallel}{v_{\text{thermal}}}. \tag{2.14}$$

Note that

$$I \approx \pi a^2 J. \tag{2.15}$$

The dissipated power density P in (2.13) can be converted into a total power dissipated by multiplying by the tokamak volume

$$P_{\text{net}} \approx P_{\text{per volume}}\, \pi a^2\, 2\pi R. \tag{2.16}$$

Combining equations (2.13) to (2.16) yields

$$\frac{I}{P} = \frac{-4en_o v_{\text{thermal}}^2 w^2}{3m\omega_p^4 \ln(\Lambda) R}. \tag{2.17}$$

Defining the thermal velocity as

$$v_{\text{thermal}} = \sqrt{\frac{kT}{m}}, \tag{2.18}$$

equation (2.17) can be recast as

$$\frac{I}{P} \cong 4\times 10^{15} \frac{T_{eV}\, w^2}{n_{m^{-3}}\, R_{\text{meters}} \ln(\Lambda)} \frac{\text{amps}}{\text{watt}}. \tag{2.19}$$

This formula is identical within a small numerical factor to one put forth by Fisch.[10] For typical conditions in the Encore tokamak; $T_e \cong 10$ eV, $R = 0.4$ meter, $n \cong 10^{18}$ m^{-3}, $\ln(\Lambda) \cong 13$, equation (2.19) predicts

$$\frac{I}{P} \cong 0.008\, w^2 \,\frac{amps}{watt}. \tag{2.20}$$

Use of equation (2.20) requires knowledge of the parameter w. In typical LHCD experiments the velocities of most of the resonant electrons greatly exceed the thermal velocity and w >> 1. Taking $w^2 \cong 20$ as a typical number[11]

$$\frac{I}{P} \cong 0.16 \frac{amps}{watt}. \tag{2.21}$$

In the LHCD experiments on Encore some 40kW of RF power was available. Assuming that only a portion of this power, say 15kW, actually interacts with the resonant electrons, equation (2.21) predicts that plasma current on the order of 2400 amps may be expected. The largest plasma current achieved was 150 amps which is more than an order of magnitude less.

To apply equation (2.19) to experiments on the PLT tokamak take $T_e = 900$ eV, $n = 3.5\times10^{18}$ m^{-3}, R = 1.32 meter, $\ln(\Lambda) = 20$.[12] The prediction of equation (2.19) is 0.8 amps per watt. In the experiments on PLT, 240 kA of current was driven by 130kW of RF power, for an efficiency of 1.85 amps per watt. Thus the prediction of (2.19) is low by more than a factor of two.

LHCD experiments were performed on the Alcator C tokamak.[13] The conditions were $n = 2\times10^{19}$ m^{-3}, $T_e = 1.2$ keV, R = 0.65 meter, $\ln(\Lambda) = 20$. Equation (2.19) predicts an efficiency of 0.375 amps per watt. The obtained efficiency under the above conditions was 0.65 amps per watt, roughly a factor of two larger than the prediction of (2.19).

Equation (2.19) is a rough formula for several reasons. The phase velocity of the plasma waves normalized to the thermal velocity w is not very well known. A spectrum of phase velocities is launched and it is now believed that possibly several processes lead to significant modifications of the launch spectrum. Use of a simple collision frequency in the derivation of (2.19) indicates that details of the evolution of the electron distribution in velocity space are being glossed over. Fisch has given a more detailed theory of current drive in the framework of the quasilinear theory and the Fokker-Planck equation.[14] However, as the above examples show, equation (2.19) correctly predicts the driven current in LHCD experiments within a factor of two or so, the predictions being too low. The fact that (2.19) predicts LHCD currents in the Encore experiments more than an order of magnitude larger than those actually observed indicates that there is something wrong with current drive on Encore. Essentially LHCD did not function as expected in the experiments on Encore.

Another way to visualize the lower hybrid current drive process is to look at changes in the electron velocity distribution as lower hybrid plasma waves are launched. The plasma waves Landau damp on the electron velocity distribution provided that the phase matching criteria is satisfied

$$\frac{\omega}{k_{\|}} = v_{\|}^{e}. \tag{2.22}$$

A further criterion is that the slope of the velocity distribution at the resonant phase velocity is negative. In the presence of a spectrum of intense lower hybrid waves, the damping tends to flatten the distribution.[15] Equilibrium between the electron distribution function and the spectrum of intense plasma waves is obtained when the slope of the distribution function in the resonant region goes to zero. This effect is depicted in Figure (2.1).

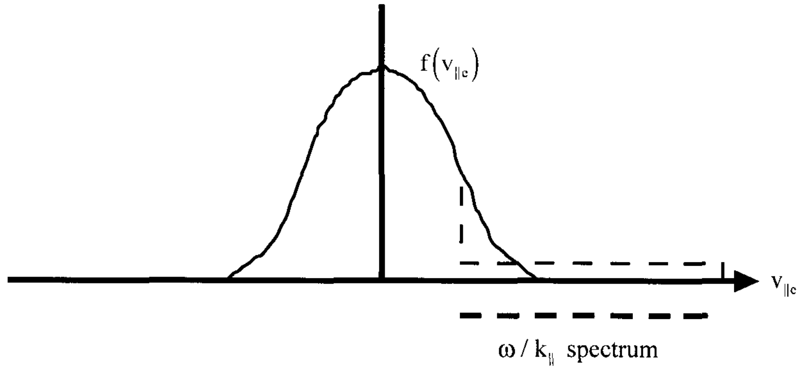

Figure 2-1. Electron velocity distribution along the toroidal magnetic field before (solid line) and after (dashed line) application of an intense spectrum of lower hybrid waves.

If the plasma wave spectrum extends to velocities well beyond the thermal velocity, then the flattened distribution function will contain electrons at velocities well in excess of the thermal velocity where previously there were few electrons. The resulting asymmetric distribution function implies net electron plasma current.

In summary, virtually all plasma waves can be employed for current drive. Slower waves carry more momentum for a given energy than fast waves. Waves that interact with supra-thermal electrons are more efficient at driving current since these electrons are less collisional. LHCD is attractive for many reasons. High power microwave sources are readily available at the necessary frequency, a few gigahertz. The antenna launching the lower hybrid waves can be a conveniently sized array of wave-guide mouths at the plasma edge. Coupling of the wave-guides to the plasma can be very efficient. The lower hybrid waves interact with supra-thermal electrons that are relatively collisionless. Simple estimates of the LH current drive effect in Encore predict large currents that were not observed in experiments.

---

[1] Nathaniel Fisch, "Theory of Current Drive in Plasmas," Rev. Mod. Phys., **59**, 1987, p. 175

[2] T. Antonsen, "Theory of RF Current Drive," in Wave Heating and Current Drive in Plasmas, V. L. Granatstein and P.L. Colestock editors, Gordon & Breach 1985, p. 281

[3] N. J. Fisch and A. H. Boozer, Phys. Rev. Lett., **45**, 1980, p. 720

[4] C. F. Karney and N. J. Fisch, Nuc. Fus, **21**, 1981, p. 1549

[5] George Schmidt, Physics of High Temperature Plasmas, Academic Press 1979, p. 21

[6] IBID reference 1, p. 204

[7] IBID reference 1, p. 205

[8] M. Porkalab et al., Phys. Rev. Lett., **53**, 1984, p. 450

[9] IBID reference 3, p. 721

[10] IBID reference 1, p. 180

[11] IBID reference 1, p. 180

[12] S. Bernabei et al., Phys. rev. Lett., **49**, 1982, p. 1255

[13] IBID reference 1, p. 214

[14] IBID reference 1, p. 183

[15] N. Krall and A. W. Trivelpiece, Principles of Plasma Physics, McGraw-Hill 1973, p. 526

3 Tokamaks

Introduction

Tokamaks are a major candidate for a fusion power reactor. Many tokamak reactor designers believe that the future of tokamaks depends upon finding a viable method of current drive. The experiments on lower hybrid current drive (LHCD) discussed in this thesis were performed on the Encore tokamak at Caltech. The following material will serve to explain tokamak geometry and nomenclature as well as rudimentary plasma confinement physics in these devices. The confinement theory will be applied to the question of confinement of the hot electron tail produced in LHCD experiments on Encore. Typical parameters of the Encore tokamak will be presented. The L/R time constant of Encore will be estimated and the Rogowsky current diagnostic discussed.

Plasma Confinement

Using the virial theorem one can show that a finite mass of plasma cannot generate fields, which in turn confine the mass in a stationary configuration.[1] In order to extend particle and energy confinement times over the values for inertial confinement, external forces have to be applied.

The solution of a charged particle moving in a constant homogeneous magnetic field suggests that magnetic fields can help confine plasma. The name "tokamak" is applied to axially symmetric toroidal systems in which the hot plasma is contained by the magnetic field of a current circulating in it, and in which a very strong longitudinal magnetic field parallel to the current is used to suppress magnetohydrodynamic instabilities.[2] The longitudinal magnetic field must be many times the intensity of the azimuthal field produced by the current. The tokamak concept of magnetic confinement will be discussed shortly.

It can be shown that magnetic confinement can never produce a true thermodynamic equilibrium. According to the Boltzmann law, in thermal equilibrium particles will arrange themselves in phase space as

$$f(\mathbf{v},\mathbf{r}) = \text{constant} * \exp\left(\frac{-H}{kT}\right), \tag{3.1}$$

where H is the Hamiltonian of the system. If spin interactions are neglected, it is seen that the energy of the system of particles is independent of the externally applied magnetic field. When the Hamiltonian of the system of particles is rewritten in terms of the generalized velocities to get the velocity dependence of equation (3.1), one finds that the vector potentials of the externally applied magnetic fields do not appear.

In the course of time the plasma will eventually reach an equilibrium configuration as though the magnetic fields were not present. Collisions are often required for this decay to thermal equilibrium as the system entropy

$$S = -k\int \int f \log(f) dr^3 dv^3 + S_o \tag{3.2}$$

is unchanged for a distribution f satisfying the collisionless Boltzmann equation. The trick of plasma confinement schemes is to delay the approach to thermal equilibrium for as long a time as is possible. One of the more successful confinement schemes has proven to be the tokamak approach.

Tokamak Geometry

In discussing tokamaks certain coordinates and language are useful to specify the geometry. The plasma in a tokamak assumes the shape of a torus, or more colloquially a "doughnut." There exist two kinds of circles one could imagine drawing on the surface of the toroidal plasma, those which enclose the hole of the doughnut and those which do not. Following along a circle on the toroidal surface which encloses the hole is going in the toroidal ϕ direction, whereas following along a circle which does not enclose the hole is going in the poloidal θ direction. In typical machines, the toroidal direction is the long way around and the poloidal direction is the short way around. The minor radius is the radius of a poloidal circle circumscribing the plasma. The major radius is the distance from the center of the hole of the torus to the center of the aforementioned poloidal circle as is shown in Figure (3-1).

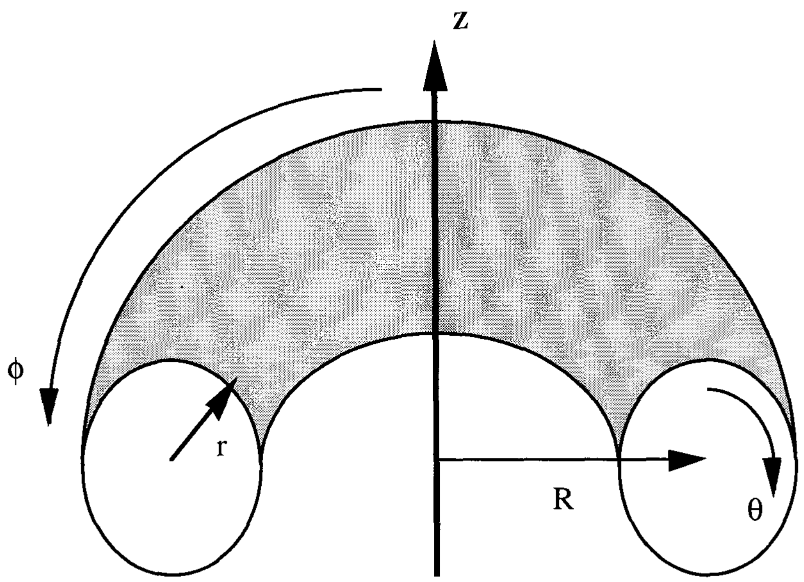

Figure 3-1. Basic coordinates used to describe tokamak geometry. R is the major radius, r is the minor radius, ϕ is the toroidal direction, θ is the poloidal direction. In virtually all devices the z direction is vertical with respect to the laboratory floor.

Single Particle Confinement Model

In a tokamak device there are several magnetic fields which play a part in delaying thermal equilibrium (i.e., confining the plasma). The primary field responsible for putting the plasma in the quasi-equilibrium of toroidal shape is a poloidal magnetic field generated by a current driven in the plasma in the toroidal direction. Using symmetry and the Hamiltonian method, single particle confinement can be investigated.

Assume that we have a toroidal vacuum chamber with a toroidal current I_ϕ localized symmetrically about the center of the poloidal cross section. This toroidal current produces a vector potential A_ϕ also pointing in the toroidal direction and a poloidal magnetic field B_θ encircling the current.

As specified, the Hamiltonian **H** for a single particle in this field is independent of ϕ. Hence the momentum P_ϕ conjugate to ϕ is a strict constant

$$\dot{P}_\phi = -\frac{\partial H}{\partial \phi} = 0. \tag{3.3}$$

This fact will be used to put bounds on the particle motions in both the major radius and z directions. The Lagrangian is

$$L = \frac{1}{2} m\mathrm{v}^2 + q\mathbf{A}\cdot\mathbf{v} - qU. \tag{3.4}$$

Using equation (3.4) the toroidal momentum is calculated as

$$P_\phi \equiv \frac{\partial L}{\partial \phi} = mR\mathrm{v}_\phi + qRA_\phi\ , \tag{3.5}$$

where $\mathrm{v}_\phi = \mathrm{R}\dot{\phi}$. Noting equation (3.3) one can write

$$0 = \delta P_\phi = m\mathrm{v}_\phi \delta R + mR\delta\mathrm{v}_\phi + q\delta(RA_\phi). \tag{3.6}$$

Consider now two toroidal circles of slightly differing major radii in the z = 0 plane. The area of the z = 0 plane located between these circles is an annulus which cuts the poloidal magnetic field lines B_θ perpendicularly. See Figure (3-2).

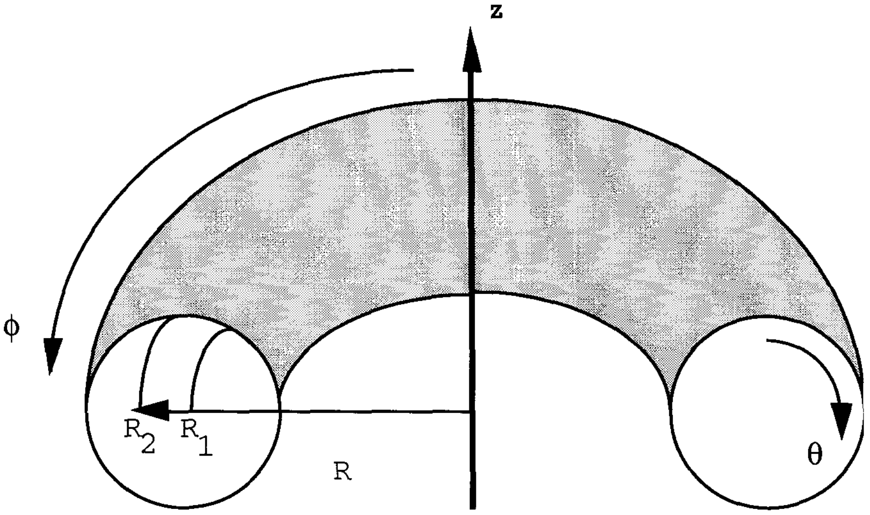

Figure 3-2. Annulus used for calculating major radius confinement in a tokamak.

The poloidal flux penetrating this annular surface is

$$\begin{aligned} 2\pi \mathrm{R}\,\delta\mathrm{R}\,\mathrm{B}_\theta &= \int_{\text{annulus}} \mathbf{B}_\theta \cdot \mathbf{ds} = \int_{\text{annulus}} (\nabla\times\mathbf{A})\cdot\mathbf{ds} = \int_{\text{circles}} \mathbf{A}\cdot\mathbf{dl} \\ &= 2\pi(\mathrm{R}_2\mathrm{A}_{\phi 2} - \mathrm{R}_1\mathrm{A}_{\phi 1}) = 2\pi\,\delta(\mathrm{R}\mathrm{A}_\phi). \end{aligned} \tag{3.7}$$

Combining equation (3.6) and (3.7), one obtains

$$0 = m\delta R\, v_\phi + mR\,\delta v_\phi + qR\,B_\theta\,\delta R . \tag{3.8}$$

Hence,

$$|\delta R| = \left| \frac{R\delta v_\phi}{v_\phi + R\frac{qB_\theta}{m}} \right| \cong \frac{|\delta v_\phi|}{\left|\frac{qB_\theta}{m}\right|} \leq \frac{2v_{thermal}}{\left|\frac{qB_\theta}{m}\right|} . \tag{3.9}$$

Thus, for a given temperature, a large enough poloidal magnetic field B_θ will insure small deviation δR in the major radius of the particle's trajectory. It should be pointed out that although thermal equilibrium is definitely not obtained in a tokamak plasma, equilibrium in velocity space is approached far more quickly than equilibrium in configuration space. Usually a temperature can be defined for the bulk plasma.

Similarly for motion along the z-axis we consider two circles of radius R, the torus major radius. These circles lie in planes of constant z and are closely spaced δz apart in the z direction. Once again, the poloidal magnetic field cuts the cylindrical area between these two circles perpendicularly.

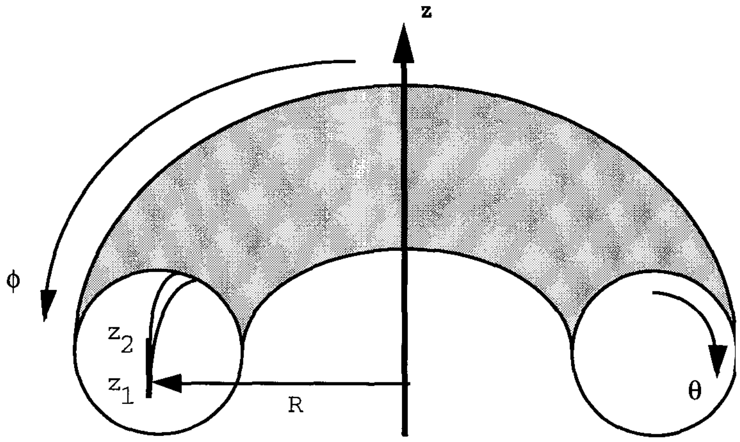

Figure 3-3. Cylinder used for calculating vertical (z-axis) confinement in a tokamak.

As in equation (3.7)

$$2\pi R\,\delta z B_\theta = \int_{\text{cylinder}} \mathbf{B}_\theta \cdot \mathbf{ds} = \int_{\text{cylinder}} (\nabla \times \mathbf{A}) \cdot \mathbf{ds} = \int_{\text{circles}} \mathbf{A} \cdot \mathbf{dl}$$

$$= 2\pi(R_2 A_{\phi 2} - R_1 A_{\phi 1}) = 2\pi\,\delta(RA_\phi). \tag{3.10}$$

And from equation (3.6)

$$0 = \delta P_\phi = mR\,\delta v_\phi + qR\,\delta A_\phi\,. \tag{3.11}$$

Combining equation (3.10) and (3.11) obtains

$$|\delta z| \cong \frac{|\delta v_\phi|}{\left|\frac{qB_\theta}{m}\right|} \leq \frac{2v_{thermal}}{\left|\frac{qB_\theta}{m}\right|}. \tag{3.12}$$

So for motion in the z-direction as well there is confinement for a given temperature if sufficient B_θ is provided.

A tokamak doesn't confine particles indefinitely. There are several reasons for this. It is assumed in the above calculations that the fields are known. In real plasma there are many particles in addition to the one considered and the interactions between these particles involve unknown fields.

On another level, the plasma current I_ϕ that produces the confining B_θ field is carried by the very plasma it is to confine. This situation leads to large-scale instability problems, which are solved by the introduction of a strong toroidal magnetic field B_ϕ with

$$\frac{B_\phi}{B_\theta} >> 1. \tag{3.13}$$

The toroidal field hinders the plasma from wiggling, kinking, pinching and various other instabilities. Image currents induced in the metal walls of the vacuum chamber also suppress large-scale plasma motions.

One further addition is necessary. A hoop of current naturally experiences forces attempting to expand the hoop to a larger diameter (opposite currents repel). These magnetic forces are balanced with the addition of a small magnetic field B_Z along the z-axis. Since all tokamaks are built with the z-axis vertical to the ground, this field B_Z is also known as the vertical field.

Toroidal Magnetic Field Dependence on Major Radius

It is of interest to know the functional dependence of the magnitude of the toroidal magnetic field with major radius. Consider a circle of major radius R in the plane $z = 0$ as shown in Figure (3-4).

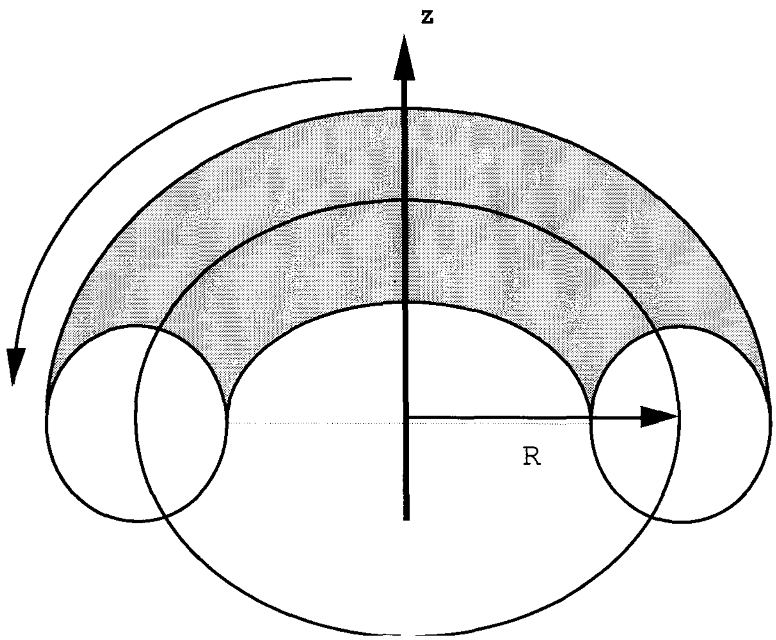

Figure 3-4. Circle used to calculate the magnitude of the toroidal field in a tokamak versus the major radius.

Integrating the toroidal field around this circle and using Maxwell's equations obtains

$$2\pi R B_\phi = \int_{\text{circle}} \mathbf{B}\cdot d\mathbf{l} = \int_{\text{disc}} \nabla\times\mathbf{B}\cdot d\mathbf{s} = \int_{\text{disc}} \mu_o \mathbf{J}\cdot d\mathbf{s} = \mu_o I_{\text{coils}}, \tag{3.14}$$

where I_{coils} is the current-turns in the toroidal field coils. Thus

$$B_\phi = \frac{\mu_o}{2\pi R} I_{\text{coils}} . \tag{3.15}$$

The toroidal field falls off inversely with the major radius. This dependence of the toroidal field on major radius causes many of the plasma parameters to vary with major radius.

Reviewing the results of this section, tokamaks are often described using the following nomenclature. The torus has major and minor radius coordinates R and r respectively. The toroidal direction (the long way around) is denoted ϕ. The poloidal direction (the short way around) is denoted θ. A strong enough toroidal current I_ϕ producing a poloidal magnetic field B_θ will confine a plasma of a given temperature with particles of given charge and mass. In order to prevent certain macroscopic instabilities from occurring, a large toroidal magnetic field B_ϕ is applied, and this field falls off in magnitude inversely with major radius. B_ϕ is typically much larger than B_θ. In addition a small vertical magnetic field B_z is applied to null out the force generated by the toroidal current which tends to expand the major radius of the plasma.

The Encore Tokamak

The experiments described in this thesis were performed on "Encore," a small research tokamak located at Caltech. This tokamak is a low temperature and low magnetic field device. The toroidal field is run continuously, and the ohmic heating supply is capable of creating plasma at a high repetition rate. The plasma is highly reproducible as evidenced by the ability to interferometrically track the propagation of lower hybrid waves over many plasma discharges.[3] Some important plasma parameters are the plasma current I_p, electron and ion plasma frequencies f_{pe} and f_{pi}, electron and ion cyclotron frequencies f_{ce} and f_{ci}, and the lower hybrid frequency f_{LH}. Typical values of these and other quantities are given in the following tables.

Parameter	Typical Value in Encore
Repetition Rate	15 PPS
Major Radius	38 cm
Minor Radius	12 cm
Toroidal Field	≤ 1.3 kG
Ohmic Plasma Current	up to several kA
Electron Temperature	5-10 eV
Electron Density	$\approx 2\times10^{12}\text{cm}^{-3}$ for $I_p = 1$ kA

In Encore, plasma density is typically proportional to the plasma current I_p. The following parameters are for a plasma current of one kiloamp, and a toroidal magnetic field of 1.3 kilogauss. In the following table, the electron and ion masses are m_e and m_i respectively and the plasma density is n.

Parameter	Formula	Argon	Hydrogen
f_{ce}	$\propto B_\phi/m_e$	3.7 GHz	3.7 GHz
f_{ci}	$\propto B_\phi/m_i$	51 kHz	2.0 MHz
f_{pe}	$\propto (n/m_e)^{0.5}$	10 GHz	10 GHz
f_{pi}	$\propto (n/m_i)^{0.5}$	37 MHz	230 MHz
f_{LH}	$\approx (f_{ce}f_{ci})^{0.5}$	14 MHz	86 MHz

Figure (3-5) shows a schematic picture of the Encore tokamak metal shell and iron core ohmic heating transformer. The plasma is essentially a one turn secondary of the transformer. In order to avoid shorting out the transformer and bypassing the plasma, an insulating break is made in the toroidal aluminum shell comprising the vacuum chamber. The voltage induced around the torus is known as loop voltage and is easily measured across the break.

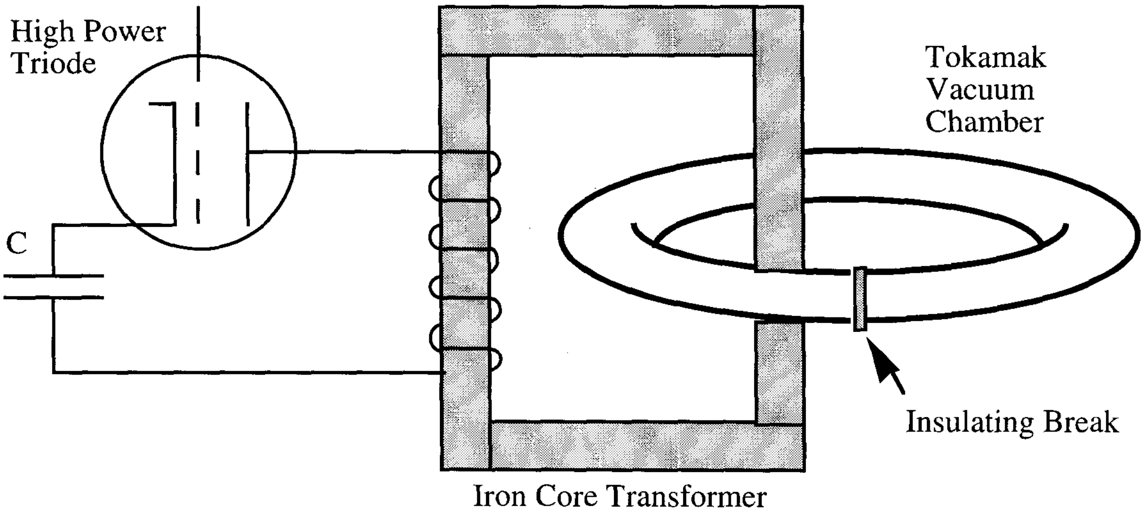

Figure 3-5. Schematic of the Encore ohmic plasma current drive system.

The ohmic heating power supply is comprised of two high power audio-frequency amplifiers of which one is shown in Figure (3-5). The two amplifiers A and B each energizes one half of a center tapped primary winding on the iron core transformer. Amplifier A operating in the opening switch mode provides plasma breakdown while amplifier B operating in the closing switch mode sustains the plasma. Figure (3-6) shows the primary current, loop voltage and plasma current versus time.

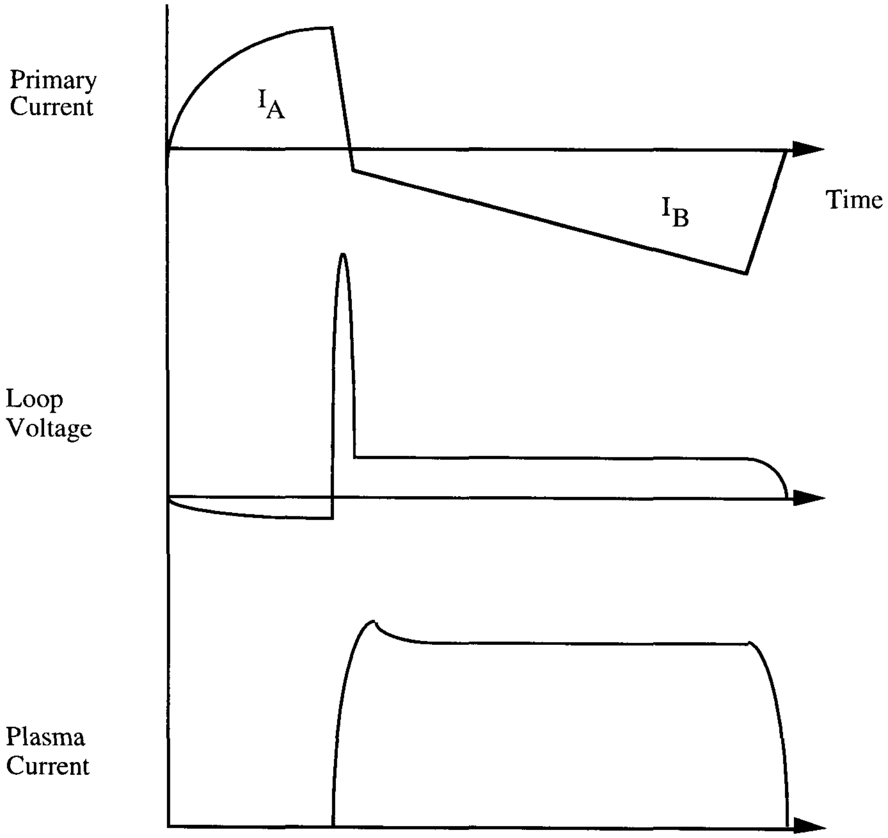

Figure 3-6. Schematic of the primary current versus time, as well as the associated loop voltage and plasma current in the Encore tokamak.

The use of audio amplifiers allows high repetition rate operation of Encore. The input waveforms to the amplifiers can be altered at will to achieve various effects on the plasma. A hot tungsten filament is maintained inside of the tokamak chamber in order to provide a source of electrons to facilitate plasma breakdown.

The tokamak vacuum chamber is composed of a 1.27cm thick aluminum toroidal shell, which acts as a plasma limiter. Access for experiments is provided by 33 4cm diameter ports located on the top and bottom of the torus and 15 8x20cm ports located around the outer wall centered about the horizontal mid-plane. The ports are sealed with o-rings and are readily removed and replaced. The vacuum base pressure is typically 5×10^{-7} torr.

During typical operation the plasma is not fully ionized. This tends to clamp the electron temperature at the ionization energy of the fill gas (≈ 10 eV). The low plasma temperature allows probes to be inserted throughout the plasma interior without damage. Plasma energy loss is dominated by line radiation. Argon is frequently used as a fill gas for two reasons. The plasmas obtained with argon fill are in general more reproducible.[4] In addition the amount of x-rays produced by runaway electrons is far less when argon instead of hydrogen fill is used. The high repetition rate operation creates a potential radiation hazard when hydrogen fill is used. Adequate shielding is provided for operation with hydrogen but it is inconvenient to have to shut down the tokamak in order to inspect equipment behind the shields. Figure (3-7) is a picture of the Encore Tokamak.

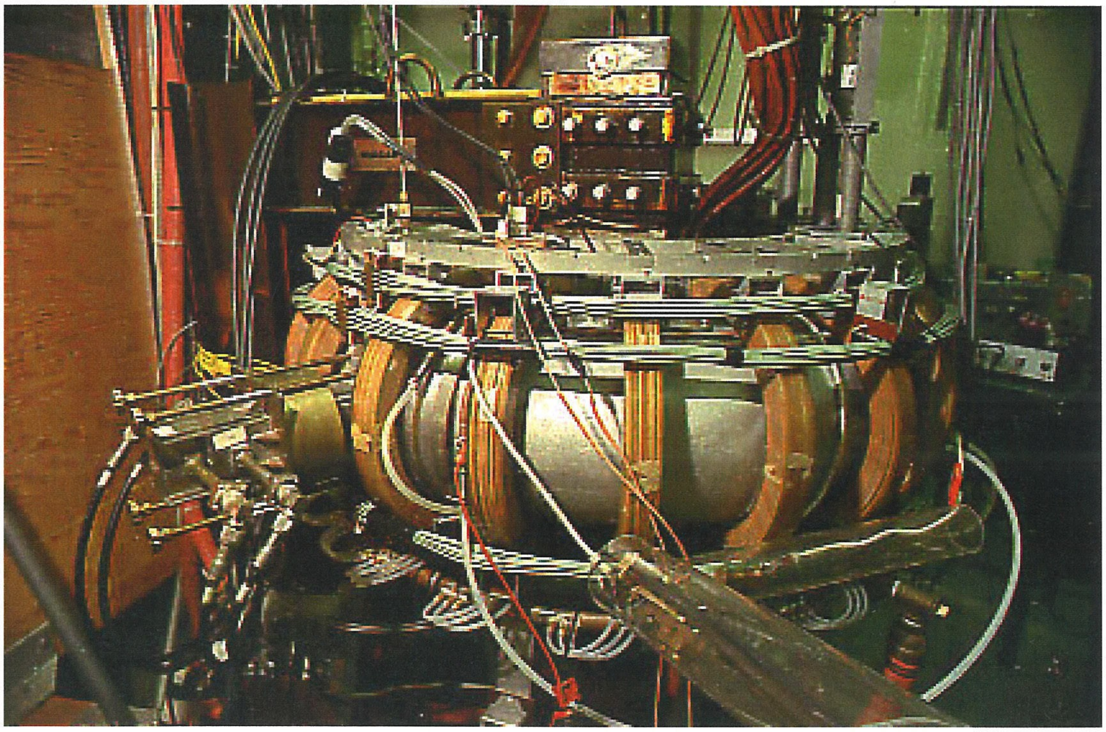

Figure 3-7. The Encore tokamak.

Confinement of Hot Electron Tails

Barring instability, equations (3.9) and (3.12) give sufficient criteria for tokamak confinement. It is of interest to estimate the maximum electron velocity, which will be confined by various plasma currents.

The poloidal field can be estimated from the plasma current by using the formula for the magnetic field of an infinite straight wire evaluated at a radius equal to half the minor radius of the tokamak. The formula for Encore parameters becomes

$$B_\theta(\text{gauss}) = 0.03 I_p(\text{amps}). \tag{3.16}$$

Setting $|\delta R|$ equal to half the minor radius, the maximum confined speed is estimated from (3.9) as

$$|v_{max}| \cong |\delta R| \left| \frac{eB_\theta}{m_e} \right| = 5.6 \times 10^5\, I_p(\text{amps})\ \text{cm/sec}. \tag{3.17}$$

Plasma waves that interact with electrons via Landau damping will have phase velocity similar to electron velocity. The phase velocity of plasma waves is often described in terms of their refractive index. The refractive index relevant to the direction parallel to the local toroidal magnetic field is denoted $N_{||}$. Plasma waves that interact with electrons moving along the toroidal magnetic field with a speed of v_{max} will have a parallel refractive index of

$$N_{||} = \frac{c}{|v_{max}|}. \tag{3.18}$$

The following table gives the result of equation (3.17) for a range of plasma currents. Also tabulated are the equivalent electron energies in electron volts and the parallel refractive index $N_{||}$ resonant with v_{max}.

Maximum Speed of Confined Electrons versus Plasma Current

I_p (amps)	$\|v_{max}\|$ (cm/sec)	$(mv_{max}^2)/2$ (eV)	$N_{\|\|}$
10	5.6×10^6	0.01	5000
100	5.6×10^7	1	500
1000	5.6×10^8	100	50
5000	2.8×10^9	2200	11
10^4	5.6×10^9	10^4	5

One significance of the above table is that in ohmic discharges in Encore with plasma currents in the range of 1 kA or more, hot electron tails with energies of a few hundred eV will be confined as part of the tokamak plasma. In the strictly rf produced plasmas to be described later, the maximum driven plasma current was of the order of 150 amps. For plasma currents of this order, hot electron tails will not be confined by the poloidal magnetic field. Instead these hot electron tails are best described as beams drifting in the combined toroidal and vertical magnetic fields.

Tokamak Inductance and L/R Time

When attempt is made to change the current in an inductance L, the fastest time scale upon which the current can alter is of the order of L/R where R is the circuit resistance. For instance, when the switch is closed in the circuit depicted in Figure (3-8) the current varies as

$$I = \frac{EMF}{R}(1 - e^{-Rt/L}). \qquad (3.19)$$

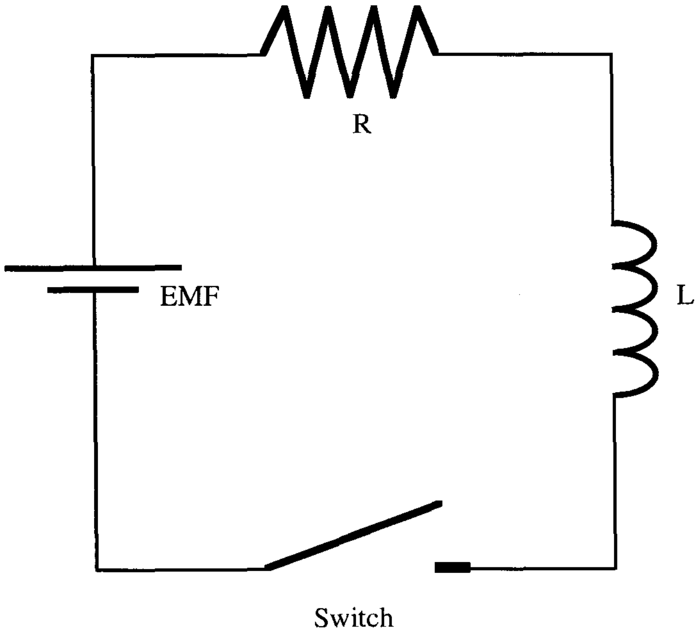

Figure 3-8. Simple L – R circuit.

In current drive experiments the plasma current cannot be expected to change significantly on shorter time scales, so an estimate of the L/R time constant is important.

The inductance of a toroidal conductor is easily computed.[5,6] Given the minor and major radius of the Encore tokamak, a value of approximately one micro-henry is obtained. The inductance of virtually all tokamaks is found to be in this neighborhood. The voltage V_{loop} induced around a tokamak by the ohmic heating supply is easily measured across the necessary gap in the toroidal metal shell enclosing the plasma. A typical operating point for ohmic plasma in Encore is

$$\left.\begin{array}{l} V_{loop} = 7.5 \text{ volt} \\ I_p = 1 \text{ kiloamp} \end{array}\right\} \Rightarrow R \approx 0.008 \text{ ohms}, \tag{3.20}$$

from which it is obtained

$$\frac{L}{R} \approx 0.13 \text{ msec.} \tag{3.21}$$

The RF power supplies employed for LHCD experiments on Encore are capable of pulse duration exceeding 16 msec. Thus in typical ohmic plasmas, the L/R time constant is incapable of hiding current drive effects.

The situation can be significantly more complicated, however, when hot electron tails are present in the plasma. If the hot electrons are relatively collisionless and if their density is high enough they can act as a small resistance in parallel with the resistance of the bulk plasma. One consequence is that the L/R time can be dramatically increased.

A second issue concerns the fact that a hot electron tail propagating counter to the RF driven tail can sometimes be generated. A reverse electron tail can be produced in current drive experiments in two distinct ways. If attempts are made to ramp up the current too quickly the electric field due to the back emf may be large enough to create a fair number of runaway electrons in the reverse direction. Alternatively, if the launch spectrum of lower hybrid waves is not sufficiently unidirectional then the reverse tail can be directly driven by the current drive mechanism. This latter case almost certainly applies to the experiments on Encore since the four port grill antenna used was capable of launching only about 75% of the power in a given direction.

The action of the "back emf" electric field on a reverse hot electron tail is to absorb energy that otherwise could have gone into forward driven current. Thus a reverse hot electron tail is detrimental to current drive. Exactly how small a resistance a reverse hot electron tail represents depends upon many factors including the confinement properties of the tail. Various authors discuss these matters more extensively.[7,8,9,10]

During current ramp up the inductive back emf will produce a measurable loop voltage change across the insulating break in the tokamak shell. For current ramp in the presence of ohmic current drive in the same direction, the loop voltage change will manifest itself as a drop in the loop voltage. Provided that the loop voltage drop is insufficient to reverse the sign of the loop voltage, a reverse electric field will not exist in the plasma. In this case poor current drive efficiency cannot be blamed on the existence of a reverse hot electron tail as no electric field exists to dump energy into this tail. LHCD experiments were performed on Encore during ohmic current drive without producing substantial plasma current or loop voltage changes, regardless of the direction of plasma wave launch.

The effect of the Encore iron core ohmic heating transformer on current drive is mainly to increase the inductance of the tokamak. A given driven current will induce a larger back emf with the iron core transformer than without it. Essentially the magnetic fields created in the iron core by the RF driven current require that more energy be extracted from the kinetic energy in the RF driven electrons. The electric field due to the increased back emf accomplishes this. The experimental effect of the iron core transformer should be an increase in the measured loop voltage drop when the RF is applied.

In LHCD experiments on Encore, very poor current drive efficiency was obtained. Loop voltage changes upon application of the RF were always very small compared to typical ohmic loop voltages. Thus, it is argued here that reverse hot electron tails and the iron core transformer are ruled out as possible causes. Were the basic current drive mechanism to be working properly, one would see either large current changes or large loop voltage changes.

Rogowsky Current Diagnostic

The object of current drive is to produce currents. Hence it is appropriate to discuss current diagnostics. The most commonly used current diagnostic is the Rogowsky coil depicted in Figure (3-9).

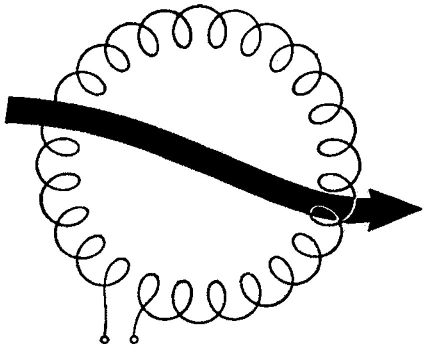

Figure 3-9. The Rogowsky coil current diagnostic. An electric current represented by the heavy black line passes through a toroidally wound coil. Changes in the amount of current are reflected in voltages at the terminals of the toroidal coil.

From Faraday's law the voltage V produced by the coil is related to the rate of change of the magnetic field B threading the coil as

$$V = nLA\frac{dB}{dt}, \tag{3.22}$$

where n is the number of turns per unit length along the circumference of the coil, L is the coil circumference and A is the coil cross-sectional area. It is assumed that the magnetic field varies little over the cross-sectional area of the coil. When the voltage produced by the coil is fed into a RC integrating circuit,[11] the result is

$$V_{RC} = \frac{nABL}{RC}. \tag{3.23}$$

R and C are the resistance and capacitance of the integrating circuit. It is necessary that the RC time constant be large compared to the time scale over which the magnetic field changes. From Ampere's law the current I threading the Rogowsky coil can be related to the magnetic field B as

$$BL = \int_{\text{loop}} \mathbf{B} \cdot \mathbf{dl} = \mu_o I. \tag{3.24}$$

As the current is ramped up, the output of the RC integrating circuit is proportional to the current

$$V_{RC} = \frac{nA\mu_o I}{RC}. \tag{3.25}$$

The calibration of the Rogowsky coil diagnostic on Encore as well as its frequency response was checked using the experimental arrangement depicted in Figure (3-10).

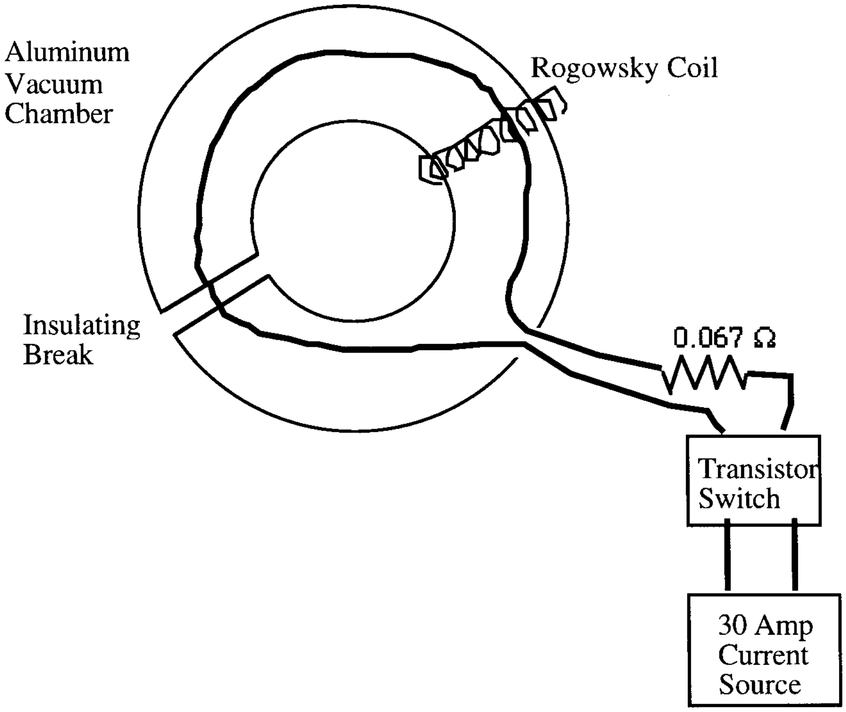

Figure 3-10. View from above the tokamak showing the Rogowsky coil and ceramic break in the metal vacuum chamber. Also shown is the experimental arrangement used to calibrate the Rogowsky coil diagnostic and check its frequency response.

When the current in the torus is ramped up, the magnetic field encircling the current must escape past the aluminum toroidal shell to reach the Rogowsky coil in order to be measured. It is interesting to note how this occurs. A diffusion equation for magnetic fields in conductors is derived as follows. From Maxwell's equations

$$\frac{\partial \mathbf{B}}{\partial t} = -\nabla \times \mathbf{E}. \tag{3.26}$$

Using Ohm's law $\mathbf{J} = \sigma\,\mathbf{E}$ this can be rewritten as

$$\frac{\partial \mathbf{B}}{\partial t} = -\nabla \times \frac{\mathbf{J}}{\sigma}. \tag{3.27}$$

Inside a good conductor conduction currents dominate displacement currents so that Ampere's law reduces to

$$\nabla \times \frac{\mathbf{B}}{\mu_o} = \mathbf{J}. \tag{3.28}$$

Combining (3.27) and (3.28) yields

$$\frac{\partial \mathbf{B}}{\partial t} = -\frac{1}{\mu_o \sigma} \nabla \times \nabla \times \mathbf{B}. \tag{3.29}$$

Finally employing

$$\nabla \cdot \mathbf{B} = 0 \tag{3.30}$$

yields

$$\frac{\partial \mathbf{B}}{\partial t} = -\frac{1}{\mu_o \sigma} \nabla^2 \mathbf{B}, \tag{3.31}$$

which is the desired diffusion equation. An estimate of the time Δt for the magnetic field to diffuse through a conductor of thickness T is obtained from (3.31) as

$$\Delta \mathrm{t} = \mathrm{T}^2 \mu_o \sigma. \tag{3.32}$$

The diffusion time scale for various thickness of aluminum metal is given below.

Magnetic Field Diffusion Time Scales in Aluminum

Time Scale	Thickness
17 msec	1.1 cm
10^{-3} sec	2.7 mm
10^{-6} sec	85 μm

The rise time of the ohmic plasma current in Encore is of the order of a millisecond. If the magnetic field from the plasma current had to diffuse out through the aluminum walls there would be a significant delay in reaching the Rogowsky coil since the walls are 1.27 cm thick. Any modulation of the plasma current on the order of a kilohertz would be seriously attenuated. However, what actually happens is that the magnetic field lines encircling the plasma current as it ramps up leak out of the toroidal metal shell through the insulating break in the torus. Hence they reach the Rogowsky coil at nearly the speed of light.

The results of the Rogowsky coil calibration experiment depicted in Figure (3-10) are given in the following three oscilloscope photographs. The calibration factor is seen to be 1.0 kiloamp per volt and is independent of modulation frequency.

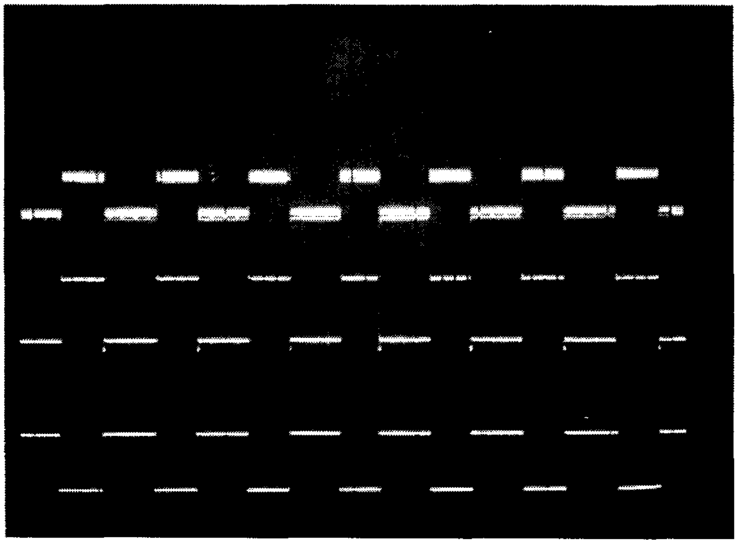

Figure 3-11. Rogowsky calibration experiment. Horizontal time scale 1 millisecond per division. Upper trace is the integrated Rogowsky signal (5mV/div). Middle trace is the voltage across the resistor (0.2V/div). Lower trace is the reference pulse.

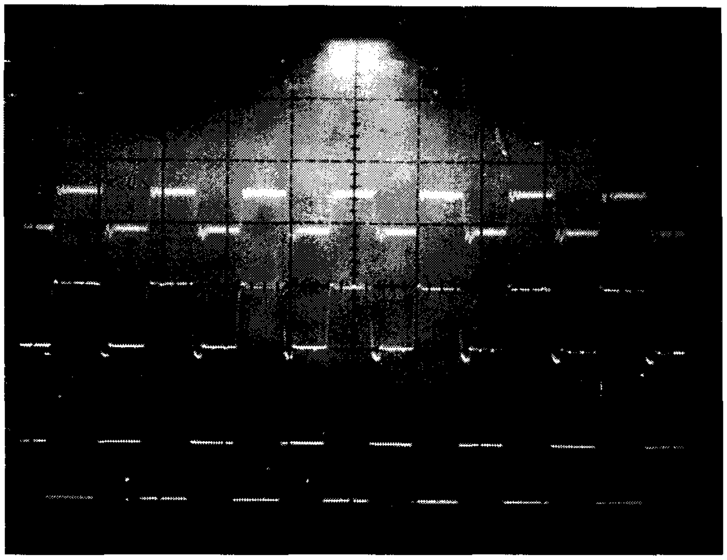

Figure 3-12. Rogowsky calibration experiment. Horizontal time scale 100 microseconds per division. Upper trace is the integrated Rogowsky signal (5mV/div). Middle trace is the voltage across the resistor (0.2V/div). Lower trace is the reference pulse.

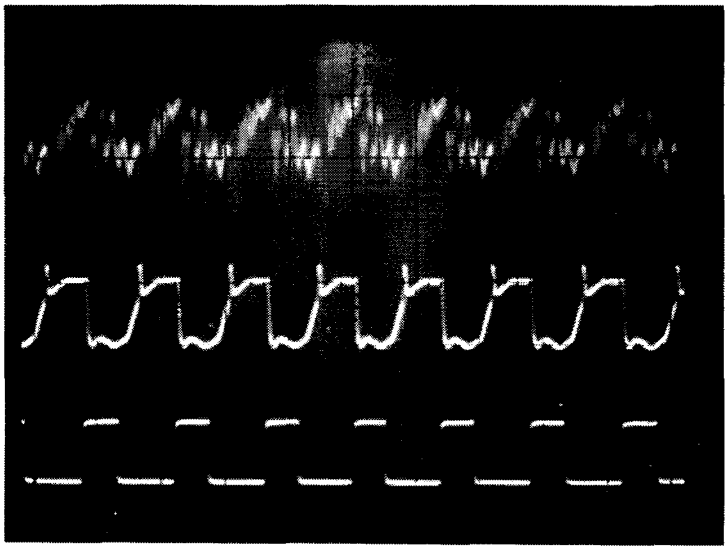

Figure 3-13. Rogowsky calibration experiment. Horizontal time scale 10 microseconds per division. Upper trace is the integrated Rogowsky signal (5mV/div). Middle trace is the voltage across the resistor (0.2V/div). Lower trace is the reference pulse.

The data in Figures 3-10 through 3-12 demonstrate that the Rogowsky current diagnostic installed on Encore has a very fast temporal response. If changes in plasma current occur, even on time scales approaching 10 microseconds, the Rogowsky coil will register them.

---

[1] Physics of high Temperature Plasmas, 2nd Edition, George Schmidt, Academic Press (1979), p. 72

[2] L. A. Artsimovich, "Tokamak Devices," Nuc. Fus. **12**, (1972) p. 215

[3] P. M. Bellan, "Electromagnetic Interference Pattern of Resonance Cones in the Far Field," Phys. Rev. Lett., **45**, (1980) p. 1407

[4] E. Fredrickson, "An Experimental and Theoretical Investigation of a Finite Beta Modified Drift Wave," thesis, California Institute of Technology, (1985) p. 5

[5] D. Halliday and R. Resnick, Fundamentals of Physics, John Wiley and Sons, Inc., NY, (1974), p. 600

[6] Bateman, MHD Instabilities, The MIT Press, Cambridge, (1980), p. 82

[7] N. J. Fisch, Rev. Mod. Phys., **59**, (1987), p. 215

[8] N. J. Fisch and C. F. Karney, "Conversion of Wave Energy to Magnetic Field Energy in a Plasma Torus," Phys. Rev. Lett., **54**, (1985), p. 897

[9] F. C. Jobes et al., "Current Ramp Up by Lower hybrid Waves in the PLT Tokamak," Phys. Rev. Lett., **55**, (1985), p. 1295

[10] C. S. Liu et al., "Inductance Effect of Runaways on Lower-Hybrid-Current Ramping," Phys. Rev. Lett., **55**, (1985), p. 2583

[11] P. Horowitz and W. Hill, The Art of Electronics, Cambridge University Press, Cambridge, MA, (1984), p. 23

4 Theory of Lower hybrid Waves

The Cold Plasma Dielectric Tensor

The general linear theory of plasma waves and in particular of lower hybrid waves is well known. A brief review of lower hybrid physics is presented in this section. Parameters relevant to the Encore tokamak are introduced and various quantities pertinent to the experimental situations are calculated. A derivation of the cold plasma dielectric tensor is presented first.

The theory of plasma waves is contained in Maxwell's equations in combination with an evaluation of the electric and magnetic permeability tensors describing the plasma. These equations may or may not be linear depending upon the nature of the permeabilities. In MKS macroscopic form, Maxwell's equations can be written as

$$\nabla \cdot \mathbf{D} = \rho_{free}, \tag{4.1}$$

$$\nabla \times \mathbf{E} = -\frac{\partial \mathbf{B}}{\partial t}, \tag{4.2}$$

$$\nabla \cdot \mathbf{B} = 0, \tag{4.3}$$

$$\nabla \times \mathbf{H} = \frac{\partial \mathbf{D}}{\partial t} + \mathbf{J}_{free}. \tag{4.4}$$

The following relations define the tensors $\boldsymbol{\varepsilon}$ and $\boldsymbol{\mu}$:

$$\mathbf{D} = \varepsilon_o \mathbf{E} + \mathbf{P} \equiv \boldsymbol{\varepsilon} \cdot \mathbf{P}, \tag{4.5}$$

$$\mathbf{H} = \frac{1}{\mu_o}\mathbf{B} - \mathbf{M} \equiv \frac{1}{\boldsymbol{\mu}} \cdot \mathbf{B}. \tag{4.6}$$

Charge density in the plasma will be considered polarization charge in a dielectric. Currents in the plasma will be considered as displacement currents in a dielectric. The dielectric tensor $\boldsymbol{\varepsilon}$ then contains much information about the plasma. Unless one is considering problems such as coupling of antennas to the plasma, the following approximations can be made:

$$\rho_{free} = 0, \tag{4.7}$$

$$\mathbf{J}_{free} = 0. \tag{4.8}$$

The approximation $\mu = \mu_0$ is made. By treating the plasma as a non-magnetic material the intrinsic magnetic moments of the ions and electrons are neglected. The plasma diamagnetism deserves some comment. When a magnetic field **H** is applied to plasma the ions and electrons gyrating about the magnetic field constitute currents wherever there is a density gradient. These currents produce a magnetic field opposing the applied field resulting in a magnetic field **B** with $\mathbf{B} < \mu_0\mathbf{H}$. One could define a relative magnetic permeability μ_r such that $\mu_r < 1$ to account for the plasma diamagnetism. This is typically not done.

The problem is that the traditional approach to the dispersion relation involves Fourier analysis of Maxwell's equations in space and time to obtain local relations. These local equations include no information about density gradients and thus do not incorporate diamagnetic effects. Most plasma waves have some oscillating magnetic field component along with some plasma density oscillation. If diamagnetic effects are sufficient to significantly alter $\mathbf{B} = \mu_0\mathbf{H}$ the wave dispersion may be affected. In most situations diamagnetic effects turn out to be small.

The shift in the toroidal field $\mathbf{B}_T$ due to the plasma diamagnetism depends on the plasma β where

$$\beta = \frac{\textit{plasma pressure}}{\textit{magnetic pressure}} = \frac{\mathrm{nkT}}{\mathrm{B}^2/8\pi}. \qquad (4.9)$$

From the MHD pressure balance equations it is found that

$$\frac{\mathrm{B}^2}{\mathrm{B}_o^2} = 1 - \beta, \qquad (4.10)$$

where B_o is the applied toroidal field and B is the actual field inside of the plasma. The difference between B and B_o for experiments performed on Encore is small since the plasma β is typically less than 1%. A typical ohmic discharge in Encore would have the following parameters:

$kT_e \approx 10\mathrm{eV}$,

$kT_i \approx 3\mathrm{eV}$,

$$n_e = n_i \approx 2\times 10^{12}\,\mathrm{cm}^{-3},$$

B_T = 350 to 1300 Gauss (on axis).

The magnetic energy density thus ranges over

$$4.7\times 10^{3}\,\mathrm{ergs\,cm}^{-3} \le \frac{B^2}{8\pi} \le 6.8\times 10^{4}\,\mathrm{ergs\,cm}^{-3}. \tag{4.11}$$

The ion and electron energy densities are roughly

$$n_i kT_i \approx 10\,\mathrm{ergs\,cm}^{-3}, \tag{4.12}$$

$$n_e kT_e \approx 32\,\mathrm{ergs\,cm}^{-3}. \tag{4.13}$$

The plasma β then falls into the range

$$0.06\% \le \beta \le 0.9\%. \tag{4.14}$$

For β = 1%,

$$\frac{B}{B_o} = \sqrt{1-\beta} = 0.995\ . \tag{4.15}$$

The shift in the magnetic field and thus the cyclotron frequencies is small for tokamak experiments in general where $\beta < 5\%$.

Consider a tube of magnetic flux that constitutes part of a plasma wave. The assumption that $\mathbf{B} = \mu_0\mathbf{H}$ for this flux tube requires that plasma diamagnetism be negligible. The diamagnetic current $\mathbf{j}_\perp$ can be written as

$$\mathbf{j}_\perp = \frac{\mathbf{B}\times\nabla p}{B^2} = \left(kT_i + kT_e\right)\frac{\mathbf{B}\times\nabla n}{B^2}. \tag{4.16}$$

Here, $\mathbf{B}$ is the total magnetic field, the sum of the toroidal and plasma wave magnetic fields. A density gradient is necessary for the diamagnetic current to exist. In large amplitude plasma waves, large density gradients can exist. It is the current per unit length along the flux tube that reduces the magnetic field inside. Equation (4.16) gives the current density. To obtain the diamagnetic current per unit length $\mathbf{i}_\perp$ one must multiply $\mathbf{j}_\perp$ by the width L of the density gradient

$$\mathbf{i}_\perp \cong \mathbf{j}_\perp L\ , \text{ where } L \equiv \frac{n}{|\nabla n|}. \tag{4.17}$$

Combining equations (4.16) and (4.17) obtains

$$\mathbf{i}_\perp = \left(n_i kT_i + n_e kT_e\right)\frac{c\mathbf{B}\times\nabla n}{|\nabla n|\,B^2}\ . \tag{4.18}$$

The magnitude of the diamagnetic current per unit length is then bounded by

$$i_\perp \le \frac{c\left(n_i kT_i + n_e kT_e\right)}{B}\ . \tag{4.19}$$

If the flux tube were a solenoid with current $\mathbf{i}_\perp$, then the field inside would be reduced in the amount $(4\pi / c)\mathbf{i}_\perp$. The fractional decrease would be less than

$$\frac{4\pi i_\perp}{cB} = \frac{1}{2}\frac{\left(n_i kT_i + n_e kT_e\right)}{B^2/8\pi} = \frac{\beta}{2}. \tag{4.20}$$

The diamagnetic correction is small if the plasma beta in the presence of the wave is small. In the case of an electrostatic lower hybrid wave

$$\tilde{B}_{\text{wave}} << B_T. \tag{4.21}$$

Thus the magnetic field energy density due to the wave is negligible compared to the toroidal field energy density. Due to ionization and collisional damping, the plasma pressure may increase in the neighborhood of the wave trajectory. However, in the case of a typical Encore plasma, β is so small to start with, it is unlikely that significant values of β and thus diamagnetism could ever be realized. Thus, the approximation $\mu = \mu_o$ is justified.

Setting

$$\mathbf{J}_{free} = \rho_{free} = 0, \tag{4.22}$$

$$\mu = \mu_o\ , \tag{4.23}$$

Maxwell's equations become

$$\nabla\cdot\boldsymbol{\varepsilon}\cdot\mathbf{E} = 0, \tag{4.24}$$

$$\nabla\times\mathbf{E} = -\frac{\partial\mathbf{B}}{\partial t}, \tag{4.25}$$

$$\nabla\cdot\mathbf{B} = 0, \tag{4.26}$$

$$\nabla\times\mathbf{B} = \mu_o\frac{\partial}{\partial t}(\boldsymbol{\varepsilon}\cdot\mathbf{E}). \tag{4.27}$$

The Fourier transformed Maxwell equations, assuming a dependence of the form

$$e^{i(\mathbf{k}\cdot\mathbf{r}-\omega t)}, \tag{4.28}$$

can be written as

$$\mathbf{k}\cdot\boldsymbol{\varepsilon}\cdot\mathbf{E}=0, \tag{4.29}$$

$$\mathbf{k}\times\mathbf{E}=\omega\mathbf{B}, \tag{4.30}$$

$$\mathbf{k}\cdot\mathbf{B}=0, \tag{4.31}$$

$$\mathbf{k}\times\mathbf{B}=-\mu_o\omega\,\boldsymbol{\varepsilon}\cdot\mathbf{E}. \tag{4.32}$$

The dielectric tensor $\boldsymbol{\varepsilon}$ must be evaluated in order to use these equations. In order to properly consider the explicit plasma currents as polarization currents it is necessary that

$$\boldsymbol{\varepsilon}\cdot\mathbf{E}=\varepsilon_o\mathbf{E}+\frac{i}{\omega}\mathbf{J}. \tag{4.33}$$

Determining $\mathbf{J}_{\mathbf{plasma}}$ as a function of $\mathbf{E}$ from the equations of motion of the charged plasma species is sufficient to specify $\boldsymbol{\varepsilon}$. More explicitly

$$\mathbf{J}_{plasma}=\sum_k q_k n_k \mathbf{v}_k. \tag{4.34}$$

The index k refers to particle species. The equation of motion for the particles of species k is

$$\text{-}i\omega\, m_k\mathbf{v}_k=q_k(\mathbf{E}+\mathbf{v}_k\times\mathbf{B}). \tag{4.35}$$

By Fourier analyzing the equation of motion in this manner, which assumes

$$\mathbf{v}_k\propto e^{i(k\cdot r-\omega t)}, \tag{4.36}$$

thermal motions are neglected. Hence the "cold plasma" dielectric tensor is being derived. If it is assumed that $\mathbf{B}$ in equation (4.35) is the known toroidal field (which means that plasma wave magnetic fields may be neglected by comparison) then (4.35) may be solved for

$$\mathbf{v}_k=\mathbf{v}_k(\mathbf{E}). \tag{4.37}$$

Substituting this solution into (4.34) returns

$$\mathbf{J}=\mathbf{J}(\mathbf{E}). \tag{4.38}$$

It turns out that the current $\mathbf{J}$ is proportional to $\mathbf{E}$ so that the dielectric tensor $\boldsymbol{\varepsilon}$ obtained is independent of $\mathbf{E}$ and depends only on the plasma parameters.[1] Defining the local z direction parallel to $\mathbf{B}$ and using the notation of Stix,

$$\varepsilon_r = \begin{pmatrix} S & -iD & 0 \\ iD & S & 0 \\ 0 & 0 & P \end{pmatrix}, \tag{4.39}$$

where

$$S = 1 - \sum_k \frac{\omega_{pk}^2}{\omega^2}\left(\frac{\omega^2}{\omega^2 - \omega_{ck}^2}\right), \tag{4.40}$$

$$D = \sum_k \frac{\omega_{pk}^2}{\omega^2}\left(\frac{\omega\,\omega_{ck}}{\omega^2 - \omega_{ck}^2}\right), \tag{4.41}$$

$$P = 1 - \sum_k \frac{\omega_{pk}^2}{\omega^2}, \tag{4.42}$$

$$\omega_{pk} = \frac{n_k q_k^2}{\varepsilon_o\, m_k}, \tag{4.43}$$

$$\omega_{ck} = \frac{q_k B}{m_k}. \tag{4.44}$$

Note that ω_{ck} takes the sign of q_k.

Definition of the Lower Hybrid Mode

Having obtained the dielectric tensor $\boldsymbol{\varepsilon}$ Maxwell's equations can be applied. From (4.25) and (4.27) the wave equation

$$\nabla \times \nabla \times \mathbf{E} = -\mu_o \frac{\partial^2}{\partial t^2}(\boldsymbol{\varepsilon} \cdot \mathbf{E}), \tag{4.45}$$

is obtained. The Fourier analyzed version is

$$\mathbf{k} \times \mathbf{k} \times \mathbf{E} = -\mu_o \omega^2 \varepsilon_o \boldsymbol{\varepsilon} \cdot \mathbf{E} = -\frac{\omega^2}{c^2} \boldsymbol{\varepsilon} \cdot \mathbf{E}. \tag{4.46}$$

Depending upon the relative values of the frequency ω and the various cyclotron and plasma frequencies, the dielectric tensor $\boldsymbol{\varepsilon}$ will take on differing character. Part of the definition of the lower hybrid modes is the condition

$$|\omega_{ci}| << \omega << |\omega_{ce}|, \tag{4.47}$$

from which it follows that

$$\frac{\omega}{|\omega_{ce}|} << 1, \tag{4.48}$$

and

$$\frac{|\omega_{ci}|}{\omega} << 1. \tag{4.49}$$

The degree to which both of these inequalities can be satisfied depends upon the disparity in electron and ion masses. To equally minimize both ratios (4.48) and (4.49) take

$$\omega = \sqrt{\omega_{ce}\,\omega_{ci}}\,. \tag{4.50}$$

Then for hydrogen and argon plasmas the ratios are

$$\frac{\omega}{|\omega_{ce}|} = \frac{|\omega_{ci}|}{\omega} = \sqrt{\frac{m_e}{m_i}} \approx \begin{cases} 2\% & hydrogen \\ 0.4\% & argon \end{cases}. \tag{4.51}$$

Assuming quasi-neutrality and ion charge states of at most +1, the ion and electron densities may be assumed equal. This allows the approximation

$$\frac{\omega_{pe}^2}{\omega_{pi}^2} = \frac{m_i}{m_e} >> 1. \tag{4.52}$$

Using equations (4.48), (4.49) and (4.52), the dielectric tensor elements relevant to the lower hybrid mode (4.40) to (4.42) can be simplified to

$$S = 1 + \frac{\omega_{pe}^2}{\omega_{ce}^2} - \frac{\omega_{pi}^2}{\omega^2}, \tag{4.53}$$

$$D = \frac{\omega_{pe}^2}{\omega|\omega_{ce}|}, \tag{4.54}$$

$$P = 1 - \frac{\omega_{pe}^2}{\omega^2}. \tag{4.55}$$

The second part of the definition of the lower hybrid mode requires examination of equation (4.46), which can be written as

$$\left(\mathbf{N}\times\mathbf{N}\times \ + \boldsymbol{\varepsilon}\cdot\right)\mathbf{E} = 0, \tag{4.56}$$

where

$$\mathbf{N} \equiv \frac{\mathbf{k}c}{\omega}. \tag{4.57}$$

If θ is the angle between the toroidal field $\mathbf{B} = B_0\,z$ and $\mathbf{N}$, and if we assume that $\mathbf{N}$ is in the x-z plane, then equation (4.56) can rewritten as

$$\begin{pmatrix} S-N_{\|}^2 & -iD & N_{\perp}N_{\|} \\ iD & S-N^2 & 0 \\ N_{\perp}N_{\|} & 0 & P-N_{\perp}^2 \end{pmatrix}\begin{pmatrix} E_x \\ E_y \\ E_z \end{pmatrix} = 0, \qquad (4.58)$$

where

$$N_{\|} = N\cos(\theta), \qquad (4.59)$$

$$N_{\perp} = N\sin(\theta). \qquad (4.60)$$

Demanding non-trivial solutions to (4.58) by setting the determinant equal to zero yields the dispersion relation which can be written as

$$AN^4 + BN^2 + C = 0. \qquad (4.61)$$

A solution to (4.61) would have

$$N^2 = f(A,B,C), \qquad (4.62)$$

allowing for propagation in opposite directions,

$$N = \pm\sqrt{f}. \qquad (4.63)$$

The important point is that in general there are two such solutions for N^2 given by equation (4.61). These two modes are distinct so long as

$$B^2 \neq 4AC. \qquad (4.64)$$

When the modes are distinct, the solution with smaller N is the fast-wave mode and the solution with larger value for N is the slow-wave mode. The lower hybrid mode is the slow mode.

In summary, lower hybrid plasma waves are those which obey the slow mode dispersion in the parameter range where $|\omega_{ci}| << \omega << |\omega_{ce}|$.

The Electrostatic Approximation

The electrostatic approximation means that **k** is parallel to **E** so that

$$\nabla \times \mathbf{E} = \mathbf{ik} \times \mathbf{E} = \mathbf{0}. \qquad (4.65)$$

Under these conditions the electric field can be calculated to sufficient accuracy by use of Poisson's equation. The electric field is derivable from a scalar potential Φ according to

$$\mathbf{E} = -\nabla\Phi = -i\mathbf{k}\Phi, \tag{4.66}$$

illustrating that **E** is parallel to **k**. Following Stix, a sufficient condition for the validity of the electrostatic approximation is found as follows.[2] Splitting **E** into components parallel and perpendicular to **k**,

$$\mathbf{E} = \mathbf{E}_L + \mathbf{E}_T \tag{4.67}$$

where

$$\mathbf{E}_L \equiv \frac{\mathbf{N}(\mathbf{N}\cdot\mathbf{E})}{N^2}, \tag{4.68}$$

$$\mathbf{E}_T \equiv \frac{-\mathbf{N}\times(\mathbf{N}\times\mathbf{E})}{N^2}. \tag{4.69}$$

The notation "L" for longitudinal and "T" for transverse is to avoid confusion with parallel and perpendicular to the magnetic field. Dotting the wave equation (4.56) by **N** obtains

$$\mathbf{N}\cdot\boldsymbol{\varepsilon}\cdot(\mathbf{E}_L + \mathbf{E}_T) = 0. \tag{4.70}$$

The electrostatic dispersion relation is obtained when **k** is parallel to **E** so that $\mathbf{E}_T \approx 0$ yielding

$$\mathbf{N}\cdot\boldsymbol{\varepsilon}\cdot\mathbf{N} = 0. \tag{4.71}$$

The wave equation (4.56) may be rewritten as

$$-N^2\mathbf{E}_T + \boldsymbol{\varepsilon}\cdot(\mathbf{E}_L + \mathbf{E}_T) = 0, \tag{4.72}$$

$$\Rightarrow \quad \boldsymbol{\varepsilon}\cdot\mathbf{E}_L = (N^2 - \boldsymbol{\varepsilon}\cdot)\mathbf{E}_T. \tag{4.73}$$

Now when

$$|N^2| >> |\varepsilon_{r\,ij}| \quad \textit{for all } i \textit{ and } j \tag{4.74}$$

equation (4.73) can be approximated as

$$\boldsymbol{\varepsilon}\cdot\mathbf{E}_L = N^2\,\mathbf{E}_T. \tag{4.75}$$

Using (4.74) on (4.75) yields

$$|\mathbf{E}_L| >> |\mathbf{E}_T|, \tag{4.76}$$

and the electrostatic approximation is valid.

Waves with large **N** = **k**c/ω, i.e., very slow waves, tend to be electrostatic. The Stix condition $|N^2| >> |\varepsilon_{ij}|$ may be overly restrictive but is sufficient to imply that **E** is parallel to **k**. To apply this criterion to the experiments considered in this thesis, typical experimental parameters have to be examined.

Experimental Parameters

The arrangement used to launch lower hybrid plasma waves into the tokamak plasma is depicted in Figure (4-1).

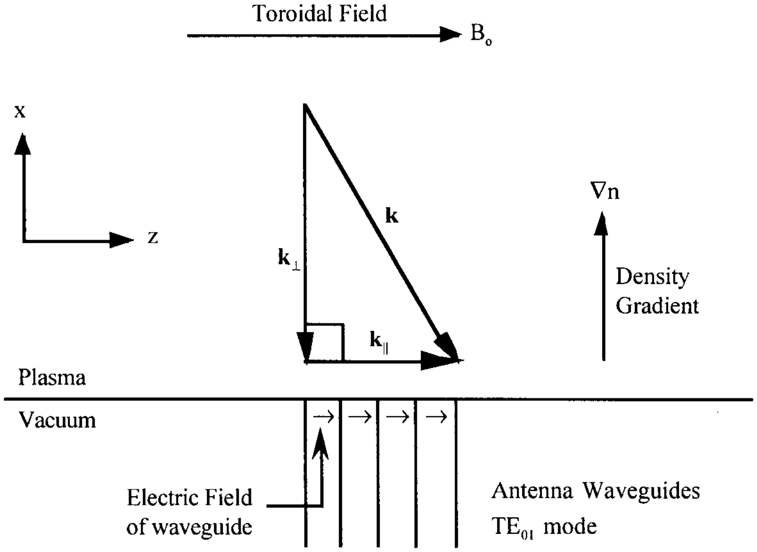

Figure 4-1. Experimental arrangement for launching lower hybrid plasma waves in a tokamak. Phasing of the wave-guides controls the launched $k_{||}$ spectrum.

The phasing of the antenna wave-guides determines $\mathbf{k}_{||}$. In slab geometry, which is a good local approximation in most tokamaks, $\mathbf{k}_{||}$ is conserved by Snell's law. The plasma dispersion then sets $\mathbf{k}_\perp$. Toroidal effects destroy the strict conservation of $\mathbf{k}_{||}$ and are discussed later. If $\mathbf{k}_\perp$ is determined from the dispersion, then one can compute

$$N^2 = \frac{c^2}{\omega^2}\left(\mathbf{k}_{||}^2 + \mathbf{k}_\perp^2\right) \tag{4.77}$$

and compare with the dielectric tensor elements as in the relation (4.74) to check the validity of the electrostatic approximation.

To determine $\mathbf{k}_\perp$ assume that the electrostatic dispersion is sufficient. Checking with the Stix criterion will prove or disprove this assumption. The electrostatic dispersion equation (4.71) can be rewritten as

$$\frac{\mathbf{k}_\perp^2}{\mathbf{k}_\parallel^2} = -\frac{P}{S}. \tag{4.78}$$

Combining (4.77) and (4.78) produces

$$N^2 = N_\parallel^2 + N_\perp^2 = \frac{c^2}{\omega^2}\left(k_\parallel^2 + k_\perp^2\right) = \frac{c^2 k_\parallel^2}{\omega^2}\left(1 - \frac{P}{S}\right) = N_\parallel^2\left(1 - \frac{P}{S}\right). \tag{4.79}$$

The parameter $N_\parallel^2 = k_\parallel^2 c^2/\omega^2$ appears frequently and is set by the antenna parameters. A typical number for quadrature phasing (90^O phase shift per channel) of the final antenna model is $N_\parallel = 10$ so that $N_\parallel^2 = 100$.

The magnetic field employed for most experiments was 1.3kG on axis. This gives the cyclotron frequencies shown in the following chart:

	H	Ar	
f_{ce}	3.7 GHz	3.7 GHz	(4.80)
f_{ci}	2.0 MHz	51 kHz	

The RF frequency used to launch the plasma waves is fixed at 450MHz by the amplifier cavity dimensions. The plasma density varies from zero at the chamber wall to 2.6×10^{12} cm^{-3} in the interior for a one-kiloamp ohmic discharge. The plasma density turns out to be roughly proportional to the plasma current and thus can be varied. Over the density range 0-5 x 10^{12} cm^{-3} the plasma frequency varies from 0 to 20 GHz. The dielectric tensor elements over this same density range vary monotonically over the ranges

$$S \approx 1 \text{ to } 31, \tag{4.81}$$

$$P \approx 1 \text{ to } -2000, \tag{4.82}$$

$$D \approx 0 \text{ to } 250\,. \tag{4.83}$$

The important ratio -P/S appearing in the electrostatic approximation rapidly becomes positive and larger than one as the density increases from the point where $\omega = \omega_{pe}$.

Many plots of plasma parameters versus the major radius in the mid-plane will be presented. The coordinate system used is depicted in Figure (4-2).

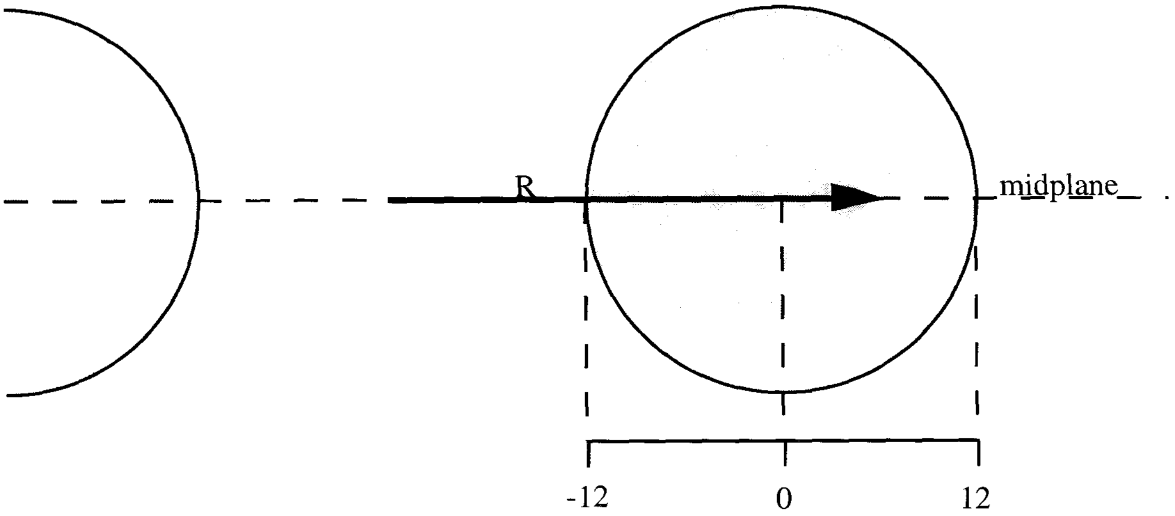

Figure 4-2. Coordinate system used in the graphs. The major radius R is measured from the center of the cross section of the tokamak chamber. All calculations are for the mid-plane.

Figure (4-3) shows numerical plots versus the tokamak minor radius of the various quantities S, P, D and the refractive index N. The index is calculated from the electrostatic dispersion. A semicircle density profile is assumed with average density of 2 x 10^{12} cm^{-3}. Being a low field tokamak with consequent large ion Larmor radius, a flat density profile would be expected. Data shows this to be the case.[3] The 1/R dependence of the toroidal field is included. For all parameters the Stix criteria is satisfied and the electrostatic approximation is valid. If the magnetic field is decreased for similar densities, then it becomes less certain that

$$N^2 \gg |P|. \qquad (4.84)$$

However, it will later be shown that lower hybrid waves are not accessible to these plasmas.

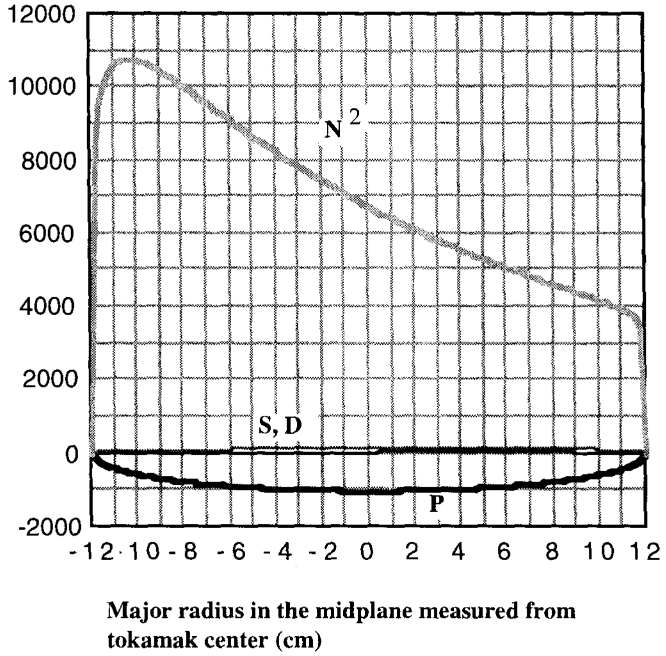
Lower Hybrid Wave Index and S, P, D Values in Encore

Figure 4-3. Plots of the dielectric tensor elements S, P, D and the index N^2 for the lower hybrid mode versus the minor radius of the Encore tokamak. A semicircle density profile is assumed with a line-average-density of 2×10^{12} cm^{-3}. The magnetic field varies inversely with major radius and is 1.3 kG on axis. The wave frequency is 450 MHz.

Resonance Cones

Since the electrostatic approximation holds for Encore parameters, the electric field can be calculated to sufficient accuracy with Poisson's equation,

$$\nabla\cdot\boldsymbol{\varepsilon}\cdot\nabla\Phi=0. \tag{4.85}$$

Utilizing the dielectric tensor (4.39), equation (4.85) becomes

$$\begin{pmatrix}\dfrac{\partial}{\partial x}\\ \dfrac{\partial}{\partial y}\\ \dfrac{\partial}{\partial z}\end{pmatrix}\cdot\begin{pmatrix}S\dfrac{\partial\phi}{\partial x}-iD\dfrac{\partial\phi}{\partial y}\\ iD\dfrac{\partial\phi}{\partial x}+S\dfrac{\partial\phi}{\partial y}\\ P\dfrac{\partial\phi}{\partial z}\end{pmatrix}=0. \tag{4.86}$$

For quadrature phasing of the antenna, the parallel wavelength is of order the width of the antenna, which is 7cm. Using typical Encore parameters and equation (4.78) the perpendicular wavelength would be significantly smaller, about 1cm. Except near the plasma edge, the fractional change in plasma parameters and tensor elements is small over the distance of a wavelength. Consequently, the tensor elements in (4.86) can be considered independent of the coordinates so that (4.86) can be solved locally resulting in the equation

$$S\left(\frac{\partial\phi^2}{\partial x^2}+\frac{\partial\phi^2}{\partial y^2}\right)+P\frac{\partial\phi^2}{\partial z^2}=0. \tag{4.87}$$

The parallel dielectric constant P is negative while S is positive. Thus (4.87) is hyperbolic and disturbances in the potential propagate along characteristics emanating from sources. For a point source at the origin the characteristics are

$$r=\left(\frac{S}{-P}\right)^{1/2} z, \tag{4.88}$$

where $r^2 = x^2 + y^2$. The propagating non-zero potential lies on a double cone with apex at the source.[4, 5] The solution will mimic the shape of an extended source. For Encore parameters with the low toroidal field, the cone angle well above cut-off can be approximated as

$$\tan(\theta)=\frac{r}{z}=\sqrt{\frac{S}{-P}}\cong\frac{\omega}{\omega_{ce}}. \tag{4.89}$$

Note that the angle is independent of density. For maximum toroidal field of about 1.3 kG on axis the angle $\theta \cong 7°$. For smaller field strengths the angle is larger. The large inverse aspect ratio of Encore (0.32) and the 1/R dependence of the toroidal field lead to substantial variations in the toroidal magnetic field within the tokamak chamber. For maximum field conditions of 1310 G on axis, the field is 46% larger at the inside wall (1920 G) and 24% less at the outer wall (996 G). The cone angle then varies from 9° at the outer wall to 5° at the inner wall.

Electromagnetic Corrections

Corrections due to electromagnetic effects have been studied both theoretically and experimentally.[6, 7] Consider the fourth of Maxwell's equations (4.4)

$$\nabla \times \mathbf{H} = \frac{\partial \mathbf{D}}{\partial t} + \mathbf{J}_{\text{free}}. \tag{4.90}$$

In order to obtain an estimate of when electromagnetic effects can be neglected, approximate (4.90) as

$$\frac{H}{r} \cong \omega D + J_{\text{free}}. \tag{4.91}$$

The condition for neglecting electromagnetic effects is that the curl of **H** is balanced by $\mathbf{J}_{\text{free}}$ so that

$$\frac{H}{r} >> \omega D. \tag{4.92}$$

This reduces to

$$r << \frac{c}{\omega\sqrt{\varepsilon}}, \tag{4.93}$$

where the intrinsic impedance has been used:

$$\frac{E}{H} = \sqrt{\frac{\mu_o}{\varepsilon_o \varepsilon_r}}. \tag{4.94}$$

If the largest of the plasma dielectric elements for Encore parameters P is substituted for **ε**, then (4.93) reduces to

$$r << \frac{c}{\omega_{pe}}. \tag{4.95}$$

Expression (4.95) can also be derived by comparing the electrostatic and radiation terms for the field of an oscillating dipole. Assuming a density of 10^{12} cm^{-3}, electromagnetic effects will become important after propagation over a distance the order of a centimeter.

The validity of the electrostatic solution is not simply the "near zone" condition (4.95) however. As discussed by Fisher and Gould, the electrostatic potential term always dominates on the cone itself.[8] Electromagnetic effects are expressed as potential disturbances developing inside and outside of the resonance cone beyond the near zone. Theory and experiment show that in essence the electromagnetic corrections add structure to the cone. This structure takes the form of a few extra fringes in the neighborhood of the cone surface.[9] Thermal effects are similar.[10]

Discussion of the Dispersion Relation

Since in slab geometry $N_{\|} = k_{\|}c/\omega$ is conserved, $N_{\|}$ can be considered a parameter determined by the launching structure. Thus the dispersion relation can be considered as an equation specifying $N_{\perp}$. The electrostatic dispersion, equation (4.78), is

$$N_{\perp}^2 = -\frac{P}{S} N_{\|}^2 . \tag{4.96}$$

The electromagnetic dispersion (4.61) can be written in the form

$$A N_{\perp}^4 + B N_{\perp}^2 + C = 0, \tag{4.97}$$

where

$$A = S, \tag{4.98}$$

$$B = (P + S)\left(N_{\|}^2 - S\right) + D^2, \tag{4.99}$$

$$C = P\left[\left(N_{\|}^2 - S\right)^2 - D^2\right] . \tag{4.100}$$

In general there are two solutions to (4.97) specifying a fast (smaller $N_{\perp}$) and slow (larger $N_{\perp}$) wave. If thermal effects are included, the dispersion relation becomes[11]

$$F N_{\perp}^6 + A N_{\perp}^4 + B N_{\perp}^2 + C = 0, \tag{4.101}$$

where A, B and C are as before and F is a new function of the plasma parameters. The new mode is a very slow ion plasma wave that is thus heavily Landau damped and useful for plasma heating. As a wave is launched from the outside of the torus, it propagates into progressively larger density. Depending upon the plasma parameters and $N_{\|}$, various events can occur as depicted in Figure (4-4).

The cutoff ($N_{\perp} = 0$) for the fast mode is at a larger density than the slow mode cutoff. For sufficiently small $N_{\|}$, a launched slow wave will mode convert to the fast wave at some density n_{T1}. The new fast wave will reflect off of its cutoff and repeat the process back and forth until damped out. The slow wave is said to be inaccessible to densities above n_{T1} from the plasma edge. For sufficiently large $N_{\|}$ the slow mode is accessible to the plasma parameters where mode conversion to the ion plasma wave occurs. This is the basic scenario of lower hybrid heating. For current drive, mode conversion to the ion plasma wave is undesirable and parameters are chosen such that the lower hybrid resonance layer does not occur in the plasma. The frequency ω is chosen well above the lower hybrid frequency.

Accessibility

Accessibility of lower hybrid waves is discussed in several papers.[12,13,14] As can be seen in Figure (4-4a), unless $N_{\parallel}^2$ is large enough, the lower hybrid wave will mode convert to the fast wave at some point in the plasma density profile. This phenomenon limits the penetration of slow waves into the plasma. Essentially it renders lower hybrid waves with certain parallel phase velocities inaccessible to the central portion of the plasma discharge.

The condition for the coalescence of the slow and fast modes is obtained from the dispersion (4.97). Solving for $N_{\perp}^2$ obtains

$$N_{\perp}^2 = \frac{-B \pm \sqrt{B^2 - 4AC}}{2A}. \tag{4.102}$$

The two modes coalesce when

$$B^2 - 4AC = 0. \tag{4.103}$$

The condition (4.103) depends on $N_{\parallel}$. Rewriting (4.103) to clearly express this dependence yields

$$\tilde{A} N_{\parallel}^4 + \tilde{B} N_{\parallel}^2 + \tilde{C} = 0, \tag{4.104}$$

where

$$\tilde{A} = (P - S)^2, \tag{4.105}$$

$$\tilde{B} = -2S(P - S)^2 + 2D^2(P + S), \tag{4.106}$$

$$\tilde{C} = S^2(P - S)^2 + D^2\left(D^2 - 2S^2 + 2SP\right). \tag{4.107}$$

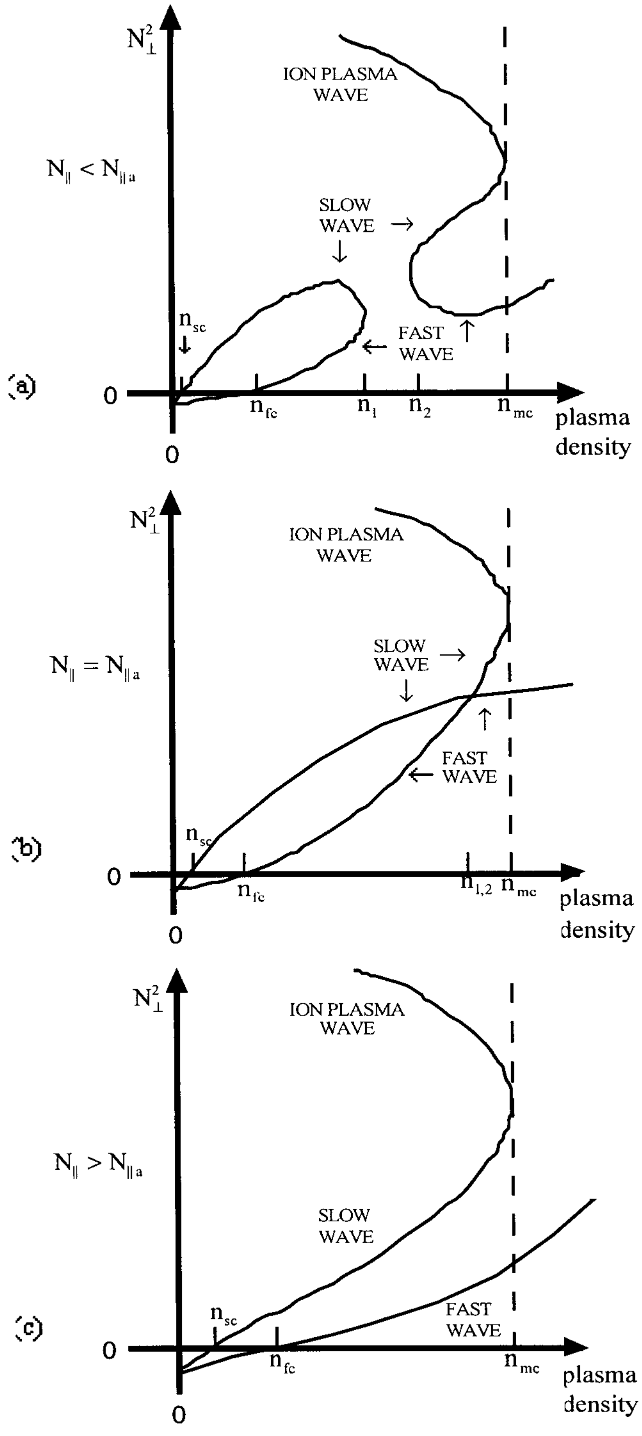

Figure 4-4. Perpendicular index versus plasma density n for fixed parallel index. The slow wave and fast wave cutoffs are subscripted "sc" and "fc" respectively. The density at which mode conversion to the ion plasma wave occurs is subscripted "mc." Mode conversion points between the slow and fast waves are subscripted with numbers. From P.T. Bonoli and E. Ott, Phys. Fluids **25** (1982) 360.

Since $\tilde{A} > 0$, equation (4.104) represents a concave upward parabola. The situation is thus as depicted in Figure (4-5).

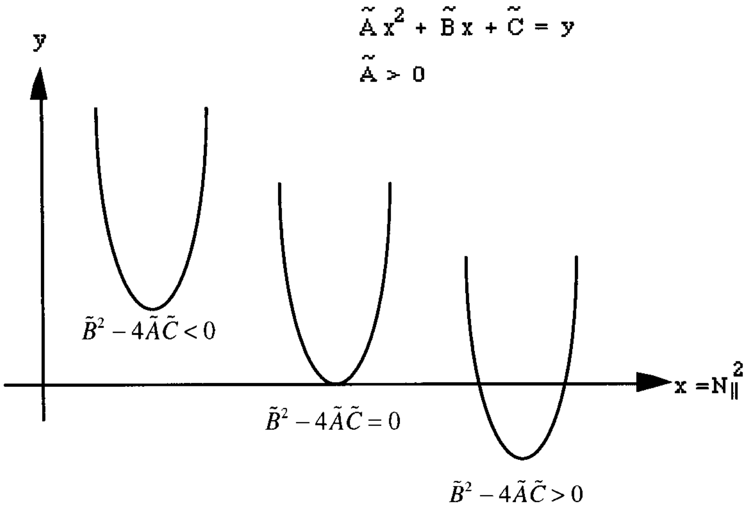

Figure 4-5. The solution to equation (4.104) is the intersection of the parabola with the horizontal axis.

Figure (4-6) shows a plot of the parameter $\tilde{B}^2 - 4\tilde{A}\tilde{C}$ in a typical ohmic discharge. The parameter is always positive and the third parabola in Figure (4-5) applies. There are two roots, two values of $N_{\|}$ at which the slow and fast modes coalesce at each point in the plasma.

The largest root of equation (4.104) is of the most interest for the following reason. $N_{\|}$ at launch in the experiments on Encore is typically peaked at 10. The phase velocity of the launched lower hybrid waves is thus a tenth the speed of light, much faster than any of the electrons in a typical ohmic plasma in Encore. $N_{\|}$ is not conserved during propagation in toroidal geometry. For launch at the outer mid-plane, the initial effect is an upshift in $N_{\|}$ and a slowing down of the parallel phase velocity.[15] Other phenomena may or may not operate to cause $N_{\|}$ shifts. However, it is only those lower hybrid waves that are slowed sufficiently to interact resonantly with electrons that are useful for current drive.

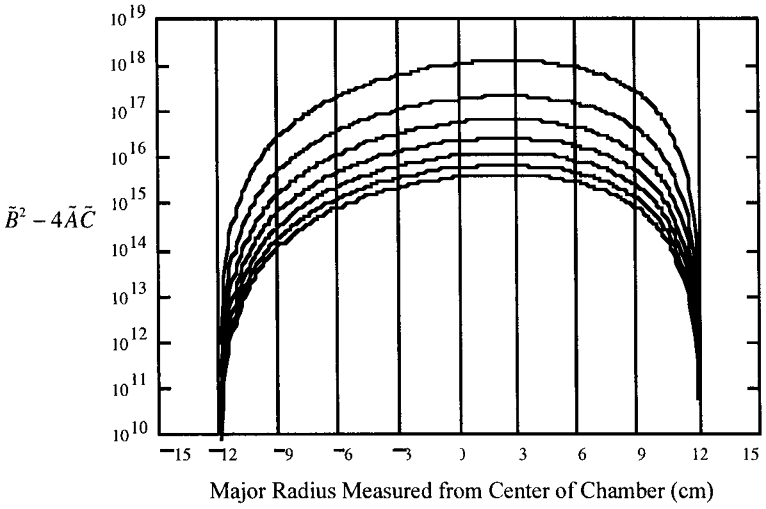

Figure 4-6. Plot of the parameter $\tilde{B}^2 - 4\tilde{A}\tilde{C}$ versus the Encore tokamak major radius for various magnetic fields on axis (186G-1300G). Since this parameter is always positive, there are two values of $N_{||}$ for which the slow and fast wave modes coincide.

For current drive it is necessary that $N_{||}$ increase after launch, and such an increase must not lead to a mode conversion to the fast wave. Thus if $N_{||}^2$ is larger than the largest root of (4.104), then $B^2 - 4AC > 0$ and the wave is accessible to the plasma parameters used. For given plasma parameters, the $N_{||}$ that represents the largest root of (4.104) is the accessibility limit $N_{||a}$. Waves with $N_{||} > N_{||a}$ propagate freely. Plasma waves with $N_{||} = N_{||a}$ will mode convert to the fast wave and propagate out of the plasma. Knowing $N_{||a}$ as a function of the minor radius of the plasma allows one to instantly see the possible depth of penetration of LH waves with various $N_{||}$. From (4.104)

$$N_{||a}^2 = \frac{-\tilde{B} + \sqrt{\tilde{B}^2 - 4\tilde{A}\tilde{C}}}{2\tilde{A}}. \tag{4.108}$$

Accessibility is important in the experiments described in this thesis. For $n_o \cong 2\times10^{12}$ cm^{-3}, B = 1.3kG and f = 450 MHz, (4.108) yields $N_{||a} \approx 7$. If the magnetic field is lowered to 800 Gauss, however, (4.108) yields $N_{||a} = 11$ and waves with $N_{||} = 10$ are inaccessible.

In Figure (4-7) calculated plots are shown of $N_{\|a}$ versus the major radius of Encore for various magnetic fields. A frequency of 450 MHz and a gas fill of singly ionized argon is assumed. The 1/R dependence of the magnetic field is included and a semicircle density profile with a line average density of 2×10^{12} cm^{-3} is assumed. The magnetic fields shown are those on axis. The left end is the inside chamber wall and the right end is the outer chamber wall. The quadrature phased wave-guide antenna used in the experiments launches a power spectrum centered at $N_{\|} = 10$ with a full width at half maximum of roughly 10. The shaded band roughly represents the $N_{\|}$ launch spectrum. This spectrum extends from $N_{\|} = 5$ to $N_{\|} = 15$. The intersection of the $N_{\|a}$ graph and the line $N_{\|} = 10$ yields the mode conversion point and the deepest possible penetration of the $N_{\|} = 10$ component into the plasma. The general trend is for worse accessibility at higher

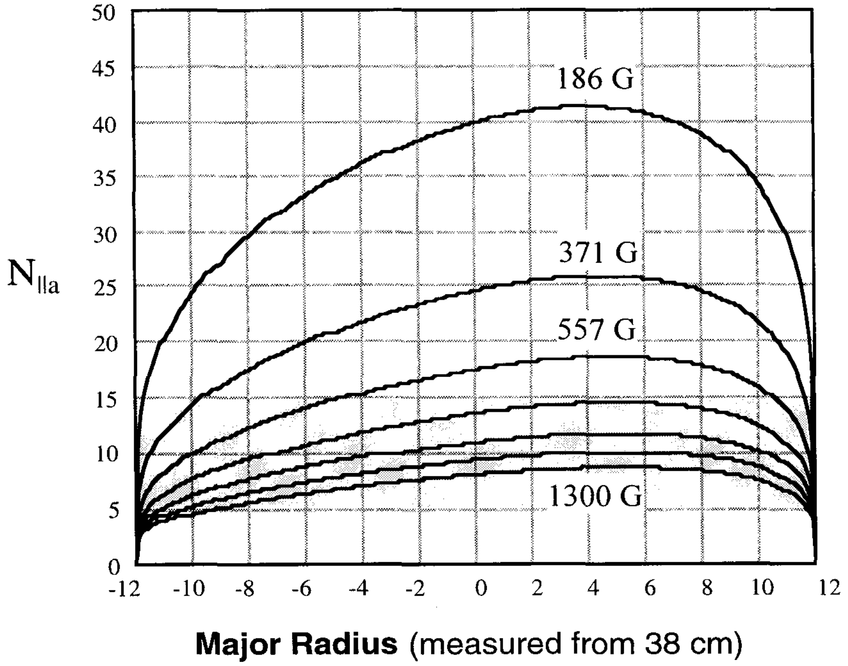

Figure 4-7. The accessibility limit $N_{\|a}$ as a function of the major radius, for various magnetic fields. The magnetic field monotonically increases from the uppermost to the lowest curve. The magnetic fields on axis are 186G, 371G, 557G, 743G, 929G, 1114G, and 1300G respectively. The shaded region indicates a typical launch spectrum for quadrature phasing of the final LH antenna. A line average plasma density of $2.0\times10^{18}m^{-3}$ is assumed.

density (i.e., near the center of the plasma) and/or lower magnetic field.

In Figure (4-8) is a similar plot showing the effect of varying the frequency. In the range 50-450 MHz, there is at best a very weak dependence on frequency. At higher and lower frequencies, accessibility begins to improve. The electron cyclotron frequency is roughly 3.6 GHz and the singly ionized argon ion cyclotron frequency is about 50 kHz. All of the frequencies in the plot lie between the cyclotron frequencies and can thus be considered lower hybrid wave frequencies. Decay lower hybrid waves generated with much lower frequency than but identical $k_{||}$ to the parent wave will be more accessible than the parent wave.

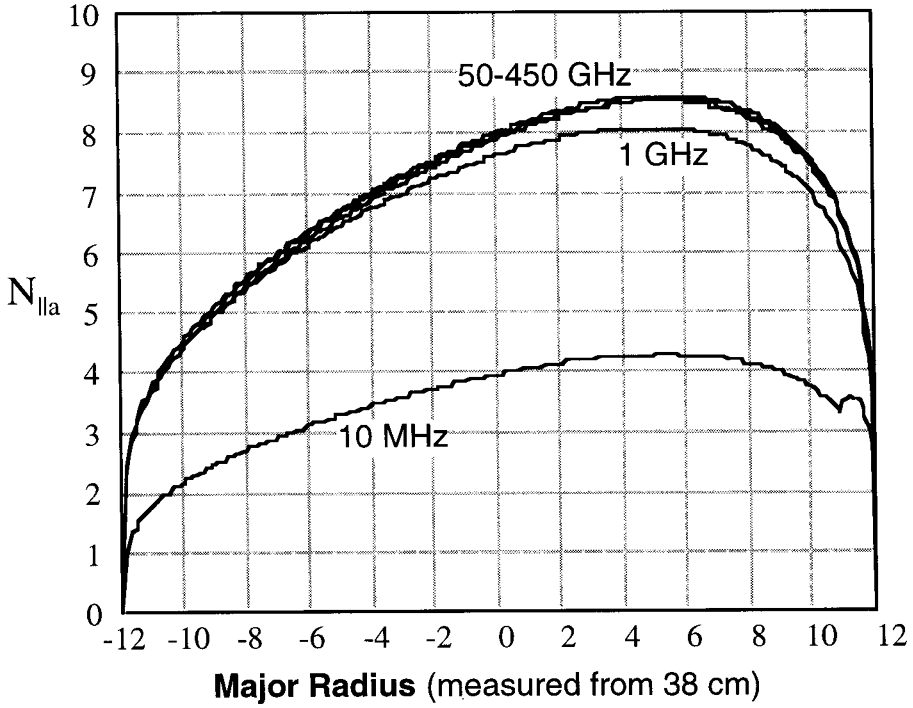

Figure 4-8. The accessibility parameter $N_{||a}$ versus the major radius (measured from 38cm) for various frequencies. The magnetic field on axis is 1300 gauss. In the range of 50-450 MHz there is only a very weak dependence on frequency.

Lower Hybrid Resonance Layer

The lower hybrid resonance occurs when

$$N_\perp^2 \rightarrow \infty \tag{4.109}$$

in equation (4.96). This happens when S = 0. From equation (4.53) this condition can be written as

$$S \cong 1 + \frac{\omega_{pe}^2}{\omega_{ce}^2} - \frac{\omega_{pi}^2}{\omega^2} = 0. \tag{4.110}$$

The frequency at which (4.110) is satisfied defines the lower hybrid frequency

$$\omega_{LH}^2 = \frac{\omega_{pi}^2}{1 + \dfrac{\omega_{pe}^2}{\omega_{ce}^2}} = \frac{\omega_{pi}^2 \omega_{ci} \omega_{ce}}{\omega_{pi}^2 + \omega_{ci}\omega_{ce}}. \tag{4.111}$$

For Encore parameters (4.111) is approximated by

$$\omega_{LH}^2 \cong \omega_{ce}\omega_{ci} , \tag{4.112}$$

while for larger field tokamaks

$$\omega_{LH}^2 \cong \omega_{pi}^2 . \tag{4.113}$$

The existence of a resonance layer could result in wave damping and thus be detrimental to current drive.

In the cold plasma approximation, in order for lower hybrid resonance heating to occur, at some place in the plasma $\omega \cong \omega_{LH}$ must hold. The wave frequency at launch for the Encore experiments is f = 450 MHz. The approximation $\omega_{LH}^2 = \omega_{ce}\omega_{ci}$ can be written as

$$f_{LH} = 6.5 \times 10^4 \; B_{Gauss} \frac{1}{\sqrt{\alpha}}, \tag{4.114}$$

where single ionization is assumed and α is the atomic mass of the ions. B_{Gauss} is the toroidal field in Gauss. If the following ratio is examined

$$\frac{f}{f_{LH}} = 6.9 \times 10^3 \; \frac{\sqrt{\alpha}}{B_{Gauss}}, \tag{4.115}$$

it is found that even for the smallest atomic number (hydrogen) and largest toroidal field currently available on Encore (1.97 kG calculated at the inside wall),

$$\frac{f}{f_{LH}} > 3.5. \tag{4.116}$$

Operation at low densities so that the approximation

$$f_{LH} \cong \sqrt{f_{ce}f_{ci}} \tag{4.117}$$

is no longer valid only makes the ratio f/f_{LH} larger. Hence, it would seem that lower hybrid resonance heating is not possible in experiments utilizing 450 MHz. At maximum toroidal field a resonance layer would exist for lower hybrid waves with frequencies less than 105 MHz.

If thermal effects are included, the electrostatic dispersion is modified from (4.96) to include the very slow ion plasma wave as shown in Figure (4-4). Mode conversion from the lower hybrid mode to the ion plasma mode occurs before the lower hybrid resonance layer defined by (4.111) is reached. Hence, the absence of the mode conversion layer is a more stringent condition than the absence of the lower hybrid resonance layer. The mode conversion layer is defined by the position at which[16] [17]

$$\omega_{LH}^2 = \omega^2\left[1 + 2\sqrt{3}\,\frac{N_{\|}v^{e}_{\text{thermal}}}{c}\left(\frac{T_i}{T_e}\right)^{1/2}\left(1 + \frac{1}{4}\frac{T_e}{T_i}\frac{\omega^4}{\omega_{ce}^2\omega_{ci}^2}\right)^{1/2}\right]^{-1}. \tag{4.118}$$

For the low field conditions of Encore where $\omega_{LH}^2 \cong \omega_{ce}\omega_{ci}$, equation (4.118) is essentially independent of magnetic field and ion mass. For the parameters $T_i = 3$ eV, $T_e = 10$ eV, f = 450 MHz, B = 1.3kG equation (4.118) yields

$$N_{\|} = 130. \tag{4.119}$$

Waves with $N_{\|} = 130$ will mode convert to ion plasma waves. The antenna used in the Encore experiments will not launch significant power at $N_{\|} = 130$. However, $N_{\|} = 130$ corresponds to the thermal velocity of 33 eV electrons and lies in the "spectral gap" between the phase velocities of launched LH waves and the thermal electrons at 10 eV in Encore. It is not known how the spectral gap is bridged in current drive experiments although decay waves and $N_{\|}$ non-conservation in toroidal geometry are possibilities. It is a possible impediment to current drive in Encore to find undesirable mode conversion associated with an $N_{\|}$ in the spectral gap. Further consideration of this result led to an understanding of the density limit encountered in all lower-hybrid current-drive experiments. This matter is discussed in more detail in chapter 8.

CMA Diagram

Figure (4-9) shows the CMA (Clemmow-Mullaly-Allis) diagram of Stix[18] upon which a heavy dashed arrow marks the trajectory of a launched lower hybrid wave in Encore. It will be shown that the cutoff for the slow mode occurs at $P = 0$. The shaded region coincides with the condition $PS < 0$ (the diagonal tensor elements are of opposite sign). For this condition (4.87) is hyperbolic and resonance cone propagation exists. The condition $L = 0$ represents the complete cutoff of the fast mode ($N \rightarrow 0$). This is in contrast to the "perpendicular" cutoff condition ($N_\perp \rightarrow 0$) to be discussed in the next section. The region 6a in which transverse plasma waves exist and the slow wave is below cutoff corresponds to a very thin layer at the tokamak edge. Numerical calculations, assuming a semicircular density profile with line average density of $2 \times 10^{12} \mathrm{cm}^{-3}$, indicate that $P=0$ occurs on the order of 5 microns from the plasma edge. Depending upon the toroidal field, the condition $L=0$ occurs between 20 and 80 microns from the plasma edge.

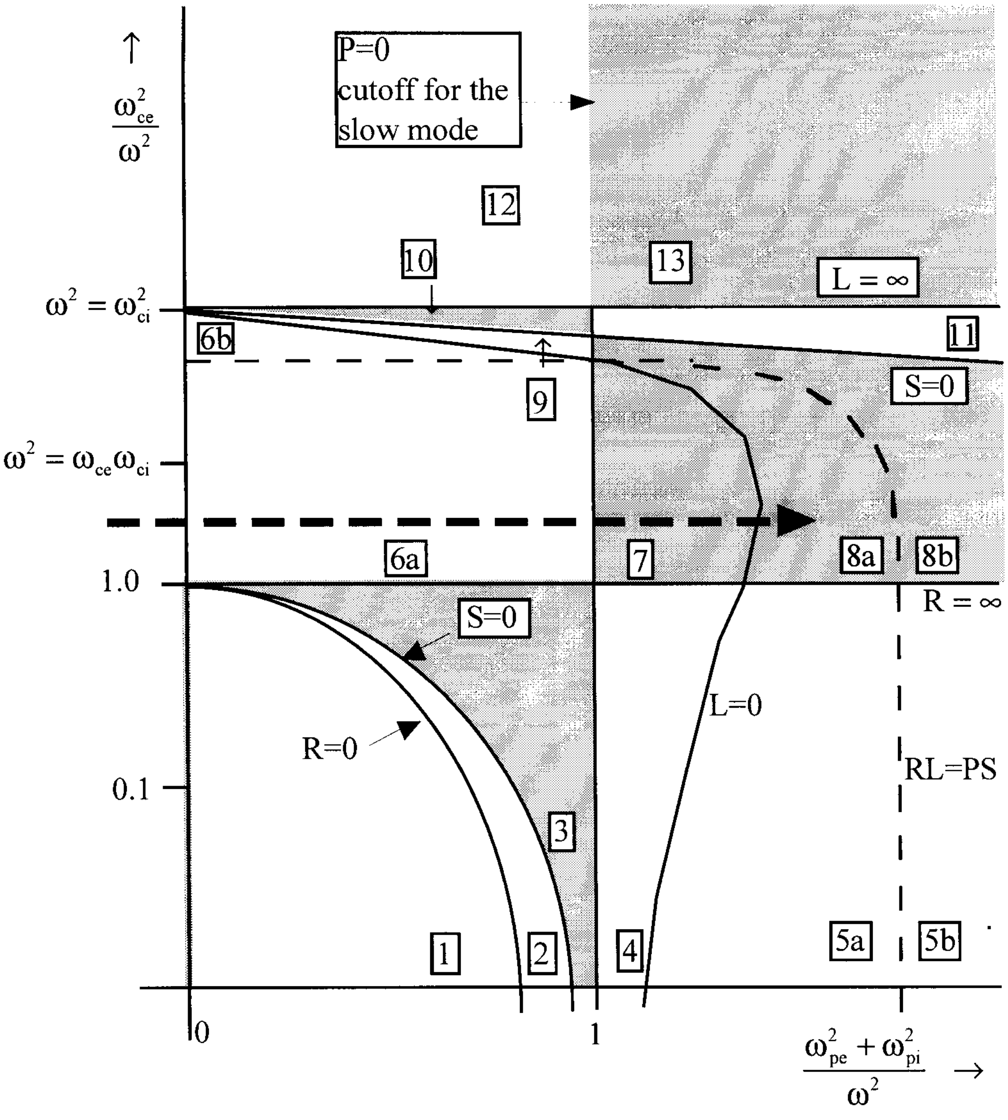

Figure 4-9. CMA diagram showing the path in parameter space taken by lower hybrid waves launched in Encore (heavy dashed line). The shaded region designates areas where PS < 0 and resonance cone propagation exists.

<u>Cutoffs</u>[19]

We assume a conserved $N_{\|}$ and look for the condition $N_{\perp} \rightarrow 0$. From the electromagnetic dispersion (4.97) the condition for cutoff, $N_{\perp} = 0$, is

$$C = P\left(\left(N_{\|}^2 - S\right)^2 - D^2\right) = 0. \tag{4.120}$$

There are two possibilities:

$$P = 0 \tag{4.121}$$

or

$$\left(N_{\parallel}^2 - S\right)^2 - D^2 = 0. \tag{4.122}$$

The first condition (4.121) is identical to the cutoff condition obtained from the electrostatic dispersion (4.96) and is the cutoff for the slow mode. Using f = 450 Mhz and (4.121) results in a cutoff density of

$$n_{\text{cutoff}}^{\text{slow mode}} = 2.5 \times 10^9\ \text{cm}^{-3}. \tag{4.123}$$

Since densities in Encore typically are in the 10^{12} cm^{-3} range with a flat profile, the slow mode cutoff occurs very near to the plasma edge and chamber wall.

From equation (4.122) the cutoff for the fast wave can be seen to depend upon $N_{\parallel}$. It may be rewritten as

$$N_{\parallel}^2 = S \pm D, \tag{4.124}$$

where $R = S + D$ and $L = S - D$ where the parameters R and L can be expressed as[20]

$$R = 1 - \frac{\omega_{pe}^2}{\omega\left(\omega + \omega_{ce}\right)} - \frac{\omega_{pi}^2}{\omega\left(\omega + \omega_{ci}\right)} \tag{4.125}$$

and

$$L = 1 - \frac{\omega_{pe}^2}{\omega\left(\omega - \omega_{ce}\right)} - \frac{\omega_{pi}^2}{\omega\left(\omega - \omega_{ci}\right)}. \tag{4.126}$$

In the above expressions ω_{ce} is negative. The two solutions for $N_{\perp} = 0$ can thus be written as

$$N_{\parallel}^2 = R, L. \tag{4.127}$$

This is reasonable because (4.127) is the dispersion obtained when it is assumed that the wavevector is parallel to the magnetic field, i.e., that $N_{\perp} = 0$.

In equations (4.125) and (4.126), the term involving the ion species is less by a factor of at least 100 compared to the term involving the electrons.[21] Hence the following approximations can be made:

$$R \cong 1 - \frac{\omega_{pe}^2}{\omega(\omega + \omega_{ce})} \tag{4.128}$$

and

$$L \cong 1 - \frac{\omega_{pe}^2}{\omega(\omega - \omega_{ce})}. \tag{4.129}$$

The fastwave cutoff condition (4.127) can now be expressed as the two possibilities

$$N_{\|}^2 = R \cong 1 - \frac{\omega_{pe}^2}{\omega(\omega + \omega_{ce})} \tag{4.130}$$

or

$$N_{\|}^2 = L \cong 1 - \frac{\omega_{pe}^2}{\omega(\omega - \omega_{ce})}. \tag{4.131}$$

Equations (4.130) and (4.131) can be rewritten respectively as

$$f_{pe}^2 = \left(N_{\|}^2 - 1\right) f \left(\left|f_{ce}\right| - f\right) \text{ for } \left(N_{\|}^2 \rightarrow R\right), \tag{4.132}$$

and

$$f_{pe}^2 = \left(1 - N_{\|}^2\right) f \left(\left|f_{ce}\right| + f\right) \text{ for } \left(N_{\|}^2 \rightarrow L\right). \tag{4.133}$$

If $N_{\|}^2 > 1$ the "L" case presented in equation (4.133) cannot happen because $f_{pe}>0$. Hence the fastwave cutoff condition is given by equation (4.130). Solving equation (4.130) for the density yields

$$n_{cutoff}^{\text{fast mode}} = \frac{\left(N_{\|}^2 - 1\right) f \left(\left|f_{ce}\right| - f\right)}{(9000)^2}. \tag{4.134}$$

Using the maximum toroidal field at the outer chamber wall (≈ 1040G), $f = 450$ MHz, and $N_{\|} = 10$ returns

$$n_{cutoff}^{\text{fast mode}} = 1.3 \times 10^{12} \text{ cm}^{-3}. \tag{4.135}$$

This is a substantial density corresponding to a position in a typical Encore discharge substantially inward from the plasma edge and chamber wall. This will tend to favor coupling of the antenna to the slow mode when the condition $N_{\|} = 10$ is imposed.

For small $N_{\|}$ obtained by identical phasing of the antenna waveguides, or by turning the antenna 90° on its side, the cutoff occurs at a much lower density. For $N_{\|} = 2$ the fast mode cutoff occurs at

$$n_{\text{cutoff}}^{\text{fast mode}} = 4 \times 10^{10}\ \text{cm}^{-3}. \tag{4.136}$$

Hence, for low $N_{\|}$ the cutoff for the fast mode will occur very close to the plasma edge and chamber wall.

Polarization

From the second and third components of the resultant vector on the left-hand side of equation (4.58), the following are obtained:

$$\frac{E_z}{E_x} = \frac{N_{\|} N_{\perp}}{N_{\perp}^2 - P}, \tag{4.137}$$

$$\frac{iE_y}{E_x} = \frac{D}{S - N^2}. \tag{4.138}$$

In the chosen coordinate system the z direction is parallel to the toroidal field, the x direction is in the direction of the density gradient, and the y axis points in the poloidal direction.

For slow wave launch, $N_{\|} = 10$ is imposed with a full width at half maximum in the $N_{\|}$ power spectrum of 10. At cutoff for the slow mode $P = 0$. The other tensor elements are $S \approx 1$ and $D \approx 0$. The electrostatic approximation is valid at cutoff since here

$$N^2 \geq N_{\|}^2 = 100 >> S, P, D. \tag{4.139}$$

Hence

$$\frac{N_{\perp}^2}{N_{\|}^2} = -\frac{P}{S} \approx 0. \tag{4.140}$$

From (4.137) and (4.138) it is found that $E = E_z$, $E_x = E_y = 0$ at the slow wave cutoff. Actually (4.137) is indeterminate when $P = N_\perp = 0$. However, it is assumed that P is not exactly zero but is slightly negative $P = \varepsilon$. Equation (4.140) then shows that

$$|N_\perp| \approx N_\parallel \sqrt{-\varepsilon}, \tag{4.141}$$

with the result that E_z/E_x diverges at cut-off. For slow wave launch the TE_{10} modes of the antenna waveguides are oriented with the electric field parallel to the magnetic field.

As the electrostatic-wave propagates into higher density regions, the polarization changes. For a density of 10^{12} cm^{-3} and a magnetic field of 1300 Gauss, the tensor elements become $P \approx -400$, $D \approx 49$, and $S \approx 7$. The electrostatic dispersion (4.96) yields

$$|N_\perp| \approx 76. \tag{4.142}$$

From Snell's law, $N_\parallel$ is conserved. Equations (4.137) and (4.138) then yield

$$\left|\frac{E_z}{E_x}\right| \approx 0.12 \tag{4.143}$$

and

$$\left|\frac{E_y}{E_x}\right| \approx 0.0084. \tag{4.144}$$

The direction of **k** and hence **E** rotates from **E** || **z** at cutoff to **E** || **x** at densities well above cutoff.

At the fast mode cutoff $P \neq 0$ and $N_\perp = 0$, so from (4.137) $E_z = 0$, regardless of $N_\parallel$. For $N_\parallel = 2$ the cutoff density from (4.136) is 4×10^{10} cm^{-3}. The tensor elements using B=1300 Gauss are $D \approx 2$ and $S \approx 1.2$. From (4.138)

$$\left|\frac{E_y}{E_x}\right| \approx 0.71 . \tag{4.145}$$

The electric field lies in the x-y plane at cutoff. For launch of the fast wave the antenna must be rotated so that the electric field of the TE_{10} modes is in the y-direction.

Single Particle Motions

Here the detailed orbits, velocities and density variations of the electrons and ions in a lower hybrid wave in Encore are examined.[22] The electrostatic approximation is assumed so that the electric field is completely specified by Poisson's equation. Poisson's equation, the equations of continuity and the Lorentz force equations are

$$-\nabla^2\phi = \frac{e}{\varepsilon_o}\left(\delta n_i - \delta n_e\right), \tag{4.146}$$

$$\frac{\partial}{\partial t}\delta n_e + \nabla\cdot\left(n_o\,\delta\mathbf{v}_e\right) = 0, \tag{4.147}$$

$$\frac{\partial}{\partial t}\delta n_i + \nabla\cdot\left(n_o\,\delta\mathbf{v}_i\right) = 0, \tag{4.148}$$

$$m_e\frac{\partial}{\partial t}\delta\mathbf{v}_e = -e\left(-\nabla\phi + \delta\mathbf{v}_e\times\mathbf{B}_o\right), \tag{4.149}$$

$$m_i\frac{\partial}{\partial t}\delta\mathbf{v}_i = e\left(-\nabla\phi + \delta\mathbf{v}_i\times\mathbf{B}_o\right). \tag{4.150}$$

Assuming a wave with dependence of the form

$$e^{i(\mathbf{k}\cdot\mathbf{r}-\omega t)}$$

and assuming small variation of the plasma parameters over a wavelength, the above equations can be rewritten as

$$k^2\phi = \frac{e}{\varepsilon_o}\left(\delta n_i - \delta n_e\right), \tag{4.151}$$

$$\delta n_e = \frac{n_o}{\omega}\mathbf{k}\cdot\delta\mathbf{v}_e, \tag{4.152}$$

$$\delta n_i = \frac{n_o}{\omega}\mathbf{k}\cdot\delta\mathbf{v}_i, \tag{4.153}$$

$$-i\omega\, m_e\,\delta\mathbf{v}_e = -e\left(-i\mathbf{k}\phi + \delta\mathbf{v}_e\times\mathbf{B}_o\right), \tag{4.154}$$

$$-i\omega\, m_i\,\delta\mathbf{v}_i = e\left(-i\mathbf{k}\phi + \delta\mathbf{v}_i\times\mathbf{B}_o\right). \tag{4.155}$$

Using the lower hybrid condition $\omega_{ce}^2 >> \omega^2 >> \omega_{ci}^2$ the above equations can be solved for the velocities

$$\delta v_{ex} = -\frac{\omega}{\omega_{ce}}\frac{k_\perp\phi}{B_o}, \tag{4.156}$$

$$\delta v_{ey} = \frac{ik_\perp\phi}{B_o}, \tag{4.157}$$

$$\delta v_{ez} = \frac{\omega_{ce}}{\omega}\frac{k_{\|}\phi}{B_o}, \tag{4.158}$$

$$\delta v_{ix} = \frac{\omega_{ci}}{\omega}\frac{k_{\perp}\phi}{B_o}, \tag{4.159}$$

$$\delta v_{ix} = 0, \tag{4.160}$$

$$\delta v_{iz} = \frac{\omega_{ci}}{\omega}\frac{k_{\|}\phi}{B_o}. \tag{4.161}$$

In the above equations the parameter $\omega_{ce} = -|\omega_{ce}|$. The positions (neglecting initial positions) are obtained by dividing the above velocities by -iω.

For Encore parameters it has been shown that the slow mode is electrostatic everywhere including cutoff, so the above apply at cutoff. (This is not necessarily true for experiments with $N_{\|}$ at launch of order 1.) At the slow mode cutoff $k = k_{\|}$ and $k_{\perp} = 0$. Equations (4.156) to (4.161) show for this case that the ions and electrons slosh back and forth parallel to the toroidal field and the antenna electric field.

Well above the cutoff density the slow mode dispersion (4.78) is used to relate $k_{\|}$ and $k_{\perp}$ obtaining

$$\frac{k_{\perp}^2}{k_{\|}^2} = -\frac{P}{S} \cong \frac{\omega_{ce}^2}{\omega^2}, \tag{4.162}$$

where approximations based on Encore parameters ($B \approx 1.3$ kG, $n_o \approx 10^{12}$) have been used. Equation (4.162) may be further simplified to

$$k_{\perp} = \pm\frac{\omega_{ce}}{\omega}k_{\|}, \tag{4.163}$$

where the sign is chosen to give inward propagating group velocity. Using (4.163) to eliminate $k_{\perp}$ from (4.156) to (4.161) yields

$$\delta v_{ex} \cong \mp\frac{k_{\|}\phi}{B_o}, \tag{4.164}$$

$$\delta v_{ey} \cong \pm\frac{i\omega_{ce}}{\omega}\frac{k_{\|}\phi}{B_o}, \tag{4.165}$$

$$\delta v_{ez} \cong \frac{\omega_{ce}}{\omega}\frac{k_{\|}\phi}{B_o}, \tag{4.166}$$

$$\delta v_{ix} \cong \pm\frac{\omega_{ce}\omega_{ci}}{\omega^2}\frac{k_{\|}\phi}{B_o}, \tag{4.167}$$

$$\delta v_{iy} \cong 0, \tag{4.168}$$

$$\delta v_{iz} \cong \frac{\omega_{ci}}{\omega}\frac{k_{\|}\phi}{B_o}. \tag{4.169}$$

From the above equations it is seen that the electrons orbit in circles about **k**, ($k \approx k_\perp$). The ions meanwhile slosh back and forth along **k**, which points nearly in the x direction.

From (4.152), (4.153), (4.156) to (4.161) and the assumption that **k** lies in the x-z plane

$$\delta n_e = \frac{n_o}{\omega}\left[\frac{\omega}{\omega_{ce}}\frac{k_\perp^2\phi}{B_o} - \frac{\omega_{ce}}{\omega}\frac{k_{\|}^2\phi}{B_o}\right], \tag{4.170}$$

$$\delta n_i = \frac{n_o}{\omega}\frac{\omega_{ci}}{\omega}\frac{k^2\phi}{B_o}. \tag{4.171}$$

Using (4.162) in (4.170) returns $\delta n_e = 0$. The electrons circle around without producing a density gradient. The electric field of the wave is due to ion density fluctuations produced as the ions slosh back and forth along **k**. Figure (4-10) depicts the single particle motions of ions and electrons in a lower hybrid wave.

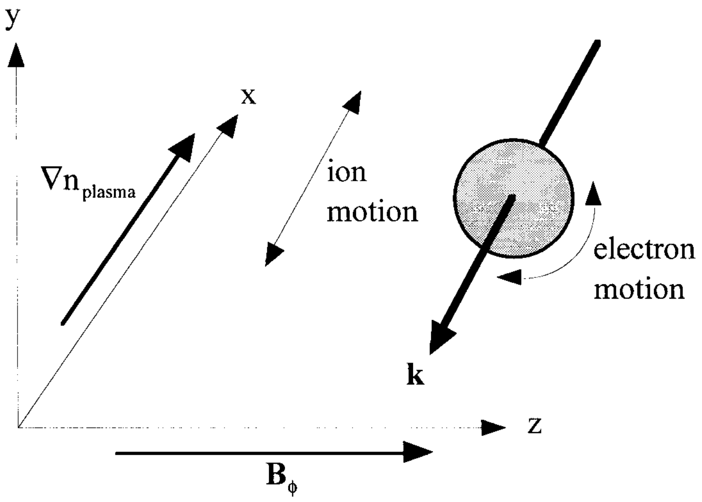

Figure 4-10. Single particle motions in a lower hybrid wave away from cutoff. The wave vector **k** lies in the x-z plane and is almost oriented parallel to the x-direction. The electrons circle around **k** without generating density variations. The ions slosh back and forth along **k** and generate density variations.

Lower hybrid theory is particularly interesting due to the fact that unlike in the situation with very high or low frequency waves, both ion and electron equations of motion are important.

Energy Relations

The electrostatic dispersion relation given in equation (4.163) can be arranged as

$$\omega = \pm \frac{k_{\|}}{k_{\perp}} \omega_{ce} . \tag{4.172}$$

Wave energy flows with the group velocity. Using (4.172) the group velocity components are calculated as

$$\frac{\partial \omega}{\partial k_{\perp}} = \mp \omega_{ce} \frac{k_{\|}}{k_{\perp}^{2}} = -\frac{\omega}{k_{\perp}} , \tag{4.173}$$

$$\frac{\partial \omega}{\partial k_{\|}} = \pm \omega_{ce} \frac{k_{\|}}{k_{\perp}} = \frac{\omega}{k_{\|}} . \tag{4.174}$$

Equation (4.173) may be further manipulated to yield

$$\frac{\partial \omega}{\partial k_{\perp}} = \mp \frac{\omega}{\omega_{ce}} \cdot \frac{\omega}{k_{\|}} . \tag{4.175}$$

From (4.173) it is seen that

$$k_{\perp} \frac{\partial \omega}{\partial k_{\perp}} < 0 . \tag{4.176}$$

The lower hybrid wave is "backward" in the perpendicular direction. Backward waves are common in filter-type transmission lines.[23] Notice that for energy flow into the plasma, $k_{\perp}$ must point out of the plasma, as it does in Figure (4-1). Using (4.174) and (4.175) obtains

$$\left| \frac{\partial \omega / \partial k_{\|}}{\partial \omega / \partial k_{\perp}} \right| = \left| \frac{\omega_{ce}}{\omega} \right| >> 1. \tag{4.177}$$

Hence although **k**, which is associated with momentum flow, is largely in the perpendicular direction, the energy flow and group velocity are largely in the parallel direction. From (4.173) and (4.174)

$$\mathbf{k}\cdot\frac{\partial\omega}{\partial\mathbf{k}} = k_{\parallel}\frac{\partial\omega}{\partial k_{\parallel}} + k_{\perp}\frac{\partial\omega}{\partial k_{\perp}} = 0, \tag{4.178}$$

demonstrating that the group velocity is orthogonal to **k**. The magnitude of the phase velocity is

$$\left|\frac{\omega}{k}\right| = \frac{\omega}{\sqrt{k_{\parallel}^2 + k_{\perp}^2}} \cong \frac{\omega}{k_{\perp}}. \tag{4.179}$$

The magnitude of the group velocity is

$$\left|\frac{\partial\omega}{\partial\mathbf{k}}\right| = \left|-\frac{\omega}{k_{\perp}}\hat{x} + \frac{\omega}{k_{\parallel}}\hat{z}\right| = \omega\sqrt{\frac{1}{k_{\perp}^2} + \frac{1}{k_{\parallel}^2}} \cong \frac{\omega}{k_{\parallel}}. \tag{4.180}$$

The group velocity is larger than the phase velocity by the ratio

$$\left|\frac{\partial\omega}{\partial\mathbf{k}}\right| \div \left|\frac{\omega}{k}\right| = \frac{\omega}{k_{\parallel}} \div \frac{\omega}{k_{\perp}} = \frac{k_{\perp}}{k_{\parallel}} = \left|\frac{\omega_{ce}}{\omega}\right| >> 1. \tag{4.181}$$

Using the dielectric tensor, the energy density in the wave may be written as[24]

$$W_o = \frac{B^2}{2\mu_o} + \frac{\varepsilon_o}{2}\mathbf{E}^*\cdot\frac{\partial}{\partial\omega}\left(\omega\boldsymbol{\varepsilon}_h\right)\cdot\mathbf{E}\ . \tag{4.182}$$

The first term on the right-hand side is the magnetic energy density. The second term is the sum of the electrostatic energy density and that portion of the charged particle kinetic energy density that is associated with the coherent wave motion. $\boldsymbol{\varepsilon}_h$ is the Hermitian part of $\boldsymbol{\varepsilon}$ defined by

$$\boldsymbol{\varepsilon}_h = \frac{1}{2}\left(\boldsymbol{\varepsilon} + \boldsymbol{\varepsilon}^{*t}\right). \tag{4.183}$$

The dielectric tensor represented by equation (4.39) in conjunction with the tensor elements (4.53) to (4.55) is already Hermitian.

In the electrostatic approximation $\mathbf{E} = -\mathbf{i}\mathbf{k}\phi$. The electrostatic dispersion relation is derived from Poison's equation (4.85) and is $\mathbf{E}^*\cdot\boldsymbol{\varepsilon}\cdot\mathbf{E} = 0$. Equation (4.182) can thus be further simplified to

$$\begin{aligned} W_o &= \frac{B^2}{2\mu_o} + \frac{\varepsilon_o}{2}\mathbf{E}^* \cdot \left(\boldsymbol{\varepsilon} + \omega\frac{\partial}{\partial\omega}\boldsymbol{\varepsilon}\right) \cdot \mathbf{E} \\ &= \frac{B^2}{2\mu_o} + \frac{\varepsilon_o}{2}\mathbf{E}^* \cdot \left(\omega\frac{\partial}{\partial\omega}\boldsymbol{\varepsilon}\right) \cdot \mathbf{E} \end{aligned} \tag{4.184}$$

Substituting the tensor elements (4.53) through (4.55) into (4.184) and evaluating yields

$$W_o = \frac{B^2}{2\mu_o} + \varepsilon_o\left(\frac{\omega_{pi}^2}{\omega^2}E_\perp^2 + \frac{\omega_{pe}^2}{\omega^2}E_\parallel^2\right). \tag{4.185}$$

From the electrostatic dispersion and Encore parameters ($n_o \approx 10^{12}$ cm^{-3}, B=1.3kG)

$$\frac{E_\perp^2}{E_\parallel^2} \cong \frac{\omega_{ce}^2}{\omega^2} \cong 68, \tag{4.186}$$

$$\frac{\omega_{pi}^2}{\omega^2} \cong \begin{cases} 0.2 & \text{hydrogen} \\ 0.006 & \text{argon} \end{cases}, \tag{4.187}$$

and

$$\frac{\omega_{pe}^2}{\omega^2} \cong 400. \tag{4.188}$$

The term containing $E_\perp$ in (4.185) is negligible compared to the term containing $E_\parallel$. Hence, neglecting the magnetic energy, the wave energy can be approximated as

$$W_{wave} \cong \varepsilon_o \frac{\omega_{pe}^2}{\omega^2}E_\parallel^2. \tag{4.189}$$

The electric field or vacuum energy is given by

$$W_{vac} = \frac{\varepsilon_o E^2}{2}. \tag{4.190}$$

The ratio of the total wave energy to the vacuum field energy is then

$$\frac{W_{wave}}{W_{vac}} = \frac{\varepsilon_o \frac{\omega_{pe}^2}{\omega^2}E_\parallel^2}{\varepsilon_o E^2/2} = 2\frac{\omega_{pe}^2}{\omega^2}\frac{E_\parallel^2}{E^2} \cong 2\frac{\omega_{pe}^2}{\omega_{ce}^2}, \tag{4.191}$$

where the dispersion relation (4.172) has been used to relate $E_\parallel$ to $E \cong E_\perp$. Using the Encore parameters mentioned earlier yields

$$\frac{W_{\text{wave}}}{W_{\text{vac}}} \cong 12. \tag{4.192}$$

The wave energy density is roughly 12 times the vacuum field electrostatic energy density. Most of the wave energy is carried by particle motions rather than by wave fields. This is consistent with the result obtained earlier that the electrons circle around **k** without bunching and forming density fluctuations. Density fluctuations are the only source of electrostatic wave fields.

The above results can be compared to the single particle motions. Based upon equations (4.164) to (4.166) the wave energy due to the kinetic energy of the electrons is

$$\begin{aligned} W_{\text{electrons}} &\cong \frac{1}{2} n m_e \left(\left(\delta v_{ey}\right)^2 + \left(\delta v_{ez}\right)^2 \right) \\ &= \frac{1}{2} n m_e \left(\left(\frac{\omega_{ce}}{\omega} \frac{k_{\|}\phi}{B_o} \right)^2 + \left(\frac{\omega_{ce}}{\omega} \frac{k_{\|}\phi}{B_o} \right)^2 \right) \\ &= n m_e \left(\frac{\omega_{ce}}{\omega} \frac{k_{\|}\phi}{B_o} \right)^2 \\ &= n m_e \left(\frac{q}{m_e \omega} k_{\|}\phi \right)^2 \\ &= \varepsilon_o \frac{n q^2}{\varepsilon_o m_e} \frac{k_{\|}^2 \phi^2}{\omega^2} \\ &= \varepsilon_o \frac{\omega_{pe}^2}{\omega^2} E_{\|}^2 \end{aligned} \tag{4.193}$$

This is identical to the formula derived in equation (4.189). Using equations (4.167) to (4.169) the kinetic energy of the ions due to the wave motion is

$$\begin{aligned} W_{\mathrm{ions}} &= \frac{1}{2} n m_i \left(\left(\delta v_{ix}\right)^2 + \left(\delta v_{iz}\right)^2 \right) \\ &= \frac{1}{2} n m_i \left(\left(\frac{\omega_{ce}\omega_{ci}}{\omega^2} \frac{k_{\parallel}\phi}{B_o} \right)^2 + \left(\frac{\omega_{ci}}{\omega} \frac{k_{\parallel}\phi}{B_o} \right)^2 \right) \\ &\cong \frac{1}{2} n m_i \left(\frac{\omega_{ce}^2\omega_{ci}^2}{\omega^4} \frac{k_{\parallel}^2\phi^2}{B_o^2} \right) \\ &= \frac{1}{2} n m_i \frac{\omega_{ce}^2 q^2 B_o^2}{\omega^4 m_i^2} \frac{k_{\parallel}^2\phi^2}{B_o^2} \\ &= \frac{\varepsilon_o}{2} \frac{\omega_{ce}^2 n q^2}{\omega^4 \varepsilon_o m_i} k_{\parallel}^2 \phi^2 \\ &= \frac{\varepsilon_o}{2} \frac{\omega_{ce}^2 \omega_{pi}^2}{\omega^4} E_{\parallel}^2 \\ &= \frac{\varepsilon_o}{2} \frac{\left|\omega_{ce}\omega_{ci}\right| \omega_{pe}^2}{\omega^4} E_{\parallel}^2 \\ &= \frac{\left|\omega_{ce}\omega_{ci}\right|}{2\omega^2} W_{\mathrm{electrons}} \, . \end{aligned} \tag{4.194}$$

For Encore parameters, the wave ion kinetic energy density is less than 2% of the wave electron kinetic energy density, assuming hydrogen ions. It is an additional factor of 40 less for argon.

It is of interest to know at what power density the energy of coherent particle wave motion equals the excitation threshold of the background neutral gas. For argon, the excitation threshold is 11.56eV.[25] The power density **Γ** in watts/cm^2, the energy density W in J/cm^3 and the group velocity in cm/sec are related by

$$\mathbf{\Gamma} = \frac{\partial \omega}{\partial \mathbf{k}} W . \tag{4.195}$$

The perpendicular and parallel components of equation (4.195) are then

$$\Gamma_{\parallel} = \frac{\partial \omega}{\partial k_{\parallel}} W \tag{4.196}$$

$$\Gamma_{\perp} = \frac{\partial \omega}{\partial k_{\perp}} W . \tag{4.197}$$

For a given power flux, slower waves have larger energy density. For lower hybrid waves in Encore, it has been shown that the energy density is in the form of particle kinetic energy. Most of the wave energy lies in electron kinetic energy. When the electron energy is 11.56eV and the electron density approximately 10^{12} cm^{-3}, the energy density of the wave is

$$\begin{aligned} W &= 10^{12} \times 11.56 \ \text{eV/cm}^3 = 1.156 \times 10^{13} \ \text{eV/cm}^3 \\ &= 1.156 \times 10^{13} \times 1.6 \times 10^{-19} \ \text{J/cm}^3 \\ &= 1.9 \times 10^{-6} \ \text{J-cm}^{-3} . \end{aligned} \tag{4.198}$$

It is perhaps simplest to compare necessary power levels with those provided by the antenna using equation (4.197). The perpendicular group velocity component is given in equation (4.175). Two cases are of interest, $\lambda_{\|} \approx 7\text{cm}$ (waveguide antenna quadrature phased) and $\lambda_{\|} \approx 1\text{cm}$ (probe launch), for which

$$\frac{\partial \omega}{\partial k_{\perp}} = \begin{cases} 3.9 \times 10^{8} \dfrac{\text{cm}}{\text{sec}} & \lambda_{\|} = 7\text{cm} \\ 5.6 \times 10^{7} \dfrac{\text{cm}}{\text{sec}} & \lambda_{\|} = 1\text{cm} \end{cases} \tag{4.199}$$

Combining (4.197), (4.198) and (4.199) yields the power density necessary for the electron sloshing energy in the wave to attain 11.56eV

$$\Gamma_{\perp} = \begin{cases} 740 \dfrac{\text{watts}}{\text{cm}^2} & \lambda_{\|} = 7\text{cm} \\ 110 \dfrac{\text{watts}}{\text{cm}^2} & \lambda_{\|} = 1\text{cm} \end{cases} \tag{4.200}$$

If instead of equation (4.197) equation (4.196) is used, the parallel component of the group velocity is a factor ω_{ce} / ω larger than the perpendicular component. The group velocity points at the resonance cone angle from the direction of the toroidal field. The projected area of the end of the antenna is decreased by the factor ω / ω_{ce}, and the antenna power levels required are the same.

The power level given in (4.200) for the $\lambda_{\|} = 7\text{cm}$ case is large compared to that typically launched in the experiments on Encore. For instance, at maximum theoretical RF power (40kW) radiating from the antenna aperture (49cm^2), the power density is roughly 800 watts/cm^2. A typical power actually obtained was of the order of 16kW for a power density of 330 watts/cm^2.

Encore has window ports, and attempts were frequently made to look for changes in the optical appearance of the plasma during injection of RF. A bright flash of light was often seen coincident with application of RF. Much if not all of this is believed to be due to excitation of background gas due to energetic tail electrons driven by the lower hybrid waves. This light emission was photographed and emanates from a cohesive beam circling the torus. No obvious "cone-like" light-emitting volume was ever seen. However, a rigorous program to look for cone-like emission was not undertaken. This qualitative result is nevertheless consistent with the power density calculations given above.

In a poorly characterized experiment, attempts were made to launch LH waves with small parallel wavelength ($\lambda_{\parallel} \approx 1\text{cm}$) from a small area using a coaxial probe. The end of the probe featured a half-centimeter length of exposed center conductor. Power levels of the order of a hundred watts were applied. No cone-like emitting volume was seen and the experiment was not pursued further.

At lower plasma densities the required power levels in (4.200) drop. Due to added electronic excitation of neutral argon atoms and ions, the resonance cone propagation may under such situations become optically visible to the eye. This may have application in plasma art.

$N_{\parallel}$ Spectrum Dynamics

An important parameter for lower hybrid current drive is the phase velocity of the launched lower hybrid waves parallel to the confining magnetic field. Normalized to the speed of light as $k_{\parallel}c/\omega$, this parameter is the parallel refractive index of the wave and is denoted by $N_{\parallel}$. Landau damping requires a velocity matching criteria

$$v_{\text{electron}} = \frac{c}{N_{\parallel}}, \tag{4.201}$$

between the lower hybrid wave and the electron velocity.

The properties of the launching antenna for the plasma-wave fix the initial $N_{||}$ spectrum. There are changes in the $N_{||}$ spectrum as the lower hybrid waves propagate through the toroidal tokamak plasma.[26,27,28,29,30] This effect has been studied for the cases where the WKB approximation is valid and geometrical optics can be used for ray tracing. For the case of a time independent dispersion function, the equations of geometrical optics in plasma take on a simple Hamiltonian form[31,32]

$$\frac{\partial \mathbf{r}}{\partial \tau} = \frac{\partial D}{\partial \mathbf{k}}, \tag{4.202}$$

$$\frac{\partial \mathbf{k}}{\partial \tau} = -\frac{\partial D}{\partial \mathbf{r}}. \tag{4.203}$$

The dispersion function $D(\mathrm{k},\omega,\mathbf{r}) = 0$ takes the place of the Hamiltonian and τ is a parameter measuring distance along the trajectory. If the tokamak coordinates are taken as $\mathbf{r} = (\mathrm{r}, \theta, \phi)$, where r is the minor radius, then the wave vector conjugate to these can be written as $\mathbf{k} = (\mathrm{k_r,m,n})$ where $\mathrm{k_r}$ is the radial wave number and

$$\mathrm{k}_\theta \equiv \frac{\mathrm{m}}{\mathrm{r}}, \tag{4.204}$$

$$\mathrm{k}_\phi \equiv \frac{\mathrm{n}}{\mathrm{R}}. \tag{4.205}$$

m and n are the poloidal and toroidal mode numbers respectively. Due to the toroidal symmetry

$$\frac{\partial D}{\partial \phi} = 0 \tag{4.206}$$

and n is a strict constant of the motion. However,

$$\frac{\partial D}{\partial \theta} \neq 0 \tag{4.207}$$

as the toroidal field B_ϕ falls off as 1/R, and the poloidal field B_θ also varies with R.

Thus as the lower hybrid wave propagates in the poloidal direction, m will change. In terms of the toroidal coordinates, $k_{||}$ can be written as[33]

$$\mathrm{k}_{||} = \left[\mathrm{k_r B_r} + \frac{\mathrm{m}}{\mathrm{r}} \mathrm{B}_\theta + \frac{\mathrm{n B}_\phi}{\mathrm{R_o + r\cos(\theta)}} \right] \frac{1}{|\mathrm{B}|}\ . \tag{4.208}$$

For an ideal equilibrium with

$$\begin{aligned} B_r &= 0 \\ B_\theta &<< B_\phi \end{aligned} \tag{4.209}$$

and defining the rotational transform q as

$$q \equiv \frac{r B_\phi}{\left(R_o + r\cos(\theta)\right) B_\theta} , \tag{4.210}$$

one obtains

$$k_{||} \approx \frac{n}{R_o + r\cos(\theta)}\left(1 + \frac{m}{nq}\right). \tag{4.211}$$

Upon launch from a grill antenna initially $k_\perp = k_r$ and $m = 0$. If m were to remain small there would be a modest change in $k_{||}$ due to the factor $(R_o + r\cos\theta)^{-1}$ which is simply the wave position in major radius. For launch at the outside mid-plane ($\theta = 0$) this shift is a small increase in $k_{||}$ and thus $N_{||}$.

If large poloidal excursions are possible, it will be seen that effects due to m changes quickly dominate the spectral shifts. Ray tracing calculations for Alcator C type equilibrium[34], PLT equilibrium[35] and others[36] show that waves which have made significant poloidal motion incur large m variations and consequent significant changes in $N_{||}$. For trajectories followed beyond $\theta = 2\pi$ in the poloidal direction, the changes in $N_{||}$ can be tremendous.

For instance in the Alcator C case mentioned above, $N_{||}$ oscillated from 4 to 0 to 6 in the range $2\pi \le \theta \le 4\pi$. The equation for $\partial m / \partial\theta$ has many m dependent terms which initially vanish at launch when m=0. The terms which result in the non-constancy of m depend on the θ-dependent terms of the toroidal equilibrium which are of order

$$\varepsilon \equiv \frac{r_o}{R_o} = \frac{\text{minor radius}}{\text{major radius}} . \tag{4.212}$$

Here, ε is the inverse aspect ratio of the tokamak, sometimes referred to as the toricity. As we have seen, in a tokamak the strict constants of motion are n and ω. For $\varepsilon = 0$, m is also a constant of the motion. In an interesting paper Bonoli and Ott[37] have investigated the effect of $\varepsilon > 0$ on the trajectories of various launched waves. They constructed a

Poincare map in (k_r, r) phase space using values of the numerical trajectories upon successive poloidal passes at $\theta = 0$. For $\varepsilon < 0.2$ strange attractors were found representing a new constant of the motion. Most inaccessible wave power is trapped in that condition. For $\varepsilon > 0.2$, however, all initial conditions resulted in ergodic ray trajectories. Initially inaccessible wave power will become accessible after a few poloidal passes. Encore tokamak is similar in aspect ratio to all major tokamaks with $\varepsilon = 0.316$. Ray trajectories should be markedly ergodic and the $N_{||}$ spectrum should be heavily shifted around after several poloidal passes. However, for reasons of accessibility, which requires lowering of

$$\frac{\omega_{pe}^2}{\omega_{ce}^2},$$

most of the experiments took place in operating conditions for which the rotational transform is weak ($q >> 1$). The cone angle for the lower hybrid wave propagation depends only on the magnetic field and is generally small.

The result of these conditions is that wave trajectories must make at least one toroidal revolution before making a poloidal revolution. The collision frequencies in a typical Encore discharge are such that thermal electron mean free paths are of the order of one toroidal revolution. One could expect observation of possible ray ergodicity in Encore to occur only when $q \cong 1$ for which case the toroidal field is usually low and the cone angle is also maximized. Hence, for most experiments on Encore, there is a slight upshift in $N_{||}$ after launch due to the decrease in major radius as described by (4.211).

Other possible mechanisms for $N_{||}$ shifts include scattering of the lower hybrid waves from other waves or from density fluctuations. Since the correlation lengths for density fluctuations in tokamaks are much longer along the toroidal field than perpendicular to it, $k_\perp^2 >> k_{||}^2$ for such density fluctuations. Scattering of the lower hybrid waves from the larger momentum perpendicular wave vector is considered to be more important. The effect of the scattering then is to alter the $k_\perp^{LH}$ of the lower hybrid wave and change the value of the poloidal mode number m. This in turn leads to large variations in $N_{||}$ upon poloidal motion as previously discussed. Parametric decay of lower hybrid waves near the plasma periphery may also lead to $N_{||}$ spectrum changes.[38]

In summary, small upward shifts in $N_{||}$ are expected due to the outside launch position and consequent decrease in major radius upon propagation. Because of the high collisionality of Encore, large $N_{||}$ shifts due to the toroidicity and m changes are unlikely except perhaps for operation near $q \cong 1$. Density fluctuations may also effect the $N_{||}$ spectrum.

---

[1] Thomas H. Stix, Waves in Plasmas, AIP 1992

[2] Thomas H. Stix, The Theory of Plasma Waves, McGraw-Hill 1962, pp. 223-224

[3] "An Experimental and Theoretical Investigation of a Finite Beta Modified Drift Wave," Thesis by Eric Fredrickson, 1985 Caltech

[4] "Resonance Cones in the Field Pattern of a Radio Frequency Probe in a Warm Anisotropic Plasma," R. K. Fisher and R. W. Gould, Phys. of Fluids, **14**, 1971 p. 857

[5] "Experimental Studies of Lower Hybrid Wave Propagation," P. M. Bellan and M. Porkolab, Phys. of Fluids, **19**, 1976

[6] "Electromagnetic interference Pattern of Resonance Cones in the Far Field," P. M. Bellan, Phys. Rev. Lett., **45**, 1980, p. 1407

[7] "Electromagnetic Effects on Plasma Resonance Cones," H. K. Kuehl, IEEE Trans. Plasma Sci., **PS-9**, 1981, p. 104

[8] IBID, R. K. Fisher, 1971, p. 866

[9] IBID, P. M. Bellan, 1980, p. 1407

[10] need reference

[11] P. T. Bonoli and E. Ott, Phys. of Fluids, **25**, 1982, p. 360

[12] IBID, Stix, 1962, p. 60

[13] "Plasma Penetration near the Lower Hybrid Frequency," V. E. Golant, Sov. Phys. Tech. Phys., **16**, 1972, p. 1980

[14] "Alcator Lower Hybrid Heating Experiment," R. R. Parker, MIT-RLE QPR\#102, 1971, p. 98

[15] See equation (4.190) and the text immediately following.

[16] "Theory of Plasma Heating in the Lower Hybrid Range of Frequencies," A. Bers, Proc. 3rd Topical Conference On Radio Frequency Plasma Heating, Caltech, 1978, A1-1

[17] Wave heating and Current Drive in Plasmas, V. L. Granatstein and P. L. Colestock editors, Gordon & Breach 1985, p. 203

[18] IBID, Stix, 1962, p. 30

[19] Originally the fastwave cutoff was correctly calculated with cumbersome formulas involving the parameters S and D. The more elegant description of the fastwave cutoff in terms of the parameters L and R was pointed out to me by Paul Bellan.

[20] Waves in Plasmas, Thomas Howard Stix, (1992) American Institute of Physics, p. 7

[21] For the largest possible magnetic field $\omega_{ce} \cong 6.5 \cdot \omega$ and $\omega_{ci} << \omega$. For hydrogen $\omega_{pe}^2 \cong 1830 \cdot \omega_{pi}^2$ while for argon $\omega_{pe}^2 \cong 1830 \cdot 40 \cdot \omega_{pi}^2$.

[22] IBID, Granatstein, 1985, p. 175

---

[23] Fields and Waves in Communication Electronics, Ramo, Whinnery and Van Duzer, (1965), John Wiley and Sons, p. 51

[24] IBID, Stix, 1962, p. 60

[25] Glow Discharge Processes, Brian Chapman, John Wiley & Sons, Inc. 1980, p.119

[26] P. Bonoli and E. Ott, "Toroidal and Scattering Effects on Lower Hybrid Wave Propagation," Phys. Fluids, **25**, 1982, p. 359

[27] D. Ignat, "Toroidal Effects on Propagation, Damping and Linear Mode Conversion of Lower Hybrid Waves," Phys. Fluids, **24**, 1981, p. 1110

[28] J. Schuss, "Lower Hybrid Wave Propagation in Toroidal Plasmas," Preprint, Plasma Fusion Center, MIT

[29] T. Maekawa et al., "Wave Trajectories and Damping of Lower Hybrid Waves in Tokamak Plasmas," IEEE Trans. Plasma Sci., **8**, 1980, p. 64

[30] P. Colestock and J. Kulp, "Geometric Optics of Lower Hybrid Waves in Non-uniform Plasmas," IEEE Trans. Plasma Sci., **8**, 1980, p. 71

[31] T. Stix, The Theory of Plasma Waves, 1962 McGraw-Hill, p. 58

[32] J. Wersinger, E. Ott and J. Finn, "Ergodic Behavior of Lower Hybrid Decay Wave Trajectories in Toroidal Geometry," Phys. Fluids, **21**, 1978, p. 2263

[33] IBID reference 5, p. 1111

[34] IBID reference 4, p. 364

[35] IBID reference 5, p. 1110

[36] IBID reference 7, p. 64

[37] IBID reference 4

[38] Y. Takase et al., "Parametric excitation of ion-sound quasimodes during lower-hybrid heating experiments in tokamaks," Phys. Fluids, **26**, (1983), p. 2992

5 Hardware Construction and Testing

In this chapter, the design, construction and testing of the waveguide array "grill" antennas for launching lower hybrid waves are described. For the solid dielectric antenna, the $N_{||}$ spectrum is calculated for various phasing. The RF power supply is briefly described. The plasma probes used for much of the data collection are discussed. Finally, the method used to obtain phase measurements on the grill antenna is presented.

Waveguide Arrays for Launching LH Waves

There is considerable literature concerning the use of open-ended waveguides for launching plasma waves.[1,2,3,4,5,6,7,8,9,10] The term "grill" antenna arose in connection with lower hybrid heating with phased waveguide arrays and comes from the analogy with the shape and use of the cooking utensil.[11] In the course of experimentation with lower hybrid waves and current drive, four different "grill" antennas were utilized, the latter three designed and built by the author. Each successive antenna model incorporated improvements in design.

As described in chapter 4, the lower hybrid waves of interest are electrostatic waves meaning that $\mathbf{k} \times \mathbf{E} = 0$. Equation (4.30) implies that the wave magnetic field is negligible compared to the electric field. Hence, the ratio of the electric-to-magnetic field at the waveguide mouth should be maximized. Modes in rectangular waveguides are categorized as either TM or TE. The ratio of E-to-H in a waveguide is known as the wave impedance and is larger for TE modes than for TM modes. Hence, TE modes are more appropriate. For unguided TEM modes, the energy contained in the electric and magnetic fields is equal. For TE modes, more energy is carried by the electric field than the magnetic field. In TM modes, more energy is carried by the magnetic field. The simplest TE mode in a rectangular waveguide is the TE_{10} mode, using the notation of Ramo, Whinnery and Van Duzer.[12] The TE_{10} mode is often employed for launching high power LH waves in tokamaks. Figure (5-1) illustrates the TE_{10} mode.

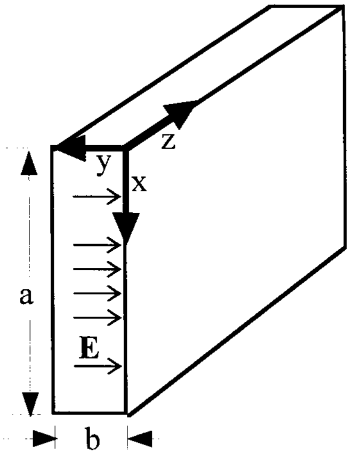

$$E_y = E_o \sin\left(\frac{\pi x}{a}\right)$$

$$E_x = 0 = H_y$$

$$H_x = -\left(\frac{E_o}{Z_{TE}}\right)\sin\left(\frac{\pi x}{a}\right)$$

$$H_z = \frac{jE_o}{\eta}\left(\frac{\lambda}{2a}\right)\cos\left(\frac{\pi x}{a}\right)$$

$$\eta = \sqrt{\frac{\mu}{\varepsilon}}$$

$$Z_{TE} = \frac{\eta}{\sqrt{1-(\lambda/2a)^2}}$$

Figure 5-1. The TE_{10} mode in a rectangular waveguide. The electric field has but one component E_x fixing the polarization. The cutoff frequency depends only on the x-dimension "a."

To maximize coupling to the lower hybrid wave, the mouths of the waveguides should be as close to the plasma wave cutoff as possible. This is particularly easy in Encore, in which due to the low plasma temperatures the metallic waveguides can act as the plasma limiter.

For the TE10 mode, the waveguide height "a" at cutoff is given by

$$a = \frac{\lambda'}{2} = \frac{c}{2f\sqrt{\varepsilon_r}}, \tag{5.1}$$

where ε_r is the relative dielectric constant of the material filling the waveguides. The high power RF source operated at a fixed frequency of 450MHz corresponding to a wavelength in air of 66.7cm. With a relative dielectric constant of one, the height of a waveguide at cutoff is 33.3cm. The waveguide should, of course, be operated well above cutoff to avoid excessive resistive wall losses. The largest vacuum ports on Encore are 18cm, and the minor diameter of the torus is only 24cm. Hence the antenna waveguides must be loaded with a dielectric material in order to reduce their dimensions.

The discussion of polarization in chapter 4 makes it evident that at cutoff near the plasma edge, the electric field of a lower hybrid wave is largely parallel to the toroidal magnetic field. Hence, the electric field at the mouths of the waveguides should be oriented parallel to the toroidal magnetic field. For the TE_{10} mode this means that what is typically the larger dimension "h" of the rectangular waveguide must be oriented perpendicular to the toroidal magnetic field.

The $N_{\|}$ spectrum at launch depends upon the waveguide phasing scheme as well as details of the construction. These calculations are presented in a later section. For purposes of estimation, a "typical" parallel refractive index for a four-waveguide, quadrature-phased antenna can be approximated as

$$N_{\|} \approx \frac{c}{\lambda_o f}, \tag{5.2}$$

where λ_o is the periodicity of the grill antenna measured parallel to the electric field. In order for Landau damping on thermal electrons at 10eV to occur, $N_{\|}$ must be of the order of 240. To achieve $N_{\|} \approx 240$ at launch would require according to equation (5.2) an antenna periodicity λ_o equal to 2.8mm. Due to the limited area at the end of the waveguides, such a narrow grill antenna would preclude the launching of the large power required for driving substantial current. The antenna structure must also be able to withstand atmospheric pressure while the waveguides are under vacuum. The design criteria was to keep the waveguides as narrow as possible consistent with the power and construction requirements. LHCD experiments at other institutions also involved LH waves with much lower $N_{\|}$ at launch than could Landau damp on thermal electrons in the plasma. It is presumed that increases in $N_{\|}$ after launch allow for the Landau damping to occur.

Early Antenna Models

Figure (5-2) shows the first three antenna models. Each had shortcomings that would prevent reliable current drive experimentation.

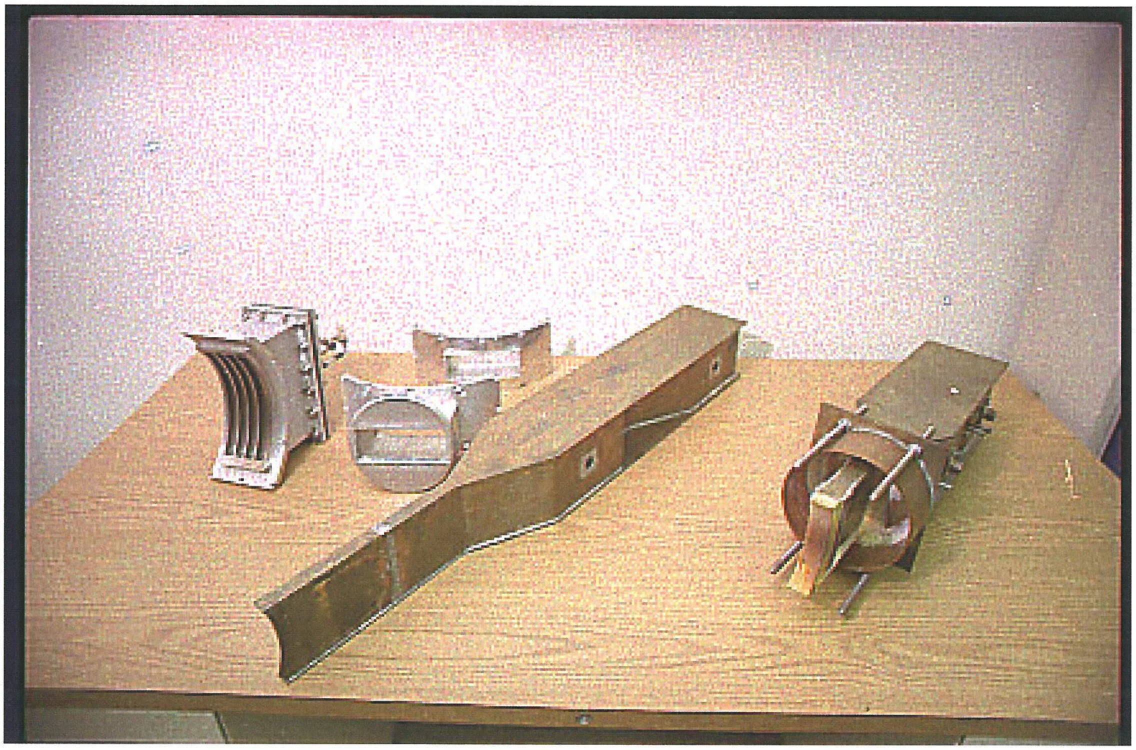

Figure 5-2. The first three grill antennas utilized for launching LH waves in Encore plasma. At far left is a pre-existing antenna that is below cutoff at 450MHz and utilizes magnetic loop coupling. In the center is the shell structure for the first powder dielectric filled antenna. At far right is the second powder dielectric antenna with tuning stubs.

The initial antenna was a pre-existing waveguide array with no dielectric fill. The magnetic loop couplers in the pre-existing antenna were not designed for efficient coupling, as they were located at the shorted end of the waveguides. In general, the loop diameter and location with respect to the short are adjusted to null out the input reactance and set the radiation resistance equal to the characteristic impedance of the input line.[13] Although this antenna is below cutoff at 450MHz, the waveguides are short enough that signal level experiments could be performed. Neglecting resistive wall losses, the electric field in the waveguides can be represented by[14]

$$E \propto e^{i(\omega t - \gamma z)} \tag{5.3}$$

where

$$\gamma = \frac{\omega\sqrt{\varepsilon_r}}{c}\sqrt{1-\frac{f_c^2}{f^2}}\,. \tag{5.4}$$

The cutoff frequency is f_c. With individual waveguide dimensions of 6.5" x 0.675", the cutoff frequency is found from equation (5.1) and is 950MHz. Equation (5.3) then yields

$$\gamma = -i(0.175)\text{cm}^{-1},$$

from which it can be determined that the e-folding distance is 5.7cm. Since the waveguides are approximately 9cm long, only 25% of the initial electric field and 6% of the power reaches the open ends of the waveguides. Were the waveguides 4cm long, as much as 25% of the power could reach the plasma. With waveguides just long enough to enclose the loop couplers, say 1cm, as much as 70% of the power could reach the plasma. This approach was not pursued. One attractive feature of this design is that with the loop couplers entering the waveguides from the shorted end, all waveguides can have the same length. This makes phasing of the array simpler, as phase delays in the couplers and waveguides do not have to be considered. This antenna array has a width λ_o of 7.0cm and from equation (5.2) a typical $N_{||}$ at launch would be 9.5.

The second antenna model was intended to rectify several problems. Using a dielectric powder with $\varepsilon_r = 12$ to fill the waveguides[15], the array would be small enough to comfortably fit into a standard port on Encore and operate well above cutoff. Provisions were made for moving the array in and out with respect to the plasma using an o-ring sealed piston, insuring proximity to the plasma cutoff. The waveguide ends nearest the plasma would be narrow so as to generate larger $N_{||}$ values at launch. At the ends away from the plasma the waveguides would be wider to facilitate coupling to coax.

To simplify construction, 1/16" sheet brass was cut, bent and soldered to form the waveguides. The shell of the first powder dielectric antenna is shown in Figure (5-3). The waveguide height was 10cm giving a cutoff frequency of 433MHz and a guide wavelength of 69.3cm. The waveguide was 5cm wide at the coupling ends. The coupling probes were copper rods 3mm in diameter, 4.5 cm long, located 7.8cm from the shorted end of the waveguide. According to calculations this resulted in an input radiation resistance of 50ohms and a residual input reactance of 14.2 ohms. The small reactance results in a 2% power reflection, which was deemed acceptable. The narrow end of the waveguide has a total width of 1.1cm, which, from equation (5.2), gives a nominal $N_{||}$ at launch of about 61. The entire waveguide assembly was 86.7cm long.

Initially the end of the waveguide array was butted up against a ceramic vacuum window mounted on the tokamak. This rectangular ceramic window mounted on a standard port is visible in the back of Figure (5-2). It was subsequently realized that this probably created too large a gap between the antenna and the slow mode cutoff in the plasma. In order to bring the end of the waveguide array closer to the plasma, the end of the array was mounted inside the vacuum chamber with an o-ring seal that allowed the position of the waveguide array to be continuously altered with respect to the plasma. The o-ring was mounted on a piston and is visible in front of the ceramic port in Figure (5-2).

To fill the waveguide assembly 27 pounds of dielectric powder were required. The powder dielectric required packing to stabilize the dielectric constant and to avoid air gaps. During packing, some of the solder joints eventually broke loose. To make a vacuum seal and contain the dielectric powder, the end of the waveguides were filled with a layer of castable dielectric resin.[16] This material was not vacuum compatible and the ends of the waveguides were coated with an additional layer of vacuum compatible epoxy (Torr Seal). In order to achieve 50-ohm input impedance, the electric couplers were required to be a certain length necessitating a wider waveguide at the coupling end. The waveguides were tapered to connect to the narrower launching end. If the waveguide tapering is gradual over several guide wavelengths, reflection from the taper should be minimal as the various reflections destructively interfere.[17] Unfortunately, the tapering was not gradual enough, and large reflections from the taper were encountered. Linear waveguide tapers in general tend to give objectionable reflections.[18] The abrupt changes in angle are a major part of the problem.[19]

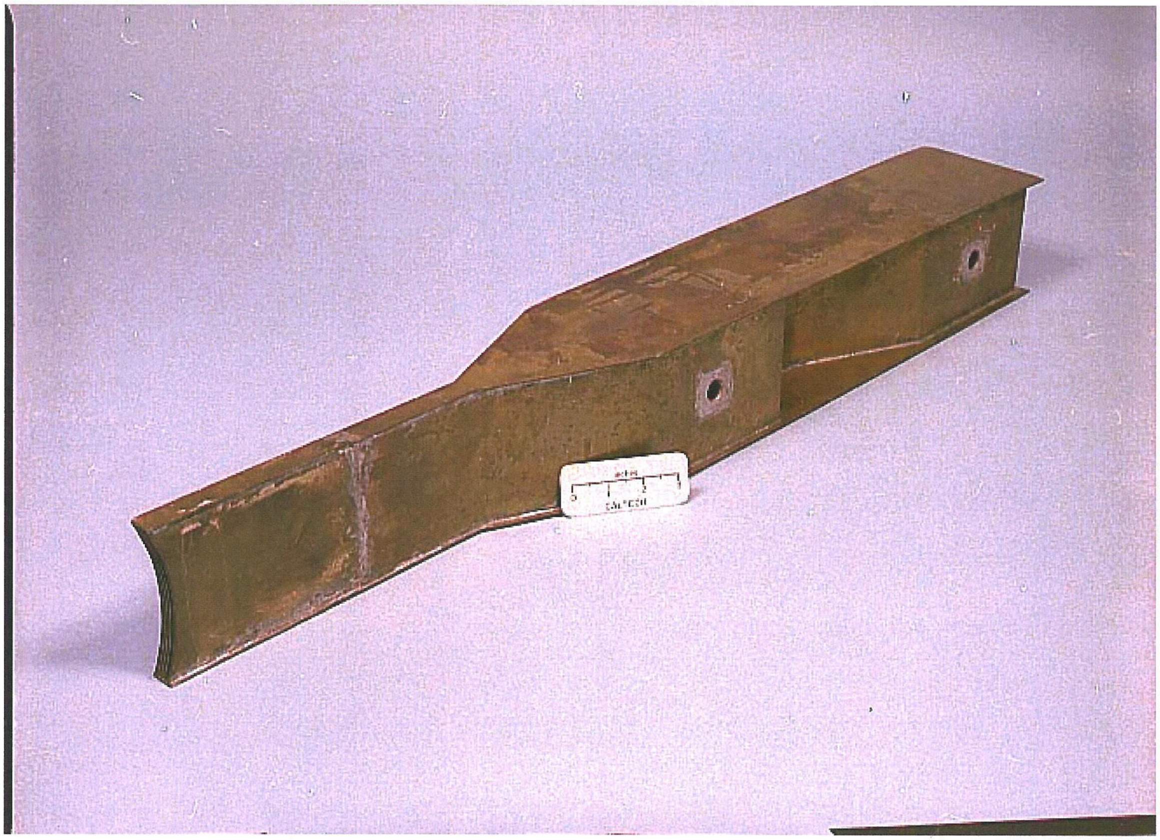

Figure 5-3. The first powder dielectric antenna. The "piston" vacuum connection and electric couplers are removed.

To remedy the problems encountered with the first powder dielectric antenna, an improved second version was constructed. To avoid the breakage of solder joints, grooves were milled in the top and bottom brass plates comprising the array in order to hold the vertical walls in position during the soldering process. The grooves increased the surface area of contact at the solder joints and eliminated the breakage problem.

To remedy the taper reflection problem, tuning stubs were added to null out the reactance introduced by the taper. A metallic screw of small diameter introduced from the broad side of a rectangular waveguide but not extending completely across the guide forms a variable shunt capacitance.[20] Since currents flow down the screw, it is necessary that good electrical contact be made between the screw and guide. When the length of the screw is approximately one-quarter of a wavelength in the guide medium, resonance occurs and the susceptance of the screw becomes infinite. Arbitrarily large mismatches can be tuned out. The second powder dielectric antenna is shown in Figure (5-4). Some of the construction details of the second powder dielectric antenna are presented in Figures (5-5), (5-6) and (5-7).

The waveguide height was 11cm giving a cutoff frequency of 394MHz and a guide wavelength of 39.8cm. The coupling ends of the waveguide were 5cm wide. The coupling probes were 4.5cm long, 3mm in diameter and located 7.0cm from the shorted ends of the waveguide. Calculations gave an input radiation resistance of 50 ohms and a residual input reactance of 14.9 ohms. The input reactance results in a 2% power reflection that was deemed acceptable. The total length of the waveguide array is 56cm. The width of the array near the plasma was about 1.1cm, giving a nominal $N_{||}$ at launch for quadrature phasing of about 61.

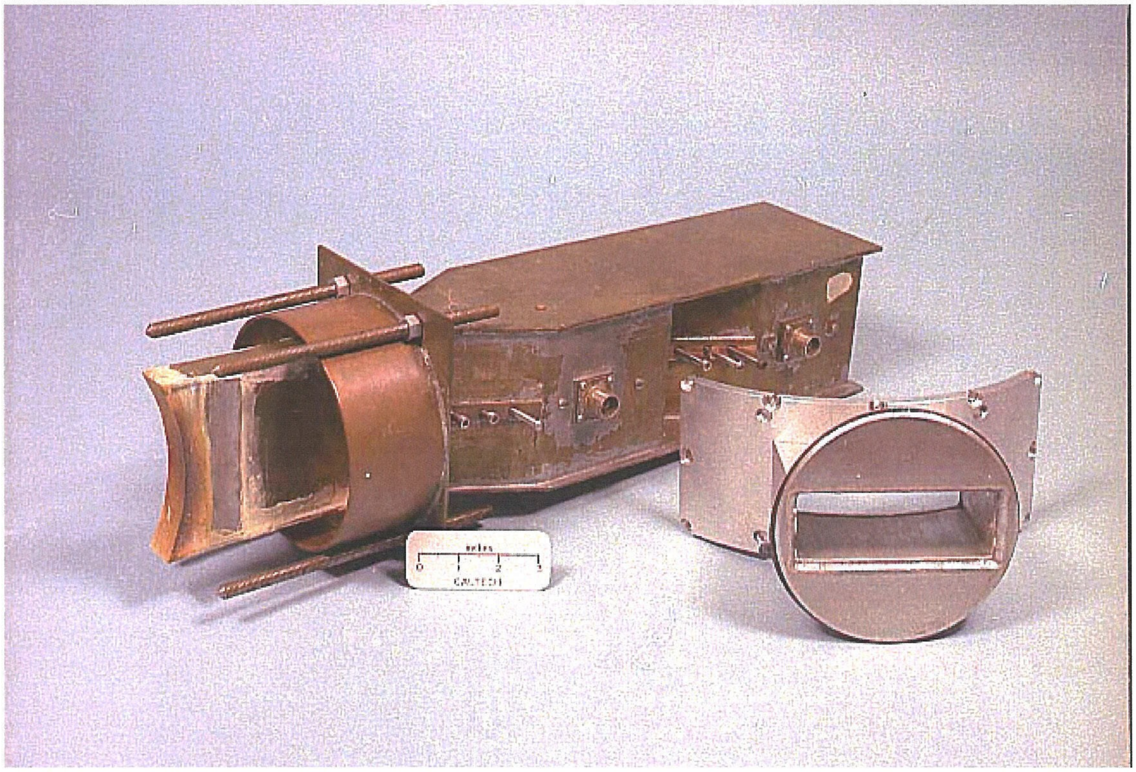

Figure 5-4. The second powder dielectric antenna. The tuning stubs are visible on the tapered portions of the waveguide. The burnt appearance of the epoxy on the plasma end of the array is evident. Steel plates to hinder bulging of the waveguides near the plasma can also be seen. The vacuum seal that allows the array to be moved in and out with respect to the plasma is also shown.

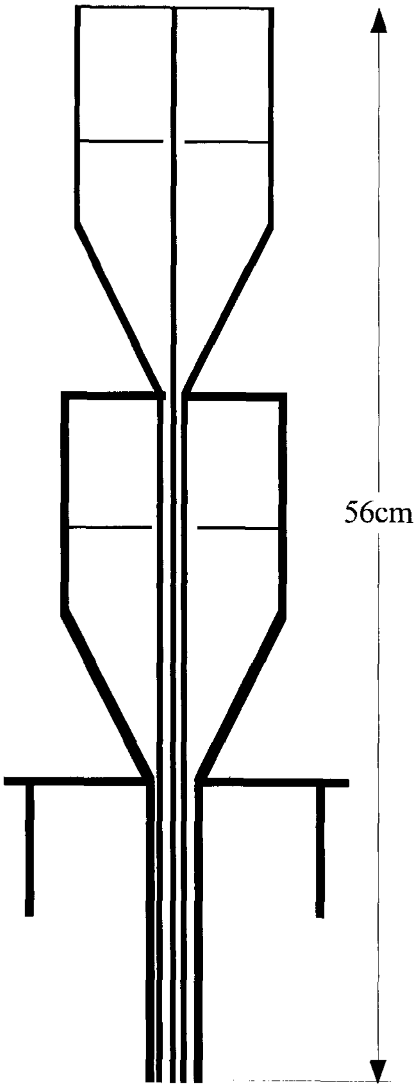

Figure 5-5. Schematic cutaway view of the second powder dielectric antenna. The longer waveguides have 1/16" walls, the shorter waveguides and the vacuum seal are made from 1/8" brass.

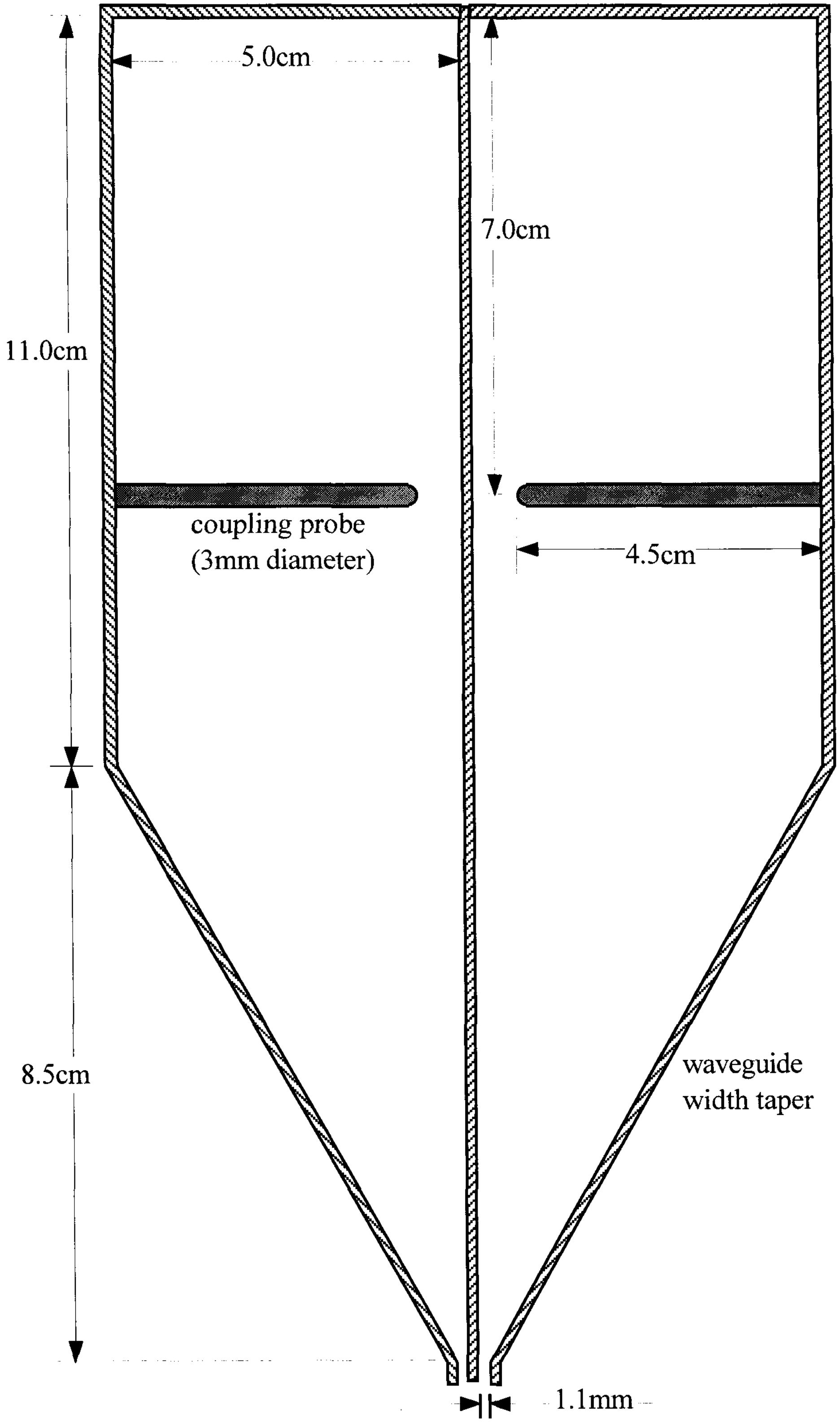

Figure 5-6. Cut away view (to scale) of the probe coupling and tapers of the two longer waveguides. Construction of the shorter waveguides is similar.

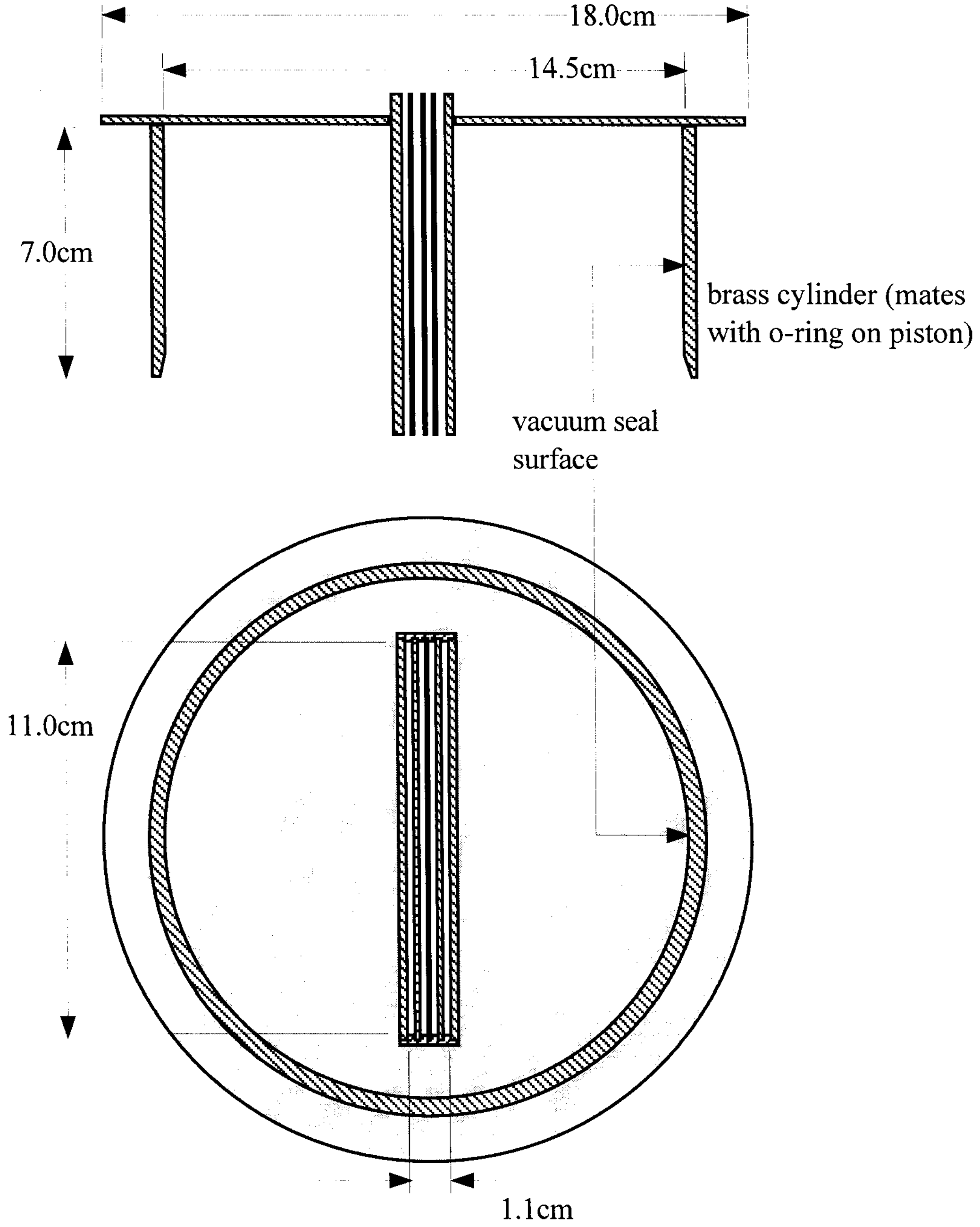

Figure 5-7. Some details of the piston vacuum seal and the launching end of the waveguide array.

The tuning stubs worked, but the antenna was not stable. The tuning stubs were very sensitive. Bumping the antenna could significantly reduce the matching achieved by the tuning stubs and also affect the phase at the waveguide mouth. The dielectric constant of the powder fill depends upon its density and is subject to change with any mechanical disturbance. The Torr Seal on end of antenna does not have the proper dielectric constant and slowly "burns" upon exposure to plasma. The narrow end of the powder antenna is not suitable for launching large power due to its small area. The use of tuning stubs to null out large reflections entails large amounts of re-circulating power in the antenna, which is undesirable for high power application since it increases chances of electrical breakdown or overheating problems. Due to the taper and stub tuning, and also to the different waveguide lengths, the inherent phase shift of each port had to be measured frequently. Difficulties were encountered due to the narrow width of the open end of the waveguides. Under vacuum, the waveguide walls near the plasma tended to bulge, lowering the density of the powder dielectric inside, or creating air gaps.

Solid Dielectric Antenna

Attempts to generate LH waves with large $N_{||}$ at launch by tapering the waveguides are responsible for most of the difficulties encountered with the powder-dielectric grill antennas. It became evident that most LHCD experiments at other institutions utilized low $N_{||}$ values at launch. Once the demand for large $N_{||}$ values at launch is removed, tapering is no longer necessary. The accompanying matching problem is eliminated. Without tapering, stable solid-dielectrics can be employed that are vacuum compatible and do not require a separate vacuum seal coating. This section describes the design and construction of the "solid dielectric" antenna.

It is still desirable to minimize the width of the waveguides to maximize the $N_{||}$ at launch. The minimum width of the solid-dielectric antenna is limited, however, by the difficulties in achieving a 50-ohm input impedance with an electric probe coupler. Larger dielectric constant helps. The largest dielectric constant available off the shelf in a microwave dielectric solid was $\varepsilon = 30.0$.[21] The "Stycast HiK 500F" material used is machinable, has low moisture absorption, has a thermal expansion well matched to brass, is useable to 260°C, and has high thermal conductivity. When using very large dielectric constants, air gaps must be avoided. The normal component of $D = \varepsilon E$ is continuous across boundaries. The electric field in an air gap will be ε times larger than in the dielectric and could result in breakdown. Capacitance values can also be dramatically altered with the presence of air gaps. To avoid air gaps, the dielectric solid is cemented into the waveguides.[22]

The radiation resistance of a probe antenna in a rectangular waveguide when the frequency is such that only the TE_{10} mode can propagate is given approximately by[23]

$$R = \frac{2Z_{TE}}{ab\beta_{10}k_o}\sin^2(\beta_{10}L)\tan^2\left(k_o\frac{d}{2}\right). \tag{5.5}$$

As shown in Figure (5-1), "a" and "b" are the dimensions of the waveguide and Z_{TE} is the characteristic impedance of the TE_{10} mode. k_o is 2π divided by the wavelength in the guide medium. β_{10} is the guide propagation constant and is given by

$$\beta_{10} = \sqrt{k_o^2 - k_c^2} = \sqrt{k_o^2 - \frac{\pi^2}{a^2}}, \tag{5.6}$$

where k_c is 2π divided by the cutoff wavelength for the TE_{10} mode. "L" and "d" in equation (5.5) are shown in Figure (5-8).

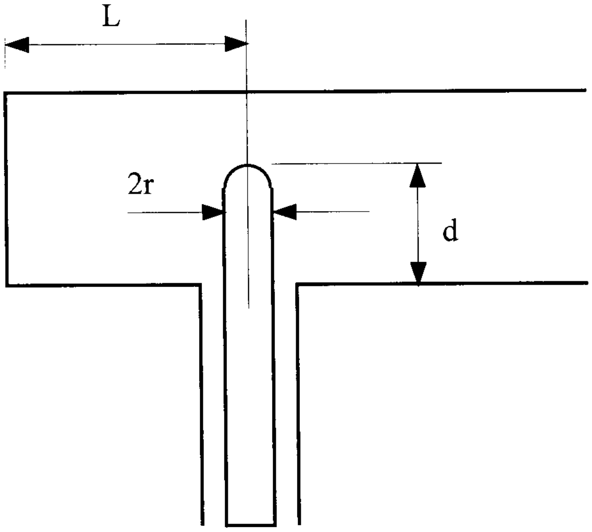

Figure 5-8. Definition of the parameters L, d and r used in the formulas for the input impedance of a probe coupler in a rectangular waveguide.

The input reactance of the probe coupler is given by[24]

$$X = \frac{Z_{TE}\tan^2(k_o d/2)}{2\pi k_o b}\left\{\begin{array}{l} \ln\left(\dfrac{2a}{\pi r}\right) + \dfrac{0.0518k_o^2a^2}{\pi^2} + \dfrac{2\pi}{\beta_{10}a}\sin(2\beta_{10}L) \\ -2\left(1-\dfrac{2r}{a}\right) - 2k_o^2\displaystyle\sum_{m=1}^{\infty}\left[1-\dfrac{\sin^2(m\pi d/2b)}{\sin^2(k_o d/2)}\right]^2\dfrac{K_o(k_m r)}{k_m^2} \end{array}\right\} \tag{5.7}$$

where

$$k_m^2 = \left(\frac{m\pi}{b}\right)^2 - k_o^2.$$

K_0 is the modified Bessel function of the second kind.

The waveguide dimensions "a" and "b" were chosen to be 6.99cm and 1.59cm respectively. Assuming that the frequency is 450MHz and the guide medium dielectric constant is 30, the values of some of the other quantities in equations (5.5) and (5.7) are $Z_{TE} = 68.8$ ohms, $\beta_{10} = 0.254\ \mathrm{cm}^{-1}$ and $k_o = 0.516\ \mathrm{cm}^{-1}$. The coax feeding the antenna is 50 ohm; thus it is desirable to have $R = 50$ ohms and $X = 0$ ohms. If $L = 3.1\mathrm{cm}$, then $2\beta_{10}L = \pi/2$, and the term containing $\sin(2\beta_{10}L)$ in equation (5.7) is maximized, which turns out to minimize X as the negative terms following are dominate. R in equation (5.5) is then maximized for the largest possible value of d. The probe length "d" is constrained to be less than the waveguide width, "b," which has been chosen to be 1.59cm. For $d = 1.5\mathrm{cm}$ and $r = 0.3\mathrm{cm}$, $X = -2.8$ ohms and $R = 7.9$ ohms are obtained. To further increase the value of R, the value of k_0d would have to be increased as was done in the design of the powder dielectric antennas. k_0d is a measure of the probe length relative to the wavelength in the guide medium. The dielectric constant cannot be increased beyond the value $\varepsilon = 30$, and d cannot be made larger without widening the waveguide, thus decreasing the $N_{||}$ at launch. It was decided to match the 8-ohm radiation resistance of the probe couplers to 50-ohm cable by using quarter-wave coax matching sections. The value $d = 1.5\mathrm{cm}$ leaves a gap filled with solid dielectric of 0.9mm between the end of the probe and the waveguide wall. At 300 volts/mil, the dielectric strength of the material in the gap is over 10 kV.

The impedance of the coax matching section is given by

$$Z_{\text{matching}} = \sqrt{Z_{\text{probe}} Z_{\text{cable}}} = \sqrt{7.9\Omega \times 50\Omega} = 19.9\,\text{ohms}. \qquad (5.8)$$

Paraffin was chosen as the dielectric material. With a dielectric constant of 2.3, a quarter wavelength in coax is 11.0 cm. The impedance of a coaxial line is given by[25]

$$Z_{\text{matching coax}} = \frac{\eta}{2\pi} \ln\left(\frac{r_2}{r_1}\right), \qquad (5.9)$$

where r_2 is the inner radius of the outer conductor, and r_1 is the outer radius of the inner conductor. With the dielectric constant of 2.3, combining (5.8) and (5.9) yields

$$\frac{r_2}{r_1} = 1.65. \tag{5.10}$$

The outside diameter of the inside conductor was chosen to be 0.616 cm and the inside diameter of the outer conductor was chosen to be 1.016 cm. This gives 2mm of paraffin between the conductors. The dielectric strength of 2mm of paraffin is at least 7.1 kV.[26] The connection to the coax was made with commercially available type-HN panel mount receptacle.[27] The dielectric constant of the Rexolite insulation in these connectors is 2.64, which is close to that of the paraffin. There is a step discontinuity in the coax line at the position of the HN connector due to the change in conductor radii. When the transverse dimensions of the conductors are negligible compared to the wavelength, the discontinuity admittance is a pure capacitance. The discontinuity capacitance is typically of the order of a few tenths of a picofarad, and is usually negligible for frequencies of a few hundred megahertz.[28]

The construction of the solid dielectric antenna is depicted in Figures (5-9) and (5-10). Brass sheet of a standard thickness of 1/16" and 1/8" was used. The top and bottom plates were milled with grooves and the entire assembly soldered. The solid dielectric pieces were cemented into the waveguides. Small threaded holes were placed at the rear ends of the guides so that excess cement could be squeezed out the back end as the dielectric slabs were pushed in. Screws would later fill the small holes. It became evident only after the dielectric slabs were halfway in, that the viscosity of the cement was dangerously large. Large weights were used to finish pushing the dielectric slabs into the guides.

The probe couplers were cemented into the waveguide dielectric. The center conductor of the matching coax was threaded at the end away from the waveguide. A mating thread was placed on a piece of rod soldered to a panel mount HN receptacle, which was then removable. The outer conductor of the coax was threaded so as to screw into the housing comprising the waveguides, and was thus also removable. The antenna assembly was tipped on its side and melted paraffin poured into the warmed coax structures to fill them, and the HN connectors then screwed in and secured in place with bolts.

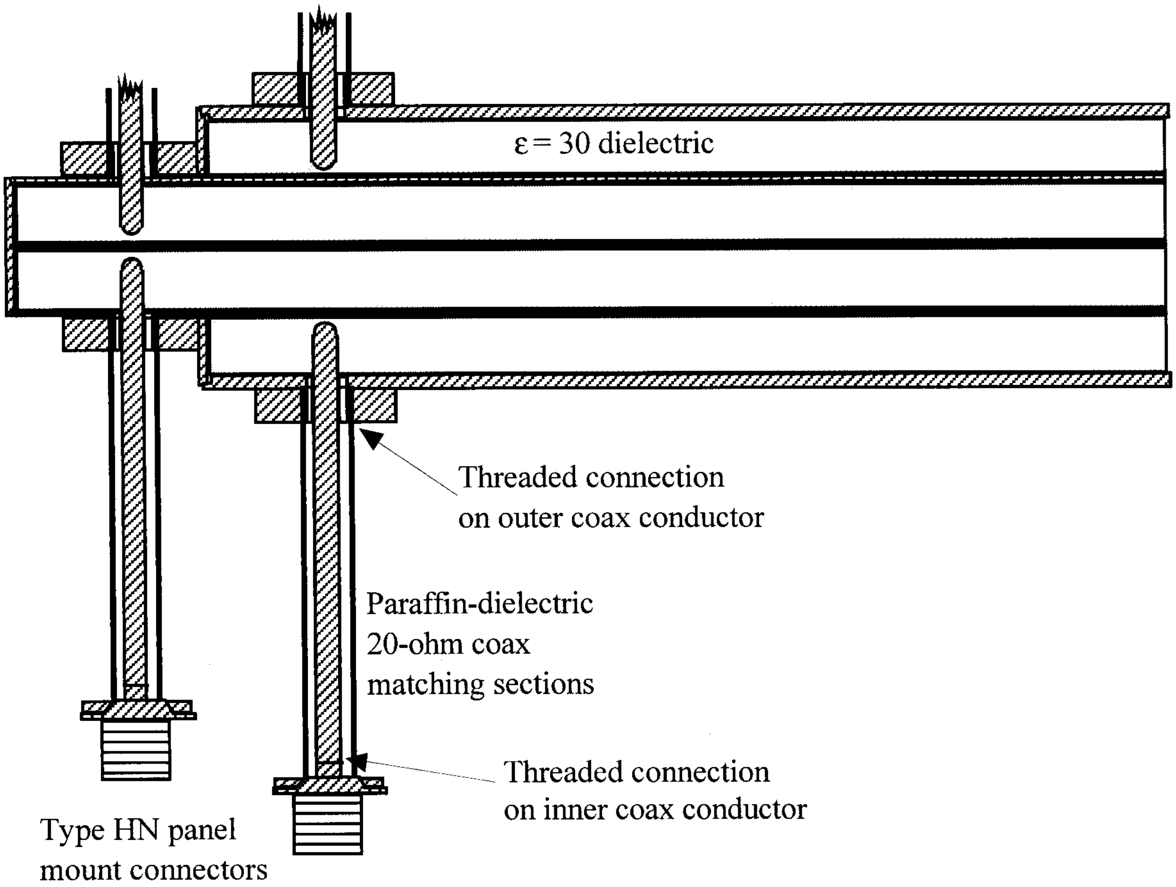

Figure 5-9. Cut away view of the construction of the solid dielectric antenna. Scale is 1:2. The waveguide material is 1/16" and 1/8" brass, all joints soldered. The quarter-wave coax matching sections utilize paraffin dielectric.

The phase at the end of the waveguides must account for the different lengths of the waveguides, and the different directions in which the electric couplers point. The phase at the open end of each waveguide was measured for purposes of determining the inherent phase shifts.

The end of the antenna was machined with a radius equal to the minor radius of Encore, in order to match the shape of the plasma.

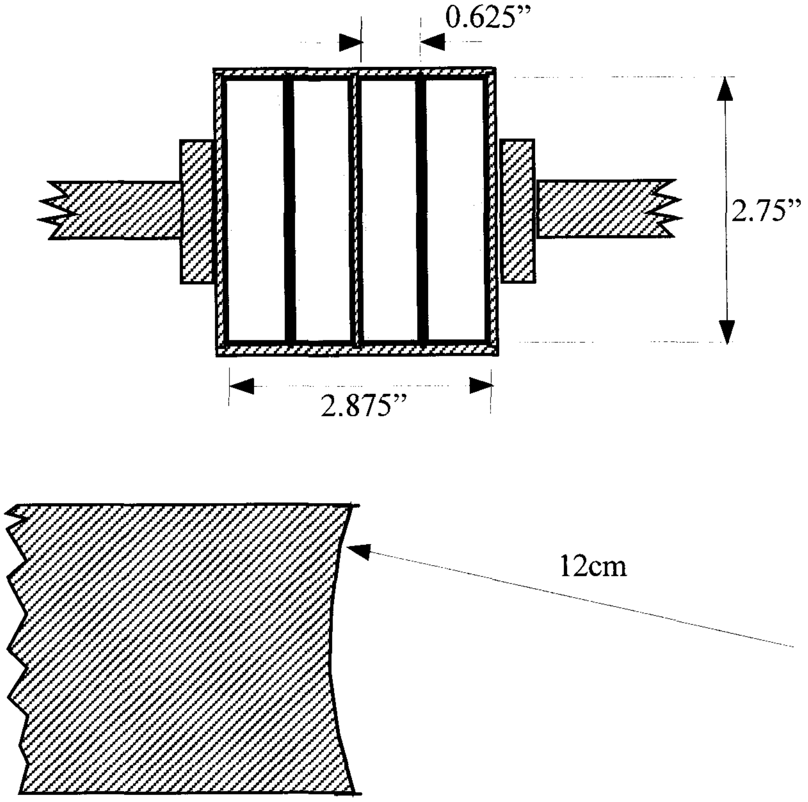

Figure 5-10. End view of the solid dielectric antenna. With the dielectric fill of $\varepsilon = 30$, the cutoff frequency is 391 MHz and the guide wavelength is 24.6 cm. The open ends of the waveguides are machined with a radius equal to the minor radius of Encore to match the edge of the plasma. The scale is 1:2.

The completed antenna is shown in Figure (5-11), and the antenna mounted on the Encore Tokamak is shown in Figure (3-7).

During operation the end of the waveguide array often acts as a plasma limiter as proximity to the slow mode cutoff would presumably be optimized for such a condition. It was discovered, however, that brass from the waveguide walls would sputter onto the ends of the dielectric slabs filling the waveguides, thus coating them with a thin conductive film. The film of brass was removed with fine sandpaper and the sputtering problem was eliminated by application of a layer of boron nitride to the brass otherwise exposed to the plasma.[29]

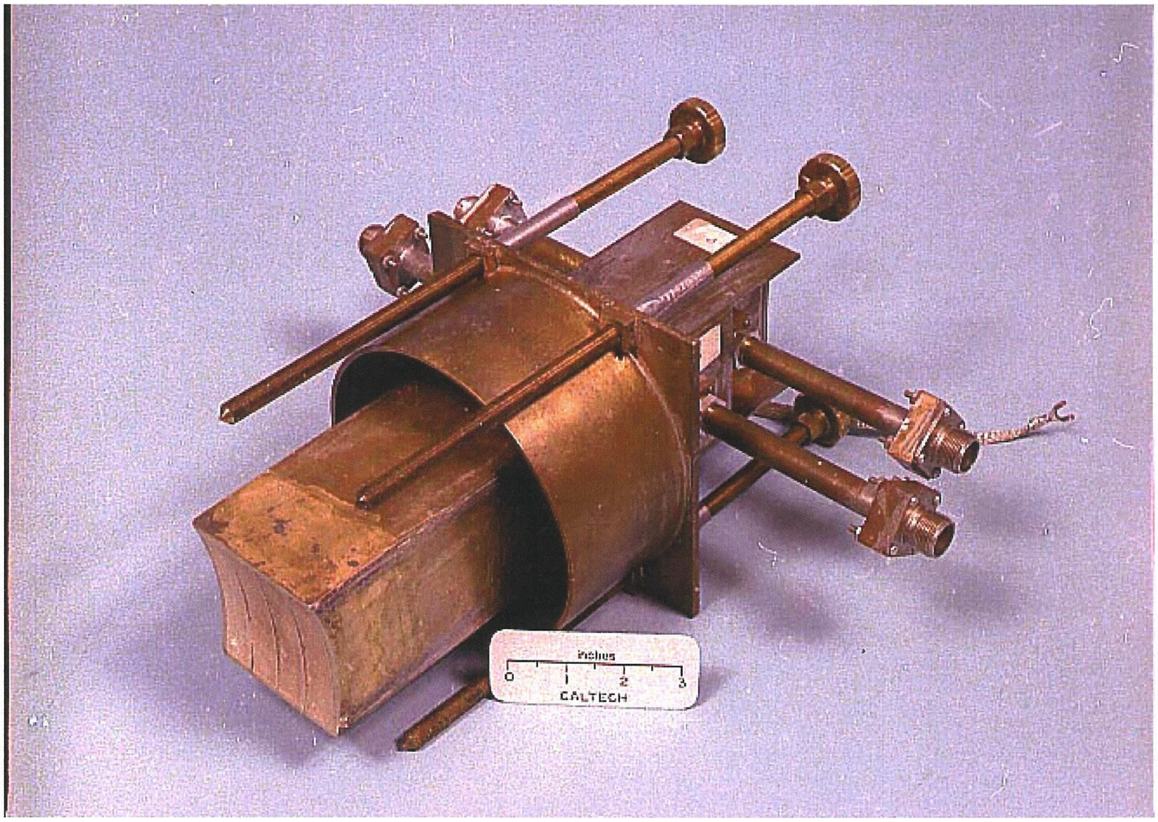

Figure 5-11. The completed solid dielectric antenna.

Calculation of Antenna $N_{||}$ Spectra

A critical parameter for lower hybrid current drive is the phase velocity of the launched lower hybrid waves parallel to the confining magnetic field. Normalized to the speed of light as $k_{||}c/\omega$, this parameter is the parallel refractive index of the wave and is denoted by $N_{||}$. Landau damping requires a velocity matching criteria

$$v_{\text{electron}} = \frac{c}{N_{||}} \tag{5.11}$$

between the lower hybrid wave and the electron velocity. The $N_{||}$ spectrum at launch is set by the antenna properties.

Consider a series of sources radiating into an open half space (vacuum) as shown in Figure (5-12).

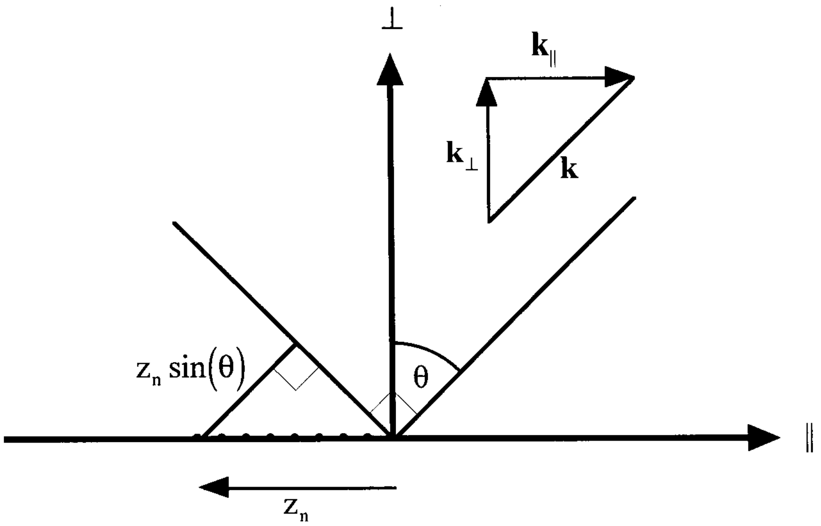

Figure 5-12. A series of point sources radiating into space. All points oscillate at the same frequency, but there are phase delays ϕ_n associated with each source. Radiation at the angle θ incurs propagation phase delays of $z_n \sin(\theta)$.

The electric field in the far field at angle θ is computed by allowing for the various phase delays and the inherent phase of the sources,

$$\begin{aligned} E &= \sum_n e^{-i(k l_n + \phi_n)} = \sum_n e^{-i(k l_0 + k z_n \sin\theta + \phi_n)} \\ &= e^{-ik l_0} \sum_n e^{-i(k_\| z_n + \phi_n)} = e^{-ik l_0} \sum_n e^{-ik_\| z_n} e^{-i\phi_n}. \end{aligned} \tag{5.12}$$

In equation (5.12) l_n is the distance from source to detector, ϕ_n is an inherent phase delay in the source, and $k\sin\theta = k_\|$. The vacuum $k_\|$ spectrum for this series of point sources is proportional to $|E|^2$. For a continuum of sources the sum goes over into a Fourier transform integral of the initial phase-amplitude function.

This procedure calculates the vacuum $k_\|$ spectrum or equivalently the $N_\|$ spectrum where $N_\| = k_\| c / \omega$. The spectrum has a peak located at $N_\| = N_\|^{peak}$. The peak has a full width at half maximum value denoted FWHM $N_\|$. The presence of plasma will modify the result, shifting the peak value an amount $\Delta N_\|^{peak}$. For instance, unequal reflection coefficients for the sources will result in unequal effective strengths. Details of a self-consistent calculation including plasma coupling can be found in references.[30, 31] Comparison of theoretical calculations with and without plasma for a typical case show that the shifts in the $N_\|$ spectrum are noticeable but small[32],

$$\frac{\Delta N_{\|}^{peak}}{\text{FWHM } N_{\|}} = \frac{0.83}{4.41} = 19\% \qquad \text{and} \qquad \frac{\Delta N_{\|}^{peak}}{N_{\|}^{peak}} = \frac{0.83}{8.0} = 10\%. \tag{5.13}$$

The shifts are towards lower $N_{\|}$ with the addition of plasma. Because the effects are small, the more difficult calculations including plasma coupling were considered inappropriate and were not pursued.

Perhaps the simplest model of the antenna is to assume that the phase varies linearly across the four waveguides

$$E(k_{\|}) = \int_0^L e^{ik_oz}e^{-ikz}dz = \left.\frac{e^{i(k_o-k)z}}{i(k_o-k)}\right|_0^L = \frac{e^{i\Delta kL}-1}{i\Delta k}, \tag{5.14}$$

where

L is the antenna width,

$k_o = (2\pi)/\lambda_o$,

$\lambda_o = (2\pi L)/(n\ \Delta\phi)$,

n = number of waveguides,

$\Delta k = k_o - k$,

$\Delta\phi$ = phase shift between waveguides.

Equation (5.14) can be rewritten as

$$\begin{aligned} E(k_{\|}) &= \frac{e^{i\Delta kL}-1}{i\,\Delta k} \\ &= e^{i\Delta kL/2}\frac{\left(e^{i\Delta kL/2} - e^{-i\Delta kL/2}\right)}{i\,\Delta k} \\ &= Le^{i\Delta kL/2}\frac{\sin(\Delta kL/2)}{\Delta kL/2}. \end{aligned} \tag{5.15}$$

The power spectrum $P(k_{\|})$ of the antenna is

$$P(k_{\|}) = |E(k_{\|})|^2 = L^2\left(\frac{\sin(\Delta kL/2)}{\Delta kL/2}\right)^2. \tag{5.16}$$

Quadrature phasing denotes a 90° phase shift between successive waveguides. A plot of $P(k_{\|})$ for the parameters of the final antenna with quadrature phasing is given in Figure (5-

13). In this case, numerical integration gives 96% of the power spectrum downstream and 4% upstream. As can be seen by differentiating equation (5.16), the major peak occurs for $k_{||} = k_o$,

$$N_{||}^{peak} = \frac{k_o c}{\omega} = \frac{c\,n\,\Delta\phi}{\omega L}. \tag{5.17}$$

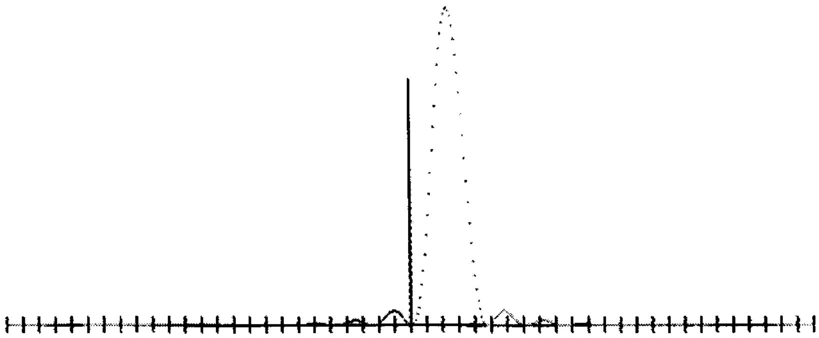

Figure 5-13. $N_{||}$ spectrum for 90° phase shift per channel using the simplest model which is a continuous 360-degree phase swing over the width of the antenna (7cm). The scale is 4 per horizontal division.

The half maximum of the power spectrum (5.16) occurs when $\Delta k L/2 \cong 1.4$ and so the FWHM of k will be $2\Delta k = 2\times 2\times 1.4/L = 5.6/L$. For L = 7cm, the FWHM will be 5.6/7 cm^{-1} and the FWHM of $N_{||}$ will be

$$\text{FWHM } N_{||} = \frac{c}{\omega}\times\frac{5.6}{L} = \frac{3\times 10^{10}}{2\pi\times 450\times 10^{6}}\times\frac{5.6}{7} = 8.5. \tag{5.18}$$

Add In Constant Phases

A refinement to the above calculation is to put in the fact that for a TE_{10} mode the phase is constant across the waveguide mouth and not continuously varying with position. In this case the spectrum is calculated as

$$E(k_{||}) = \frac{1}{2\pi}\left[\int_0^{\Delta z} e^{-ikz}dz + e^{i\Delta\phi}\int_{\Delta z}^{2\Delta z} e^{-ikz}dz + e^{2i\Delta\phi}\int_{2\Delta z}^{3\Delta z} e^{-ikz}dz + e^{3i\Delta\phi}\int_{3\Delta z}^{4\Delta z} e^{-ikz}dz\right]. \tag{5.19}$$

The result of this refined calculation applied to the antenna parameters is shown in Figure (5-14). Numerical integration gives 89% of the power spectrum downstream and 11% upstream.

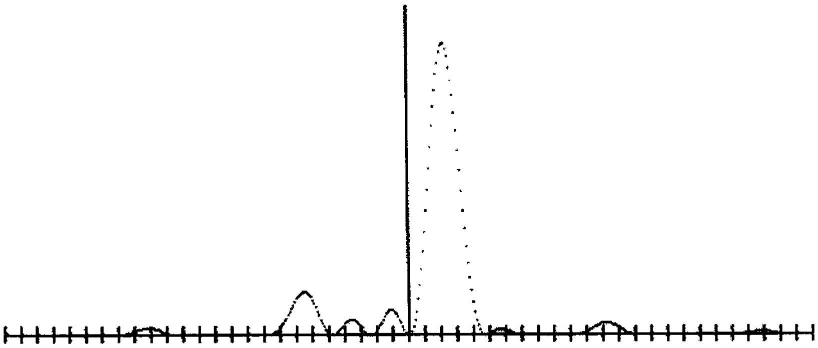

Figure 5-14. $N_{||}$ spectrum for 90° phase shift per channel using constant phases of 0°, 90°, 180° and 270° over the mouths of the four waveguides. The scale is 4 per horizontal division.

Include Waveguide Walls

A last refinement is to include the thickness of the waveguide walls as sources with zero amplitude. The result applied to our case is shown in Figure (5-15). The effect on the spectrum is significant. Numerical integration gives 76% of the power spectrum downstream and 24% upstream. The inclusion of a finite wall thickness and constant phases seriously decreased the directionality of the antenna. Note also that the undesirable upstream power is at lower phase velocities than the downstream power. To better define the $N_{||}$ spectrum and improve directionality, more waveguides are needed.

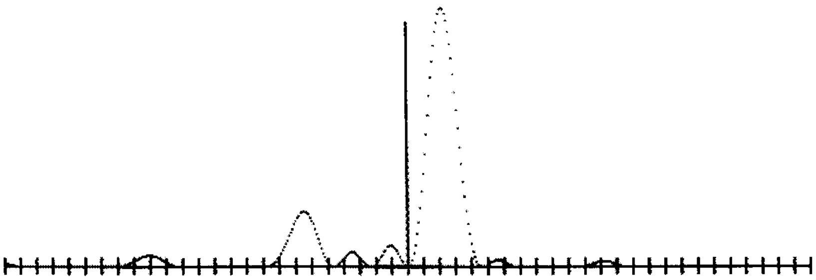

Figure 5-15. $N_{||}$ spectrum for 90° phase shift per channel, constant phase across the individual waveguide mouths, with waveguide wall thickness included. The scale is 4 per horizontal division.

In Figure (5-16), calculations for a whole range of $\Delta\phi$ are shown. Note that the slowest phase velocities are obtained for the case $\Delta\phi = 180$ degrees.

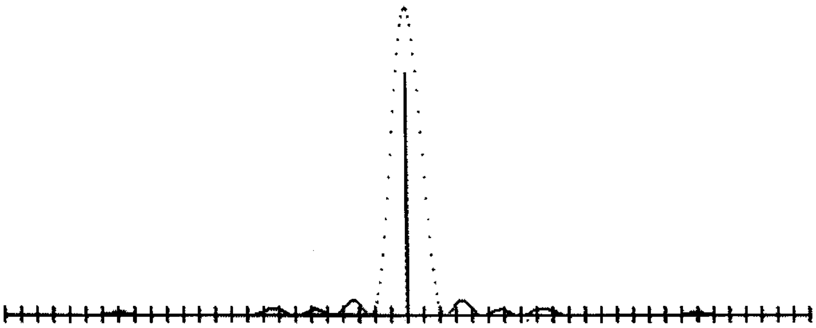

a) 0° phase shift per channel

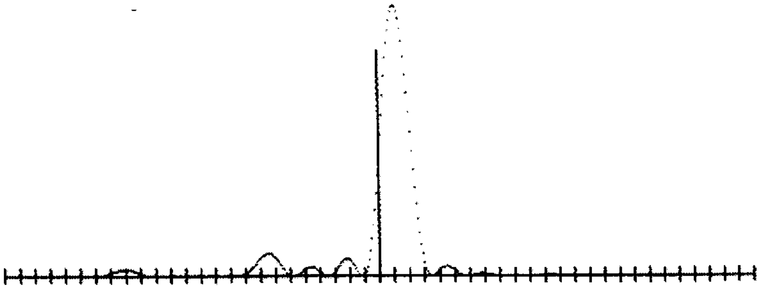

b) 45° phase shift per channel

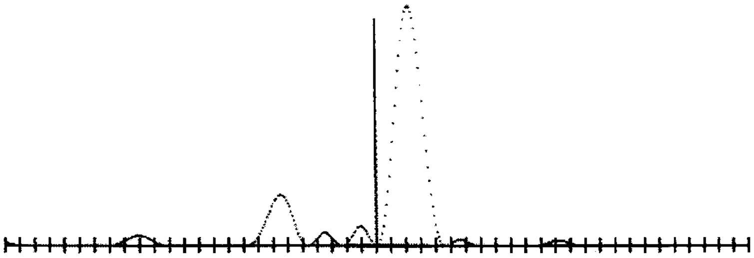

c) 90° phase shift per channel

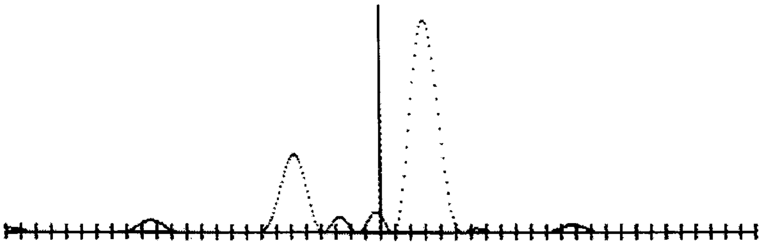

d) 120° phase shift per channel

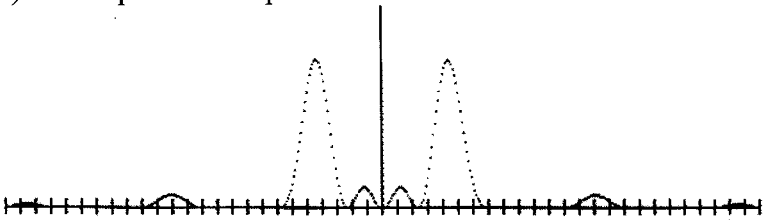

e) 180° phase shift per channel

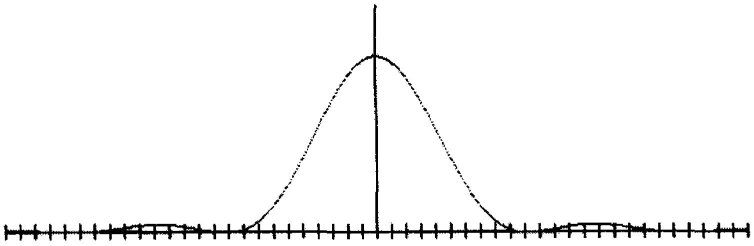

f) Only a single waveguide powered

Figure 5-16. $N_{||}$ spectrum for various phasing of the antenna. The horizontal scale is 4 per division.

Calculations of this type were made for lower hybrid antennas located at other institutions, and the results concur with the published data for those experiments.[33]

Antenna Testing and Evaluation

After all the calculations and construction, the antenna must be tested to insure that it functions properly. It is possible, for instance, that some or all of the waveguide channels exhibit large losses. There may be unexpected points of reflection in some of the waveguides. Under high power operation, breakdown might occur in hidden air gaps for instance.

Two methods were used to evaluate the antenna. The first and simplest uses the set-up shown in Figure (5-17).

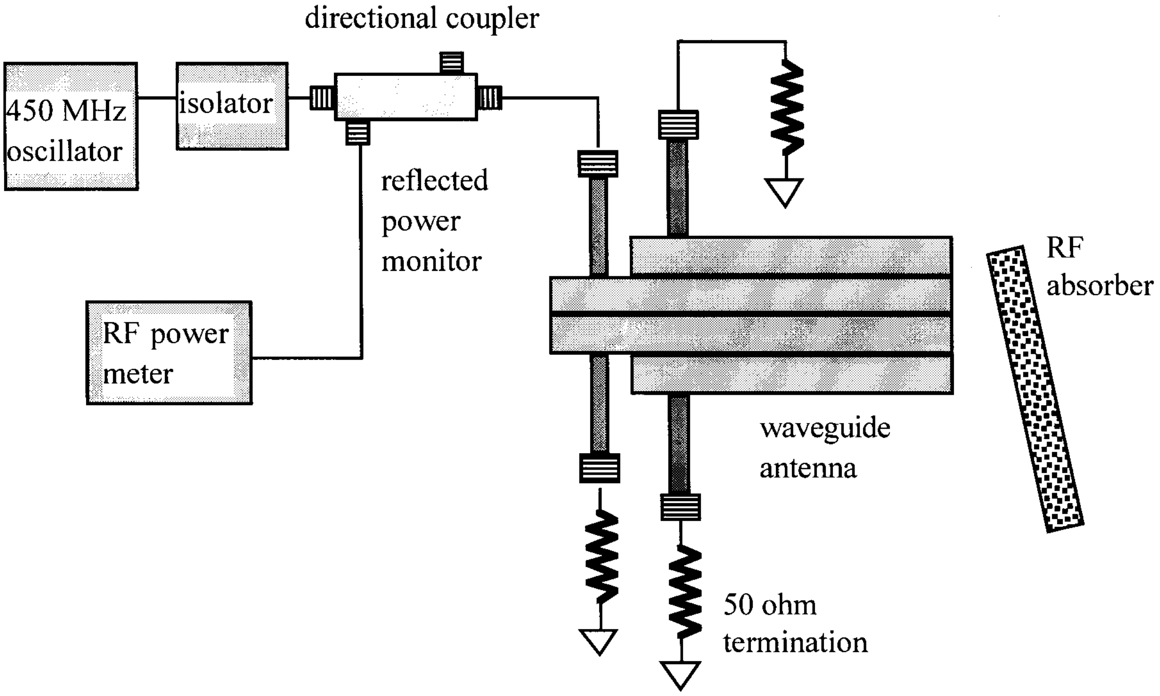

Figure 5-17. Experimental arrangement used for testing the antenna for proper matching and loss. The reflected power is monitored as RF reflecting and absorbing materials are played against the open ends of the waveguides.

A certain power level is put into a wave-guide channel, while the other three inputs are terminated into 50-ohm loads. Looking at the reflected power, one plays with RF absorbing material and metal foil on the exposed waveguide end. If the reflected power can be affected at all then it is proved that at least some RF power reaches the waveguide end. In this manner it was possible, by proper positioning on the end of the waveguides, to drop the reflected powers 30 dB or more on all channels. Similarly, it was possible to push the reflected power up to within 2 dB of the forward power. These results are consistent with properly matched waveguides with a loss per pass of about 1 dB.

The static reflection coefficients looking into air are about 3 dB down from the forward power. Figuring 1 dB loss per pass, 80% of the power makes it to the wave-guide end. In order to come out with 1 dB loss at the wave-guide end, 13% of the original power must be lost there, through radiation into space and coupling to adjacent wave-guides.

An important aspect governing the end reflection is the accessibility of the $k_{||}$ spectrum of the wave-guide end fields to free space. Radiation in free space must satisfy the dispersion

$$N^2 = \frac{k^2c^2}{\omega^2} = 1, \tag{5.20}$$

where $k^2 = k_\perp^2 + k_{||}^2$. Wave-guide power with $N_{||}^2 > 1$ cannot satisfy this dispersion. Calculations of the $N_{||}$ spectrum for a single waveguide are shown in Figure (5-13f). Numerical integration of the result for this case gives only 6% of the spectral power accessible to free space, that is with $|N_{||}| \leq 1$. The reason so little can be radiated is due to the fact that a large free space wavelength (67cm) has been squeezed into a very small waveguide (1.6cm x 7cm) with an appropriate dielectric. A wider waveguide would shift the spectral power towards smaller $N_{||}$. The fact that 20% of the power making it to the waveguide end is lost (which corresponds to a 1-dB loss) suggests that coupling to adjacent wave-guides is small but non-negligible. The result is consistent with an adequately functioning antenna.

A 1-dB loss per pass for the antenna is not unreasonable considering the insertion losses of many commercial items. However, estimates of the losses in the waveguides and coax matching sections due to dielectric and resistive wall losses do not account for it. The Emerson and Cumming, Inc., HiHiK ($\varepsilon = 30$) wave-guide material has a loss tangent of 0.001 and the paraffin coax filler a loss tangent of 0.0003.[34] The skin effect resistivity of a typical brass is $5.01\times10^{-7}\sqrt{f}$ Ohms.[35] Using the formulas of Ramo, Whinnery, and Van Duzer[36] losses of 0.68 dB/m for the waveguide and 0.2 dB/m for the coax matching section are obtained. The wave-guide is 20cm long while the coax section is 11cm in length. The solder joints and dielectric cement have been neglected. Measurements with an IR thermometer of the antenna temperature rise after significant energy throughput show the greatest temperature increases occur near the ends of the 20 ohm coax matching sections. After prolonged running at high powers and large duty cycle, the paraffin dielectric of the matching sections sometimes softens and partially leaks out. Paraffin expands significantly as it melts. It has been necessary to occasionally repack the matching sections with paraffin. Evidently, most of the antenna losses occur in these matching sections.

The type-HN cables connecting the antenna to the RF power supply were found to have 1.4 dB loss. The loss was assumed to be small until a significant temperature increase of the cable was observed with the IR thermometer. IR thermometers are inexpensive and are extremely useful for all kinds of debugging operations.

Calorimeter Test

A more definitive test of the antenna is a high power calorimeter test. This will unambiguously give an estimate of the power throughput and thus antenna loss under conditions of high power. Problems unique to high power operation such as voltage breakdown in air gaps or filler materials will be exposed. The original motivation for this test was provided by initial current drive experiments that yielded little effect on the plasma current.

The idea is to immerse the end of the antenna into a fluid that will act as an effective RF load. Applying a known amount of RF watt-seconds to the antenna, the temperature rise of the fluid and reflected power is measured to obtain an upper bound on the antenna loss. A schematic diagram of the set up is shown in Figure (5-18).

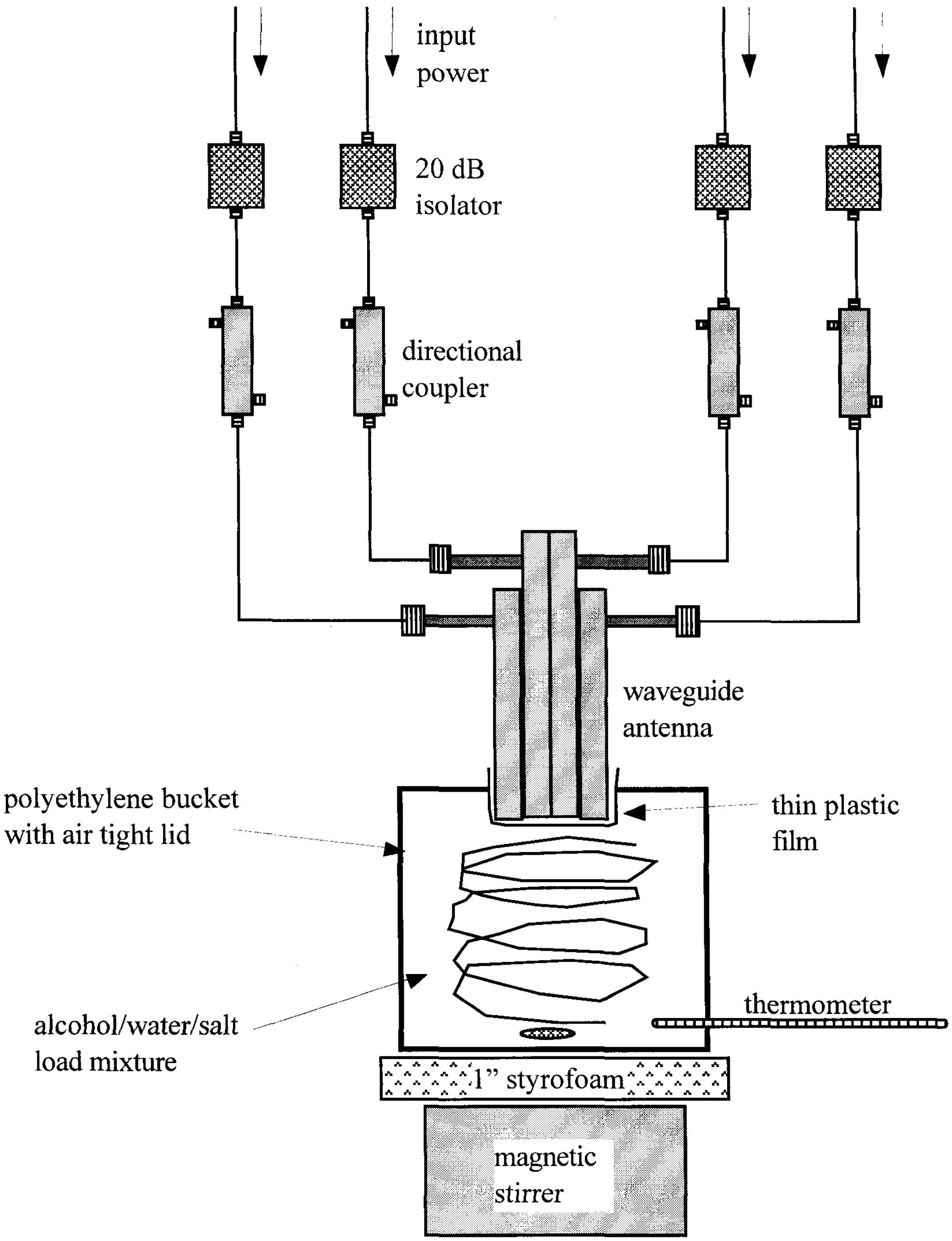

Figure 5-18. Schematic of experimental arrangement used for the calorimetric tests to check power flow through the antenna.

Alcohol was chosen as the base for the liquid load medium in order to match the impedance of the antenna dielectric and increase the dimensions of the evanescent region. The wave-guide material has a dielectric constant of $\varepsilon = 30$. A mixture of 95% alcohol and 5% water has a similar dielectric constant at radio frequencies.[37] By comparison, distilled water has $\varepsilon \cong 80$. The loss tangent must be increased to the point that the e-folding distance for the RF power is a fraction of the load dimensions. The e-folding distance should, in fact, be a fraction of the e-folding distance of the evanescent wave-guide end-field. Utilizing data from King[38] it is seen that dissolving salt in the amount of 10gm/liter in the dielectric load increases the conductivity into the range $\sigma \cong 1$ Si/m. For this concentration the real part of the dielectric constant is essentially unchanged. The increased conductivity gives a loss tangent of

$$\delta \approx \frac{\sigma}{\omega \varepsilon} \geq 1. \tag{5.21}$$

The resulting e-folding distance for our parameters is of the order of a few centimeters, while the wavelength for plane waves in the fluid (≈ 12 cm) is only slightly increased.

An indication of the effectiveness of the load is given by the drop in reflected power to 10 dB or more below forward power upon immersion of the antenna end.

Styrofoam was placed between the polyethylene bucket and magnetic stirrer because the stirrer became warm after running. The mechanical energy of stirring was negligible for the duration of the experiment and the pre-experiment temperature was stable to a tenth of a degree centigrade. The end of the antenna was covered with a thin sheet of plastic to prevent salt water from soaking into the wave-guide dielectric. The antenna and RF load were placed remote from personnel behind a metal door, and fire extinguishers were available. Temperature measurements were made both with an alcohol thermometer located at the bottom of the bucket and with an IR thermometer. These two measurements were in agreement. All seals were made air tight with RTV to prevent evaporative cooling. The heat capacity of the NaCl, H_2O, polyethylene bucket, thermometer and stir-bar were included. Collectively, however, the heat capacity of these materials is an order of magnitude less than that of the alcohol.

Only one wave-guide was powered. The forward RF power was measured by a directional coupler hooked directly to the antenna. The coupler insertion loss of 0.2 dB was noted. The power reflected back into the non-powered wave-guides was measured and was negligible.

Average RF power levels of 233 watts incident to the antenna were used. The experiment was run twice, with RF on times of 120 and 180 seconds. The results for the two trials agree within 1%. The result is that the thermal energy measured in the load is 66% of the RF energy input to the antenna. The missing energy is 34% of the RF energy input to the antenna and could be accounted for by losses in the antenna structure. A 1-dB loss in the antenna as suggested by the earlier tests would account for 17% of the input RF energy. A 1.8-dB loss in the antenna would be required to account for the entire 34%.

There are two principle sources of error, both of which tend to make the antenna appear to have more loss. RF power that is not damped in the load, but escapes as radiation will not heat the load. Second, the antenna has a large thermal mass and is essentially at room temperature. Since the antenna has thermal contact with the load it can act as a heat sink. Since the evanescent waves are damped close to the antenna, this heat sink is all the more important.

In conclusion, antenna losses of 1.0 to1.8 dB need to be invoked to explain the calorimeter data. Considering the possible errors, a 1.0-dB loss per pass, as was suggested by the earlier bench test, seems reasonable.

RF Power Supply

A 4-channel, 450 MHz power supply with a combined output of 50 kW was designed and built.[39] A schematic of the RF supply is shown in Figure (5-19), and a picture of the operational unit is shown in Figure (5-20). A considerable amount of time was spent debugging problems with the RF supply. Kapton bypass capacitors in the Eimac RF amplifier cavities occasionally failed accompanied by big arcs, so a fast protection circuit utilizing ignitrons was installed to quickly crowbar the HV supply in the event of an arc. The high voltage connections to the final amplifiers had to be well shielded. To stabilize the amplifier chain, numerous isolators as well as substantial shielding were installed in the low power sections. It was found necessary to pay particular attention to isolating and shielding the low power stages from the high power stages.

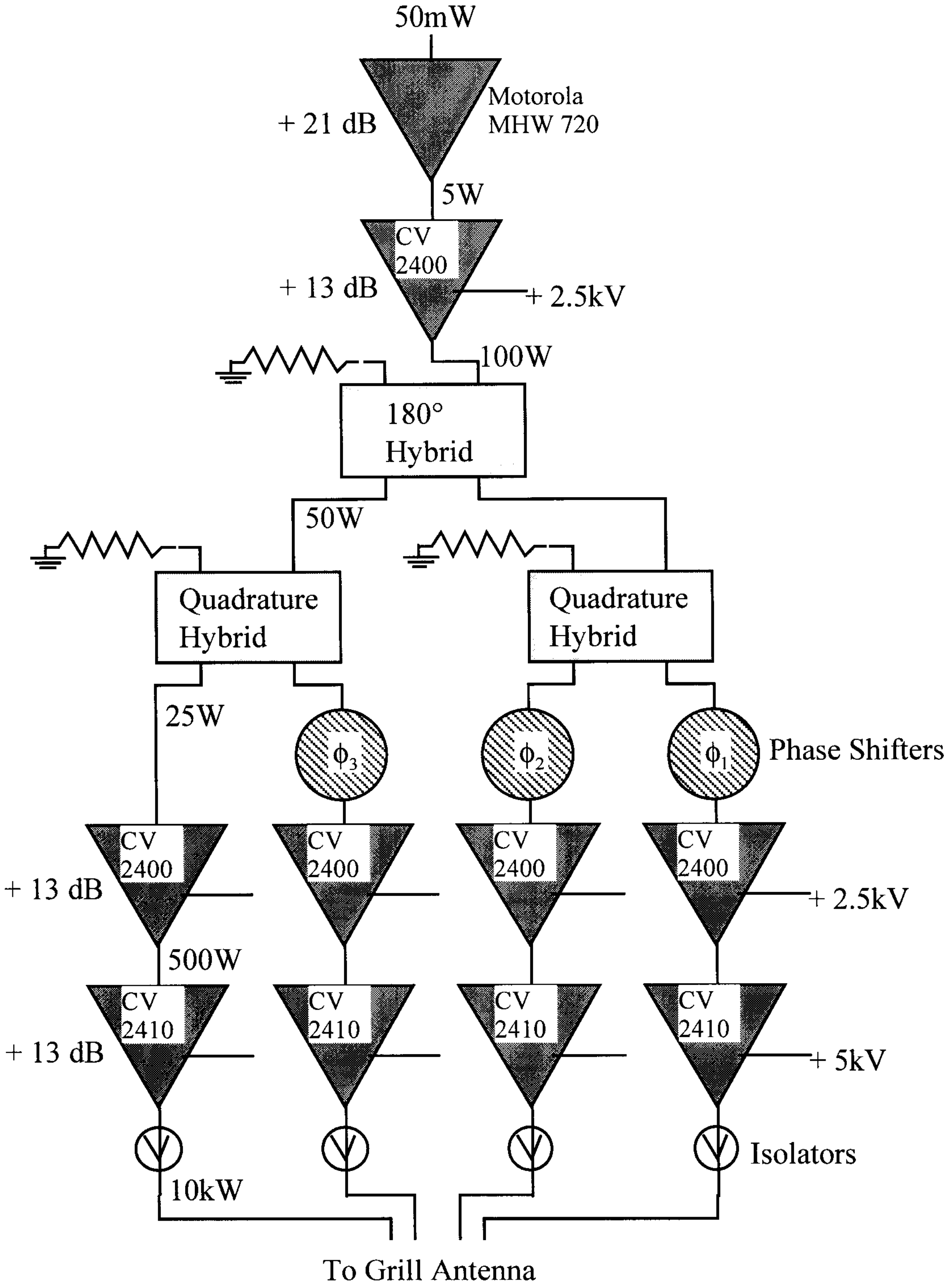

Figure 5-19. Schematic of the 50kW RF power supply. The phase shifters and isolators were obtained from Micon Inc.[40], the RF tubes and cavities from Varian Eimac[41], and the hybrids from Merrimac.[42] The output directional couplers and additional isolation to stabilize the amplifier chain is not shown.

The output power and sometimes the phase of RF amplifiers depend upon the amount of reflected power. To make the phase and power of the RF supply immune to the cabling, antenna structures and changing plasma conditions, high power ferrite isolators where purchased and installed on the outputs of the final amplifiers.[43] These devices dump reflected power to dummy loads so that the final amplifiers see a constant and almost negligible amount of reflected power. In the event of sustained large reflection, the isolator dummy loads included temperature sensors capable of detecting thermal overload and shutting down the RF supply. Output and reflected power could be monitored with high power directional couplers on the output of the final amplifiers.

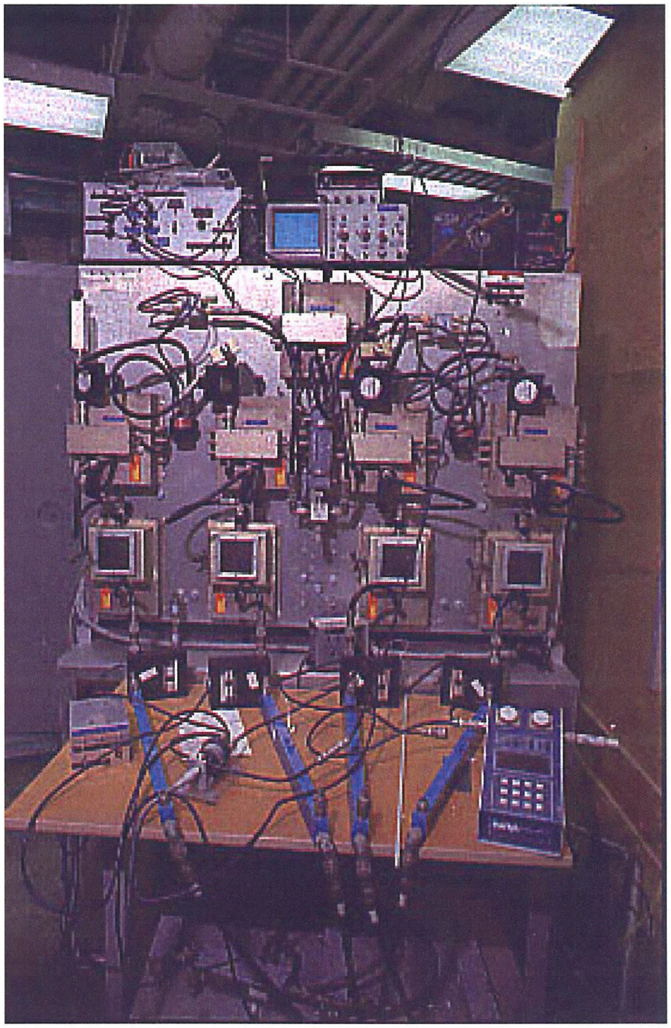

Figure 5-20. The four channel RF power supply used for the LHCD experiments. On the table are directional couplers for measuring forward and reflected power (long blue devices).

Quadrature hybrid modules employed in the low power sections of the amplifier chains gave nominal output phasing at 0, 90, 180 and 270 degrees. Due to the phase shifts inherent in the antenna, other phases were required. Phasing was accomplished with the addition of phase shift modules. Cable delays in the low power sections were also occasionally employed. At 450MHz, the wavelength in air is about 67cm. The wavelength is roughly 2/3 of the vacuum value in the coax dielectric. These distances make cable phasing a very reasonable alternative.

The OSHA average continuous exposure limit for RF radiation at frequencies from 10MHz to 100GHz is 10mW/cm^2. Using a Narda-8611 survey meter with the 0.3-26GHz probe, no average exposure was measurable on the lowest scale (0.1mW average power) near any of the equipment. Window ports on the tokamak were checked as well as the antenna structure, cabling and RF supply. Conditions involving plasma as well as no plasma were checked. With a spectrum analyzer and a loop of area 1 cm^2 on the end of coax, instantaneous levels as high as roughly 7 mW/cm^2 were observed very close to the air cooling intakes on the final RF output cavities. Since the duty factor was generally 0.04 or less, the average power was considerably less. A small fluorescent lamp was often carried around to detect any gross RF leakage, but none was ever seen.

The passive RF hardware was not immune to failure. In one incident, an audible "ticking" sound was heard coincident with the repetitive RF bursts. The sound turned out to be a spark on the RF connector of one of the high-power directional couplers. The connector was defective and was repaired.

RF Plasma Probes

Considerable amounts of data were collected with the use of plasma probes, which were scanned across minor cross sections of the Encore plasma. In this section aspects of the construction of these probes is given, and their function is discussed.

Basic construction of the plasma probes involves telescoping cylinders of stainless steel and alumina with a central conductor of tungsten wire. The construction aims to produce coax protected by an outer cylinder of alumina as shown in Figure (5-21).

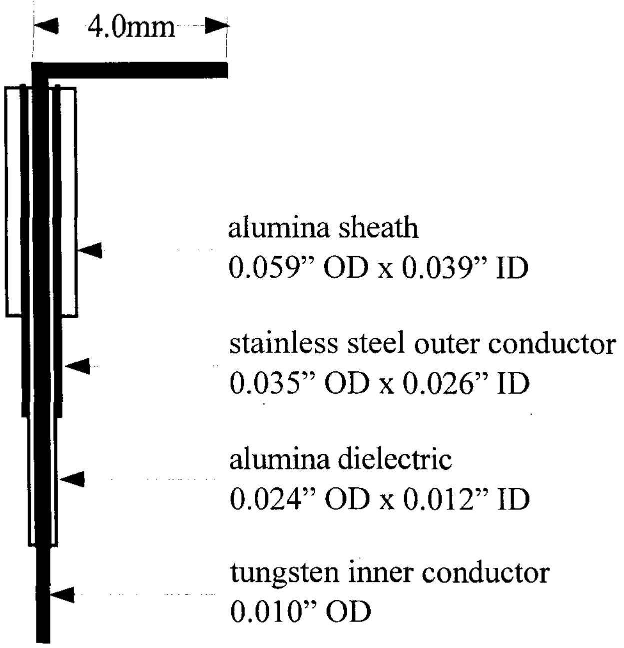

Figure 5-21. Cut away view of end of RF plasma probe, not to scale. The alumina sheath is 25cm long. The exposed tungsten is treated with a tesla coil to remove sharp edges.

Tungsten wire and alumina are chosen for their resistance to sputtering. Alumina has one of the lowest sputtering yields of any known material.[44] The sputtering threshold for tungsten is 33eV[45] and is considerably greater than a typical plasma temperature in Encore ($\approx 10\text{eV}$). Of the elemental metals, only rhenium at 35eV has a higher sputtering threshold. Plasma in Encore typically involves atomic or molecular species that are not fully ionized. As such, the plasma temperature is clamped close to the ionization potential of the tokamak fill gas. For argon this is 15.8eV and for hydrogen is 13.6eV.

The exposed portion of the tungsten wire is bent over at 90° and in the plasma is oriented parallel to the toroidal magnetic field. See Figure (5-22). The reason for this is as follows. From equation (4.78)

$$\frac{k_\perp^2}{k_\parallel^2} = \frac{\lambda_\parallel^2}{\lambda_\perp^2} = -\frac{P}{S} >> 0. \qquad (5.22)$$

Except at the plasma edge, the ratio -P/S is a large positive number. This implies that $\lambda_\parallel >> \lambda_\perp$. Thus LH wave phase variations along the toroidal field are slower than perpendicular to the toroidal field. Increases of probe area to increase sensitivity should therefore be along the toroidal field rather than perpendicular to it.

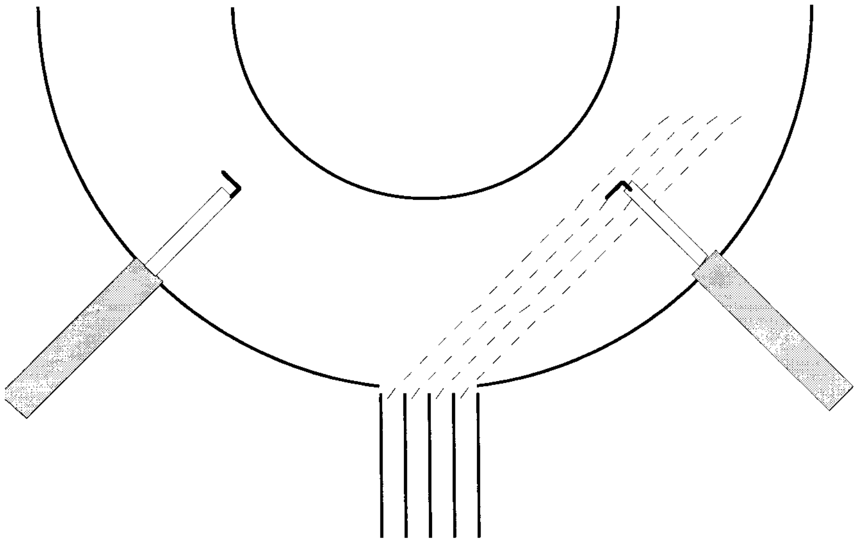

Figure 5-22. Schematic layout of the grill antenna and RF plasma probes. The probes can be scanned over the two-dimensional minor cross section.[46] In addition, the probes can be moved to any port around the tokamak. On Encore there are 20 ports around the outer circumference, located every 18°.

The central conductor of the RF plasma probes is floating. Capacitive coupling allows high frequencies to pass unimpeded down 50-ohm cable to a power detector, often a spectrum analyzer. As discussed in the LH theory section, LH waves in Encore are electrostatic. Wave energy is carried primarily by particle motion rather than by electric or magnetic fields. The electrostatic field is generated by ion density fluctuations oscillating along **k**. The electrons circle around **k** without producing a density gradient. What the probe sees is an ion density varying at 450MHz.

According to elementary gas-kinetic theory, the number of particles of a given species Γ crossing per unit area per unit time (from one side only) is[47]

$$\Gamma = \frac{1}{4} n \bar{v}, \qquad (5.23)$$

where $\bar{v}$ is the mean particle speed. For comparable electron and ion temperatures, the mean speed of the electrons is much greater. The mean electron current greatly exceeds the mean ion current and the floating probe potential is negative. From (5.23) the ion current is proportional to the ion density, which includes a component fluctuating at 450MHz. Since the mean floating potential does not change, the plasma sheath surrounding the probe does not change and the frequency response is limited only by the capacitance of the probe. Since the capacitance is likely of the order of one picofarad, the frequency response is probably limited to something like

$$\frac{1}{\mathrm{RC}} = \frac{1}{(50\,\mathrm{ohms})(10^{-12}\,\mathrm{farad})} = 20\,\mathrm{GHz}. \tag{5.24}$$

If the ion density fluctuations become large enough, the assumption that the plasma sheath remains unaffected may become false. It is assumed, however, that the signal level detected varies monotonically with the wave power. In this case, the location of the LH wave power in the scanned minor cross section can be unambiguously identified.

Two-Sided DC Probe

Some data was taken with a Two-sided current collecting probe shown in Figure (7-23). The purpose of this probe was to discriminate direction of electrons moving at high speed along the toroidal field. Each of the two exposed pieces of tungsten wire intercepts toroidal magnetic field lines from a direction opposite that of the other. The wires are biased negatively so that they collect ion saturation current. When bombarded by fast tail electrons, electrons are collected despite the negative bias. This flow of electrons can dwarf the ion saturation current. Hence, toroidally accelerated electrons can be detected and their direction ascertained. By varying the probe bias, some information regarding the electron energy can be obtained. The electron cyclotron radius is given by

$$r_c^e \cong 3.4 \cdot \frac{\sqrt{T_e}}{B_{\mathrm{gauss}}}\,\mathrm{cm}. \tag{5.25}$$

For B_{gauss}=1300 gauss and T_e=100eV, equation (5.25) returns $r_c^e \cong 0.026\,\mathrm{cm}$. This is about 0.010" and too small for an electron to "hop" around the alumina separating the two tungsten wires. On the other hand, for argon ions with T_i=3eV, $r_c^{Ar} \cong 1.2\,\mathrm{cm}$ and ions could pass around the alumina shield separating the two wires.

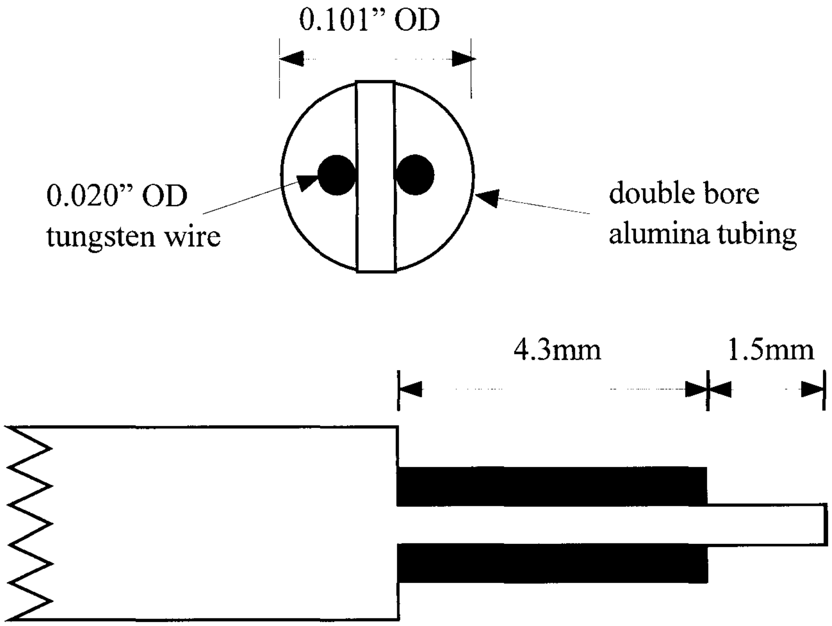

Figure 7-23. Schematic of the end of a two-sided current collecting probe used to determine tail-electron direction. In the plasma, the two tungsten wires lie in the same horizontal plane and are oriented perpendicular to the toroidal-field. In this manner, each tungsten wire intercepts hot tail electrons from a single toroidal direction.

Phase Measurements

The inherent phase delays in the individual waveguides must be measured so that the grill antenna can be properly phased to launch (as nearly as possible) unidirectional LH waves. Phase delay in cabling and passive components such as directional couplers must also be known. Calculations for these quantities cannot be considered reliable.

Initially, phase measurements were attempted with small electric-dipole probes maneuvered in front of the grill antenna. Reproducibility was a problem. The electric probes were particularly sensitive to motions and positions of objects in the vicinity. The exact position of the probe was important. The measured phase could vary by up to ± 20° depending on the position. In order to measure the phase at the end of one of the central waveguides, a cable connected to the dipole antenna crossed in front of other waveguides, altering the boundary conditions.

A magnetic-coupled loop antenna proved to be much more reliable, and was totally insensitive to motion of nearby objects. More importantly, it was insensitive to the exact position of the loop. In addition, the cable connected to the loop could be made to approach the open end of the waveguide without crossing in front of other waveguides. Further reproducibility was obtained by enclosing the magnetic pick-up loop as well as the end of the grill antenna in a box of RF absorbing foam.

Originally, a pair of mixers and a local oscillator was used to display a sinusoidal waveform on an oscilloscope, from which the phase could be measured. Later, a vector voltmeter was used to obtain more precise measurements. The vector voltmeter measurement scheme was capable of determining phase to ± 5°. A schematic of the phase measurement arrangement is shown in Figure (5-24). The phase shifts of cabling and directional couplers could be determined by adding them between the RF source and antenna and noting the additional phase lag.

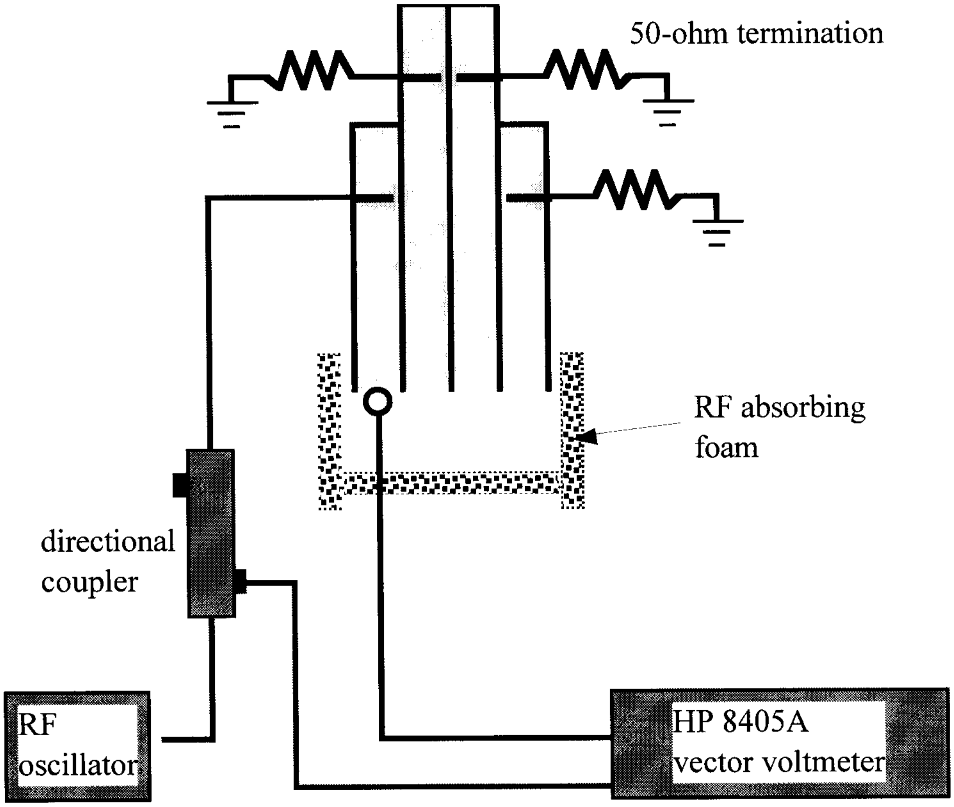

Figure 5-24. Set up for determining phase delay in the individual waveguides of the grill antenna.

The vector voltmeter could not be used for checking the phase of the high-power RF system due to the pulsed output. Measurements of the RF supply phase were made with the oscilloscope system.

---

[1] R. J. Briggs et al., "Transport of energy to the lower hybrid resonance in an inhomogeneous plasma," Phys. Rev. Lett., **29**, (1972), p. 852

[2] P. Lallia, "A LHR slow wave launching structure suited for large toroidal experiments," 1974 Topical RF Conference, Texas, p. C3-1

[3] M. Brambilla, "Slow-wave launching at the lower hybrid frequency using a phased waveguide array," Nuc. Fus., **16**, (1976), p. 47

[4] S. Bernabi et al., "A theoretical and experimental study of plasma-wave coupling and propagation using phased waveguide arrays and electrostatic structures," PPPL-1288, Sept. 1976, Princeton U., Plasma Physics Laboratory, Princeton, NJ

[5] V. Krapchev et al., "Waveguide array excitation of lower hybrid fields in a tokamak plasma," Nuc. Fus., **18**, (1978), p. 519

[6] O. N. Scherbinin et al., "effect of wall corrugations on the lower hybrid wave spectrum of a waveguide array," Nuc. Fus., **19**, (1979), p. 1675

[7] V. B. Krapchev et al., "Non-linear coupling of lower-hybrid waves at the edge of tokamak plasmas," Phys. Rev. Lett., **46**, (1981), p. 1398

[8] J. Rodney et al., "Multipactor in the Brambilla grill," Proc. of the IEEE, **70**, (1982), p. 203

[9] F. Gardiol, "Open-Ended Waveguides: Principles and Applications," in Advances in Electronics and Electron Physics, vol. **63**, (1985), p. 139

[10] J. Preinhaelter, "Optimization of the muti-junction grill for lower hybrid current drive," Nuc. Fus., **29**, (1989), p. 1729

[11] P. Lallia, "A LHR slow wave launching structure suited for large toroidal experiments," 1974 Topical RF Conference, Texas, p. C3-1

[12] Fields and Waves in Communication Electronics, Ramo, Whinnery and Van Duzer, (1965) John Wiley & Sons, p. 289

[13] R. E. Collins, Field Theory of Guided Waves, 2nd edition, (1991) IEEE Press, p. 483

[14] Fields and Waves in Communication Electronics, Ramo, Whinnery and Van Duzer, (1965) John Wiley & Sons, p. 421

[15] Eccoflo HiK free flowing dielectric powders, dissipation factor 0.0007, density 2.70 gm/cc, $\varepsilon = 12$, Emerson & Cuming, Inc., Canton, MA 02021

[16] Stycast 35D, dielectric casting resin, dissipation factor 0.002, Emerson & Cuming, Inc., Canton, MA 02021

[17] F. Sporleder and H. Unger, Waveguide tapers, transitions and couplers, (1979) Institution of Electrical Engineers, London, p. 2

[18] R. A. Waldron, "The theory of reflections in a tapered waveguide," The Radio and Electronic Engineer, Oct. 1966, p. 245

[19] F. Sporleder and H. Unger, Waveguide tapers, transitions and couplers, (1979) Institution of Electrical Engineers, London, p. 2

[20] Montgomery, Dicke and Purcell, principles of Microwave Circuits, (1948) McGraw-Hill, p. 168

[21] Stycast HiK 500F, high temperature, high dielectric constant stock, dissipation factor < 0.002, dielectric strength > 300 volts/mil, Emerson & Cuming, Inc., Canton, MA 02021

---

[22] Stycast HiK cement, dissipation factor 0.01, $\varepsilon = 20$, Emerson & Cuming, Inc., Canton, MA 02021

[23] Robert E. Collin, Field Theory of Guided Waves, 1st edition, McGraw-Hill, NY, (1960), p. 266

[24] Robert E. Collin, Field Theory of Guided Waves, 1st edition, McGraw-Hill, NY, (1960), p. 270

[25] Fields and Waves in Communication Electronics, Ramo, Whinnery and Van Duzer, (1965) John Wiley & Sons, table 8.09, p. 444a

[26] G. W. Pierce, Phys. Rev., **2**, (1985), p. 99, (claim 12 kV/3.5mm)

[27] UG 496/U, Amphenol 82-92

[28] J. R. Whinnery et al., "Coaxial-Line Discontinuities," Proc. of the I.R.E., (November 1944), p. 695

[29] "Combat-BN Coatings" available from Carborundum Corporation, 168 Creekside Drive, Amherst, NY 14228

[30] V. Krapchev and A. Bers, "Wave-guide Array Excitation of Lower Hybrid Fields in a Tokamak Plasma," Nuc. Fus., **18**, 1978, p. 519

[31] M. Brambilla, "Slow Wave Launching at the Lower Hybrid Frequency using a Phased Wave-guide Array," Nuc. Fus., **16**, 1976, p. 47

[32] V. Krapchev et al., "Waveguide array excitation of lower hybrid fields in a tokamak plasma," Nuc. Fus., **18**, (1978), p. 519

[33] P. Lallia, "A LHR slow wave launching structure suited for large toroidal experiments," 1974 Topical RF Conference, Texas, p. C3-1

[34] "Dielectric Materials Chart," Emerson & Cuming, Inc., Canton, MA 02021, 1975

[35] Fields and Waves in Communication Electronics, Ramo, Whinnery and Van Duzer, (1965), John Wiley & Sons, p. 289

[36] Fields and Waves in Communication Electronics, Ramo, Whinnery and Van Duzer, (1965), John Wiley & Sons, p. 426, 444a

[37] Antennas in Matter, R. King and G. smith, MIT Press 1981, p. 740

[38] Antennas in Matter, R. King and G. smith, MIT Press 1981, p. 741

[39] The basic construction was largely carried out by Frank Cosso. The author of this thesis was extensively involved in the debugging required to make the RF supply operational.

[40] Micon Inc., Ferrite Control Div., 1105 Industrial Parkway, Bricktown, New Jersey 08723

[41] Varian, Eimac Division, 301 Industrial Way, San Carlos, California 94070

[42] Merrimac Industries, Inc., 41 Fairfield Place, West Caldwell, NJ 07006

[43] R. O. Collado et al., "Specification of high-power ferrite circulators," in Microwaves & RF, November, (1987), p. 107

[44] Brian Chapman, Glow Discharge Processes, John Wiley & Sons, NY, (1980), p.379, p. 396

[45] Brian Chapman, Glow Discharge Processes, John Wiley & Sons, NY, (1980), p.394

[46] E. Fredrickson, "An experimental and theoretical investigation of a finite beta modified drift wave," Thesis, Caltech (1985), p. 5

[47] I. H. Hutchinson, principles of Plasma Diagnostics, Cambridge University Press, NY, (1987), p. 51

6 Data from Ohmic Plasmas

The Encore tokamak produces repetitive and highly reproducible ohmically generated target plasma for LHCD. The plasma is well characterized and the magnetic field and density can be easily varied. LH waves were launched with the solid dielectric antenna into plasmas with a variety of plasma parameters in order to verify LH accessibility, propagation angle and antenna phasing asymmetry. High power LH waves were launched in attempts to generate significant changes in plasma current.

Low Power Measurements

Early measurements verified that proper antenna phasing can launch directional plasma waves and verified the propagation-angle dependence on the toroidal magnetic field expected of lower-hybrid waves. The antenna utilized was the first antenna model discussed in chapter 5, which is shown in Figure (5-2) at the far left. This antenna had identical phase delays for all four ports and setting the phase was particularly simple. The RF power supply is shown schematically in Figure (6-1) and automatically generates the directional quadrature phasing.

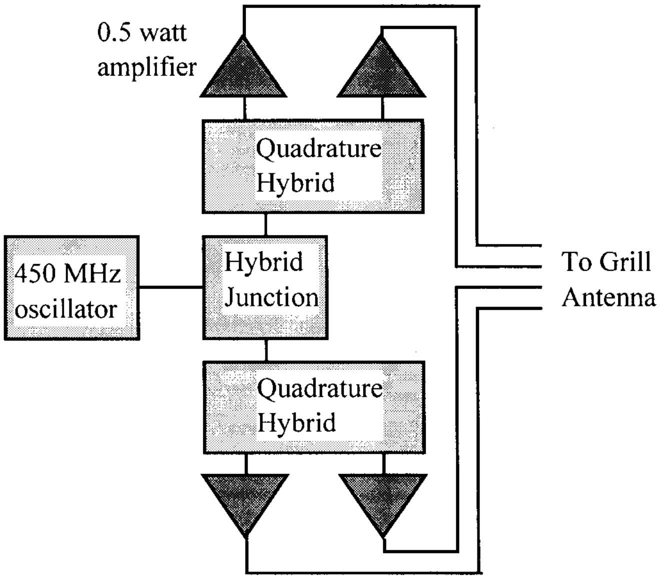

Figure 6-1. Low power (2-watt) RF supply for launching signal-level LH waves with quadrature phasing from a 4-port grill antenna.

The experimental arrangement is shown in Figure (6-2). Two linear RF-probes operating in the tokamak mid-plane are located on either side of the grill antenna. The probes scan parallel to major radii of the torus.

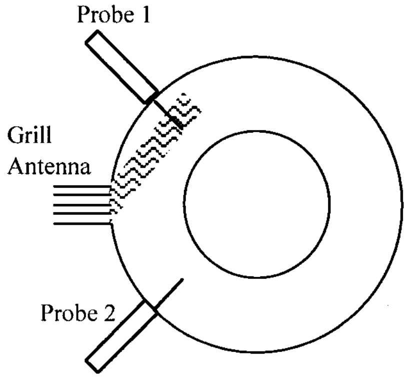

Figure 6-2. Experimental arrangement for launching and detecting signal level LH waves in Encore.

The grill antenna excited a cavity mode in the torus that could obscure the plasma wave signal. Using a "boxcar" sampling device to look for the LH wave during a specific portion of the plasma shot was found necessary. The detection electronics is shown schematically in Figure (6-3). Capacitive coupling prevented DC probe voltages from damaging the RF electronics. The low pass filter eliminated any constant RF signal such as RF broadcast from other installations.

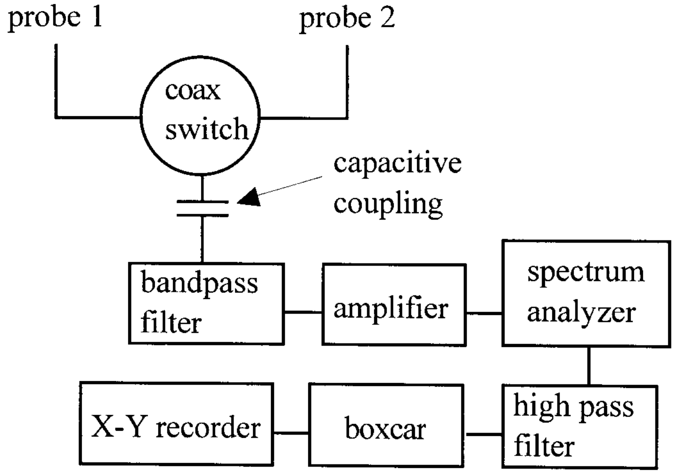

Figure 6-3. Schematic of electronics used for signal level detection of lower hybrid waves in Encore.

Data showing directionality is given in Figure (6-4). The toroidal magnetic field was 345 gauss, allowing deep penetration of the LH waves. The coils generating the vertical magnetic field on Encore were often configured to simultaneously produce a radial-horizontal magnetic field to null out magnetic errors in the toroidal magnetic field. It was found necessary to keep the vertical and radial-horizontal coil currents identical to obtain reproducibility. The probes are not unidirectional. LH waves impinging from either toroidal direction or from multiple toroidal revolutions in the same direction are detected. LH wave damping is necessary to demonstrate the directionality. Better than 10dB of directionality was noted in the probe measurements.

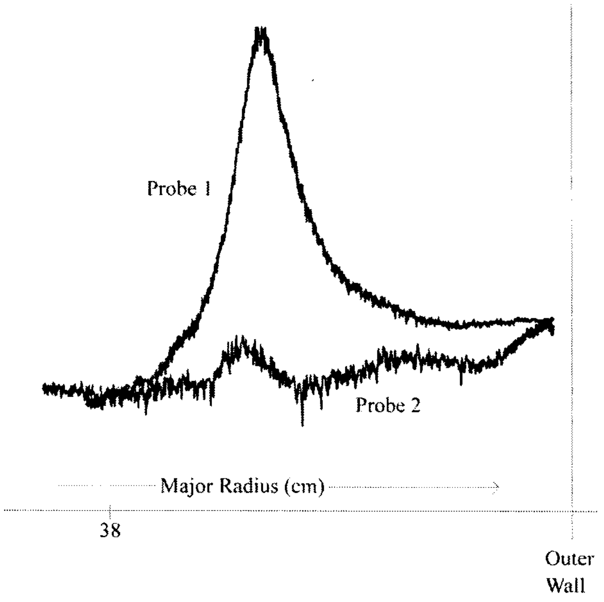

Figure 6-4. RF-voltage versus position in major radius for the two probes located on either side of the grill antenna. With quadrature phasing better than 10dB directionality was noted.

The propagation angle of LH waves with respect to the toroidal magnetic field is given by equation (4.89). The angle is inversely proportional to the magnitude of the magnetic field and independent of plasma density. The LH waves are launched from the grill antenna located on the tokamak outer wall. Faster penetration into the torus is expected for lower magnetic fields. This is indeed seen in the probe measurements, providing confirmation that LH waves are being launched and observed. See Figure (6-5).

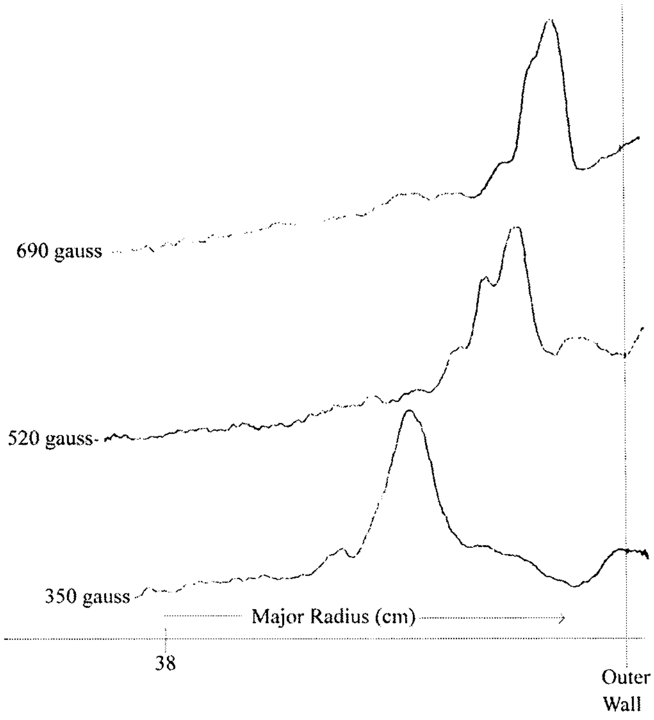

Figure 6-5. RF-voltage versus position in major radius for three different toroidal magnetic fields. The location of the peaks moves as expected for LH wave propagation.

Set-Up for Measurements with the Solid Dielectric Antenna

Considerable data was taken using the solid dielectric antenna and an X-Y probe capable of scanning a square inscribed in the minor cross section of Encore. The arrangement of the antenna and X-Y probe on the tokamak is shown schematically in Figure (6-6). The probe and antenna are separated by 45 degrees in the toroidal direction. The grill antenna was phased to launch LH waves preferentially in the counter clockwise direction, which is the direction in which electrons are accelerated by the ohmic supply. Data taken on the side of the antenna to which LH waves are preferentially launched are denoted "downstream" data. To obtain data on the "upstream" side of the antenna, the positions of the antenna and probe were swapped, using the same two ports. The RF power to the four channels was 260, 240, 250, and 270 watts, for a combined total of 1.2kW. The tokamak was filled with argon to a pressure of 5.0×10^{-5} torr. The vertical magnetic field was varied to maximize the plasma current and its stability.

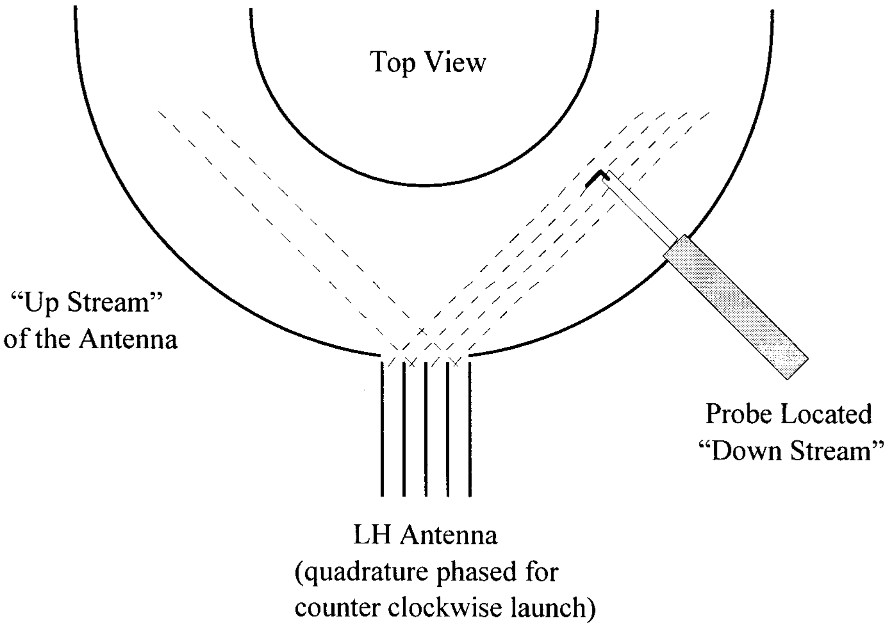

Figure 6-6. Experimental arrangement of the antenna and X-Y probe. To obtain the "upstream" data, the positions of the antenna and probe were reversed, using the same two ports.

The orientation of the data plots is described in Figure (6-7). The grill antenna is installed in a port on the outer wall. Consequently, plasma waves are generated near the outer wall and then propagate to other locations in the minor cross section. Accessibility limits the depth of penetration, and the LH propagation angle affects the rate of penetration into the plasma. The physical size of the scanned square was measured as 16cm by 16cm. The diagonal of this square is 22.6cm and is close to the diameter of the minor cross section (24cm).

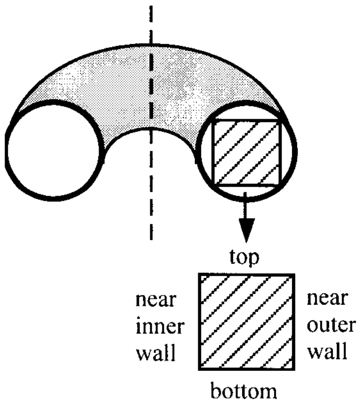

Figure 6-7. Description of the orientation of the X-Y data plots.

The electronics used to collect the data is shown in Figure (6-8). Due to the large plasma wave power utilized, the set up is somewhat simplified from that required for signal level measurements. The spectrum analyzer was tuned to 450MHz by inputting the oscillator signal driving the high power RF supply. The computer controls the position of the probe which stops at 32 by 32 positions per scan to take data.

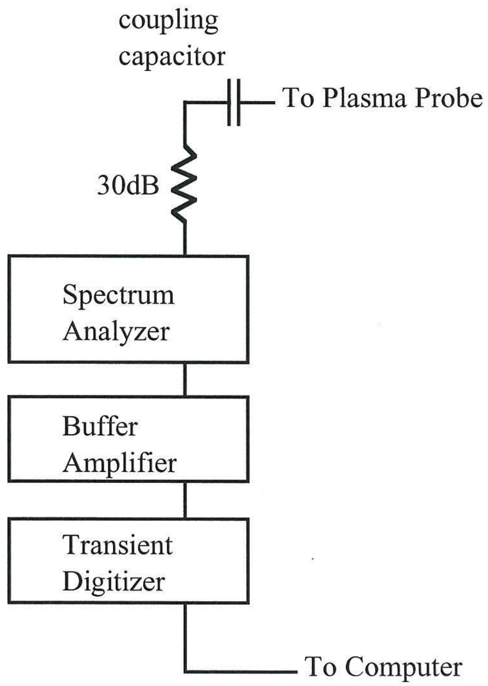

Figure 6-8. Electronics used in taking the two-dimensional data arrays of plasma wave power.

The data is displayed with a color-coding for relative RF power level. The scale is two and one-third dB per color and there are ten colors. The color code is displayed in Figure (6-9). Any data outside of the 23.3dB range is aliased into the nearest color range. Care was taken to avoid aliasing into the top green bin through proper choice of the reference level.

Figure 6-9. Color code for the X-Y data plots. The scale is 2 and 1/3 dB per color. Power increases from left to right. Green colors represent large RF power.

Data from the Solid Dielectric Antenna

Due to the antenna phasing, LH waves are preferentially launched in the counter-clockwise direction as seen from above. When the RF-probe is located slightly counter-clockwise from the antenna it is considered "downstream." Two matrices of data where taken. One matrix is with the RF-probe located downstream of the antenna, the other with the RF-probe located upstream of the antenna.

Plasma currents utilized were 0.25, 0.50, 0.75. 1.00, 1.25, 1.50, 1.75, and 2.00 kilo-amps. Toroidal magnetic fields utilized were 345, 518, 690, 863, 1040, 1210 and 1360 gauss, measured at the axis of the minor cross section. The individual matrices involve all possible combinations of plasma current and toroidal magnetic field. Rows are associated with specific plasma current; columns are associated with specific toroidal magnetic field. Higher rows are associated with higher plasma current. Columns further to the right are associated with larger toroidal magnetic field.

Plasma density is roughly proportional to plasma current in Encore. Figure (6-10) shows data of this nature.[1] This means that in the matrix of plotted data, plasma density can be assumed to be greater in higher rows. Plasma current increases monotonically with the ohmic power. Since argon plasma in Encore is not fully ionized, it is reasonable to expect that the degree of ionization and thus plasma density will increase monotonically with ohmic power and thus with plasma current.

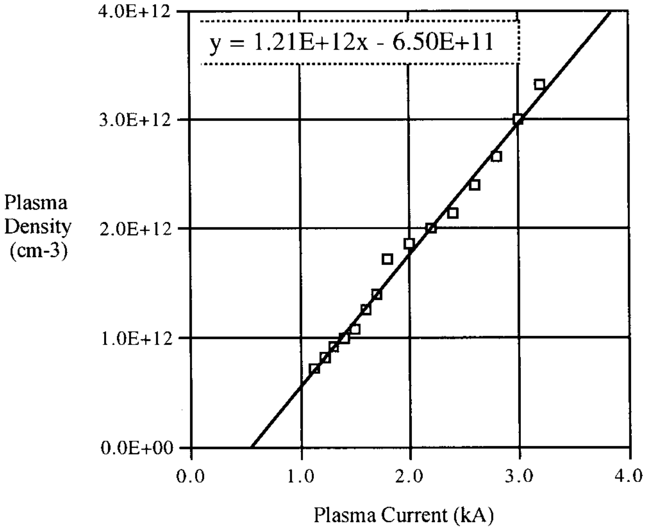

Figure 6-10. Data showing that plasma density in Encore is roughly proportional to plasma current.

Plasma in Encore at large minor radius where the grill antenna is located is not always "smooth." The RF power reflected from the antenna is seen to drop when plasma is present. The drop in reflected power is not steady but can show quite a bit of temporal structure. The reflected power from one channel of the grill antenna is shown in Figure (6-11). The plasma parameters were 345-gauss and 250-amps. Similar but less dramatic oscillations were noted at 1 kilo-amp and 518-gauss. The structure of the plasma changes with changes in the plasma current and toroidal field. These structure changes in turn affect the antenna/plasma coupling. The oscillations shown in Figure (6-11) are probably due to naturally occurring drift waves in the plasma.[2]

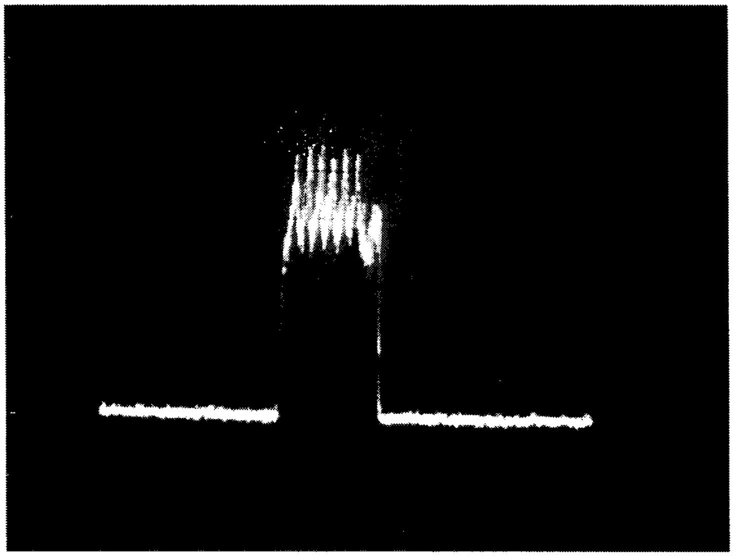

Figure 6-11. Oscillations in the reflected power from one channel of the grill-antenna. The plasma parameters are 250-amp current and 345-gauss toroidal field. The vertical scale is 10dB per division. The horizontal scale is one millisecond per division.

The matrices of data are shown on the following three pages. For reference, the plasma current and toroidal magnetic field vary across the matrices as in Table (6.1).

	345G	**518G**	**690G**	**863G**	**1040G**	**1210G**	**1360G**
2.00 kA	☐	☐	☐	☐	☐	☐	☐
1.75 kA	☐	☐	☐	☐	☐	☐	☐
1.50 kA	☐	☐	☐	☐	☐	☐	☐
1.25 kA	☐	☐	☐	☐	☐	☐	☐
1.00 kA	☐	☐	☐	☐	☐	☐	☐
0.75 kA	☐	☐	☐	☐	☐	☐	☐
0.50 kA	☐	☐	☐	☐	☐	☐	☐
0.25 kA	☐	☐	☐	☐	☐	☐	☐

Table 6.1. Plasma current and the magnetic field on the toroidal axis for the arrays of plots shown on the following pages.

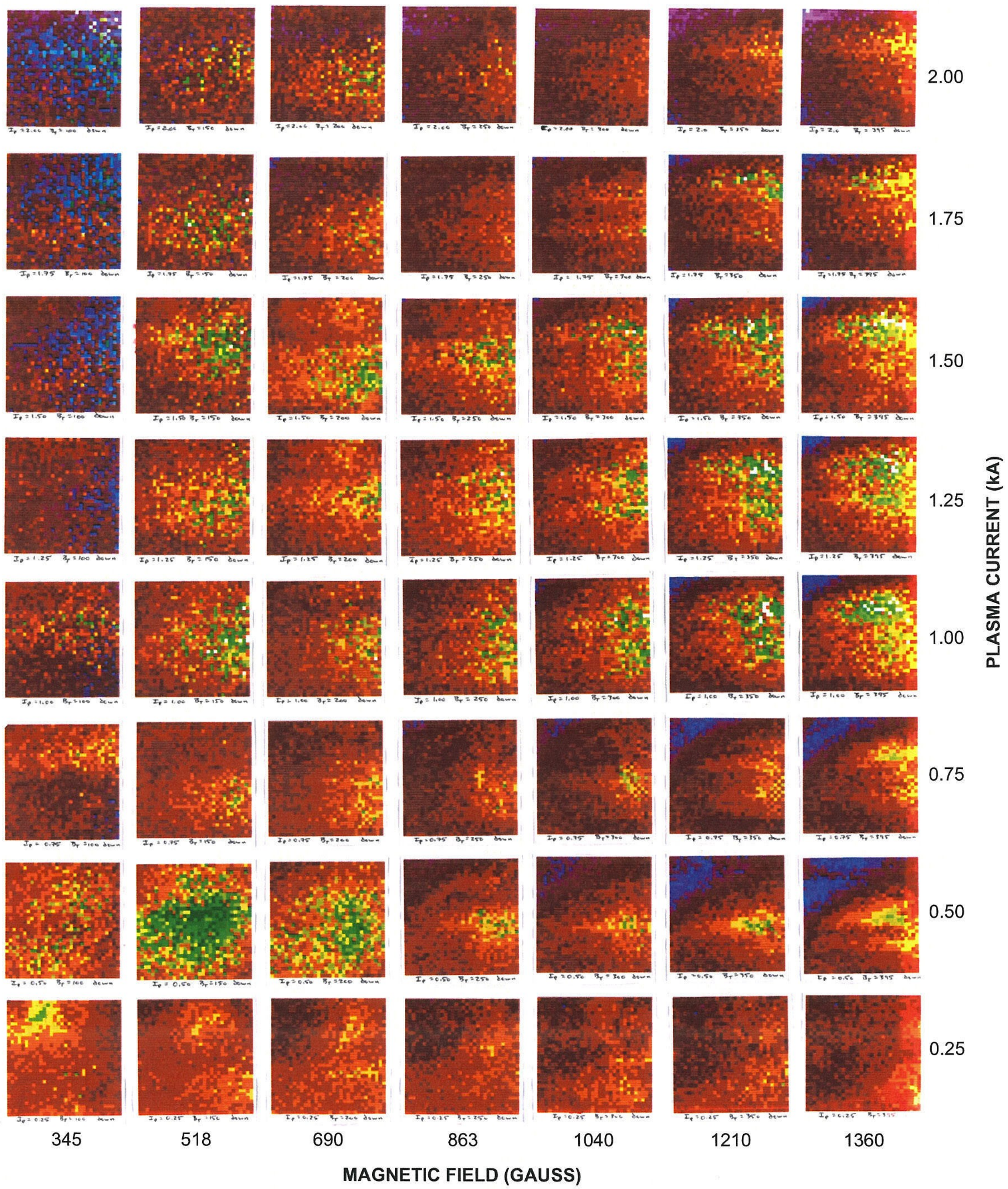

Figure 6-12a. Downstream data.

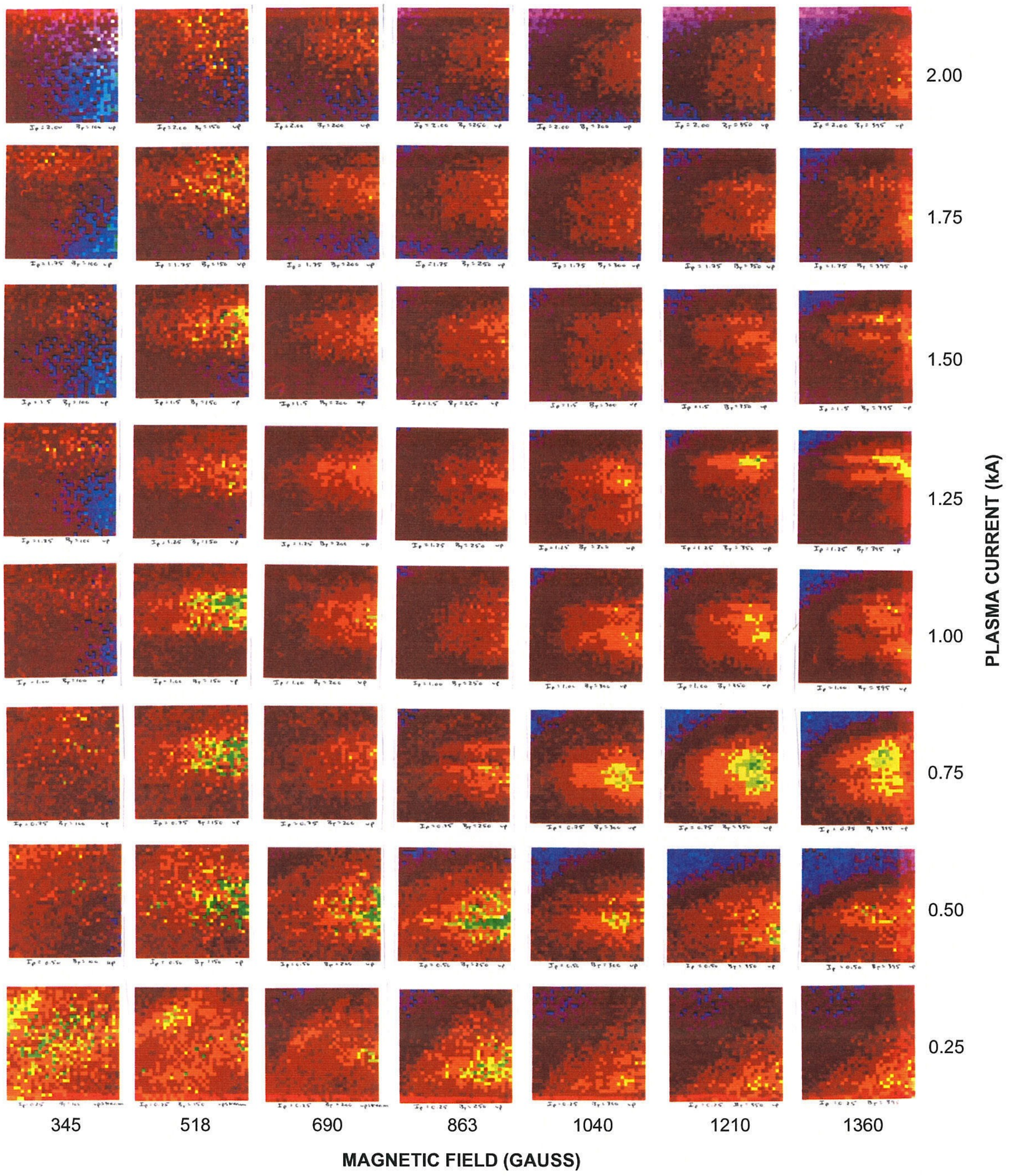

Figure 6-12b. Upstream data.

Verification of LH Wave Accessibility

In Figure (4-7) the $N_{||}$ accessibility limit is plotted versus the major radius for various toroidal magnetic fields, assuming a line average plasma density of 2×10^{12} cm^{-3}. Graphs specifically applicable to the matrices of data are given below. The major radius is measured from the center of the minor cross section. Thus R=0 corresponds to the center of the minor cross section. Each curve corresponds to a particular toroidal magnetic field. The toroidal fields on axis are 345, 518, 690, 863, 1040, 1210, and 1360 gauss. For a given major radius, the curves are monotonically lower in value as the magnetic field is increased.

The 1/R dependence of the toroidal magnetic field upon the major radius is included in the calculations. The plasma density profile in Encore is known to be flatter than parabolic.[3] A semi-circle plasma density profile is assumed. The line average density is obtained from the data in Figure (6-10). The linear fit in Figure (6-10) does not have a zero intercept, and there is no data below one kiloamp. The line average densities for plasma currents below one kiloamp were estimated from an extrapolation of the lowest data point linearly to zero. The line average densities used are 1.77, 1.47, and 1.17×10^{12} cm^{-3}, and 8.6, 5.6, 4.2, 2.8, and 1.4×10^{11} cm^{-3}.

The shaded regions designate the $N_{||}$ range launched by the grill antenna. The spectrum peaks at $N_{||} = 10$ (see Figure (5-15)). $N_{||}$ values equal to the accessibility limit mode convert to the fast wave and propagate back out of the plasma. $N_{||}$ values less than or equal to the accessibility limit are consequently prevented from penetrating further into the plasma. The shaded area above the center of the graph represents launched LH wave power that is capable of propagating to the center of the plasma.

The right-hand side of the plots corresponds to the outer wall of the tokamak from which the LH waves are launched. Under conditions of low toroidal magnetic field and high plasma current, it would be possible for LH waves launched near the outer wall to propagate around the periphery of the plasma and appear near the inner wall. The inner wall of the tokamak corresponds to the left-hand side of the plots. Accessibility is marginally improved near the inner wall due to the larger magnetic field at that location.

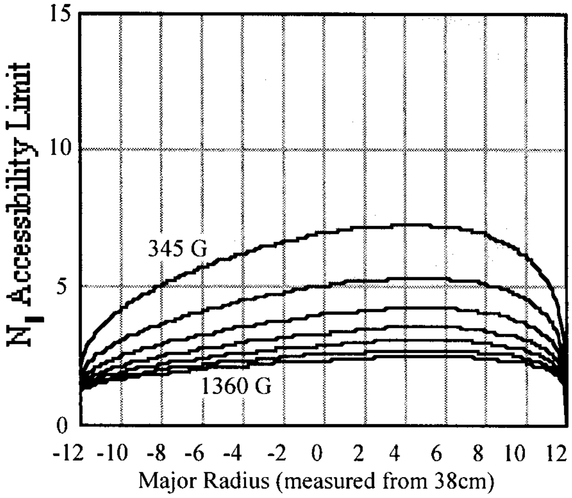

$I_P = 0.25\text{kA}$

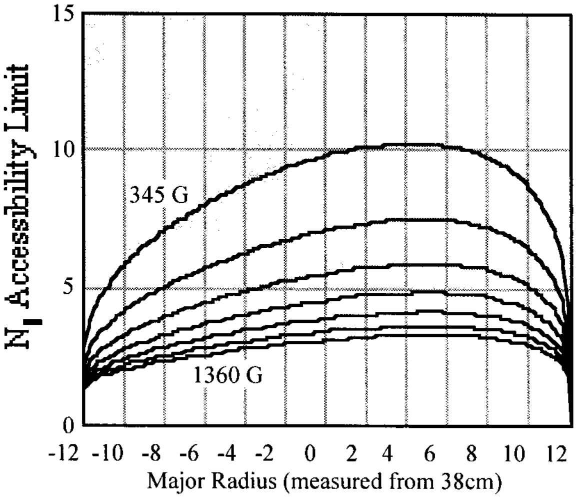

$I_P = 0.50\text{kA}$

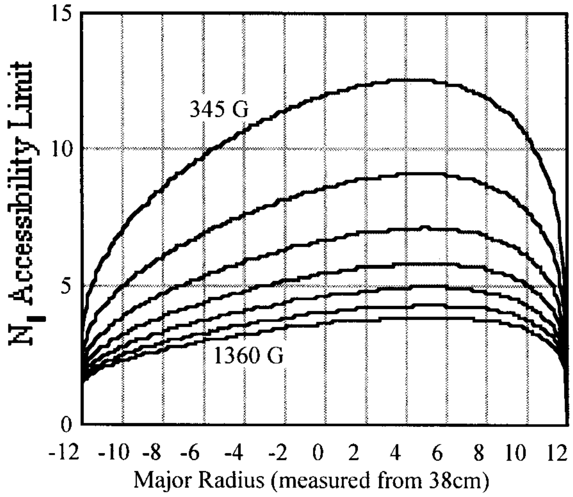

$I_P = 0.75\text{kA}$

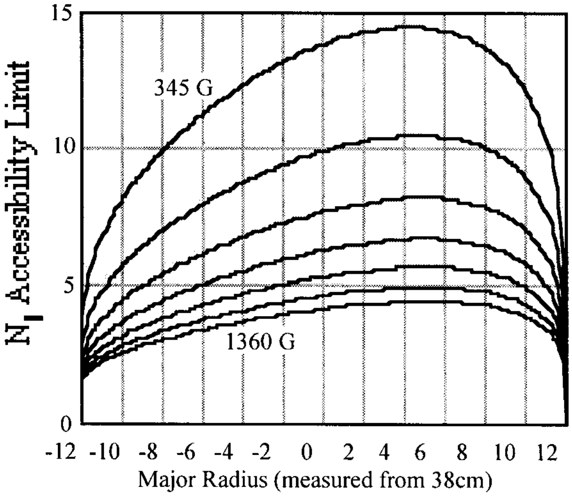

$I_P = 1.00\text{kA}$

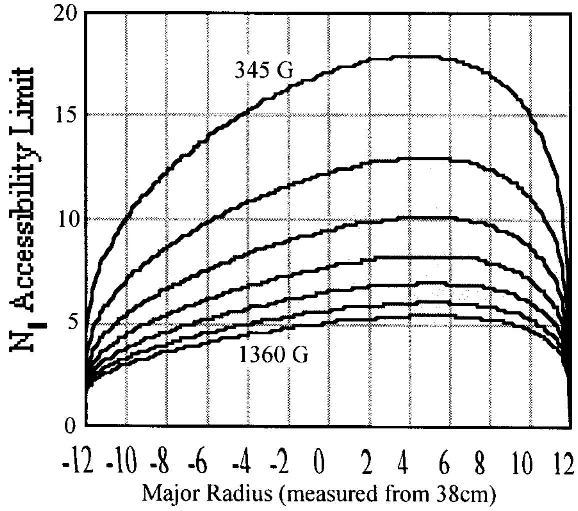

$I_P = 1.25\text{kA}$

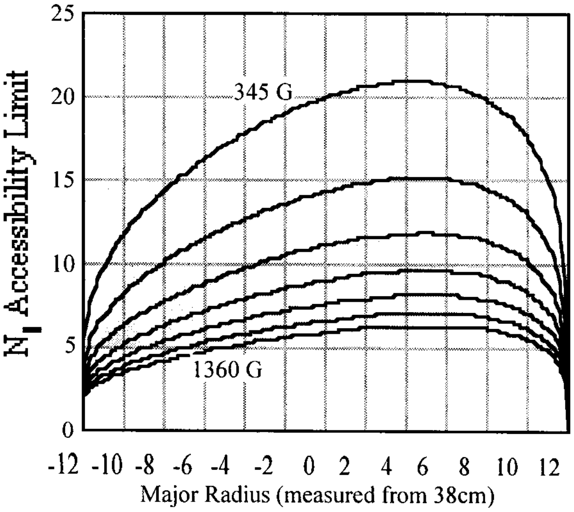

$I_P = 1.50\text{kA}$

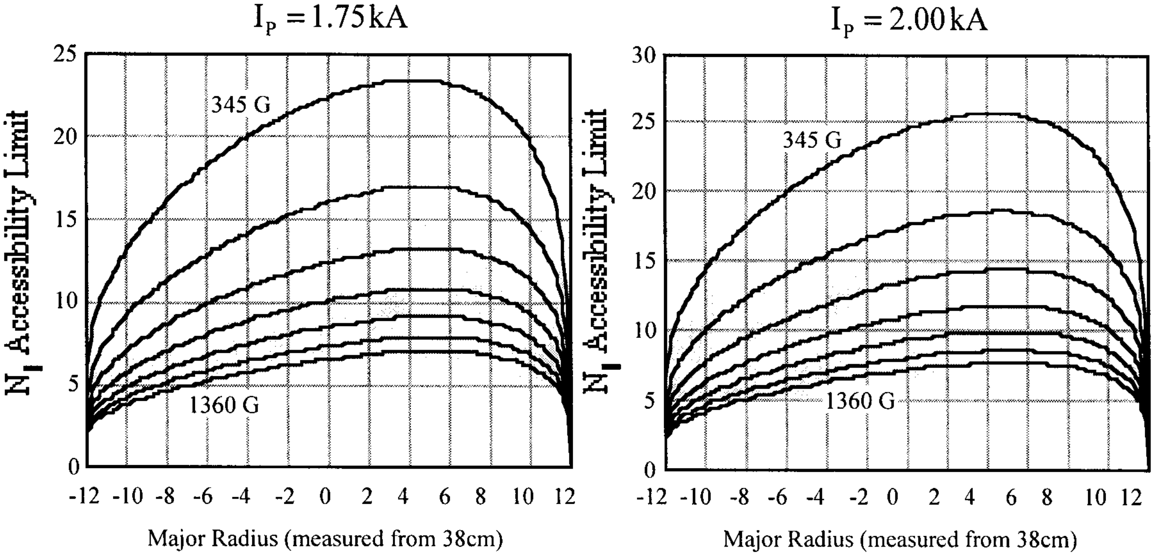

Figure 6-13. The accessibility limit $N_{\|a}$ as a function of the major radius, for various magnetic fields. The magnetic field monotonically increases from the uppermost to the lowest curve. The magnetic fields on axis are 345G, 518G, 690G, 863G, 1040G, 1210G, and 1360G respectively. The shaded region indicates a typical launch spectrum for quadrature phasing of the final LH antenna. A line average plasma density of $2.0 \times 10^{12} cm^{-3}$ is assumed.

For the lowest toroidal field (uppermost curve in each plot), only the lowest plasma current (0.25kA) shows good accessibility. This predicts that the left-hand column of plots will show little if any green regions near R=0, except possibly for the plot at the bottom. This is the case. In fact many plots in the left-hand column contain large amounts of blue, which represents the lowest power bin.

Accessibility is best for the largest magnetic fields, which corresponds to the right hand columns of the data matrices. Accessibility is also best for the lowest plasma currents, which corresponds to the lower rows of plots in the data matrices. In the downstream data matrix, most of the data plots with substantial amounts of green area (corresponding to large plasma wave power) occur in the right-hand columns or lower rows.

There are some data plots at 518 gauss and one at 690 gauss that have some regions of green pixels, despite also having substantial plasma currents of at least 1kA. These are plasmas with a large poloidal field to toroidal field ratio, and thus larger rotational transform. The $N_{||}$ spectrum will alter upon significant poloidal propagation.[4] Provided that the poloidal propagation is rapid compared to wave damping, $N_{||}$ changes should occur and accessibility would be impacted. Accessibility is so poor for the lowest magnetic field that little power can even enter the plasma, and thus have a chance for subsequent $N_{||}$ changes.

Larger $N_{||}$ at launch are preferable for improved accessibility. For a four-port grill antenna that would require narrower waveguides. That in turn would limit the total RF power available. Limiting factors include waveguide electrical breakdown, multipacting behavior and pondermotive forces upon the nearby plasma. The remedy is to have more waveguides. This dramatically increases the control of the launched $N_{||}$ spectrum, provided the ability to continuously vary the phasing to the waveguides is included.

In attempts to drive plasma current with LH waves launched into ohmic plasmas, it was consistently noted that ΔI_P was largest for smaller plasma current. This is entirely consistent with the improved accessibility at low plasma current.

LH Propagation Angle

The launched LH waves propagate at a specific angle with respect to the toroidal magnetic field. Even if the waves are accessible to the plasma interior, if they propagate inwards along too shallow a path, the power may be damped long before reaching the plasma interior. The propagation angle is given in equation (4.89) and depends only on the frequency (which is fixed) and the magnetic field. The values are given in Table (6.2). Also given in the chart is an estimate of the maximum inward deviation of a LH wave on a single pass between the antenna and probe. It is assumed that the LH wave is launched near the outer wall, and that the toroidal separation of the antenna and probe is 45°. The major radius of the outer wall is 50cm, and 45° represents a portion of the circumference measuring 39.3cm. The inward deviation is calculated as

$$\Delta R \cong 39.3\text{cm} \times \theta_{\text{radians}} \ . \tag{6.1}$$

B_ϕ (gauss)	345	518	690	863	1040	1210	1360
θ (degrees)	25°	17°	13°	11°	9°	8°	7°
ΔR (cm)	17.1	11.7	8.9	7.5	6.2	5.5	4.8

Table 6.2. Resonance cone angle and inward deviation versus magnetic field on axis.

The data plots represent a physical dimension of 16cm on a side. The minor diameter is 24cm. Hence, there is a gap of the order of 4cm between the outer wall and the right-hand side of the plots.

Consider the second row from the bottom where accessibility is good. The data plots show a clear indication that the penetration of the green areas into the plasma from the right-hand side varies in a monotonic fashion with the magnetic field. The penetration is greatest for lower magnetic field. The plot with the largest number of green pixels is the one with 518-gauss and 500-amp plasma current. This set of parameters enjoys both good accessibility and fast penetration due to a large propagation angle.

The lowest row appears anomalous in that although accessibility is excellent and for some magnetic fields the penetration should be rapid, few green areas appear. The plasma current for this row is 250-amps. From equation (3.17) the maximum confined electron velocity for a plasma current of 250-amps is 1.4×10^8 cm/sec. This corresponds to an electron-energy of only 5.6 eV. Electrons more energetic than 5.6 eV are not confined by the poloidal field. Since the ionization potential of argon is 15.8eV, electron temperatures in Encore are clamped near this value. The lowest row of data plots represents anomalous plasmas in that they are poorly confined.

For maximum magnetic field and plasma current between 1kA-1.5kA, significant penetration appears despite the small propagation angle. There is good accessibility for these plots. If LH wave damping were small, an additional toroidal revolution would add additional deviation of up to 38cm. This deviation is so large that the power could appear anywhere in the minor cross section. Because the plots appear to show wave power creeping in from the right-hand side, significant contribution to the data from more than one toroidal-propagation would be unlikely. Plasma turbulence may play a role.

Directionality due to Antenna Phasing

The phase of waveguides is such that the antenna launches power preferentially in what is called the "downstream" direction in the data. If the upstream and downstream data matrices are compared, it is immediately evident that significantly larger plasma wave power is launched downstream compared to upstream. This demonstrates that the quadrature phasing of the antenna produces an asymmetry in the $N_{||}$ spectrum just as it is supposed to do. Phasing appears to work in these ohmic plasmas.

Looking at the upstream data, few plots show yellow or green areas representing significant power. In most instances, where significant power is found upstream, even more power is detected downstream. This is evidence for the stability of the measurements and the stability of the calibration. The only plots to buck this trend lie on the third row at the three highest magnetic fields. In this case one has once again the issue that the penetration appears excessive given the propagation angle. This phenomenon has been noted at high magnetic field with plasma current between 0.75 and 1.5 kiloamp.

The RF-probe will detect power propagating from either toroidal direction. The fact that so little power is seen upstream compared to downstream is strong evidence that wave damping is sufficient to curtail contribution from paths of the order of one toroidal revolution.

Attempts to Drive Large Plasma Current

The LH grill antenna was phased to launch waves primarily in the direction of the ohmic accelerated electrons. The forward and reflected power in kilowatts to the four waveguides during plasma launch for this experiment is as follows:

Channel	0	1	2	3
Reflected	0.6	1.1	2.1	0.1
Forward	4.0	4.0	3.3	3.0

There was some difficulty with channel two during this period.

The tokamak was filled to a pressure of 3.0×10^{-5} torr of hydrogen. Target plasma with approximately 1kA ohmic current was used. The associated loop voltage was recorded as 2.5 volts giving an ohmic power of 2.5kW. However, the calibration of the loop voltage was later called into question. Judging from recorded data for other plasmas, it is highly unlikely that the ohmic power could have exceeded 10kW. The 10.5kW of RF power coupled to the plasma is comparable to if not greater than the ohmic power. In this case the plasma absorbs 73% of the RF power and only 27% is reflected. In other cases more than 75% of the power was absorbed. The toroidal field was set to 1360 gauss on axis. A pulsed vertical magnetic field was used. The data is shown in Figure (6-14). Plasma current is increased by as much as 300 amps, and the loop voltage is decreased roughly 0.4 volts (16%) upon application of RF. Other settings of the plasma parameters were tested. However, no other plasma conditions, antenna phasing, or power settings resulted in a larger current increase by as much as a factor of 2. When the phase shifters in the RF supply were slowly adjusted, the current increase could be made to decrease, but not increase. This suggests that the phasing was properly adjusted and that the current drive effects are phase sensitive.

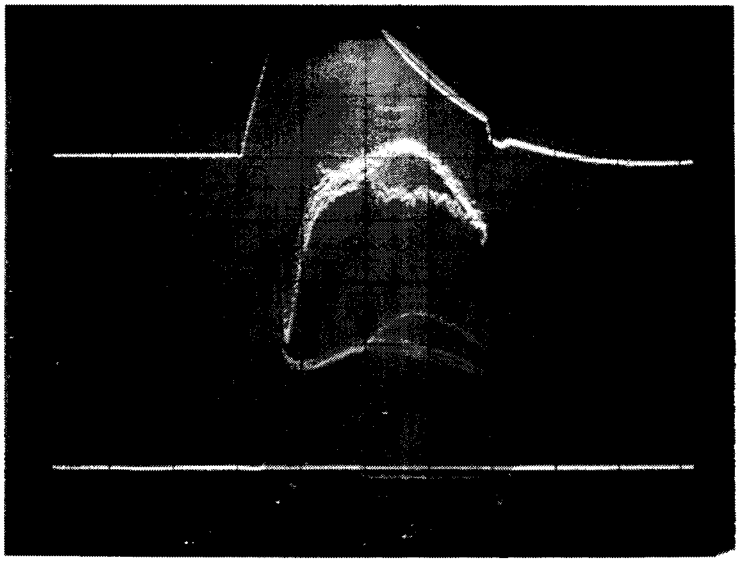

Figure 6-14. LHCD results in hydrogen. The top trace registers the vertical magnetic field. The second trace down is the loop voltage with and without RF, 0.5V per division. The third trace down is the plasma current with and without RF, 0.5kA per division. The bottom trace registers the RF timing. Horizontal scale is 1msec per division. The loop voltage is decreased, and the plasma current increased with application of RF. The traces involve superposition of many plasma shots.

The overall efficiency for current drive in Encore is of the order of

$$\frac{I_{\mathrm{amps}}}{P_{\mathrm{watts}}} \approx \frac{300\,\mathrm{amps}}{10500\,\mathrm{watts}} = 0.03\ \mathrm{amps/watt}. \tag{6.2}$$

For comparison, a LHCD experiment on PLT maintained a plasma current of 183kA with a RF power of 40kW.[5] The overall efficiency is

$$\frac{I_{\mathrm{amps}}}{P_{\mathrm{watts}}} \approx \frac{183000\,\mathrm{amps}}{40000\,\mathrm{watts}} = 4.6\ \mathrm{amps/watt}. \tag{6.3}$$

It is known that the current drive efficiency scales inversely with the plasma density[6]

$$\frac{J_{\mathrm{amps/m^2}}}{P_{\mathrm{watts/m^2}}} \propto \frac{1}{n}. \tag{6.4}$$

The PLT experiment involved a plasma density of $2.2\times10^{12}\ \mathrm{cm}^{-3}$. Experiments on Encore involved comparable or lower plasma density, so the current drive efficiency should not be less due to density effects. Many successful LHCD demonstrations at other institutions involved grill antennas comprised of four waveguides. Some other phenomenon is hindering lower hybrid current drive on Encore. It will be argued in chapter 8 that the cause of the poor current drive efficiency is related to the so-called "density limit" problem.

Similar experiments were performed with the tokamak filled with argon to a pressure of 3.5×10^{-5} torr. The results are shown in Figure (6-15). In this case, little if any effect is seen on the plasma current or loop voltage upon application of RF.

Noticeable effects in argon were evident at lower plasma current. See Figure (6-16). In this instance roughly 80 amps are driven on top of a 400-amp ohmic plasma current. The ohmic power involved is only 2kW.

The question arises as to why LHCD in argon appears weaker than in hydrogen. It was checked that the LH cone angle and the LH accessibility criteria are essentially unaffected by the change in ion mass, for the plasma parameters used.

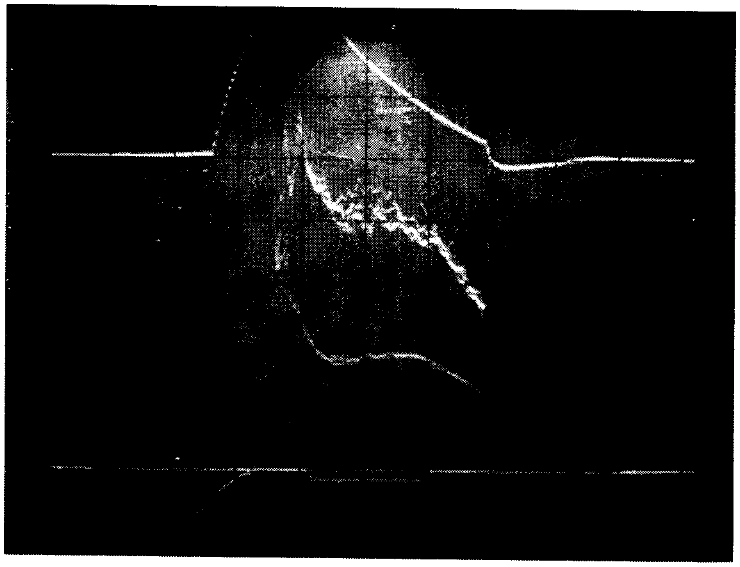

Figure 6-15. LHCD results in argon. The top trace registers the vertical magnetic field. The second trace down is the loop voltage with and without RF, 0.5V per division. The third trace down is the plasma current with and without RF, 0.5kA per division. The bottom trace registers the RF timing. Horizontal scale is 1msec per division. The traces involve superposition of many plasma shots.

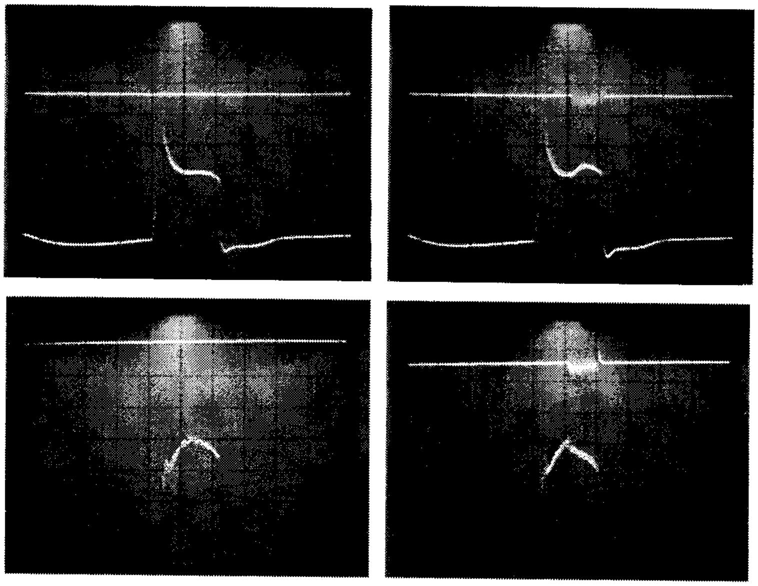

Figure 6-16. Plasma current and loop voltage changes upon RF application to an argon plasma. In all four photos, the top trace is the RF marker. The upper photos are the plasma current, 200 amps per division. The lower photos are the loop voltages, 0.5 volts per division, 5-volt total signal.

One difference, however, involves the mass density. For a given pressure, argon is twenty times as dense as diatomic hydrogen, and argon has twenty times as many total electrons per unit volume (bound and free) as hydrogen. This means that argon has twenty times the stopping power for high-energy electrons compared to hydrogen. The lower density in hydrogen has the effect of making it easier to produce high-energy electrons. In fact, when running the tokamak with hydrogen, care must be taken to avoid unnecessary x-ray exposure. X-rays are generated when the high-energy electrons collide with the chamber walls.

There are two possible effects. One is that LHCD generates high-energy electrons. The collisional lifetime of LHCD generated high-energy electrons is longer in hydrogen. The second effect is that the spectral gap between the $N_{||}$ spectrum at launch and the high-energy tail of the thermal electron distribution is smaller if the thermal electron distribution extends to higher energies. In hydrogen the thermal distribution extends to higher energies and the spectral gap is thus smaller versus in argon.

Interpretation of loop voltage drops and current increases in ohmic plasmas is subject to some degree of controversy. It could be argued, for instance, that plasma wave heating would be expected to decrease plasma resistance. This lower resistance would cause the ohmic supply to drive more current for a given loop voltage.[7] Other groups have demonstrated that LHCD works, and in chapter 7 LHCD will be demonstrated in non-ohmic plasma. What is unique and interesting in these measurements is the extremely low current drive efficiency.

Generation of Plasma Waves at Other Frequencies

With the 2-watt RF-supply energizing the solid dielectric antenna, it was observed that the signal from a plasma probe was symmetrically broadened. This data is shown in Figure (6-17). The probe and antenna were separated by 67.5 degrees toroidally. The tokamak was filled with argon to a pressure of 3×10^{-5} torr. The toroidal field on axis was 1040 gauss. The plasma current was one kiloamp. The antenna was phased to launch LH waves preferentially in the direction of the probe.

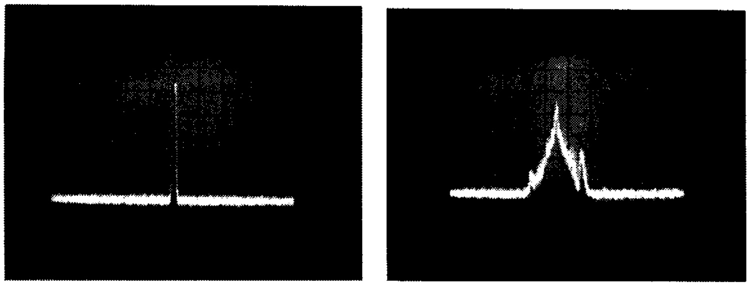

Figure 6-17. At left is the 2-watt input signal to the antenna. At right is the symmetrically broadened signal measured with a plasma probe. The horizontal scale is 5MHz per division. The vertical scale is 10dB per division.

At high power, a different behavior was noted. The plasma probe detected a band of lower frequencies than the input signal. The data is shown in Figure (6-18). In this case the tokamak was filled with hydrogen to a pressure of 4×10^{-5} torr. The toroidal field is 1040 gauss, and the plasma current one kiloamp. The antenna is located 45 degrees clockwise from the probe in the toroidal direction (as viewed from above). The antenna is quadrature phased to preferentially launch LH waves counter-clockwise. The ohmically accelerated electrons also travel counter-clockwise. The power to the antenna was 2kW per channel.

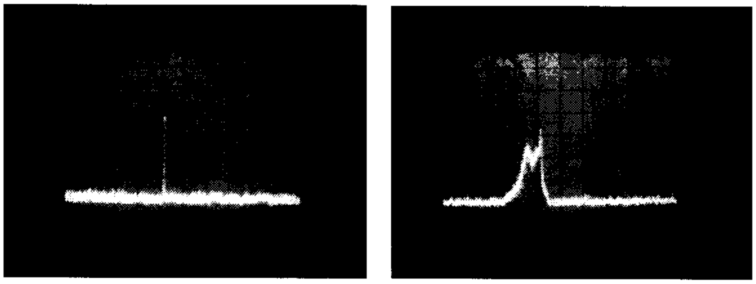

Figure 6-18. The antenna power is 2kW per channel. At left is the input signal to the antenna. At right is the non-symmetrically broadened signal measured with a plasma probe. The horizontal scale is 50MHz per division. The vertical scale is 10dB per division.

Measurements show that under similar conditions, the spectrum of lower frequency waves generated is broadest for hydrogen, intermediate for helium, and narrowest for argon. This data is shown in Figure (6-19). The toroidal magnetic field is 1310 gauss. The plasma current peaks at roughly 1.5 kA.

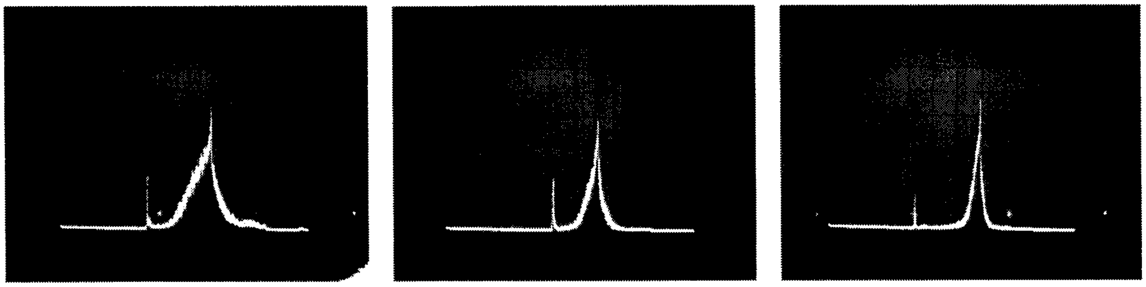

Figure 6-19. Observed spectrum of waves for various gas fill. At left is 5×10^{-5} torr hydrogen. The center trace is 4×10^{-5} torr helium. At right is 4×10^{-5} argon. Horizontal scale is 50MHz per division. Vertical scale is 10dB per division.

The plasma probe utilized was the X-Y probe. Scans were made of the minor cross section for various frequencies noted in Figure (6-18). The plasma current and the timing of the plots are shown in Figure (6-20). A 400MHz scan was taken at the marker shown in Figure (6-20). A 417MHz scan was taken 0.34msec later. A 433MHz scan was taken 0.67msec after the marker. A 450MHz scan was taken 1.0msec after the marker. The resulting contour plots are shown in Figure (6-21).

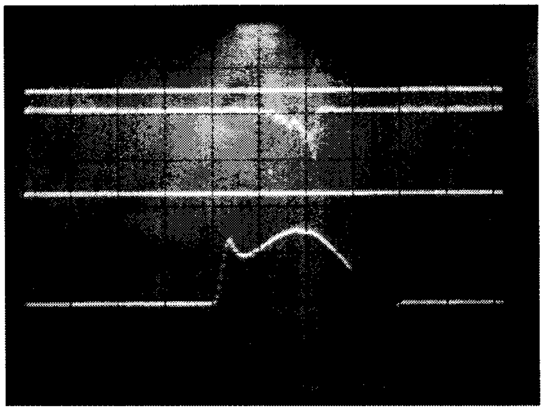

Figure 6-20. Timing of the contour plot data. Second trace from the top is the spectrum analyzer signal, 50MHZ per division. Third trace is the timing marker for the 400MHz scan. Lowest curve is the plasma current, 1kA per division. For the lower two curves the horizontal scale is one millisecond per division.

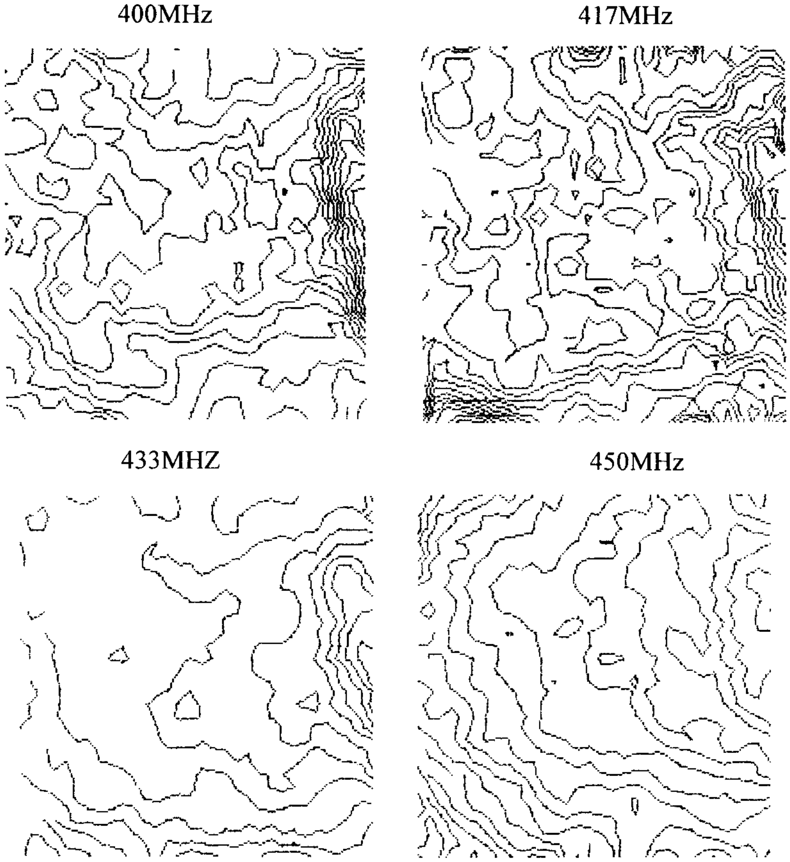

Figure 6-21. Contour plots of detected power at various frequencies as noted. The right-hand side of the plots corresponds to the outer wall where the LH waves are launched by the grill antenna.

Figure (6-21) shows that the lower frequency waves are concentrated at the plasma periphery near the outer wall. The lower the frequency, the more the plasma wave power is restricted to the outer edge of the plots. These waves are likely associated with parametric instability at the plasma edge.[8]

Summary

Experiments on Encore show that LH waves launched by several grill antennas including the solid dielectric antenna behave as one would expect. Accessibility depends upon both the magnetic field and the plasma density and affects the maximum depth of penetration. The LH propagation angle depends upon the magnetic field and affects the rate of penetration. The directionality of the launched waves depends upon the antenna phasing. The solid dielectric antenna launches directional LH waves into Encore that are accessible to the center of the plasma and do indeed propagate there.

LHCD effects are observed in Encore. The changes in plasma current observed are larger at smaller plasma current (and thus smaller density) as one would expect from accessibility considerations. However, the lower hybrid current drive efficiency in Encore is low by orders of magnitude compared to LHCD experiments on other tokamaks. This cannot be explained as due to problems with accessibility, propagation angle or the directionality of the launched spectrum.

During high power LHCD experiments, a spectrum of waves with frequencies lower than that of the launched waves is detected. These waves appear to be concentrated at the plasma periphery.

---

[1] Eric Fredrickson obtained the data indicating linearity. The author obtained the microwave measurement yielding the density calibration.

[2] See for instance "An Experimental and Theoretical Investigation of a Finite Beta Modified Drift Wave," Eric Fredrickson, thesis, California Institute of Technology, Pasadena, CA, (1985).

[3] Eric Fredrickson, private communication

[4] See the discussion at the end of chapter 4.

[5] F. C. Jobes et al., Phys. Rev. Lett., (1985), **55**, p. 1295

[6] N. J. Fisch, "Theory of current drive in plasmas," Rev. Mod. Phys., (1987), **59**, p. 214

[7] N. J. Fisch, "Theory of current drive in plasmas," Rev. Mod. Phys., (1987), **59**, p. 212

[8] Paul Bellan, private communication

7 Data from RF-Sustained Plasmas

The small LH current drive efficiency on Encore is explained in chapter 8 as related to the so-called "density limit." Despite this problem, significant amounts of LHCD current could be generated in Encore. It was found possible to sustain plasma discharges without the aid of the ohmic heating system. This chapter reviews the experiments of this nature.

Magnetic-Error-Field Current-Drive

Current drive experiments in ohmic discharges can be difficult to interpret. Changes in plasma current may be directly due to current drive or they may instead be due to plasma heating which increases the conductivity of the plasma, thus increasing the ohmic plasma current. For ohmic discharges it was found that plasma current is increased for antenna phasing to launch $N_{||}$ parallel to the ohmically accelerated electrons, which in Encore is counterclockwise as viewed from above. The plasma current increases ΔI_P are of the order of a few hundred amps at most, which is small considering that the RF power is a considerable fraction of the ohmic power.

It is desirable to eliminate the effects of the ohmic EMF in order to study the LH-wave/plasma interaction. To this end RF was applied to afterglow plasmas in Encore for which the ohmic input is disconnected and the plasma current and loop-voltage decay on a L/R time scale. The idea is to use the ohmic drive to break down the plasma, and then sustain a RF-current driven discharge beyond the ohmic decay period. Referring to Figure (3-6), amplifier "B" operating in the closing switch mode to sustain the plasma is not utilized. Only amplifier "A," operating in an opening switch mode, is used to partially ionize the tokamak fill gas. In the opening switch mode a quick high-voltage spike is produced as the current in the triode amplifier is disconnected. After amplifier "A" disconnects, the ohmic supply is no longer engaged.

Initial experiments along this line appeared to yield no plasma beyond the ohmic decay zone. The antenna was phased to launch lower hybrid waves parallel to the ohmic electron drift and one expected that the decay of ohmic plasma current would reverse or plateau as the RF current drive was established. Close examination of the I_P trace showed, however, that not only was the plasma current decaying to zero but was in fact overshooting to a negative value which was maintained for the duration of the RF pulse. This negative overshoot was small, on the order of 10-20 amps and thus difficult to see except on an expanded current scale. See Figure (7-1).

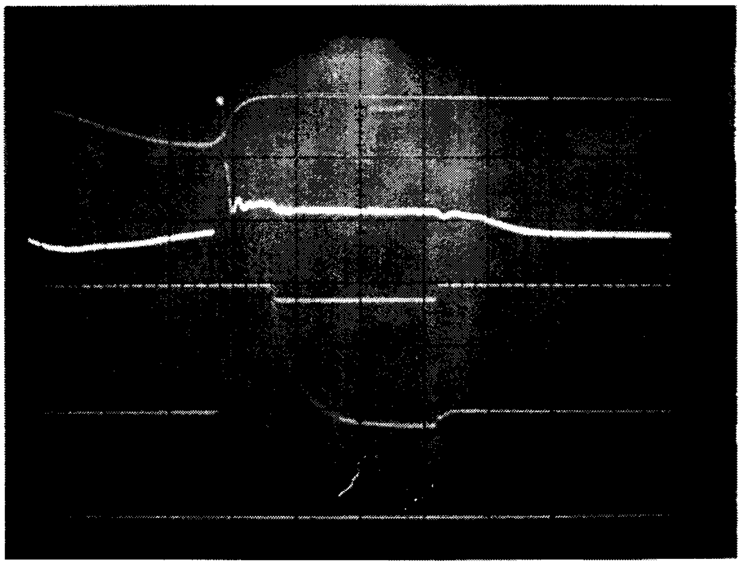

Figure 7-1. Example of a RF sustained plasma in Encore. Upper trace is the "B" amplifier current. Next is the loop voltage (1V/div). Next is a reference pulse coincident with application of RF. The forth trace is the plasma current (100A/div). Note the spike in the loop voltage trace when the ohmic supply ionizes the fill gas, and at the termination of RF.

Initial suspicion was that the Rogowsky circuits were picking up RF interference and giving a rectified output. The current was proven to be real in the following way.

An optical emission diagnostic showed emission coincident with the RF pulse. Looking at the plasma in the tokamak through a window port when the RF was turned on, a bright flash could be seen in place of the subdued blue glow of the short ohmic pulses. The RF pulse duration was increased to eight milliseconds, considerably longer than the one millisecond ohmic afterglow. The plasma light emission seen upon application of RF matched the Rogowsky signal in duration. At the very least, the RF was maintaining plasma breakdown.

The loop voltage due to the ohmic afterglow plasma decayed to zero value during the RF discharge and then exhibited a negative spike coincident with the end of the RF pulse. This negative spike is consistent with the back EMF one would expect due to a decaying reverse (negative) plasma current as shown by the Rogowsky diagnostic. The loop voltage diagnostic is so simple, it is difficult to imagine it giving a misleading result.

Thus, because of the optical, Rogowsky and loop voltage diagnostics, there can be no doubt that during application of RF a current carrying plasma is maintained devoid of ohmic input. However, the direction of the current was opposite to what one would expect based on LHCD theory and the antenna phasing.

Perhaps the phasing is backwards to what it is presumed to be. Upon reversing the phasing so as to flip the $N_{||}$ spectrum at launch to the other direction, *exactly the same reverse plasma current is obtained.* In fact, for no phasing at all, that is, a symmetrical $N_{||}$ distribution launched by a single waveguide, the same result is obtained. Application of RF gives negative plasma current regardless of antenna phasing. The tokamak/RF-antenna system has a handedness. The amount of current driven is linearly proportional to the applied RF power. See Figure (7-2).

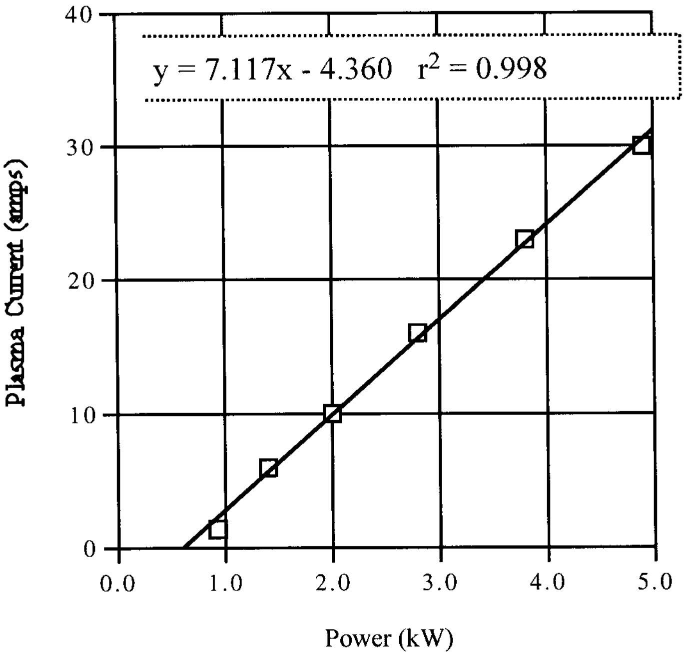

Figure 7-2. I_p^{RF} versus RF power in kilowatts. Only one of the outer waveguides is powered. The current is proportional to the power, and appears to have a threshold just below 1 kW.

What gives the handedness? What property of the system gives the direction of the RF discharge current? To answer this question a great number of aspects of the tokamak were varied in an attempt to alter the magnitude, and possibly change the direction of the RF discharge plasma current I_P^{RF}.

The polarity of the ohmic target plasma current was reversed without effect on I_P^{RF}. Moving the antenna in and out with respect to the chamber wall affected the amount but not the direction of I_P^{RF}. The antenna was moved to different ports around the torus without effect on I_P^{RF}. Thus, local chamber wall features are not responsible.

All four ports of the grill antenna were powered one at a time and each gave an identical result, reverse plasma current. The antenna was flipped upside down and the same experiment repeated without change in the result. Thus the non-powered waveguides or other construction features of the grill antenna can be eliminated.

Varying the vertical magnetic field B_{vert} direction and magnitude could affect the amount of current to some degree but not its direction. This result also eliminates the vertical component of the earth's magnetic field. The horizontal component of the earth's field does not give a net direction to the torus. Encore is a low magnetic field tokamak and it is not out of the question that the earth's magnetic field could have an effect. Reversing the toroidal field B_ϕ had absolutely no effect on I_P^{RF}. The iron core transformer for the ohmic drive on Encore was partially pulled apart with no detectable affect on I_P^{RF}. The position of the filaments used to provide electrons for breakdown was varied without effect.

The vertical field coils were hooked up to generate a radial horizontal magnetic field B_H. The RF plasma current was found to be a strong function of this horizontal field and the direction of I_P^{RF} could be reversed for certain values and direction of B_H. Data was taken, I_P^{RF} versus B_H, for both directions of the toroidal field B_ϕ and the results are shown in Figures (7-3) and (7-4). Note that the direction of B_H needed to zero or reverse I_P^{RF} depends on the direction of B_ϕ. It is the combination of B_ϕ and B_H that gives the handedness. A small horizontal radial field superposed on the large toroidal field simply leads to a small change in direction of the toroidal field, causing the field lines to spiral in or out depending on the directions of B_H and B_ϕ .

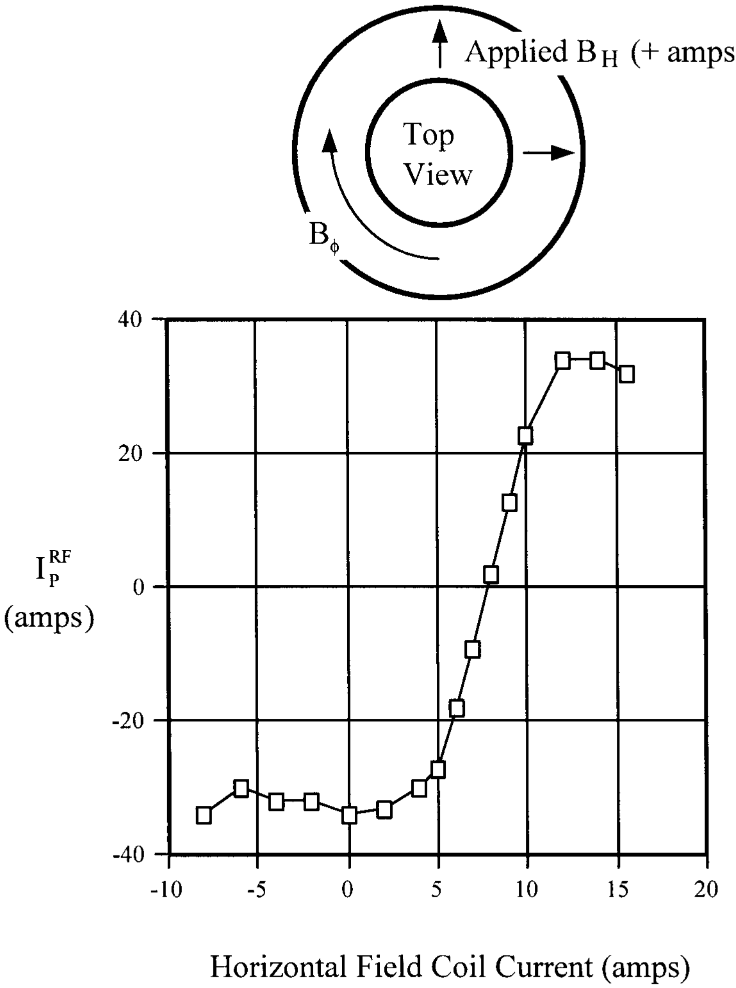

Figure 7-3. RF induced plasma current I_P^{RF} versus the current in a set of coils generating a radial horizontal magnetic field in the Encore tokamak. It is increasingly difficult to obtain an ohmic breakdown for increasingly negative coil current.

The data is consistent with the following picture. An inherent radial horizontal magnetic "error" field B_H^{error} in the Encore tokamak causes the magnetic field lines to spiral in a horizontal plane. Suppose that the lower hybrid antenna generates electron beams in both directions, localized near the chamber wall. The electron beam spiraling out toward the chamber wall will be attenuated with respect to the electron beam spiraling inwards toward the chamber center. Thus a net current I_P^{RF} is produced. See Figure (7-5).

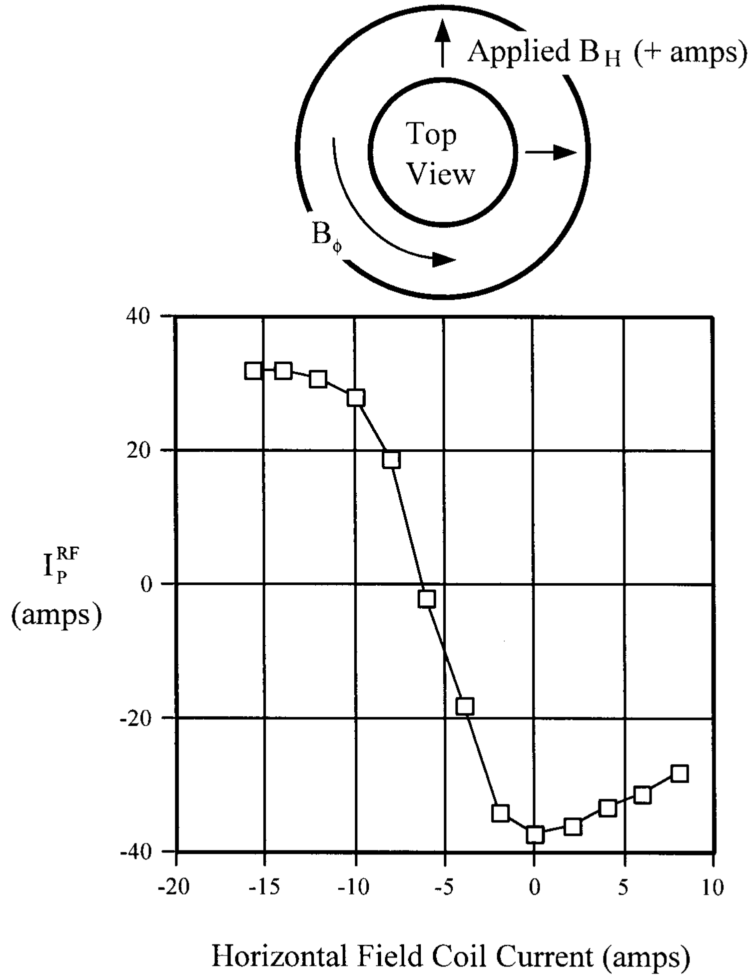

Figure 7-4. RF induced plasma current I_P^{RF} versus the current in a set of coils generating a radial horizontal magnetic field in the Encore tokamak. The direction of the toroidal field is opposite to that in Figure 7-3. It is increasingly difficult to obtain an ohmic breakdown for increasingly positive coil current.

If the horizontal error field B_H^{error} is due to the toroidal field currents, then upon reversing B_ϕ, B_H^{error} also will also reverse and the direction of the spiral is unchanged. This explains the insensitivity of I_P^{RF} to the toroidal field direction. It also explains why the direction of the applied correction B_H necessary to zero or reverse I_P^{RF} changes with the direction of B_ϕ as shown in Figures (7-3) and (7-4).

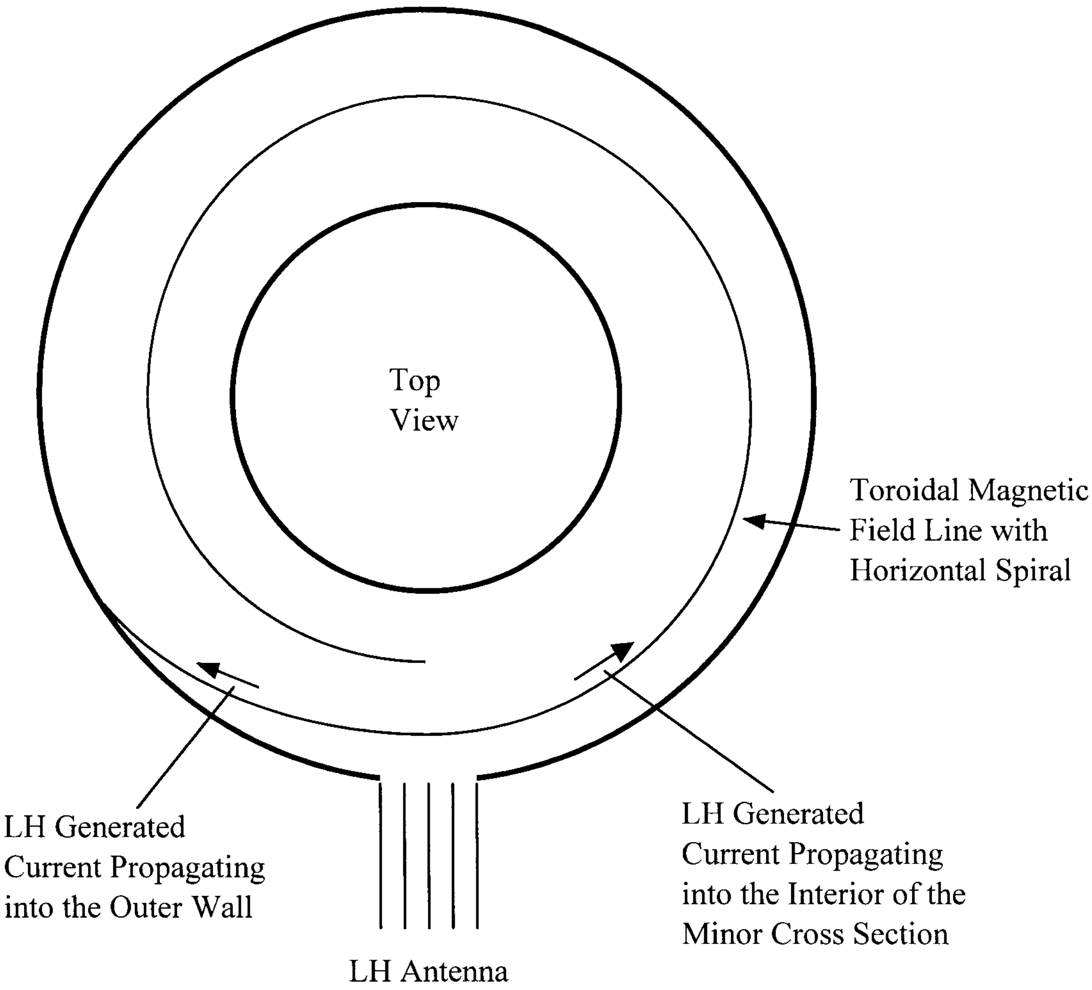

Figure 7-5. Schematic of the proposed theory explaining the production of net toroidal current with a symmetric LH antenna phasing. Spiraling of the toroidal field lines in a horizontal plane (highly exaggerated in the figure) breaks the symmetry. LH current generated near the outer wall of the torus propagates in both toroidal directions. Current spiraling outward to the chamber wall is rapidly attenuated with respect to current propagating into the interior of the minor cross section.

If the antenna is generating beams in opposite directions then perhaps plasma exists even when B_H is applied to zero I_P^{RF}. Optical emission shows that a plasma exists for the condition $I_P^{RF} = 0$. However, optical emission is less for this case than when a net current exists. A toroidal current is, of course, necessary for plasma confinement.

Further bolstering the spiral theory is the data shown in Figures (7-6) and (7-7) where the necessary B_H to zero I_P^{RF} is shown to be proportional to the toroidal field. This confirms that the inherent horizontal radial error field is due to toroidal field coil currents. The discrepancy at low toroidal field is an indication that smaller contributions to the horizontal error field not due to toroidal field coil errors exist. One possible source for this is the iron core transformer for the ohmic supply on Encore. This transformer has a small gap at the tokamak center point to lower the inductance for impedance matching purposes.

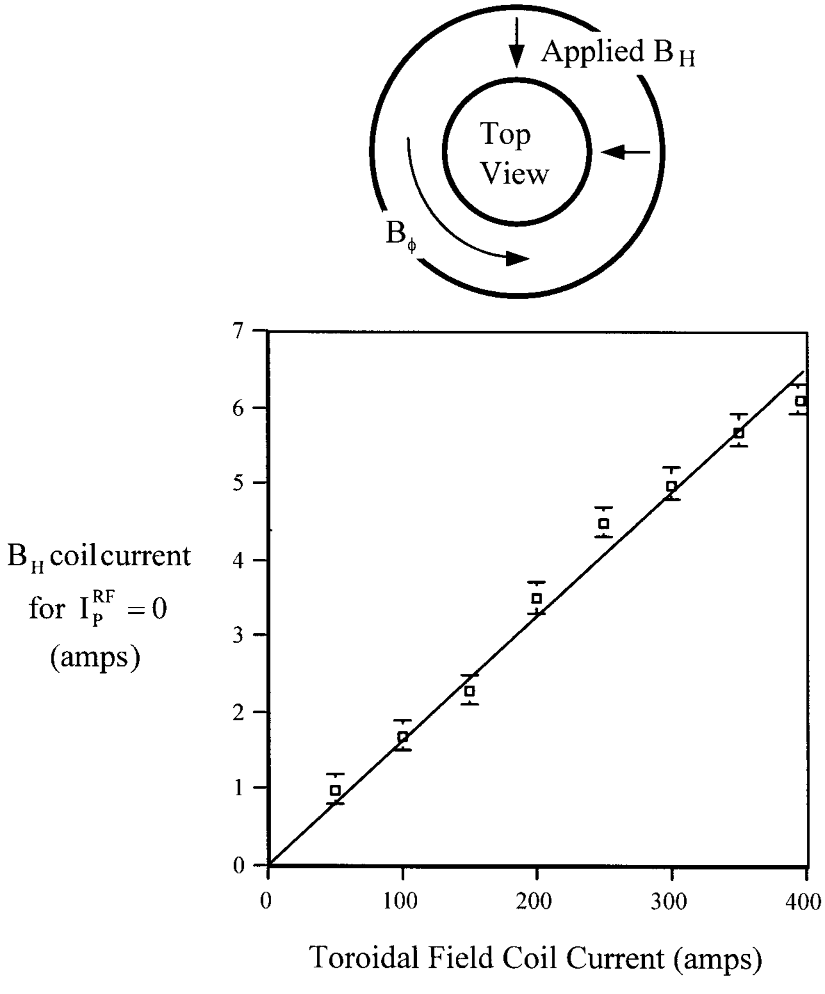

Figure 7-6. Current in the coils which produce a radial horizontal magnetic field necessary to achieve $I_P^{RF} = 0$ versus current in the toroidal field windings.

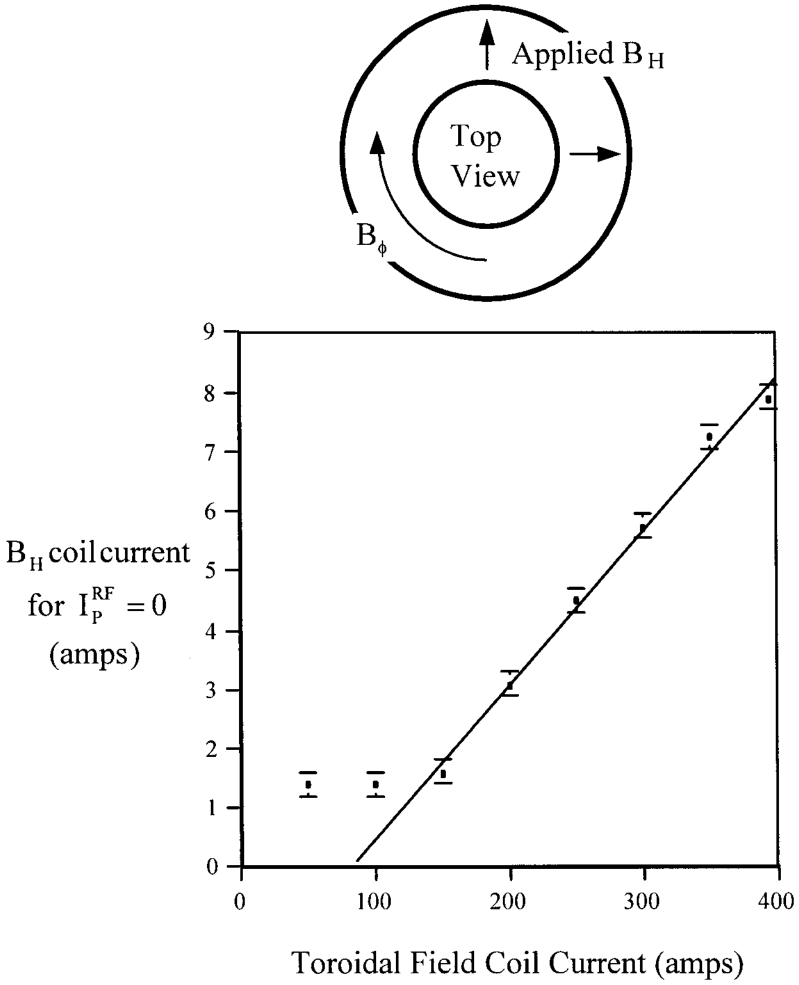

Figure 7-7. Current in the coils which produce a radial horizontal magnetic field necessary to achieve $I_P^{RF} = 0$ versus current in the toroidal field windings.

With the toroidal field on, one cannot simply stick a magnetic probe into the machine to measure the inherent horizontal error field. Inferring from the applied B_H necessary to correct the error and zero I_P^{RF}, the error is of the order of a few gauss. The effect of the error is simply to slightly alter the direction of the toroidal field lines ($\approx 1300\,\text{gauss}$) and this simply cannot be seen with a handheld probe. However, the direction of the inherent error field can be deduced from the correction field necessary to eliminate it. When this is done the direction of the magnetic field line spiral thus inferred agrees with that necessary to produce the observed direction of I_P^{RF}.

Three gauss out of 1300 represents a deviation in angle of 2.3 milliradians. After traversing one circumference of the tokamak (major radius 38cm), the deviation in position will be of the order of half a centimeter. Since the minor radius is 12cm, an electron beam generated at the outer portion of the tokamak could expect to remain in the chamber for something of the order of 48 passes before colliding with the inner wall.

It might be mentioned at this point how one can decide the direction of a magnetic field. A useful picture is shown in Figure (7-8). The north pole is that from which magnetic field lines emerge. Since north poles point north, the earth's North Pole is thus technically a magnetic south pole. It is known that cosmic ray primaries (positively charged ions) are bent to the east as they approach the earth.[1] Given their positive charge, this is only possible if the magnetic field of the earth in space points to the north. In the Northern Hemisphere the earth's magnetic field points north and down. Knowing this, any magnetic probe may be quickly calibrated as to direction, by simply looking at the earth's field. The absolute direction of a magnetic field rarely needs to be known. The handedness of the spiraling field lines is insensitive to the convention used for the direction of the magnetic field. If both the horizontal error field and the toroidal field are assumed to point in the opposite direction, the field lines still spiral with the same handedness.

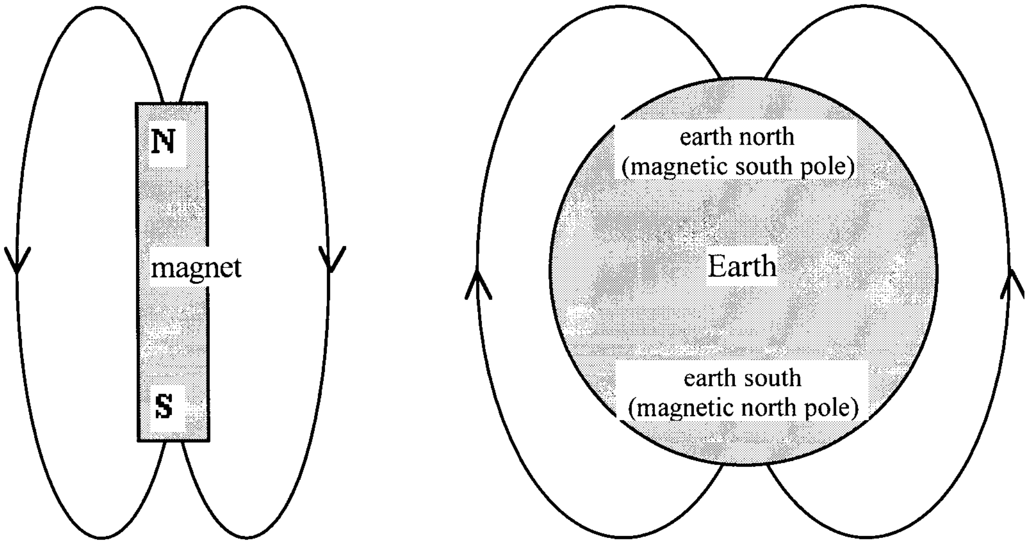

Figure 7-8. Accepted convention for the direction of magnetic field lines produced by two common sources.

There are several ways to see how the toroidal field coils on Encore could produce such a horizontal radial magnetic error field. To minimize errors and to avoid encircling the ohmic transformer, the return current lead for the coils doubles back underneath the input lead which is located underneath the coils. As can be seen in Figure (7-9), the currents in the input lead sections do not entirely match the return current because of the pancake coils. Because these connection leads are underneath the toroidal coils a horizontal error will exist in the tokamak chamber. Another source of horizontal error is due to coil tilt. A consistent tilt of the pancake coils about a vertical axis will also result in horizontally spiraling field lines. By properly adjusting the tilt of the coils on Encore it was later found possible to eliminate the horizontal error so that $I_P^{RF} = 0$ for $B_H = 0$.

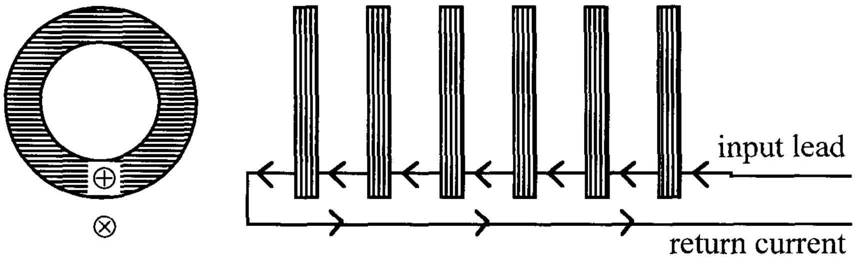

Figure 7-9. One source of the horizontal magnetic error field involves the return current lead. There is no local cancellation of the return current lead at the positions of the toroidal field coils.

In general, localized horizontal radial magnetic error fields in tokamaks can be measured only by electron beam studies in which the beam spiraling can be detected.[2] Average global magnetic error fields can be detected by the EMF induced in a toroidal loop when the toroidal magnetic field is pulsed. Typical practice is simply to apply a correcting B_H that is adjusted to maximize the plasma parameters.[3] Encore, being a high rep-rate, probe-compatible tokamak, usually contains low temperature collisional plasma not fully ionized. For this reason, it is not sensitive to small horizontal errors. Collisional current carriers in a typical Encore discharge simply do not have a long enough mean free path to sample the slight spiraling. However, higher velocity RF generated electrons are not so collisional. At 100eV, the mean free path of an electron is of the order of a dozen circumferences of the torus, plenty of distance for the horizontal spiral to have effect.

In Figure (7-10) RF-sustained plasma current is demonstrated in both toroidal directions by manipulation of the radial horizontal magnetic error field. An ohmic target plasma comprised of argon is used. A single waveguide is powered with 3.9kW. The RF-current is sustained for more than 8 milliseconds, limited only by the RF power supply.

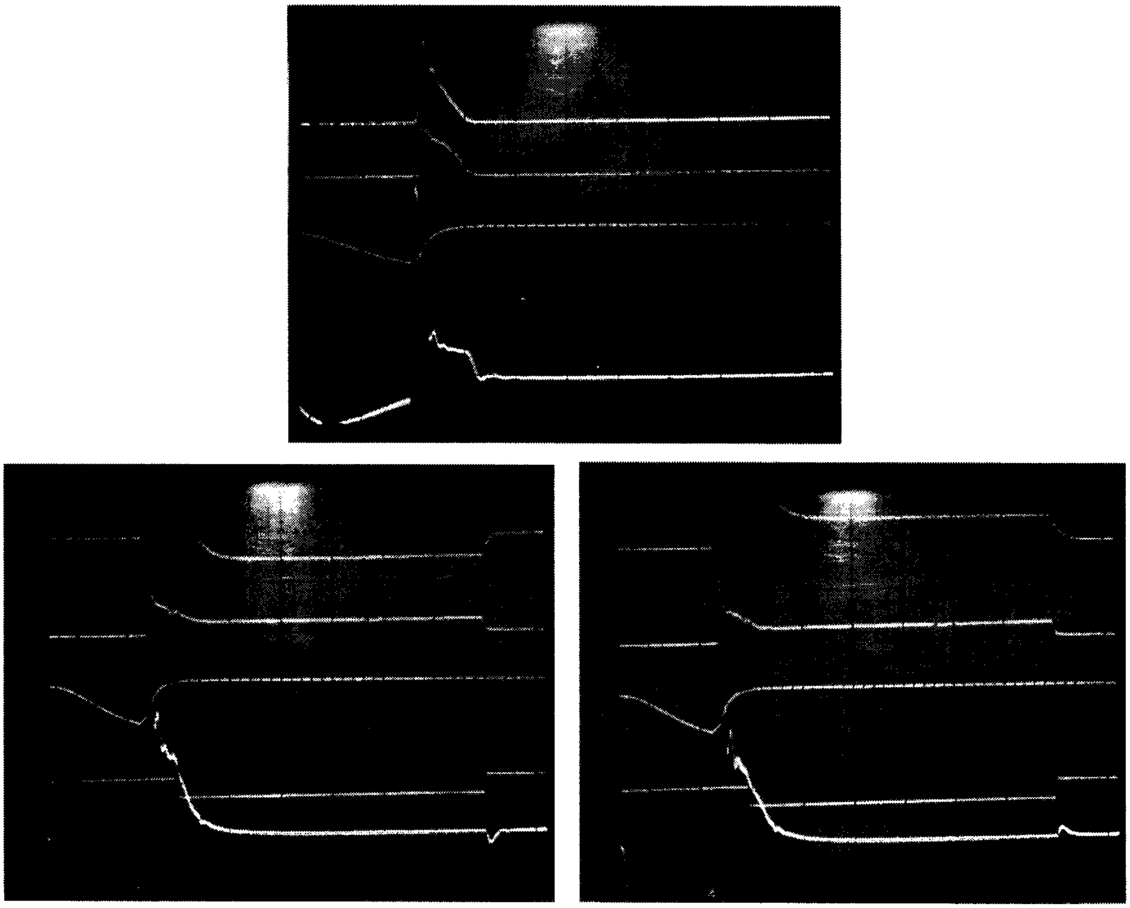

Figure 7-10. Photos demonstrating RF-sustained plasma current. In all photos, the top trace is the plasma current, 500A/div. upper photo, 50A/div. lower photos. The second trace from the top is the optical emission signal. The third trace is the ohmic primary. The fourth trace is the RF marker. The bottom trace is the loop voltage, 5V/div. top photo, 2V/div. lower photos. For the bottom right photo, a radial horizontal magnetic field of 6.5 gauss was applied to reverse the spiraling of the toroidal field lines.

Effects Due to Phasing

The RF current drive discussed in the previous section produced net current from a symmetric $N_{||}$ spectrum by creating an asymmetry in the magnetic paths available to the opposing beams. This section discusses experiments in which the magnetic error fields were eliminated and quadrature phasing was utilized to generate non-symmetric $N_{||}$ distributions at launch. Very little net RF current was generated in this manner. Some possible reasons for this are discussed.

The vertical field correction coils on Encore were reconnected in a parallel configuration that allowed independent application of a correcting radial horizontal magnetic field B_H as well as a vertical magnetic field B_V. For ohmically generated plasma, it was standard to use a pulsed vertical magnetic field supply. This was replaced with a DC current supply to prevent confusion due to transient behavior. B_H was generated by a DC current supply as well.

With a single channel of the antenna powered the launched LH spectrum should be symmetrical as shown in Figure (5-16f). With a 7.4kW to a single port and no magnetic correction applied, the RF driven current was -23 amps.[4] The settings of the correction coils necessary to achieve $I_P^{RF} = 0$ could then be measured. The necessary values of the correction coil currents to achieve $I_P^{RF} = 0$ varied with time. Some factors that might influence this were examined.

Fourteen magnetic socket screws were removed form the torus without effect. A magnetic optics table recently placed near the torus was moved without effect. Pieces of iron placed on top of the torus leaning against the iron core of the ohmic transformer had no effect. Pieces of iron placed near the outer mid-plane of the torus could completely reverse the direction of I_P^{RF} depending upon their position. Lifting the torus slightly with respect to the various magnetic coils had no effect. Moving the iron core of the ohmic transformer back and forth had no effect. Moving around the toroidal magnetic field current leads had no effect. Rotating the torus with respect to the iron core several centimeters had no effect. A small hand magnet held near the torus had a detectable effect on I_P^{RF}. Increasing the gap in the iron core transformer had a definite effect as shown in Figure (7-11).

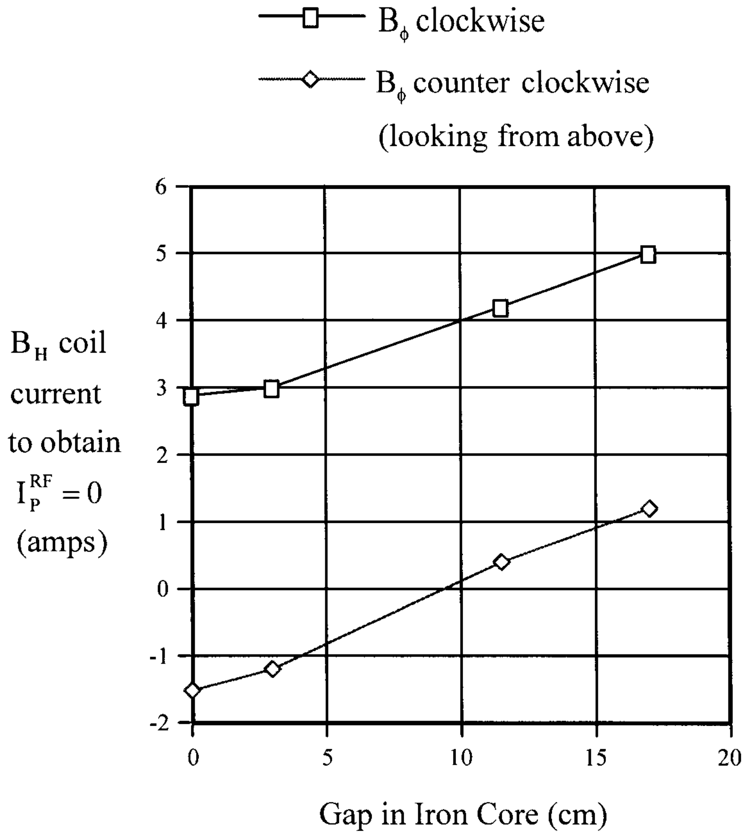

Figure 7-11. The current in the B_H correction coils necessary to make $I_P^{RF} = 0$ for various gaps in the iron core transformer of the ohmic supply. Data is presented for both polarities of the toroidal field.

An attempt was made to disengage the ohmic supply as much as possible by removing the movable portion of the ohmic transformer core completely. Breakdown of the plasma was found to be still possible. However, the initial ohmic loop voltage was then found to decay on a very long time scale in the presence of RF sustained plasma. The iron core transformer was restored to its original configuration.

For comparison, I_P^{RF} generated by each of the four channels of the antenna was examined and the results are shown in table (7-A). No magnetic correction B_H or B_V was applied for these measurements. The power to channel #1 was slightly less than that of the other channels due to problems with the amplifier chain. In any event, the powers are not equalized and this will cause degradation to the directionality of the $N_{||}$ spectrum. Channel #1 was less efficient in driving plasma current than the other channels for unknown reasons. It is possible that there is an air gap in the coax paraffin or ceramic dielectric for that channel. Also of interest, the interior waveguides (#1 & #2) have significantly higher reflection coefficients from the plasma than the exterior waveguides. Altering the power to individual channels was not simple. Continuously variable attenuators were not included in the amplifier chains. In retrospect, optimum $N_{||}$ directionality probably requires fine adjustment of power to each waveguide, so that the plasma-coupled power can be equalized for all four channels.

Channel	Fwd. Power (kW)	Ref. Power (kW)	I_P^{RF} (amps)
#0	5.1	10%	-15
#1	4.3	23%	-8
#2	5.1	23%	-16
#3	4.1	4%	-15

Table 7-A. Comparison of the performance of each individual waveguide in generating RF driven plasma current with no magnetic correction fields B_H or B_V.

With one channel of the antenna powered, B_H was carefully adjusted so as to achieve $I_P^{RF} = 0$. The current in the B_H coils necessary to null out the RF driven plasma current was determined to be 3.1 amps. In this condition it was found that $I_P^{RF} = 0$ was insensitive to the vertical magnetic correction field B_V. This makes sense from the symmetry of the situation. The fast electron beams are generated equidistant from the top and bottom of the chamber. The vertical field will induce a vertically oriented helix rather than a horizontal spiral. No direction is favored by creating such a path for the two beams.

All four ports of the antenna were then energized with quadrature phasing. According to Figure (5-16c) this should give a fairly unidirectional $N_{||}$ spectrum at launch. Numerical integration shows that 76% of the power should launch in one direction, and 24% in the opposite direction. The amount of current driven was 3 amps. The horizontal magnetic correction field was varied so as to maximize the RF driven current and as much as 60 amps was obtained. See Figure (7-12).

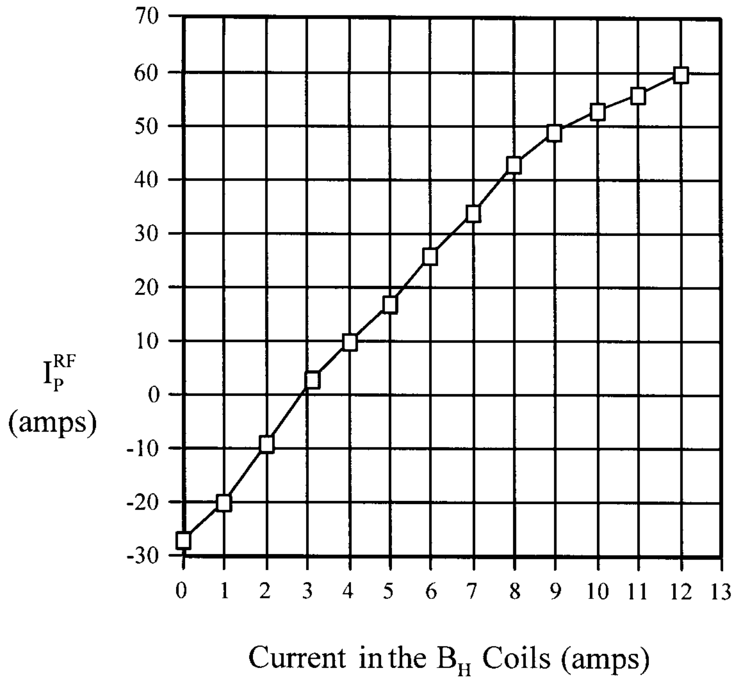

Figure 7-12. RF driven plasma current versus the current in the horizontal magnetic correction field coils. The antenna is quadrature phased. At 3.1 amps the error field is nullified but only 3 amps are obtained. 60 amps are obtained at the maximum current used.

Next, the vertical magnetic field was adjusted so as to maximize the RF driven current. 100 amps of plasma current were obtained in this manner. Finally, the argon fill pressure was varied to obtain an even larger plasma current of 144 amps as shown in Figure (7-13). The largest RF-driven plasma current obtained by such procedures was 158 amps. A typical result is shown in Figure (7-14).

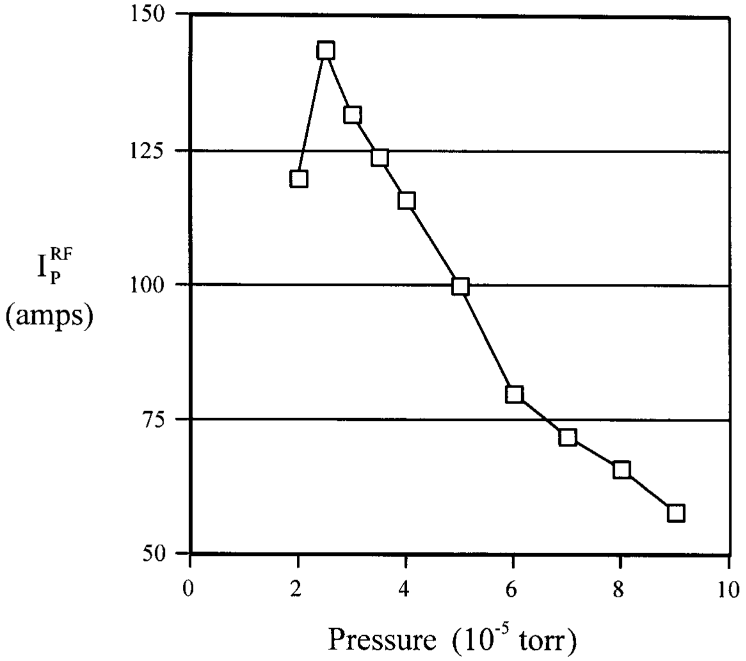

Figure 7-13. RF driven plasma current versus the argon fill pressure. A peak of roughly 144 amps is obtained at a pressure of 2.5×10^{-5} torr.

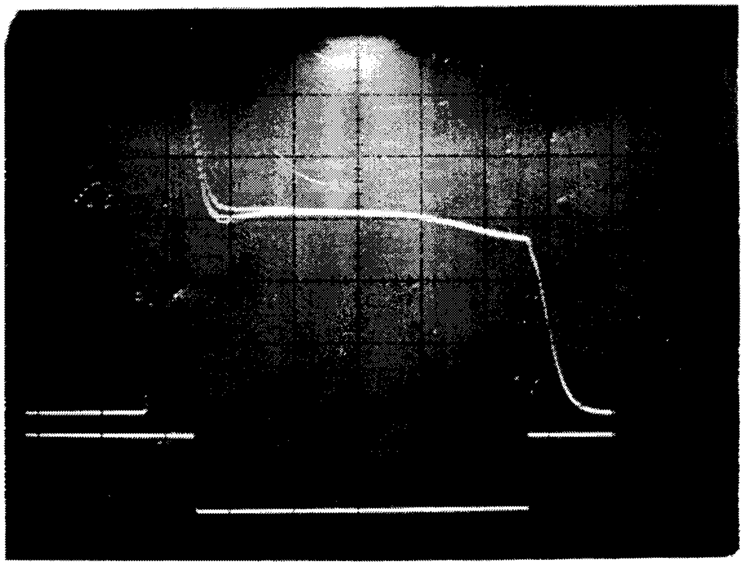

Figure 5-14a. Magnetic error field assisted LHCD result. Upper trace is the plasma current (50 amps/division). Lower trace is the RF-on reference. Horizontal scale is 1 msec per division.

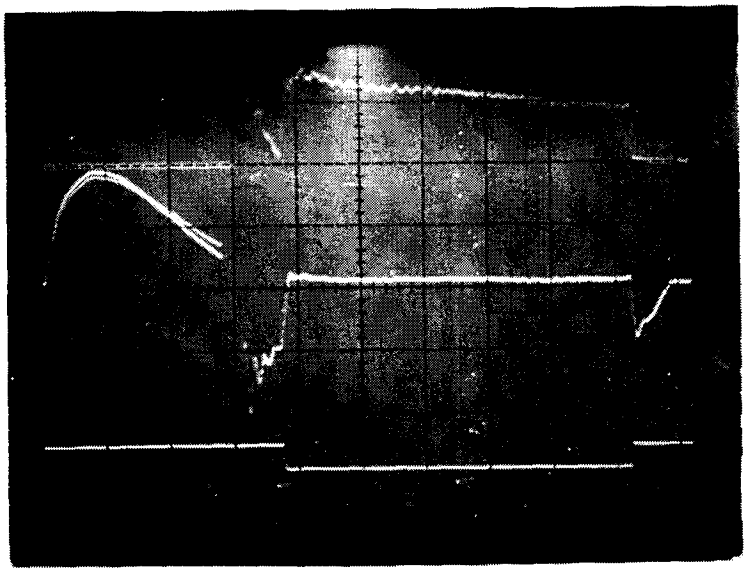

Figure 5-14b. Magnetic error field assisted LHCD result. Upper trace is the plasma optical radiation output. Middle trace is the loop voltage (2V/division). Lower trace is the RF-on reference. Horizontal scale is 1 msec per division.

On the chance that there was an error in the method of setting the waveguide phasing, many other phasings were experimented with. None was found to produce as much plasma current as quadrature phasing (90° shift per waveguide). In particular, experiments with zero phase shifts (all waveguides have the same phase) produced a maximum net plasma current of 100 amps. 180° phase shift produced a maximum net plasma current with other parameters optimized of 75 amps. These results suggest that the phasing was as measured.

It is interesting to note that the vertical magnetic field which maximizes I_p^{RF} for 0° phase shift per waveguide is only slightly less than for quadrature phasing (coil current 3.4 amps versus 3.8 amps). For 180° phase shift I_p^{RF} is maximized for a vertical field coil current of 3.75 amp. The vertical field induced helix negates a drift that is proportional to the electron toroidal velocity. This suggests that the typical toroidal electron velocities in the RF driven current are similar independent of phasing. This is despite the fact that $N_{||}$ at launch is dramatically different according to the calculations shown in Figure (5-16). Regardless of the $N_{||}$ spectrum at launch, in bridging the "spectral gap" to reach thermal

10eV electrons, presumably similar spectra composed of large $N_{||}$ values are created after launch.

The failure of phasing by itself to produce a unidirectional plasma current can at least partly be attributed to the poor directionality of a four-waveguide system. Ideal calculations indicate a 0.76 - 0.24 directionality. More waveguides are needed to improve upon this. Failure to equalize the plasma-coupled power from the four waveguides will only further deteriorate the ideal calculations. Another factor may involve the nature of the target plasma to which the RF is applied. The RF generated plasma is not homogeneous. Plasma density is likely highest where the RF generated electron beams exist. The antenna is not presented with uniform plasma with a steep density gradient in the major radius direction. If the four waveguides are not presented with LH cutoffs located at similar distances, then further degradation in directionality is sure to result. If the distance to the cutoff is significant compared to the separation between waveguide centers, the $N_{||}$ spectrum will be altered from the ideal calculations. Factors that might play a role in this include the field curvature in the fringing fields as well as superposition of fields from neighboring waveguides.

Correlation of Reflected Power

The RF power reflected from the plasma varies slightly as a function of time. Presumably this is due to the turbulent nature of the plasma. Simultaneous data was taken of the reflected power versus time from the two outermost waveguides. These two waveguides have the largest separation. The question was whether or not the variation in reflected power versus time from the two waveguides would be correlated or not. Lack of correlation would be evidence that due to plasma turbulence, the waveguides are not each exposed to identical launch plasma. This in turn would offer evidence of a possible mechanism for disruption of the calculated $N_{||}$ spectrum. The data is shown in Figure (7-15). The reflected power levels appear to be correlated.

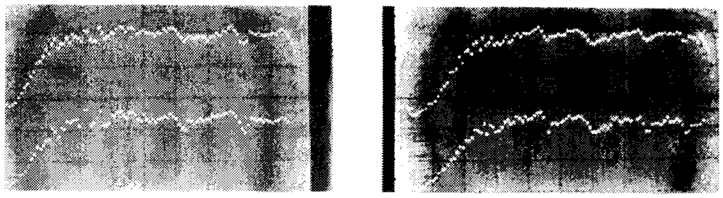

Figure 7-15. Reflected power of the two outermost waveguides versus time. A RF sustained discharge in hydrogen with $I_P^{RF} = 30$ amps is used. The horizontal scale is 0.2 msec per division. The vertical scale is 2dB per division. The upper traces are one waveguide, and the lower traces, the other.

Microwave Density Measurement

A microwave density diagnostic on Encore was capable of measuring line average density. A measurement was taken during LHCD and the data is shown in Figure (7-16). The measurements were calibrated against ohmically generated plasma that reached a peak current of 3 kA. Line average density in Encore is proportional to the plasma current and is roughly 2×10^{12} cm^{-3} for $I_P^{ohmic} = 2\,\mathrm{kA}$. Thus the calibration data involves a line average density of about 3×10^{12} cm^{-3}. This line average density corresponds to 1.3 fringes in the microwave data. The LHCD data shows $I_P^{RF} \approx 100$ amps. The microwave data shows about 0.3 fringes. Thus the line average density in the RF sustained plasma is of the order of 7×10^{11} cm^{-3}. This is well above the cutoff (P=0) for the slow mode which is 2.5×10^{9} cm^{-3}.

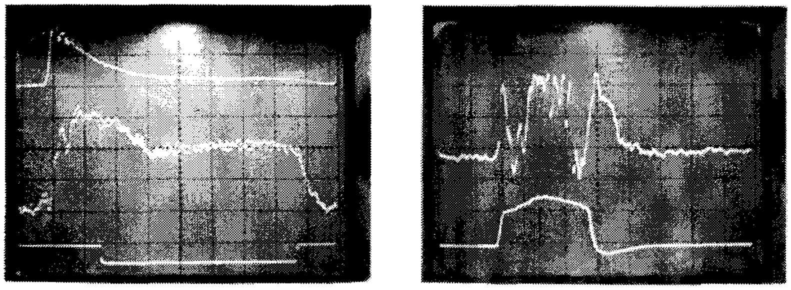

Figure 7-16. Microwave density diagnostic data. At left is the LHCD data. Upper trace is plasma current (500A/division). Middle trace is the microwave fringe data. Lower trace is the RF reference. At right is ohmic plasma calibration data. Upper trace is microwave fringe data. Lower trace is plasma current (2kA/division). Horizontal scale is 0.5 msec per division for both photographs.

Dependence on the Toroidal Magnetic Field

The effect of B_ϕ on the maximum I_P^{RF} was looked at. Except for B_H, which was varied, the parameters are the same as for the record I_P^{RF}. Quadrature phasing was used. B_H was adjusted for each B_ϕ so as to maximize I_P^{RF}. B_V for maximizing I_P^{RF} was found to be independent of B_ϕ. In tokamak mode, the vertical magnetic field balances the "hoop" force of the toroidal current and there is no B_ϕ dependence to B_V. The result of the experiment is shown in Figure (7-17).

At lower magnetic fields, the net RF driven plasma current falls off. It is likely that this is due to problems with accessibility. Figure (4-7) shows that accessibility for a typical quadrature phase launch spectrum becomes hindered for magnetic fields below 929 gauss (300 amps coil current). Below this value the accessibility limit curve lies entirely within the launch spectrum for quadrature phasing. Remarkably, this is exactly where I_P^{RF} begins to drop in Figure (7-17).

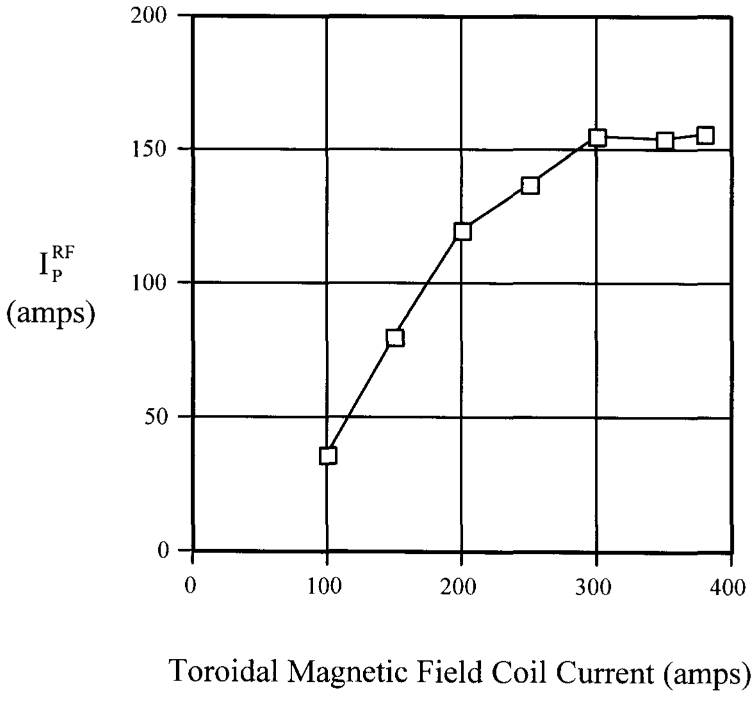

Figure 7-17. Maximized net RF driven plasma current versus the toroidal magnetic field coil current. Below 300 amps there is a monotonic fall in plasma current.

Ion Mass Dependence

The atomic species used for the fill gas in Encore was varied to see what effect if any it would have on I_P^{RF}. Presumably the fill gas would affect primarily the ion mass value. This in turn would affect the ion plasma frequency and the ion cyclotron frequency. When an effect seemed to be apparent, the experiment was pushed to the point that six different fill gases had been tried. The gases utilized are listed in table (7-B).

Atomic Species	Mass (amu)	Ion Gauge Factor
Hydrogen	1.0	2.3
Deuterium	2.0	2.7
Helium	4.0	6.9
Nitrogen	14.0	1
Neon	20.2	3.3
Argon	39.9	0.89

Table 7-B. Fill gases used in the ion mass dependence experiment. The "ion gauge factor" is the calibration factor for correct reading of ion-gauge pressure based upon the ease of ionization of the various gases.[5]

The gas fill pressure was kept at approximately 3×10^{-5} torr for all of the gases. The toroidal field was maximized to provide the best possible accessibility. The horizontal error field was adjusted to maximize I_P^{RF} for argon fill, and held constant for all of the data. The result of the experiment is shown in Figure (7-18). Larger values of I_P^{RF} but very similar mass dependence were obtained by adjusting the vertical field independently in each case so as to maximize the RF driven current.

Since the "ion gauge factor" (related to the ease of ionization) as listed in table (7-B) does not have a monotonic relationship with the atomic mass, it is difficult to imagine that this factor plays a major role in the phenomena.

The LHCD density limit to be described in chapter 8 depends upon many variables including the value of the ion mass. The equation for the density limit can be written as[6]

$$n_{\mathrm{limit}} = \frac{\omega^2}{4\cdot\pi^2\cdot 9000^2}\cdot\left[\frac{2}{\gamma}\left(\frac{3}{4}\beta_e\frac{\omega^4}{\omega_{ce}^4}+3\beta_i\frac{m_e^2}{m_i^2}\frac{T_i}{T_e}\right)^{0.5}+\frac{m_e}{m_i}-\frac{\omega^2}{\omega_{ce}^2}\right]^{-1}. \tag{7.1}$$

The units of n_{limit} are cm^{-3}. The parameter γ is defined by

$$\frac{\omega}{k_{\|}} = \gamma \cdot v^{e}_{thermal} \, , \tag{7.2}$$

where $v^{e}_{thermal}$ is the electron thermal velocity. It characterizes the degree of upshift in $k_{\|}$ occurring in the plasma, enabling a resonant interaction between the launched LH waves and the slower thermal distribution of electrons. The parameters β_e and β_i are temperature enhancement factors and multiply the electron and ion temperatures respectively. β_e exceeds unity when the fast electrons providing the current drive have a total energy comparable to the bulk, and characterizes the change in the electron distribution due to the LH waves. β_i exceeds unity when there is ion heating, and characterizes the change in the ion distribution due to the LH waves.

Taking values pertinent to Encore (B=1300 gauss, T_i=3eV, T_e=10eV, $\omega = 2\pi \cdot 450 \times 10^6 \sec^{-1}$), and choosing $\gamma = \beta_e = \beta_i = 1$, the results shown in Figure (7-19) are obtained. For Encore parameters, the density limit is totally insensitive to the values of T_e, T_i, and β_i. The monotonic relationship is preserved for other choices of γ and β_e.

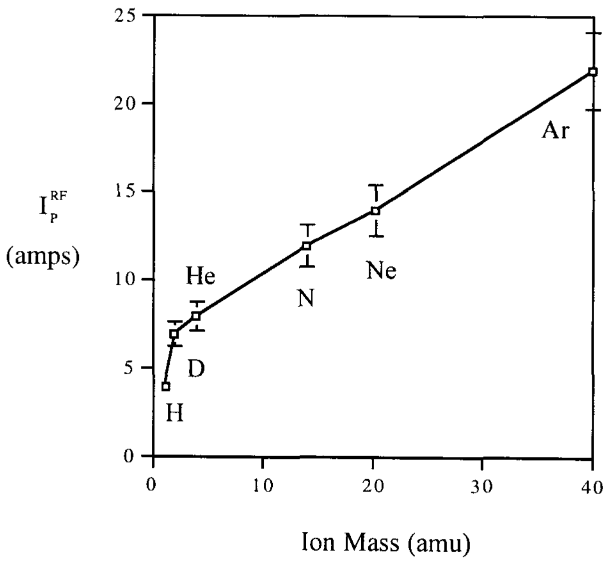

Figure 7-18. Dependence of the amount of RF driven plasma current on the type of gas used to fill the tokamak. There is a monotonic increase in I_P^{RF} with atomic weight. The sharp rise in the dependence rolls off above the mass of helium.

It is difficult to create plasma in Encore with line average density less than 10^{12} cm^{-3} with the ohmic heating system. Ohmic breakdown cannot be achieved with line average densities of the order of 2×10^{11} cm^{-3}. Densities of the order of 2×10^{11} cm^{-3} occur very close to the edge of the plasma. It is quite plausible that as the density limit is increased, greater penetration of the LH waves is achieved causing the RF driven plasma current to increase.

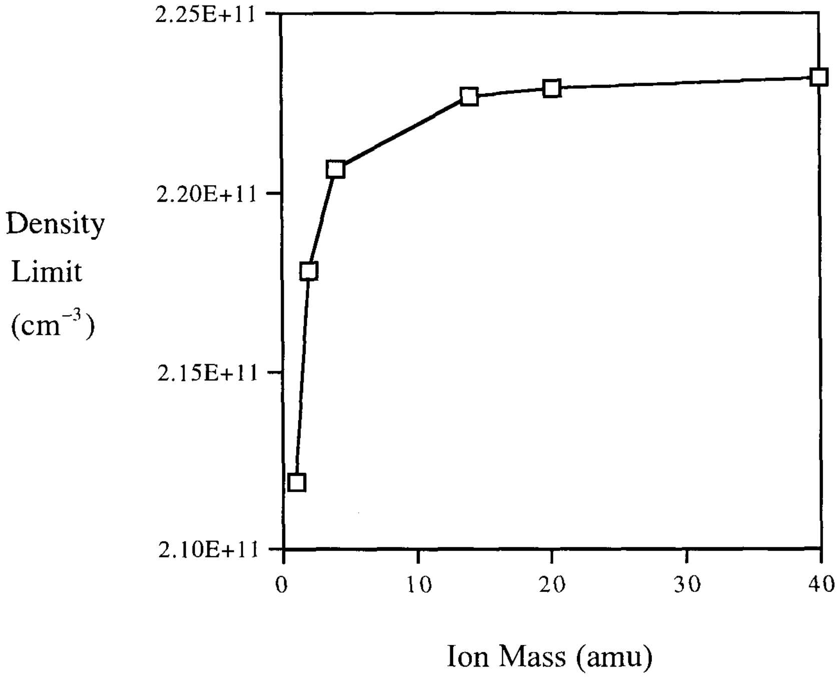

Figure 7-19. Dependence of the LHCD density limit in Encore on ion mass. There is a monotonic relationship with larger ion mass associated with a larger density limit. The sharp rise in the dependence rolls off above the mass of helium.

RF Tokamak

An attempt was made to eliminate the use of the Encore ohmic supply for the purpose of ionizing target plasma for LHCD. To replace the ohmic supply, a tungsten filament was installed on the tokamak. This filament was biased to 400 volts and emitted a current of 50-75 milliamperes. Using 180° phase shifts with 2.3kW per channel, $I_P^{RF} = \pm 65$amps were obtained, the sign depending upon the direction of B_H enhancement. See Figures (7-20a) and (7-20b). The maximized I_P^{RF} was found to be insensitive to the filament voltage over the range of 100-500 volts. Without ohmic generation of target plasma, the tokamak loop voltage signal is due entirely to the rise and fall of the RF driven current. The RF driven plasma current appeared to jump between discrete levels of approximately 20, 40 and 60 amps as B_H was varied. Unlike the RF sustained plasma generated from ohmic target plasma, these plasmas showed large sensitivity to B_V. Varying the vertical magnetic field could alter the polarity of I_P^{RF}, much as B_H did for the ohmic initiated RF plasmas.

Encore was now operating in a pure RF mode. The ohmic supply makes quite a bit of noise, whereas the RF system makes virtually none. In the pure RF mode, silent blue flashes of light appeared in the tokamak window ports coincident with RF application.

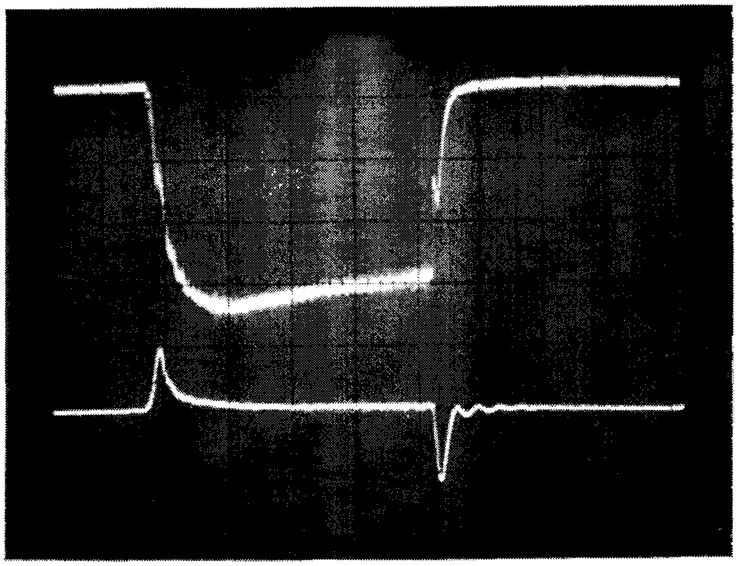

Figure 7-20a. LHCD without an ohmic target plasma. Phasing is 180° shift per waveguide. Upper trace is plasma current (20 amps per division). Lower trace is the loop voltage (1 volt per division). Horizontal scale is 1 msec per division.

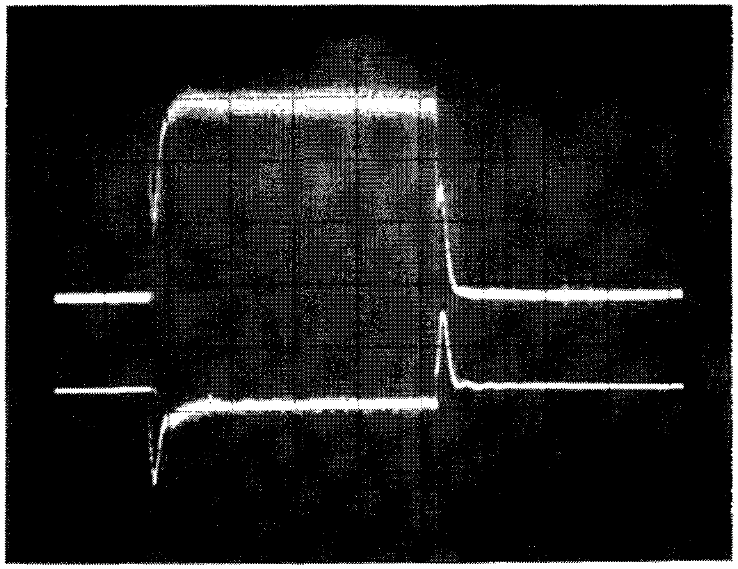

Figure 7-20b. Same as Figure 7-20a, but B_H adjusted to maximize the RF driven current in the opposite direction. Upper trace is plasma current (20 amps per division). Lower trace is the loop voltage (1 volt per division). Horizontal scale is 1 msec per division.

In Figures (7-20) the symmetry between the forward and reverse driven plasma current for symmetric 180° phasing of the antenna is good. In Figure (7-21a) similar results are shown for quadrature phasing to enhance the positive current. There is now a notable asymmetry. Repeating this experiment with quadrature phasing to enhance the negative current does not retain the asymmetry however. See Figure (7-21b). The conclusion is once again that the effects of phasing in RF sustained plasma appears to be weak.

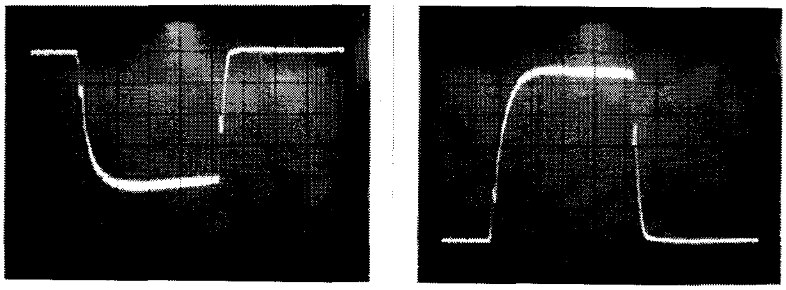

Figure 7-21a. B_H and B_V adjusted to maximize reverse I_P^{RF} (left) and forward I_P^{RF} (right). Phasing is quadrature for forward direction.

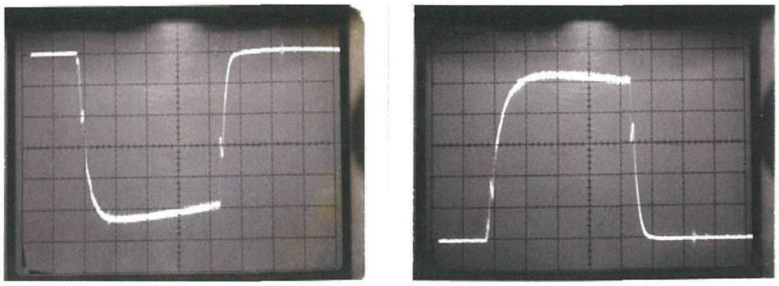

Figure 7-21b. B_H and B_V adjusted to maximize reverse I_P^{RF} (left) and forward I_P^{RF} (right). Phasing is quadrature for reverse direction.

When the ohmic supply is used to break down the target plasma, there is a bright flash of light. Due to the persistence of vision, the RF sustained plasma cannot be seen independently with the naked eye. Without the ohmic breakdown, the RF sustained plasma became instantly visible. There is a background glow from the volume inside of the vacuum chamber. Superimposed is a very bright narrow beam that would move around in response to changes in B_H and B_V. With no vertical field the glow was concentrated at the top of the vacuum chamber as shown in Figure (7-22).

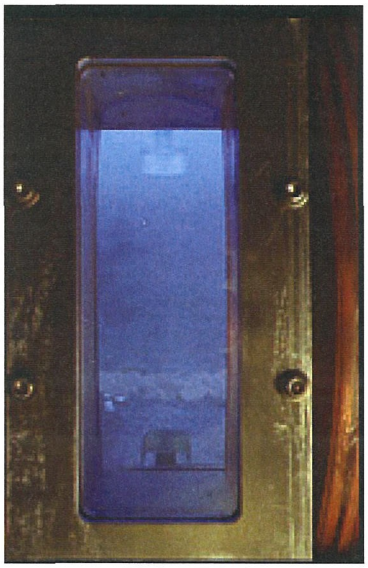

Figure 7-22. Glow from a RF produced plasma in Encore. The glow is concentrated at the top of the vacuum chamber. The toroidal magnetic field polarity is such that the guiding center drifts for electrons are directed upwards.

From equation (3.12) the vertical confinement in a tokamak can be written as

$$\left|\delta z\right| \le \frac{2 v_\phi}{\left|\frac{qB_\theta}{m}\right|}. \tag{7.3}$$

The electron toroidal velocity can be associated with a parallel energy according to

$$v_{\parallel e} = \sqrt{\frac{2E_\parallel}{m_e}} \approx 5.93\times10^7 \sqrt{E_{\parallel\, eV}}\ \ \mathrm{cm/sec}. \tag{7.4}$$

The poloidal cyclotron frequency (denominator of equation (7.3)) can be written as

$$\left|\frac{qB_\theta}{m}\right| \approx 3.5\times10^6 \frac{I_{amps}}{r_{cm}}\ \mathrm{sec}^{-1}, \tag{7.5}$$

where the formula for the magnetic field a distance r_{cm} from a straight wire carrying a current I_{amps} has been used. Combining (7.3), (7.4) and (7.5) yields

$$\left|\delta z\right| \le 34 \cdot \frac{r_{cm}\sqrt{E_{\parallel eV}}}{I_{amps}}\ \mathrm{cm}. \tag{7.6}$$

It will be shown in the double-sided probe measurements that the energy of the tail electrons in the "beam" exceeds 100 eV. Taking values of r_{cm}=1cm, I_{amps}= 65amps and T_{eV}=100eV returns $\left|\delta z\right| \le 5\mathrm{cm}$. 100eV is a lower bound. Confinement is worse for larger energies. Since the minor radius of Encore is only 12cm, these RF discharges do not appear to be confined in the conventional tokamak sense.

In the absence of sufficient poloidal current to provide confinement, drifts due to the magnetic field curvature and gradient force the electrons and ions out of the tokamak. The **∇B** and curvature-**B** drifts in a tokamak are oriented in the vertical direction. Collectively these two drifts are sometimes referred to as the guiding center drifts. Electrons drift one direction (up or down), and the ions the other. The resulting vertical electric field causes an $\mathbf{E}\times\mathbf{B}$ drift in the major radius direction. The formula for the gradient and curvature drift is[7]

$$v_z = \frac{\frac{1}{2}mv_\perp^2}{qB} \cdot \frac{\mathbf{B}\times\nabla\left(B^2/2\right)}{B^3} + \frac{m}{qB} \cdot \frac{\mathbf{B}\times\frac{d}{dt}\left(\mathbf{v}_\parallel\right)}{B}. \tag{7.7}$$

The first term in equation (7.7) is the magnetic field gradient drift, and the second term is the field curvature or centripetal drift. Equation (7.7) can be approximated as

$$v_z \approx \frac{m}{qB_o}\cdot\frac{1}{4}\cdot v_\perp^2 \cdot \frac{B_{max}^2 - B_{min}^2}{B_o^2 2 r_{minor}} + \frac{m}{qB_o}\cdot\frac{v_\parallel^2}{R_{major}}, \qquad (7.8)$$

where r_{minor} is the minor radius of Encore, R_{major} is the major radius, B_{max} is the toroidal field at the inner wall, B_{min} is the toroidal field at the outer wall, and B_o is the toroidal field on axis. Using the values for maximum toroidal field (1300 gauss on axis), assuming 100eV to calculate $v_\parallel$ and assuming T_e=10eV to compute $v_\perp^2$ obtains $v_z \cong 4.1\times10^5$ cm/sec. The second "centripetal" term in equation (7.7) dominates. The speed of an electron accelerated to 100eV in the toroidal direction is $v_\phi \cong 5.9\times10^8$ cm/sec. The ratio of these two quantities is

$$\frac{v_z}{v_\phi} = 0.0007. \qquad (7.9)$$

This represents a small angle. The vertical displacement per toroidal revolution is of the order of 0.2 centimeter. The fact that the luminous "beam" appears at the top of the tokamak is puzzling. It would seem unlikely that it could drift up there from an initial location coincident with the end of the LH grill antenna without creating luminosity in the intervening region as well. Even for electrons accelerated to $N_\parallel = 10$ ($v_\parallel = 0.1c$), equation (7.8) returns an angle of 0.003 radians. The vertical displacement per toroidal revolution is 0.8 cm. What is perhaps more likely, the beam is generated along the toroidal field lines nearest the filament which supplies the electrons for the breakdown. What is surprising is that these field lines pass some distance from the end of the LH grill antenna, probably of the order of the minor radius when the filament is located on a top or bottom port.

With the addition of a vertical magnetic field B_V, the vertically oriented helical path of the beam could be observed through an optical window mounted on a port located at the outer mid-plane as shown in Figure (7-23). With the filament emitting electrons but with no applied RF, no luminosity whatsoever was visible in the torus.

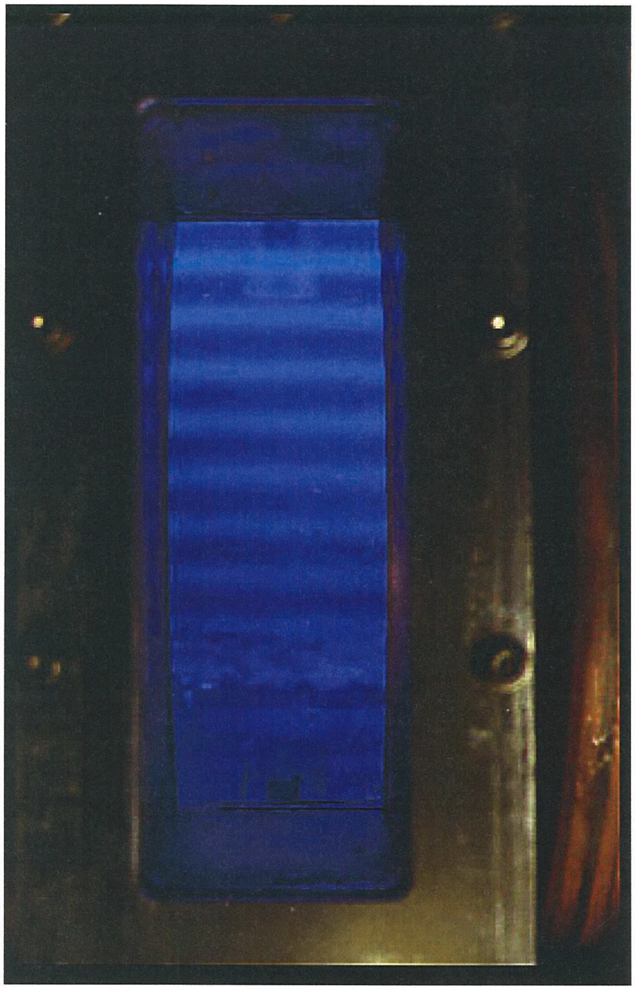

Figure 7-23. Helical path of RF-driven plasma current in Encore. For this photo a vertical magnetic field was applied. The optical window is located on a side port of Encore.

Note that the luminous beam is quite narrow from top to bottom. The launching LH antenna is 7cm tall. The window port in Figure (7-23) is roughly 17cm tall. Estimating from photos, the luminous beam is about 0.6cm thick. This could be explained if the filament dimensions set the beam size.

It was determined that indeed the filament was the source of the luminous beams. In Figure (7-22) the guiding center drifts for electrons are directed upwards and the filament was located at the top of the torus. For other locations of the filament, the luminous beam would appear in different locations as expected. The beam location near the top of the torus explains the sensitivity of I_P^{RF} to the vertical magnetic field. By adjusting B_V the symmetrically generated beams suffer differential attenuation against the top of the chamber and the polarity of I_P^{RF} can be altered. This is analogous to the horizontal spiraling phenomena for obtaining net current discovered earlier.

In Figure (7-23) the luminosity appears to decay over the ten or so revolutions visible in the tokamak. The energy of an electron that can travel this distance in 2.5×10^{-5} torr argon before coming to rest can be estimated. With a major radius of 38cm, ten revolutions corresponds to a distance of 2400cm. It can be determined that room temperature argon at a pressure of 2.5×10^{-5} torr has a density of 5.5×10^{-11} gm/cc. The CSDA (Continuous Slowing Down Approximation) range is a very close approximation to the average path length traveled by a charged particle as it slows down to rest. The CSDA range is obtained by integrating the reciprocal of the total stopping power with respect to energy. The path will generally not be straight and the "projected" range is the average depth measured along the initial direction to which a charged particle will penetrate in the course of slowing down. However, the CSDA range is a measure of the greatest possible depth of penetration. Tables of CSDA range for electrons in argon are available.[8] The data for argon are plotted in Figure (7-24).

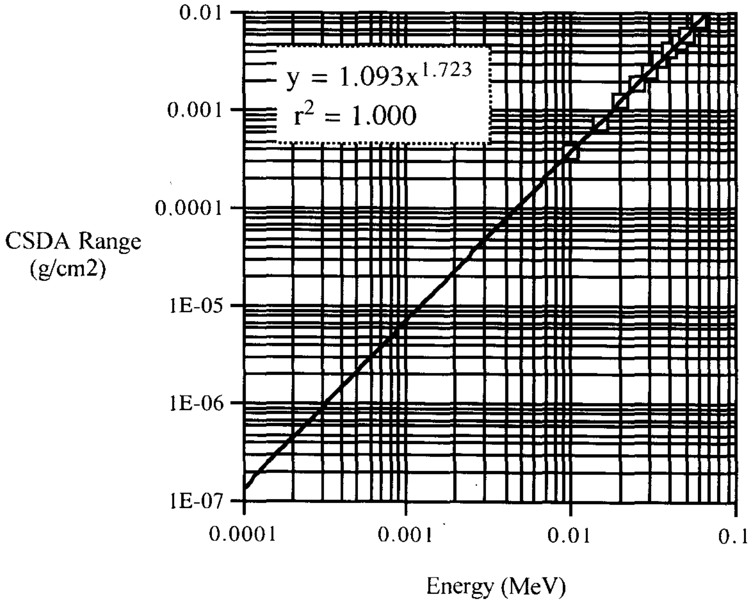

Figure 7-24. The CSDA range for electrons in argon according to reference 8.

Using a distance of 2400cm and a density of 5.5×10^{-11} gm/cc, it is determined that the CSDA range must be 1.3×10^{-7} gm/cm^2. From Figure (7-24) this corresponds to an energy of about 100eV.

From Figure (5-15) it can be seen that the grill antenna with quadrature phasing generates an $N_{||}$ spectrum at launch from roughly 5-to-15. Electrons accelerated to velocities corresponding to $N_{||}=15$ have a parallel energy of 1140eV, while those accelerated to correspond to $N_{||}=5$ have energies of 10.3keV. Electrons with a parallel energy of 100ev correspond to $N_{||}=51$. If these electrons are produced or sustained by a LH wave interaction, then the spectral gap has been bridged. If a toroidal "cavity mode" were responsible then the beam would not extinguish in luminosity moving away from the top of the torus.

The LH wave interaction with the electron beam may persist as the electron beam makes many revolutions of the torus. The electrons may continuously lose energy to the argon atoms, but continuously gain some back from the LH waves. The RF sustained plasma may be most concentrated at the top of the torus where the filament is located. The beam may lose luminosity simply because it propagates out of the region at the top of the chamber where the plasma necessary to support LH waves is most concentrated.

There happened to be a very narrow window port on top of Encore and pictures were taken through it of the luminous beam from above. See Figure (7-25). For these photos, the vertical field was adjusted to maximize I_P^{RF}. As B_H was adjusted, the position of the luminous beam would move in major radius as expected. As in the picture taken from the side, the dimensions of the beam were quite narrow compared to the dimensions of the launching LH antenna. The beam is located at the top of the tokamak and very close to the window port.

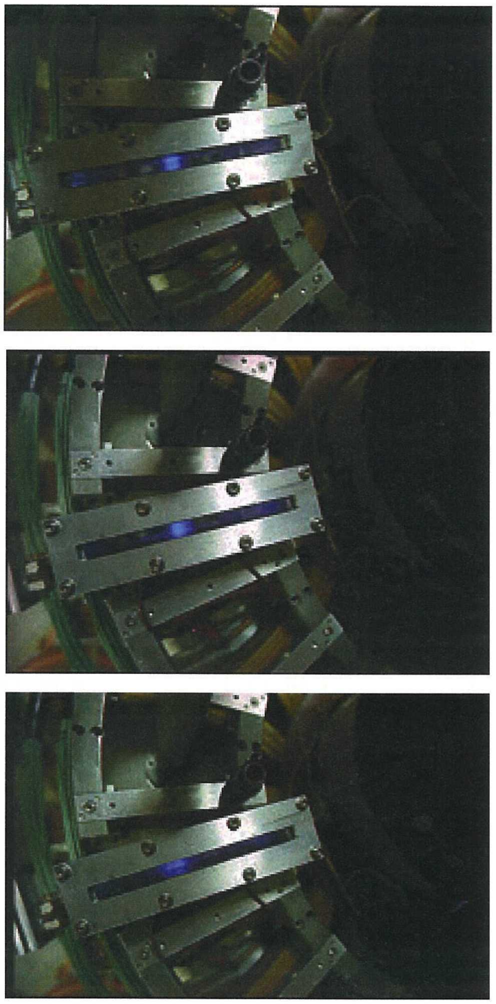

Figure 7-25. Luminous "beam" of RF driven plasma current as seen through a window port located on top of the tokamak. The beam progressively moves from right to left going down the photos. B_H is varied to cause this motion.

X-Y Probe Measurements of Error Fields

The spiral nature of the magnetic field in Encore was observed in a more direct fashion. A tiny filament was mounted on the end of an alumina probe and inserted horizontally into the vacuum chamber from the outer mid-plane. The filament location was approximately 6-7cm from the outer wall of the vacuum chamber. The vacuum level in the chamber was of the order of 2×10^{-6} torr. The filament was heated and biased 20-volts negative to produce an emission current of 1.4 microamps. The toroidal magnetic field current was set to 395 amps producing a field on axis of approximately 1360 gauss.

The direction of the toroidal field is set clockwise as viewed from above.[9] The two-sided current probe described in chapter 5 was used to detect the current launched along the toroidal field lines. Only one side of the probe was utilized. The orientation of the plots is described in Figure (7-26). The probe measurements are shown in Figure (7-27). It appears in these Figures that the filament is emitting from two distinct locations.

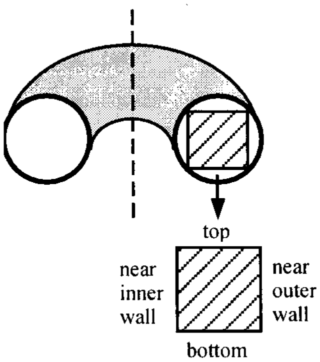

Figure 7-26. Orientation of the X-Y plots. The right-hand edge is nearest the outer wall, the left-hand edge is nearest the inner wall.

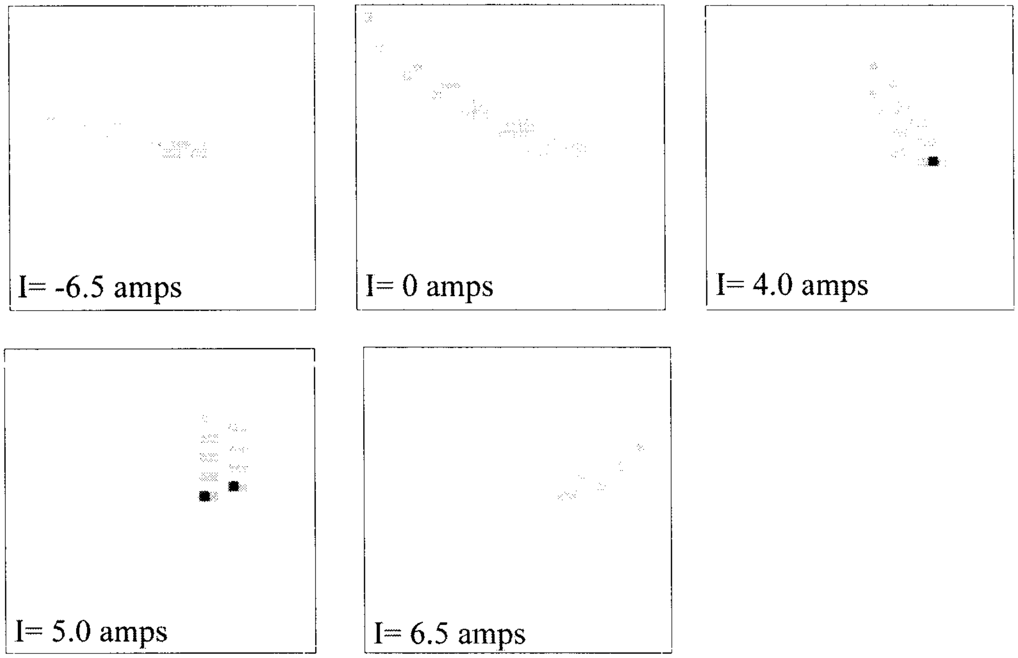

Figure 7-27. Electron current (dark patches) detected with one side of the two-sided probe. The scanned area is a square inscribing the circular cross section of the vacuum chamber. The left side of the square is nearest the inner wall. The currents listed are those in the radial-horizontal correction field coils. No current was placed in the vertical field coils.

The vertical and radial components of the toroidal magnetic field of Encore cannot be simply measured with a handheld magnetic probe. Since the toroidal field is so large compared to the components of interest, small changes in the probe angle would cause large changes in the probe measurement.

Probe measurements show that positive current in the radial-horizontal correction field coils generates a magnetic field directed radially outward. Since this corrects the radial drift seen in Figure (7-27), the radial field inherent to Encore is directed inward. Since the uncorrected drift as visualized in Figure (7-27) is toward the inner wall and the toroidal field is oriented clockwise (as seen from above), the current collecting probe must face the filament on the "downstream" side of the filament in terms of the toroidal field. In other words, the toroidal field lines must point from the filament to the current collecting side of the double probe, rather than the other way around.

The vertical component of earth's magnetic fields points downward in the Northern Hemisphere and is of the order of a half gauss.[10] In the absence of a vertical component from the toroidal field coils, the toroidal field would spiral slightly downward. The current collecting side of the double-probe faces the filament on the "downstream" side and yet upward drifts are seen in Figure (7-27). The inherent vertical field of Encore must be either directed upward or else must be insufficient to overcome the electron curvature and gradient-**B** drifts.

For the given polarity of the toroidal magnetic field, the gradient-**B** and curvature-**B** drifts for the electrons are upward, independent of toroidal direction. In Figure (7-27) upward drifts are seen. The vertical height of the scanned area was determined to be 15.9cm. In Figure (7-27) for the case of I=5amps, the vertical shift of the spiraling electron beam per revolution is roughly 1.0cm. The maximum guiding center drift velocity occurs when the 20eV energy of the source electrons goes entirely into $v_{||}$. For this case equation (7.8) gives a vertical drift velocity of 8×10^4 cm/sec. Electrons with $E_{||}$=20eV have a toroidal velocity of 2.65×10^8 cm/sec. The ratio of these two speeds is 0.0003. The maximum vertical displacement per revolution due to the guiding center drifts is then about 0.07cm. The fact that the measured drift exceeds the maximum possible guiding center drift implies that there is an inherent vertical magnetic field due to the toroidal field coils and/or the horizontal field coils. The polarity of the vertical field must be upwards in order to enhance the guiding center drifts. A lower bound to the magnitude necessary is that which accounts for a 0.93cm drift per revolution. The relevant equation is

$$\frac{B_V}{B_\phi}\cdot 2\pi R = 0.93\,\text{cm}. \qquad (7.10)$$

It may be estimated from Figure (7-27) that the location in major radius of the emitting filament is the axis of the chamber (38cm) plus 3.2cm. The toroidal field on axis is 1360 gauss and at the location of the filament would be 1254 gauss. Solving equation (7.10) for B_V returns 4.5 gauss. This is the net vertical error field. Subtracting the downward 0.5 gauss due to the earth's magnetic field means that the vertical field due to Encore when 5 amps are placed in the horizontal coils is of the order of 5.0 gauss (at the measured location).[11] This is a lower bound since the electron source does not produce a beam that is mono-energetic in parallel energy.

Ideally one would place the electron source on an X-Y probe so that the field error could be mapped as a function of position in the minor cross section of the torus. Errors are not necessarily evenly distributed in the toroidal direction. For instance on Encore, the iron core of the ohmic transformer induces localized field errors. Errors accumulated in complete revolutions of the torus should be examined. Apparatus for such measurements has been described.[12]

Energetic Electrons in RF Sustained Plasma

Hot electron measurements similar to those described in the previous section were made in RF-sustained plasma. An ohmic target plasma was utilized. The scanned area was a square, but rather than being inscribed in the minor cross section, it was displaced 3.8cm outward in major radius. This was done because many hot electrons were found near the outer wall where the end of the grill antenna is located.

The toroidal field was set to circulate counterclockwise which is opposite to the direction of the previous section. The inherent radial, horizontal, magnetic field is consequently now directed outward. The magnitude of the toroidal field was 1300 gauss on axis. The "two sided" X-Y scanning probe was located 157.5° counterclockwise from the grill antenna as seen from above the tokamak. The experimental arrangement is shown in Figure (7-28). The two probes were biased 100 volts negative so that detected electron current must occur from energetic electrons. The two probes are labeled "1" and "2," probe "2" facing into the toroidal field.

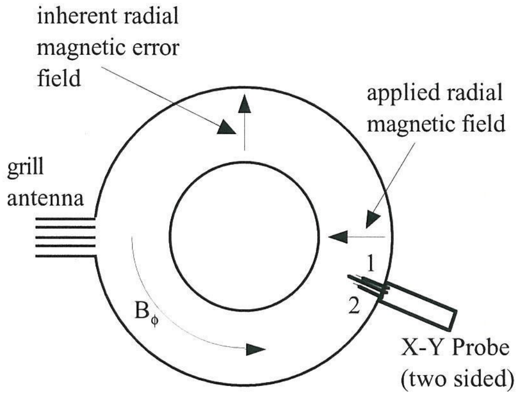

Figure 7-28. Experimental arrangement as seen from above the tokamak.

4.9 kW power was delivered to a single channel of the four port grill antenna (one of the two interior waveguides). The tokamak was filled with argon to a pressure of 2.5×10^{-5} torr.

The data is presented in the form of two-dimensional color-coded plots. Ten colors represent the current ranges and the color code is given in Figure (7-29). Blue and black represent negative ranges where ion current dominates. Shades of green represent the most intense regions of hot electrons.

Figure 7-29. Color code for the data plots. The scale is linear with lowest to highest going from left to right. The upper bound of the lowest color is -7.4mV (across the input resistance of the amplifier). The upper bounds of the next eight colors in mV are 2.6, 12.6, 22.6, 32.6, 42.6, 52.6, 62.6 and 72.6. The lower bound of the largest color is 72.6mV.

In Figure (7-30) data for the case with no correcting radial horizontal magnetic field and no vertical field is given. The location of the most intense hot electrons is near the outer wall where the mouth of the grill antenna is located. From Figure (7-28) it can be seen that the uncorrected spiraling of the toroidal field lines should push the hot electrons nearer the outer wall for probe "2" and away from the outer wall for probe "1." This is born out by the shifts in the outer border of the green regions in Figure (7-30). For the direction of the toroidal field, the gradient-**B** and curvature-**B** drifts are downward for electrons, independent of toroidal direction. The green regions in both plots of Figure (7-30) are shifted downward from center.

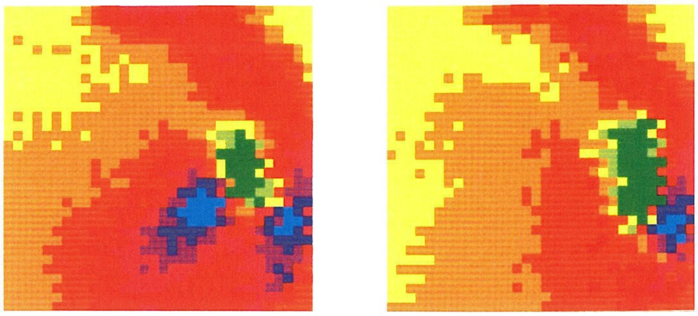

Figure 7-30. Color-coded plots of hot electrons. No correcting horizontal or vertical magnetic field is employed. The left plot is from probe "1" and the right plot is from probe "2." The outer wall of the tokamak is very near the right side of the plots, and the inner wall is nearest the left side.

In Figure (7-31), the results of applying a strong radial-horizontal magnetic field to more than reverse the horizontal error field is shown. I_P^{RF} is reversed as a consequence. This time electrons impinging on probe "2" have spiraled into the interior of the tokamak, while electrons that would have impinged on probe "1" have spiraled toward the outer wall to such a degree that practically no green regions are evident.

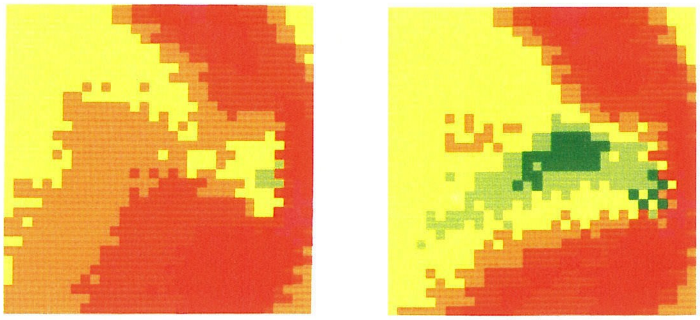

Figure 7-31. 13 amps are applied to the radial-horizontal magnetic field coils to reverse the direction of I_P^{RF}. The applied radial magnetic field is roughly 7.1 gauss. The left plot is from probe "1" and the right plot is from probe "2." The outer wall of the tokamak is very near the right side of the plots, and the inner wall is nearest the left side.

In Figure 7-32, the applied radial-horizontal field is adjusted to make $I_P^{RF} = 0$. The right-hand boundaries of the green regions of denser hot electrons are comparable distances from the outer wall.

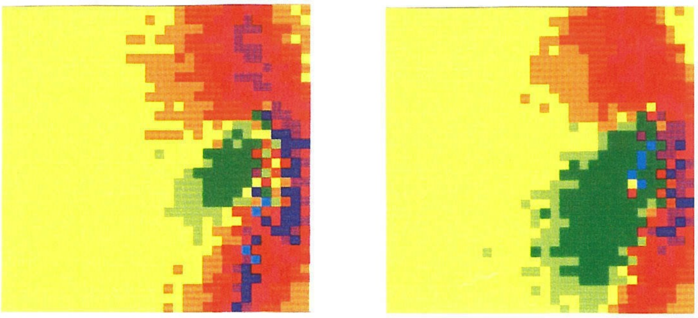

Figure 7-31. Approximately 4.5 amps are place in the radial-horizontal magnetic field coils to achieve $I_P^{RF} = 0$. The left plot is from probe "1" and the right plot is from probe "2." The outer wall of the tokamak is very near the right side of the plots, and the inner wall is nearest the left side.

In Figure (7-33) no correcting radial-horizontal magnetic field is applied. However, +4.8 amps are applied to the vertical field coils. Probe measurements indicate that this produces a field that points upwards with a magnitude of approximately 4.3 gauss. This was found to help the ohmic breakdown. The gradient and curvature-**B** drifts for electrons are downward. The easier ohmic breakdown is consistent with the fact that the ohmic supply drives electrons counterclockwise (as seen from above), and the addition of the upward vertical field causes these accelerated electrons to spirals upwards counteracting the downward drifts. Since no correcting radial-horizontal magnetic field is applied, electrons impinging on probe "2" should be closer to the outer wall than those impinging on probe "1." In Figure (7-33) this appears to be the case judging form the right-most boundaries of the green regions. Electrons impinging on probe "2" (second plot in Figure (7-33)) travel in the same direction as the ohmic electrons and appear well confined. Electrons impinging on probe "1" (first plot in Figure (7-33)) appear less well confined. In this case the electrons spiral downward due to the vertical field and also drift downward due to the gradient and curvature-**B** drifts.

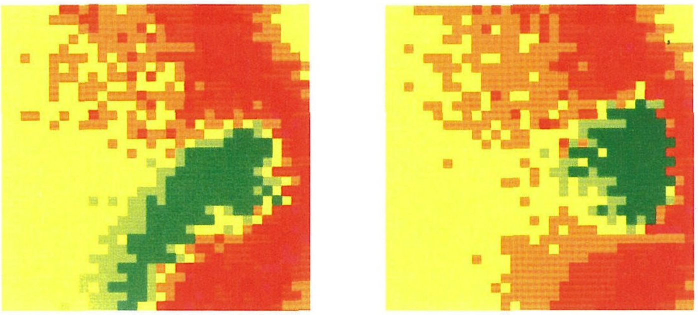

Figure 7-33. Approximately 4.8 amps are placed in the vertical magnetic field coils creating a toroidal field that spirals upward. No radial-horizontal field is applied. The left plot is from probe "1" and the right plot is from probe "2." The outer wall of the tokamak is very near the right side of the plots, and the inner wall is nearest the left side.

Fast Wave Launch

In the previous section it was noted that a considerable fraction of the detected hot electrons were found very close to the end of the grill antenna. It could be conjectured that the evanescent fields between the end of the grill antenna and the slow wave cutoff could accelerate electrons passing by. From Figure (5-16f) the $N_{||}$ spectrum for a single waveguide is much broader than for quadrature phasing, but is still concentrated below $N_{||} = 36$. Acceleration is more likely if the initial toroidal velocity of the electron is resonant with an $N_{||}$ in the spectrum. For $N_{||} = 36$ the resonant electron would have an energy of 198eV. In Figure (5-15f) some miniscule amount of power is available as high as $N_{||} = 72$. For $N_{||} = 72$ the resonant electron would have an energy of about 50eV. Such energies are unlikely to be produced by the filament source but could possibly be generated in the ohmic target plasma. It is also possible that electrons of these energies generated by Landau damping of LH waves could subsequently be accelerated by the evanescent region, thus enhancing the current drive.

There is an interesting way to test these ideas. If the grill antenna is rotated 90°, then the electric field of the TE_{10} mode is no longer parallel to the toroidal field but perpendicular to it. In this configuration it would be impossible for the evanescent fields to accelerate electrons passing by in the toroidal direction. From equation (4.137) the electric field perpendicular to both the toroidal magnetic field and the density gradient is the appropriate polarization for launching fast waves. Fast waves have been launched and well characterized in toroidal plasmas.[13] Experimental results agree with predictions from the cold-plasma dispersion relation. Fast waves can also drive current in toroidal plasmas.[14,15,16] The current drive efficiencies for the slow and fast mode are comparable.

From equation (4.128) the cutoff for the fast mode is at a slightly higher plasma density than for the slow mode (equation (4.124)). If distance from the cutoff were any concern, matters would be worse for the launch of fast waves.

The orientation of the antenna for fast wave launch is toroidally symmetric. For the LH case with a single powered waveguide, toroidal symmetry is compromised due to the presence of the uneven number of non-powered waveguides.

For the experiment, 4.9 kW was applied to a single waveguide, the third from the top. The torus was filled with argon to a pressure of 2.5×10^{-5} torr. The toroidal field was set to 1300 gauss on axis with polarity such that circulation was clockwise. For this polarity the guiding center drifts for electrons are upwards. The radial-horizontal magnetic error field is directed inwards. No radial-horizontal correction field was applied. The preferred direction for accelerated electrons (spirals into the chamber rather than out toward the outer wall) is clockwise.

When RF power was applied, 20 amps of plasma current were driven. For a single waveguide the current drive efficiency is comparable to that from the launch of slow waves. The larger density required to reach cutoff was not a serious impediment.

The direction of the net electron flow was clockwise as expected from the spiraling of the field lines. To obtain the 20 amp current a downward directed vertical-magnetic-field of approximately 2.4 gauss was applied.[17] The resulting downward spiral for electrons propagating in the clockwise direction counteracts the upward guiding center drifts.

Hot electron measurements were made as described in the previous section. The measured square was shifted 3.8 centimeters outward from being inscribed in the minor cross section to capture hot electrons near the outer wall where the end of the grill antenna is located. The antenna was located 135¡ clockwise from the X-Y probe as seen from above. The color code is as previously described. The results are shown in Figure (7-34).

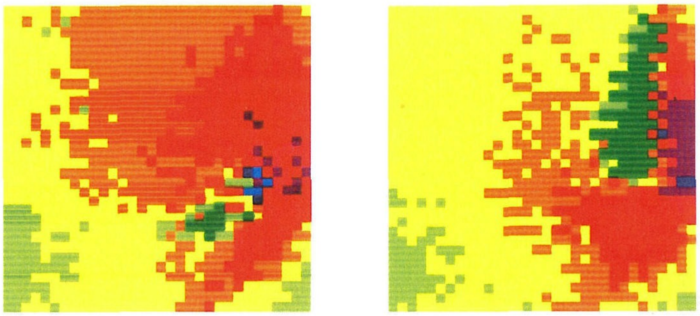

Figure 7-34. Plots of hot electrons with fast wave launch. The left plot records hot electrons accelerated clockwise in the torus. The right plot records hot electrons accelerated counter-clockwise in the torus.

Hot electrons were detected traveling in both directions. Orienting the antenna electric field parallel to the toroidal electric field is not a requirement to generate hot electrons. Electrons traveling in the preferred clockwise direction are vertically well confined in Figure (7-34). Electrons travelling in the counterclockwise direction follow magnetic field lines that spiral upwards in addition to drifting upwards due to the guiding center drifts. Figure (7-34) demonstrates this behavior.

I_P^{RF} varied with the combination of radial and vertical magnetic field settings. By altering the combination of radial and vertical fields slightly, a current of 26 amps was obtained.

A radial-horizontal magnetic field was applied so as to reverse the preferred direction for accelerated electrons. Now electrons traveling in the counterclockwise direction spiral inwards rather than toward the outer wall. With the aid of an upward directed vertical field of about 4 gauss, a current of 20 amps in the opposite direct was obtained. This is the same magnitude of current obtained in the previous case.

In summary, several important observations can be made. Significantly increasing the cutoff density does not seem to affect the current drive efficiency. This suggests that proximity to the cutoff is adequate for both slow and fast waves. Rotating the antenna electric field perpendicular to the toroidal direction does not hinder the generation of fast toroidal electrons. Nor does it affect the basic current drive efficiency. This suggests that the evanescent fields at the end of the grill antenna prior to the cutoff location are not a major source of the hot electrons observed.

Role of the Vertical Magnetic Field

In Figure (7-33) apparent vertical confinement is achieved with an applied vertical magnetic field of 4.3 gauss directed upward. It was previously estimated that the toroidal field coils cause a vertical error of roughly 5.0 gauss directed upward when the toroidal field circulates clockwise as seen from above, and the field on axis is 1360 gauss. With the toroidal field now circulating counterclockwise as seen from above, and with the field on axis being 1300 gauss, this 5.0 gauss error would be reduced proportionally to 4.8 gauss and point downwards. The vertical component of the earth's magnetic field is about 0.5 gauss directed downward. Combining these would predict that there was a net vertical magnetic field of roughly 1.0 gauss directed downwards. However, the electron drifts are also downward for this toroidal field polarity. Hence the net vertical magnetic field must be directed upwards to explain the confinement seen with probe #2 in Figure (7-33). The magnitude of the discrepancy is not large. It is possible that the vertical error field changed in magnitude, or that only a portion of it was due to the toroidal field coils and thus changed polartity when the toroidal field was reversed.

The probe bias of -100 volts requires that detected electrons be more energetic than 100eV. From the estimate of the CSDA range given earlier, one would anticipate that the energy of the electrons creating the luminous beam would not be too much larger than 100eV. One might estimate the necessary vertical field by equating the vertical pitch of the toroidal magnetic field to the ratio of the vertical drift velocity and the toroidal velocity. For electrons moving very fast along the toroidal field lines, the second "centripetal" term of equation (7.7) dominates. The relationship becomes

$$\frac{B_{\text{vertical}}}{B_\phi} = \frac{v_{z-\text{drift}}}{v_\phi} \cong \frac{m_e}{q_e B_o} \cdot \frac{v_\phi}{R_{\text{major}}}. \qquad (7.11)$$

Using 100eV as the appropriate electron parallel energy, one can solve equation (7.11) for the necessary net vertical magnetic field. The result is 0.9 gauss, a very modest magnetic field. For 2.6 keV electrons corresponding $N_{||} = 10$, the necessary field would be 4.5 gauss.

Equation (7.10) implies that larger vertical fields are necessary to confine more energetic electrons. Large vertical fields are incompatible with the ohmically generated target plasma and would present a problem. When the vertical field is used to confine the hot electrons, there is a juggling problem because the confinement is energy selective. Not all energies will be properly confined.

The arguments of the previous paragraph apply to very low current densities. It must not be forgotten, however, that Encore is a tokamak. Even for currents as small as 20 amps, it is the current *density* that determines the poloidal magnetic field, which in turn provides conventional tokamak confinement. The dark green "beam" in the first plot of Figure (7-34) has a diameter of the order of 1.5 cm. Were the beam to contain the bulk of the 20 amps, the poloidal magnetic field at the edge of the beam would be of the order of 5 gauss. From equation (3.12), however, a strict vertical confinement of 1.5cm for 100eV electrons requires a poloidal field of 280 gauss. It seems difficult to explain the confinement of the hot electron beams in a conventional tokamak sense. However, another factor to consider include the fact that current is driven in both directions in separate "beams." It is only the net current that is measured. The current in the beam could be much larger than 20 amps.

In true tokamak operation, the purpose of the vertical field is not to combat guiding center drifts at all, but rather to combat the tendency of the toroidal current to expand in major radius. The poloidal magnetic field confines the plasma. The tendency for the toroidal current to expand can be seen as follows. Lengths of current traveling in opposite directions on opposite sides of the torus repel each other.

It should be noted that I_P^{RF} does not monotonically increase with increases in the vertical magnetic field. There is always a peak observed in I_P^{RF} as the vertical field is varied. Sometimes the peak is rather weak.

The issue of confinement in these unusual low-current RF-sustained discharges requires further study. It appears as though the vertical magnetic field provides enhanced confinement for the hot electrons. The fact that there is insufficient plasma current to provide conventional tokamak confinement will be explained in the next chapter as due to the density limit.

Toroidal Field Scan

Hot electron plots were recorded as a function of toroidal magnetic field. If the location of the hot electrons varied with the toroidal field in a manner analogous to that of lower hybrid waves, it would act as a confirmation that LHCD was taking place. It was earlier argued that the sudden decrease in I_P^{RF} as the toroidal field is decreased agrees remarkably well with the theory of accessibility of LH waves. This is strong evidence for LHCD. In this section, comparison will be made with the LH cone angle.

The toroidal magnetic field was set to circulate counterclockwise, so the inherent radial error field is directed outwards as seen from above. The grill antenna was located 157.5 degrees clockwise from the X-Y probe. For this orientation, the toroidal field lines spiral toward the outer wall travelling from the antenna to the X-Y two-sided probe. The tokamak was filled with argon to a pressure of 2.5×10^{-5} torr. The probe bias was -100 volts as before. The color code is given in Figure (7-29). 3.9kW was applied to one of the interior waveguides. Data was taken using the probe closest to the antenna. To avoid any confusion, no vertical or radial-horizontal magnetic field was applied. The data is shown in Figure (7-35).

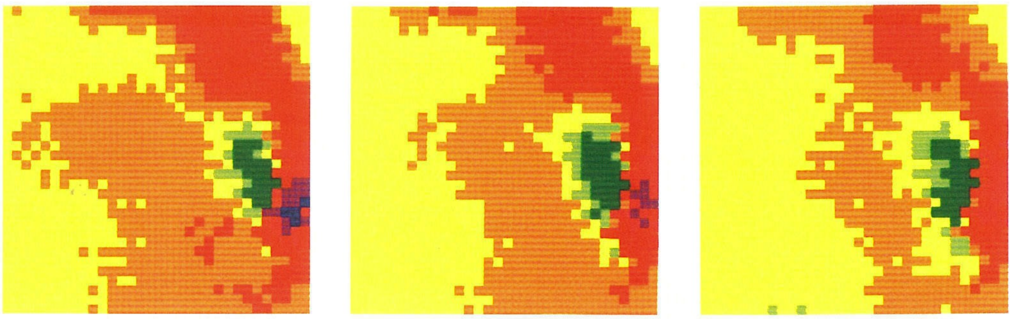

1360 gauss 1210 gauss 1040 gauss

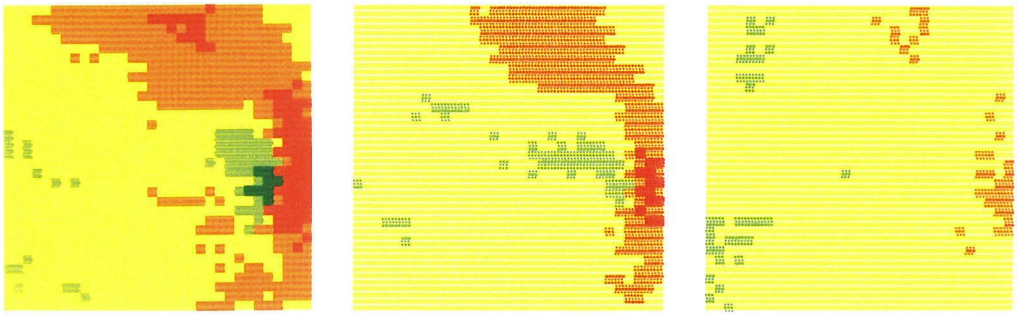

863 gauss 690 gauss 518 gauss

Figure 7-35. Plots of hot electrons for various magnetic fields. The outer wall of the tokamak is very near the right side of the plots, and the inner wall is nearest the left side.

In Figure (7-35) the areas of intense hot electrons, colored green, suddenly begin to disappear by 863 gauss. A possible explanation for this behavior is that accessibility of the antenna launch spectrum becomes significantly compromised at a toroidal field of 863 gauss. The $N_{\|}$ spectrum for a single waveguide is given in Figure (5-16f). The spectrum is peaked at $N_{\|} = 0$, and falls monotonically to zero by roughly $N_{\|} = 32$. The slope of the curve in Figure (5-16f) is steepest in the region $8 \le N_{\|} \le 24$, so once the accessibility limit moves above $N_{\|} = 8$ there will be a rapid drop in accessible power. Most of the power involves $N_{\|} < 20$.

Microwave density measurements were made during a RF sustained discharge and the measurement is shown in Figure (6-13). The measured line average plasma density was $7 \times 10^{11}\ cm^{-3}$. Evidence has been presented that RF discharges tend to form concentrated beams, so the peak plasma density may be significantly higher than the line average density. At the stated fill pressure there are roughly 8×10^{11} argon atoms per cubic centimeter, and single ionization will produce a plasma density of the order of

8×10^{11} cm^{-3}. For sake of argument assume a plasma density of $8.6\times10^{11}\text{cm}^{-3}$ corresponding to the 1.5kA graph in Figure (6-13). What this figure shows is that the accessibility limit for a toroidal field on axis of 863 gauss has reached $N_{||} = 10$ and accessibility is beginning to become a problem for a single waveguide spectrum. Any further decrease in the toroidal field will rapidly hinder accessibility.

The lower hybrid "cone" angle is the angle with respect to the local magnetic field at which LH waves propagate. From equation (4.89), the tangent of the LH cone angle for Encore parameters is given by ω / ω_{ce} and is independent of the plasma density. In Figure (7-36) the LH "cone" angle is given as a function of magnetic field for 450 MHz.

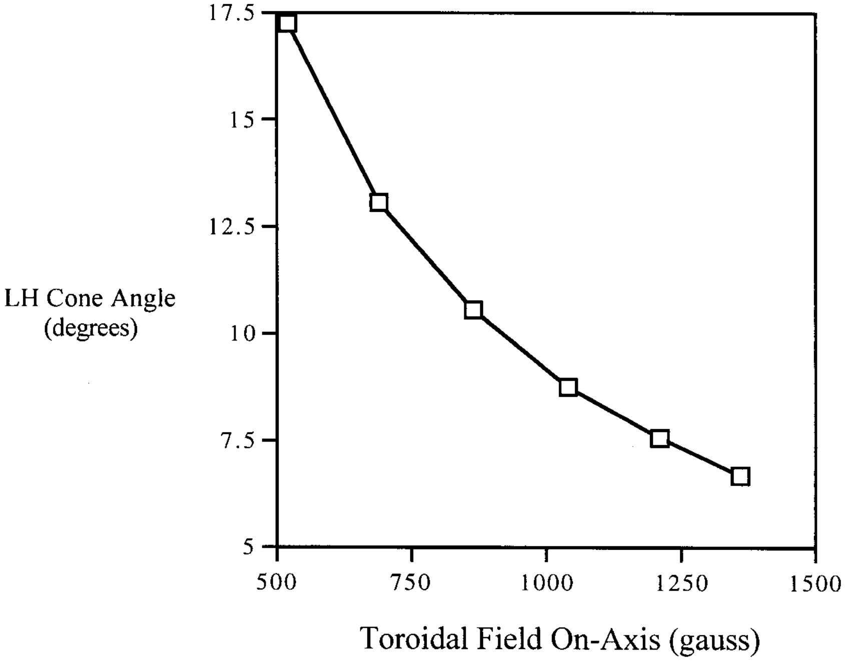

Figure 7-36. The propagation angle of lower hybrid waves with respect to the local magnetic field. At lower magnetic fields the angle is considerably larger.

Possibly because accessibility decreases the amount of LH power injected as the magnetic field is decreased, the amount of current represented by the dark and light green areas in Figure (7-35) decreases as the magnetic field is reduced. The question is whether the distribution of the current protrudes further from the outer wall (near the right-hand side of the plots) as the magnetic field is decreased and the LH cone angle increased. The distance from the grill antenna to the X-Y probe is 104cm. Due to the very small plasma current the poloidal field is negligible compared to the toroidal field and twisting of the field lines can be ignored. The maximum displacement of the LH wave front across the minor cross section is given by multiplying the propagation angle in radians by the distance. These values are given in the following table.

B_{axis}(gauss)	Angle (degrees)	Displacement (cm)
1360	6.7	12
1210	7.6	14
1040	8.8	16
863	10.6	19
690	13.1	24
518	17.3	32

The minor diameter of Encore is 26cm. The square containing the data is roughly 16cm in width. There is roughly a 5cm gap from the center of the edges of the square to the chamber wall. For the three lowest magnetic fields, the LH waves have opportunity to deliver energy and form hot electrons at the left-hand boundary of the plots. Since the magnetic field lines spiral towards the outer chamber wall travelling from the antenna to the X-Y probe, hot electrons cannot reach the left hand boundaries of the plots by propagating along the toroidal field for multiple revolutions of the torus. Inspection of Figure (7-35) shows that indeed areas of green exist near the left-hand boundaries for the three cases featuring the lowest magnetic fields. For the three highest magnetic fields the angle is insufficient to produce hot electrons at the left-hand edge of the plots. In Figure (7-35) no areas of green exist near the left-hand edge for the three cases featuring the largest magnetic fields.

Computing the horizontal centroid of the current and plotting this versus the propagation angle is more quantitative. This is done in Figure (7-37).[18] The results show that indeed the centroid of the current moves further into the chamber as the LH angle increases. The results are consistent with LHCD.

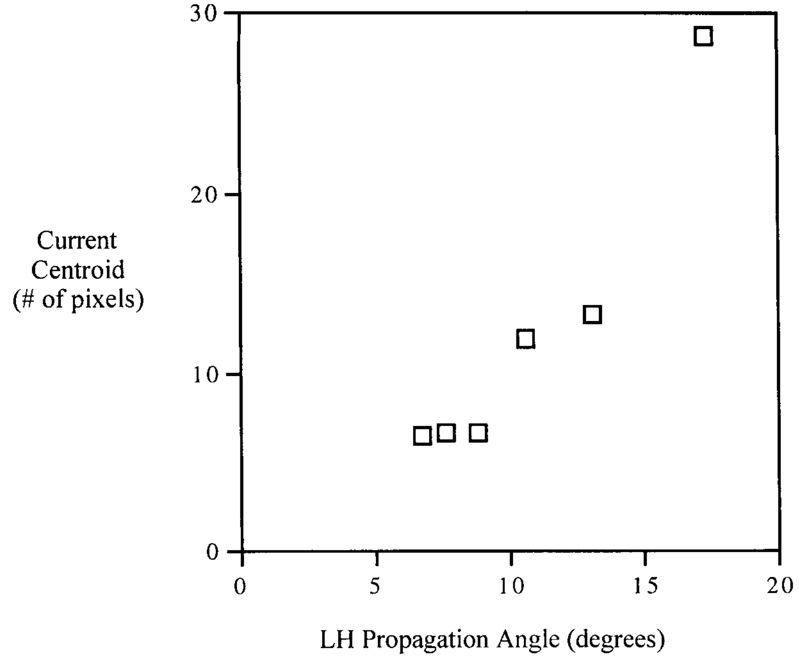

Figure 7-37. Graph of the horizontal centroid of the hot electron current versus the LH propagation angle. The plots are 32×32 pixels.

Effect of Initial Conditions

Under most circumstances, the initial conditions of the ohmic target plasma were not noticed to have an impact on the plasma current I_P^{RF} in RF sustained discharges. For instance, when RF sustained plasma current was first discovered in Encore, the polarity of the ohmic plasma was reversed without effect on the direction of I_P^{RF} and with little effect on its magnitude. However, it must be admitted that for most experiments great care was taken to insure that the initial conditions were identical, and these effects were not looked for. In the following instance a dependence on the conditions of the ohmic target plasma was documented.

The configuration of the tokamak is shown in Figure (7-38). The toroidal field was set to circulate clockwise as seen from above. The toroidal field was 1311gauss on axis. The inherent radial magnetic error field is directed radially inward for this toroidal field polarity. An over correction was made to the radial magnetic error field. The applied correcting field was directed radially outward and was of a magnitude to completely reverse I_P^{RF} (roughly 5gauss). For this configuration, the preferred direction for electrons accelerated near the outer wall is counter clockwise. Electrons accelerated in the counterclockwise direction will spiral into the chamber, rather than outward toward the nearby wall. The ohmic system on Encore also accelerates electrons in the counterclockwise direction. The plasma current was maximized for a vertical magnetic field of 3.3 gauss directed upward, and this field was used to take the data..

The tokamak was filled with argon to a pressure of 2.5×10^{-5} torr. All four waveguides were energized with identical phase. According to Figure (5-16a) this produces a very narrow $N_{||}$ spectrum centered on zero, with virtually all of the power satisfying $N_{||} \leq 8$, although some miniscule amount of power is available at $N_{||}$ values as high as 36. The RF power to the four waveguides in kilowatts was 4.7, 2.7, 4.7 and 3.7 respectively. The imbalance will broaden the $N_{||}$ spectrum somewhat.

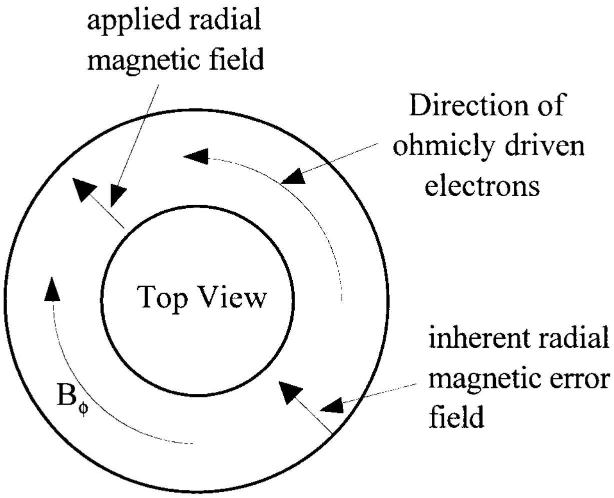

Figure 7-38. Configuration of the tokamak for the experiment showing an effect of initial ohmic plasma level on the RF-sustained plasma current. RF driven electrons representing the net RF current travel counterclockwise as do ohmic driven electrons.

The I_P^{RF} data is shown in Figure (7-39). Two different settings of the ohmic plasma setting were utilized (1.6 and 2.8). With the 2.8 setting, larger ohmic current was produced, taking longer to decay. The larger initial ohmic current is associated with the smaller RF-sustained plasma current (70 amps versus 100 amps). The ohmic and RF-sustained current have identical polarity.

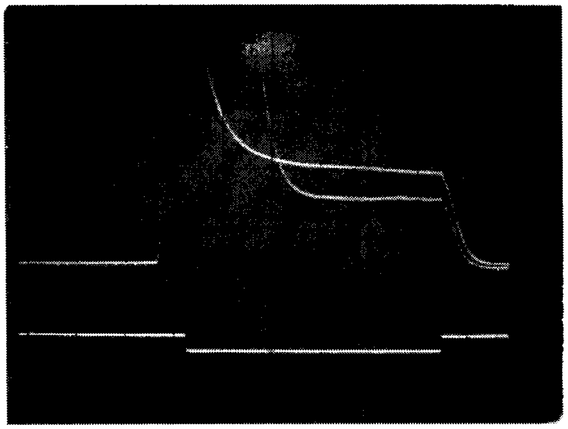

Figure 7-39. Plasma current versus time for two different settings of the ohmic amplifier. The larger initial ohmic current is associated with the smaller I_p^{RF}. Horizontal scale is 1msec per division. Vertical scale is 50amps per division. Lower trace tracks the RF.

The loop voltage is shown in Figure (7-40). With no RF, the loop voltage quickly decays to zero. With RF, the loop voltage never decays to zero during the RF-sustained plasma, but instead appears to even plateau for the lower ohmic setting. There is a large spike in the loop voltage when the RF is turned off and the plasma current decays. This data is reproducible and several photographs of the same data were made.

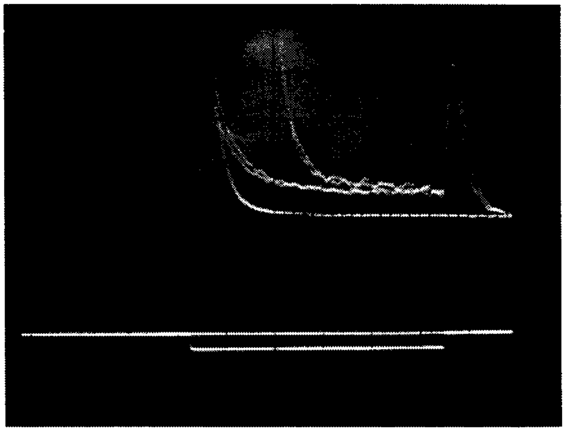

Figure 7-40. Loop voltage versus time for two different settings of the ohmic amplifier. Loop voltage is also shown for the lower ohmic setting without RF. The loop voltage takes longer to decay with the larger initial ohmic current. There is a large spike in the loop voltage when the RF sustained current decays. Horizontal scale is 1msec per division. Vertical scale is 200mV per division. Lower trace tracks the RF.

A possible explanation for why the larger ohmic plasma current results in smaller RF-sustained plasma current involves the distribution in the minor cross section of the plasma electrons to be accelerated by LHCD. It is not known if the target electrons are primarily thermal electrons or tail electrons. Experiments by others have shown that LH waves launched parallel to ohmically driven electrons contribute to much greater increases in plasma current than LH waves launched the other direction, suggesting that thermal electrons are not the target electrons.[19] Whichever, if the target electrons are primarily formed at larger major radius, then I_P^{RF} will be larger due to the fact that the path length before spiraling into the inner wall is larger. It is possible that the smaller ohmic setting causes the bulk of the target electrons to be formed at larger major radius. It would be possible to check this with probe measurements.

The loop voltage maintains a low but non-zero value during the RF-sustained discharge. Three possible explanations are discussed in the following.

One possibility is that the RF induced plasma conductivity is such that the L/R decay time is long compared to duration of the RF plasma. Since the RF is on long before the loop voltage decays to the almost constant level of roughly 100mV, one would have to argue that the conductivity took a few milliseconds to develop. The inductance of Encore is of the order of one micro-henry.[20] A typical ohmic discharge in Encore might have a plasma current of 1kA and a loop voltage of 8 volts for a resistance of the order of 8 milli-ohms. The L/R time is of the order of 0.1milli-second. In order to achieve an L/R time on the order of 10 milliseconds or larger, the resistance of the plasma would have to be of the order of 0.1 milli-ohm or less.

Another possibility is that the RF-sustained plasma is slowly decaying. If the decay rate is one amp per millisecond, which is certainly possible in Figure (7-39), then the loop voltage would be

$$V_{\mathrm{loop}} = L\frac{dI}{dt} = (10^{-6}\,\mathrm{henry}) \times (10^{3}\,\mathrm{amp/sec}) = 1\mathrm{mV}. \tag{7.12}$$

In order to get a loop voltage of 100 mV as in Figure (7-38), the decay rate would have to be 100 amps per millisecond, and this is ruled out in Figure (7-39).

Yet another possibility is that the spiraling RF-driven electron beam impinges the tokamak chamber inner wall at a location that is not 180 degrees from the gap in the torus across which the loop voltage is measured. The roughly 100 amp plasma current must then flow in the aluminum chamber wall. In order to drop 100 mV, a resistance of the order of one milli-ohm across some portion of the torus is necessary. Although this seems plausible, there is the question of why the two differing plasma currents end up with virtually identical loop voltages.

Summary

Low current (≤ 160 amp) discharges were maintained in Encore by application of RF with the grill antenna. Net plasma current is obtained not by antenna phasing but rather with the aid of subsidiary magnetic fields that induce spiraling of the toroidal field lines. When the electron acceleration is near the plasma periphery, the spiraling presents an asymmetry that favors one toroidal direction over the other. It is not known why the antenna phasing failed to produce significant asymmetry in the plasma current. The highly inhomogeneous nature of the unusual plasma may play a role.

The decrease in plasma current at low toroidal field strength appears to closely coincide with the onset of LH accessibility problems. This is strong evidence that LHCD is involved. The dependence of the amount of plasma current on the ion mass correlates with the ion mass scaling of the density limit discussed in chapter 8. There is some evidence that the hot electrons produced distribute themselves in correspondence to the LH propagation angle.

Fast wave launch produces similar plasma current, so acceleration of electrons by the antenna evanescent fields prior to the plasma mode cutoff can be ruled out. The fast wave cutoff is at a higher density than for the slow mode. Hence, proximity to the cutoff is not an impediment to LHCD.

With the use of a miniature electron source and a probe capable of scanning the minor cross section and detecting the electrons, the field errors in Encore can be observed and quantified. Electrons with energies above 100eV have been observed in RF sustained discharges. These beams of electrons are not confined in the conventional tokamak sense due to the low poloidal magnetic field. The vertical field plays an important role in the propagation of the low current beams. The behavior of the hot electrons confirms the spiral nature of the toroidal field lines. Encore has been operated in a purely RF mode without the use of an ohmic target plasma. When RF sustained discharges utilize an ohmic target plasma, the nature of the target plasma can sometimes affect the RF driven current level.

---

[1] This was an important discovery in the early study of cosmic rays. See I. Asimov, Understanding Physics, Dorset Press, (1988), volume II, p. 218

[2] Pete Politzer, tokamak designer, GA Technologies, Inc., San Diego, CA, private communication

[3] Hiroyuki Ikezi, GA Technologies, Inc., San Diego, CA, private communication

[4] The convention for current direction is based upon the normal ohmic current direction in Encore being positive.

[5] Obtained from the operating manual for the Varian Ratiomatic Ion Gauge used to measure pressure in Encore. Essentially it measures the difficulty in ionization by a 150-volt electron beam.

[6] L. H. Sverdrup and P. M. Bellan, "Cause of the Lower-Hybrid Current-Drive Density Limit," Phys. Rev. Lett., **59**, (1987), p. 1197, equation (6).

[7] George Schmidt, Physics of High Temperature Plasmas, second edition, 1979 Academic Press, p. 23, equation 2-102

[8] See http://physics.nist.gov/PhysRefData/Star/Text/contents.html or Stopping Powers for Electrons and Positrons, M. J. Berger et al., ICRU Report #37, International Commission on Radiation Units and Measurements, Bethesda, MD, (1984), ISBN 0-913394-31-9, p.82

[9] The switch used to energize the toroidal field is in the "up" position to achieve this polarity. Placing the switch in the "down" position produces a toroidal field that is counterclockwise as viewed from above the tokamak. The calibration for gauss on axis is 3.45 times the coil current in amps.

[10] http://www.ngdc.noaa.gov/cgi-bin/seg/gmag/igrfpg.pl

[11] Probe measurements demonstrate that at the center of the minor cross section, the horizontal coils produce a negligible vertical field component.

---

[12] P. M. Bellan, "Simple system for mapping magnetic field errors in tori," Rev. Sci. Instrum., **58**, (1987), p. 148

[13] R. C. Platt and R. McWilliams, "Excitation of fast waves near the mean gyrofrequency," Phys. Rev. Lett., **57**, (1986), p. 2276

[14] J. Goree et al., "Fast-wave current drive in a toroidal plasma," Phys. Rev. Lett., **55**, (1985), p. 1669

[15] S. C. Chiu et al., "Theory of fast wave current drive for tokamak plasmas," Nuc. Fus., **29**, (1989), p. 2175

[16] D. P. Sheehan, R. McWilliams et al., "Fast-wave current drive above the slow-wave density limit," Phys. Rev. Lett., **64**, (1990), p. 1258

[17] The value of 2.4 gauss is a measured value near the center of the torus and includes the earth's magnetic field but not any vertical field errors due to the toroidal field or the radial-horizontal field. The applied field near the outer wall of the tokamak is of the order of 64% of the center value. Application of the radial-horizontal field alters the vertical field slightly.

[18] The background level appears to be yellow. The red colors represent less current than the yellow background. The presence of the red shades may indicate enhanced ion current due to higher plasma density. The green shades represent electron current above the background level. In any event, the computed centroid uses the green shaded areas only. The dark green areas were weighted per the given current range despite the fact that dark green may include saturated pixels.

[19] N. J. Fisch, "Theory of current drive in plasmas," Rev. Mod. Phys., **59**, (1987), p. 213

[20] See the text prior to equation (3.20). The iron core transformer is neglected for this estimate. It is assumed that the ohmic windings are open circuits.

8 Lower Hybrid Current Drive Density Limit

Introduction

In the early days of lower hybrid current drive experiments, there were numerous reports of success. Many groups built coupling antennas and associated power supplies. When they flipped the switch, large currents were driven in tokamak plasmas.[1] This did not happen in the LHCD experiments on Encore. Eventually currents as large as 150 amps were driven in Encore, but considering the available RF power of 40 kW, the efficiency was well below that observed in other experiments, as described in chapter 2.

The "successful" LHCD experiments noted that the current drive efficiency plummeted at some plasma density. As described in chapter 2, the current drive efficiency is supposed to drop with increasing plasma density, being proportional to the inverse of the density. However, the "density limit" encountered in experiments across the world was a more precipitous phenomena, and nobody knew what the explanation was. The density limit varied from tokamak to tokamak. Encore is an unusual tokamak, having a very low magnetic field and highly collisional plasma. Data shows that plasma density in Encore is proportional to the plasma current.[2] It is therefore not possible to have significant plasma current without a significant concomitant plasma density. Was it possible that the density limit for Encore was such that any significant plasma current would raise the plasma density above the limit? The density limit was shown to depend on the frequency, with higher frequencies corresponding to higher density limits.[3] Experiments on Encore utilized a frequency of 450MHz, which is possibly the lowest frequency employed in any experiment.

Many possible explanations for poor current drive efficiency on Encore were examined. Directional couplers on the RF power supply output enabled demonstration of large output power. As described in chapter 5, the antenna was found to effectively couple large RF power to a dummy load. The antenna and RF power supplies function properly.

In chapter 4 it is argued that the cutoff coincides with such a low plasma density that it occurs very close to the antenna waveguides. Hence coupling of the antenna to the plasma should not be a problem. In chapter 7 it is shown that RF generated plasma could be sustained in Encore. This demonstrates that the antenna is capable of coupling significant amounts of power to the plasma.

In chapter 4 it is argued that for large enough toroidal magnetic field, accessibility is not a problem. In chapter 6 data from ohmicly generated plasmas confirms these calculations. Therefore, accessibility is not a problem.

In chapter 3 the L/R time constant of Encore was demonstrated to be short enough so as not to hide significant changes in plasma current. The Rogowski current diagnostic was shown to have a fast time response. If lower hybrid waves generated significant amounts of plasma current, then either the loop voltage diagnostic or the Rogowsky current diagnostic would see it.

It was in writing up the physics of lower hybrid waves and calculating the various parameters as they related to Encore experiments that the idea for what might cause the density limit occurred. The question was posed, "under what conditions can the launched lower hybrid waves mode convert to the ion plasma mode in Encore?" The ion plasma modes are heavily Landau-damped and useful for heating, but not current drive.

Mode conversion from the lower hybrid mode to the ion plasma mode occurs before the lower hybrid resonance layer defined by (4.112) is reached. The mode conversion layer is defined by equation (4.119). For the low field conditions of Encore where $\omega_{LH}^2 \cong \omega_{ce}\omega_{ci}$, equation (4.119) is essentially independent of magnetic field and ion mass. For the Encore parameters $T_i = 3$ eV, $T_e = 10$ eV, f = 450MHz, B = 1.3kG equation (4.119) yields $N_{||} = 130$. Waves with $N_{||} = 130$ will mode convert to ion plasma waves. The antenna used in the Encore experiments will not launch significant power at $N_{||} = 130$. However, $N_{||} = 130$ corresponds to the thermal velocity of 15.2eV electrons and lies in the "spectral gap" between the phase velocities of launched LH waves ($N_{||} \approx 10$ corresponding to 2.6 keV electrons) and the thermal electrons at 10eV in Encore (corresponding to $N_{||} \approx 240$). See Figure (8-1). It is not known how the spectral gap is bridged in current drive experiments although decay waves and $N_{||}$ non-conservation in toroidal geometry are possibilities. The presumption is that by some means, waves with $N_{||}$ values corresponding to electrons in the thermal distribution must be generated. If in bridging the spectral gap the $N_{||}$ spectrum must slide in a continuous fashion from values corresponding to high phase velocity to those corresponding to thermal velocities, then if the mode conversion lies in the spectral gap, no waves will make it past this road block. So the idea is that the density limit occurs when the undesirable mode conversion to an ion plasma wave moves into the "spectral gap."

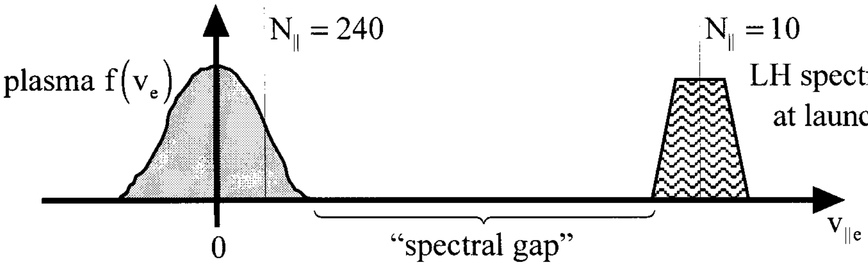

Figure 8-1. Schematic of the plasma electron velocity distribution along the toroidal magnetic field juxtaposed with the lower hybrid wave $N_{\|}$ spectrum at launch. In order for Landau damping to occur, there must be a phase matching where $N_{\|} = c / v_{\|e}$. The "spectral gap" is the region between $f(v_{\|e})$ and the launch $N_{\|}$ spectrum.

In attempts to explain the density limit, difficult theories involving parametric decay were looked at.[4] Other theories were more like ad hoc rules designed to cover all known cases.[5] In contrast, the proposed theory is simple and appealing, and unlike other theories, offers a physical explanation that fits the data well. The issue of exactly how the spectral gap is bridged is not addressed.

The following paper published in Physical Review Letters presents the above-mentioned theory.[6] In the paper a comparison is made between the theory and experimental results from many other tokamaks. Compelling agreement is demonstrated.

---

[1] For instance see papers on LHCD in the proceedings of the fifth topical conference on "Radio Frequency Plasma Heating," February 21-23, 1983, U. of Wisconsin-Madison.

[2] Data from Eric Fredrickson

[3] M. J. Mayberry et al., Phys. Rev. Lett., **55**, 829 (1985)

[4] C. S. Liu, V. S. Chan et al., "Density Threshold for Parametric Instability of Lower Hybrid Waves in a Tokamak," GA Technologies, Inc., San Diego, CA

[5] J. G. Wegrowe et al., "The density Limit in lower-Hybrid Current Drive," Comment on Plasma Physics and Controlled Fusion, **8**, 211, (1984)

[6] The idea behind the theory presented in the paper is due to the author of this thesis. The paper, however, was largely written by Paul Bellan.

Cause of the Lower-Hybrid Current-Drive Density Limit

L. H. Sverdrup[(a)] and P. M. Bellan
California Institute of Technology, Pasadena, California 91125

(Received 13 April 1987)

We derive a simple model which predicts the observed lower-hybrid current-drive density limit for all major experiments to within a factor of 2. The model is based on (i) the experimentally observed upshift in $k_\parallel$ and (ii) the $k_\parallel$ dependence of the mode coalescence condition of the linear model conversion of a lower-hybrid wave into a hot-plasma wave.

PACS numbers: 52.40.Db, 52.25.Sw, 52.50.Gj, 52.55.Fa

Fisch[1] predicted in 1978 that dc toroidal currents could be driven in tokamaks by the injection of suitably phased lower-hybrid waves. Prior to 1978, lower-hybrid experiments had been designed to provide ion heating via the linear mode conversion process predicted by Stix[2] to occur at the lower-hybrid layer where $\omega = \omega_{\mathrm{lh}}$. Initial attempts to reconfigure these heating experiments so as to produce current drive were unsuccessful, until Yamamoto *et al.*[3] demonstrated on the JFT-2 tokamak that current could be driven provided that the plasma density was reduced substantially from the values typically used in the heating experiments (i.e., the density was reduced so that $\omega > 2\omega_{\mathrm{lh}}$). The JFT-2 results have been subsequently reproduced and extended in a large number of devices,[4-18] and it has always been found that current drive works only up to a (rather low) "density limit" where mode conversion would not be expected since $\omega > 2\omega_{\mathrm{lh}}$. Experiments indicate that the density limit increases with[16] ω and[13] m_i. The density limit is not predicted in Fisch's theory. Tonon and Moulin,[19] and Wegrowe and Engelmann[20] postulated a density-limit mechanism based on the wave interacting with hot ions, but (as we will show) their model predicts the density limit to have a strong singularity, inconsistent with experimental observations.

We present here a new and very simple model which predicts within a factor of 2 the observed density limits of all major current-drive experiments. This model is based upon (i) the dependence on parallel wave number $k_\parallel$ of the coalescence of the two modes involved in linear mode conversion of a lower-hybrid wave into a hot-plasma wave and (ii) the upshift in $k_\parallel$ that is associated with the filling of the spectral gap in current drive. Before deriving the model, let us briefly review (i) and (ii).

$k_\parallel$ dependence of mode coalescence.—Stix[2] showed that when hot-plasma effects are included, the lower-hybrid dispersion relation becomes

$$k_\perp^4\epsilon_{\mathrm{th}} + k_\perp^2\epsilon_\perp + k_\parallel^2\epsilon_\parallel = 0, \tag{1}$$

where

$$\epsilon_\perp = 1 - \frac{\omega_{pi}^2}{\omega^2} + \frac{\omega_{pe}^2}{\omega_{ce}^2}, \quad \epsilon_\parallel = 1 - \frac{\omega_{pe}^2}{\omega^2}, \quad \epsilon_{\mathrm{th}} = -\left(\frac{3}{4}\frac{\omega_{pe}^2}{\omega_{ce}^2}\frac{u_{T_e}^2}{\omega_{ce}^2} + 3\frac{\omega_{pi}^2}{\omega^2}\frac{u_{T_i}^2}{\omega^2}\right). \tag{2}$$

Equation (1) is quadratic in $k_\perp$ giving two modes,

$$k_\perp^2 = [-\epsilon_\perp \pm (\epsilon_\perp^2 - 4k_\parallel^2\epsilon_\parallel\epsilon_{\mathrm{th}})^{1/2}]/2\epsilon_{\mathrm{th}}, \tag{3}$$

which are plotted in Fig. 1. The small-$k_\perp$ mode is the launched lower-hybrid wave (cold mode) which propagates from the plasma periphery towards the lower-hybrid layer (where $\epsilon_\perp = 0$); in the vicinity of this layer the cold mode converts[2] linearly to the large-$k_\perp$ hot-plasma mode which propagates back towards the periphery and is strongly damped. It was originally assumed[2] that mode conversion occurred at the lower-hybrid layer where $\epsilon_\perp = 0$ (or equivalently $\omega = \omega_{\mathrm{lh}}$), but it was later noted[21,22] that the mode conversion actually occurs at the point where the two modes described by Eq. (3) coalesce, i.e., where

$$k_\parallel = \epsilon_\perp^2/4\epsilon_{\mathrm{th}}\epsilon_\parallel. \tag{4}$$

Examination of Fig. 1 shows that the location of mode coalescence is at a lower density than the lower-hybrid layer, and Eq. (4) shows that this location depends on a large number of parameters.

Upshift of $k_\parallel$.—There is a well-known[23,24] problem

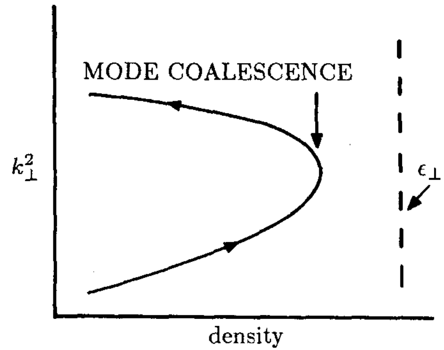

FIG. 1. Plot of $k_\perp^2$ vs density. Note that the location of mode coalescence occurs at lower density (Ref. 21) than the location of the lower-hybrid layer.

concerning the use of Fisch's theory to explain the results of current-drive experiments. According to Fisch's theory, lower-hybrid waves drive current by imparting momentum to electrons in the tail of the distribution function. These electrons can interact with the wave because their velocity u satisfies the resonance condition $u = \omega/k_\parallel$. Yet, in all experiments[14] the parallel refractive index launched is typically $n_\parallel = ck_\parallel/\omega = 1.5-10$ so that, in order for electrons to be resonant with the wave, they must have $3\times 10^9 < u < 2\times 10^{10}$. In the experiments the electron temperature has ranged from 50 to 2000 eV ($3\times 10^8 < u_{T_e} < 1.3\times 10^9$). Thus, except for the hottest of these plasmas, there ought to be essentially zero electrons capable of resonantly interacting with the wave. What seems to happen is that the wave creates its own tail by pulling electrons from the bulk out to high velocities via parallel-wave-partial resonant interaction. In order to do this, at least some component of the launched wave $k_\parallel$ spectrum must interact resonantly with electrons in the bulk, and so a spectral component must develop which has a parallel phase velocity much lower than the launched value. In effect, $k_\parallel$ has been shifted up for some fraction of the launched wave power (the remainder is, of course, unshifted and interacts with the newly created tail electrons to give current drive as predicted by Fisch). Various mechanisms for the upshift have been proposed, such as toroidal-poloidal[22] and ponderomotive[24] effects. It has also been suggested[23] that there is no upshift, but that the antenna spectrum includes enough of a large-$k_\parallel$ component to pull electrons from the bulk to high velocities.

We will not attempt here to decide which (if any) of the above mechanisms cause the $k_\parallel$ upshift. Instead, we will simply accept the upshift as an experimentally observed fact; i.e., experiment has shown that $k_\parallel$ is shifted up for part of the launched power in such a way that

$$k_\parallel = \omega/\gamma u_{T_e}, \tag{5}$$

where $\gamma \approx 1-2$.

We postulate that the density limit occurs when the $k_\parallel$ predicted by Eq. (5)—i.e., the $k_\parallel$ interacting with the bulk—is of such a value to satisfy Eq. (4). When this occurs, (i) mode conversion takes place for the upshifted $k_\parallel$ component which thus becomes strongly attenuated by *perpendicular*[2] damping processes, and so cannot pull electrons from the bulk to the tail by *parallel*-wave–particle resonance, so that (ii) there are no tail electrons to resonantly interact with the unshifted (i.e., high phase velocity) component of the incoming wave, and so (iii) there is no current drive. We emphasize that, for the upshifted $k_\parallel$ component, mode conversion takes place even though $\omega > \omega_{\text{lh}}$.

Proceeding with the mathematical derivation, we define $x = \omega_{pe}^2/\omega^2$, so that $\epsilon_\parallel = -x$, $\epsilon_\perp = 1 - \lambda x$, where $\lambda = m_e/m_i - \omega^2/\omega_{ce}^2$, and $\epsilon_{\text{th}} = -x\alpha u_{T_e}^2/\omega^2$ where $\alpha = \frac{3}{4}\beta_e\omega^4/\omega_{ce}^4 + 3(m_e/m_i)^2\beta_i T_i/T_e$. (Here, we have introduced the temperature enhancement factors β_e, β_i which multiply the bulk temperatures T_e, T_i. These enhancement factors take into account the fact that the total energy in rf-produced suprathermal tails can, depending on rf power levels, be comparable to the energy of the bulk; in particular, β_e will exceed unity when the fast electrons providing current drive have a total energy comparable to the bulk,[5] while β_i will exceed unity when there is ion heating.[20]) Using Eq. (5) in Eq. (4), we find $x = 1/(2\alpha^{1/2} + \lambda)$, or in terms of the original variables

$$\frac{\omega_{pe}^2}{\omega^2} = \left[\frac{2}{\gamma}\left(\frac{3}{4}\beta_e\frac{\omega^4}{\omega_{ce}^4} + 3\beta_i\frac{m_e^2}{m_i^2}\frac{T_i}{T_e}\right)^{1/2} + \frac{m_e}{m_i} - \frac{\omega^2}{\omega_{ce}^2}\right]^{-1}. \tag{6}$$

All the major current-drive experiments had $T_i/T_e \simeq 0.3-1$; however, there was a fairly large range of frequencies, magnetic fields, and observed density limits. Figure 2 plots Eq. (6) for hydrogen (solid lines) and for deuterium (dashed lines) and also shows the experimentally measured normalized density limits of a large number of experiments. Here we have chosen $\gamma = \beta_e = \beta_i = 1$ as plausible values which give a good fit to the observations [note, that according to Eq. (6), equally plausible values of $\gamma = 1.4$, $\beta_e = \beta_i = 2$ would give the same results]. Figure 2 also plots Eq. (6) for argon which was used in the Caltech Encore plasma.[25] Table I presents the same information but with nonnormalized parameters; hydrogen gas is assumed, unless specified otherwise, and for case where T_i and/or T_e were unspecified, an estimate of $T_i/T_e = 0.3$ was used to calculate the predicted density limit.

It is clear from Fig. 2 and Table I that Eq. (6) predicts the experimental observations for a wide variety of parameters. Several[8,13,16] experiments were carefully controlled so as to determine the dependence on just one parameter. Equation (6) is consistent with the observations of these experiments: in particular, Eq. (6) is consistent with the dependence on ω observed in Versator[16] and Petula-B,[11,18] the dependence on B observed in FT,[8] and the dependence on m_i observed in ASDEX.[13]

From Eq. (6) and Fig. 2 it is seen that there are essentially two regimes of interest: (i) a low-field region (slope on left-hand side of Fig. 2) where the density limit is independent of ω and proportional to B^2, and (ii) a high-field region (flat portion of curve in Fig. 2) where the density limit is independent of B and is instead determined by T_i/T_e, ω, and m_i. The change from regime (i) to regime (ii) occurs at $\omega \approx \omega_{\text{gm}}(2T_i/T_e)^{1/2}$, where $\omega_{\text{gm}} = (\omega_{ci}\omega_{ce})^{1/2}$ is the geometric mean frequency.

It is worthwhile to compare our model to that proposed by Wegrowe and Engelmann[20] (the Tonon and

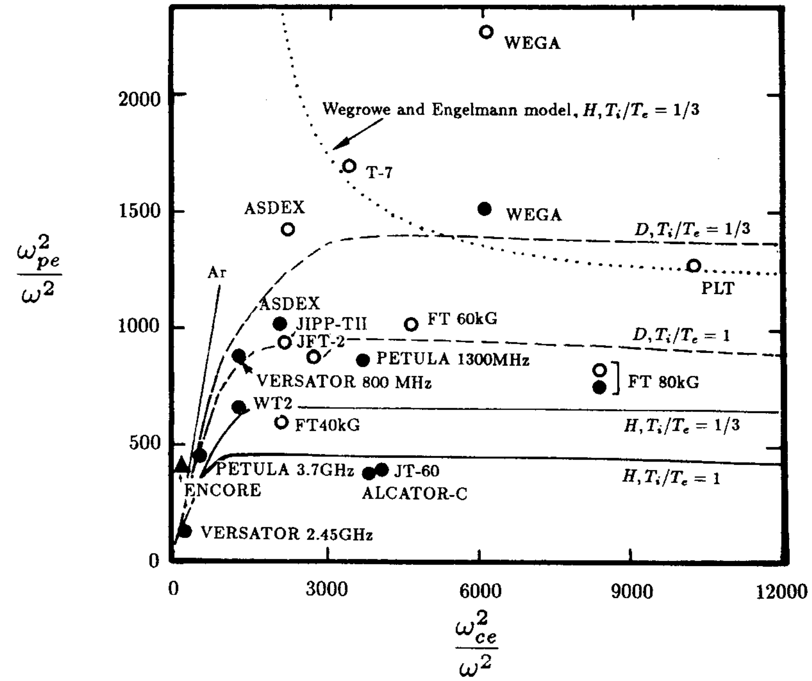

FIG. 2. Density limit predicted by Eq. (6) vs experiments: The solid line is Eq. (6) for hydrogen and the dashed line is for deuterium. For experiments, solid circles indicate hydrogen, open circles indicate deuterium, and the triangle indicates argon (all references in Table I). For comparison, the dotted line shows the Wegrowe and Engelmann model (Ref. 20) [Eq. (7) in text] for hydrogen, $T_i/T_e = \frac{1}{3}$.

TABLE I. Comparison of observed density limit with prediction of Eq. (6).

	f (MHz)	B (kG)	T_i (eV)	T_e (eV)	n_{observed} (10^{12} cm^{-3})	$n_{\text{Eq. (6)}}$ (10^{12} cm^{-3})
JFT-2 (D gas)[a,b]	750	14		250	6	9
Versator[c]	800	10	120	350	7	5
Versator[c]	2450	10	120	350	10	12
PLT (D gas)[d,b]	800	30			10	11
WT-2[e,b]	915	11	50	200	7	7
Alcator-C[f]	4600	100			100	180
FT (D gas)[g,h,i]	2450	40			45	94
FT (D gas)[g,h,i]	2450	60			75	103
FT (D gas)[g,h,i]	2450	80			60	100
FT[g,h,i]	2450	80			55	48
WEGA[i]	800	22.5			12	5
WEGA (D gas)[i]	800	22.5			18	11
T7(D gas)[j]	900	19			17	14
Petula-B[k]	1300	28		1000	18	14
Petula-B[l]	3700	28		1000	80	73
JIPP-TII[m,f]	750	14			8	6
ASDEX[n]	1300	22			20	15
ASDEX (D gas)[n]	1300	22			30	27
JT-60[o]	2000	45			20	34
Encore (Ar gas)[p]	450	1.5	5	10	1	0.3

[a] Reference 3.
[b] Reference 14.
[c] Reference 16.
[d] Reference 5.
[e] Reference 6.
[f] Reference 15.
[g] Reference 8.
[h] Reference 9.
[i] Reference 20.
[j] Reference 10.
[k] Reference 11.
[l] Reference 18.
[m] Reference 12.
[n] Reference 13.
[o] Reference 17.
[p] Reference 25.

Moulin model[19] is essentially the same as the one in Ref. 20). We consider the standard case where there is one ion species and $Z=1$. Expressing Eq. (12a) of Ref. 20 in our notation gives the Wegrowe and Engelmann density limit as

$$\frac{\omega_{pe}^2}{\omega^2}=\left[\frac{\phi^2}{z_0^2}\frac{m_e}{m_i}\frac{T_i}{T_e}+\frac{m_e}{m_i}-\frac{\omega^2}{\omega_{ce}^2}\right]^{-1}, \tag{7}$$

where ϕ^2/z_0^2 is an adjustable parameter,[20] the value of which is given in Ref. 20 to be $\phi^2/z_0^2=2$. It is easily seen that the right-hand side of Eq. (7) becomes singular when $T_i/T_e=(\omega^2/\omega_{gm}^2-1)/2$; this singular behavior is also shown in Fig. 2, where Eq. (7) has been plotted as a dotted line for the typical case of hydrogen, $T_i/T_e=\frac{1}{3}$.

Finally, let us consider the predictions of our model for typical fusion-reactor parameters. With $T_e=T_i$, average atomic mass ≈ 2.5, $f=8$ GHz, and $\gamma=\beta_e=\beta_i=1$, Eq. (6) gives density limits of 4×10^{14} cm^{-3} for $B=6$ T, and 8×10^{14} cm^{-3} for $B=10$ T.

In summary, we have described how the combination of (i) the experimentally observed upshift of $k_\parallel$ to $k_\parallel=\omega/\gamma u_{T_e}$ and (ii) the $k_\parallel$ dependence of linear mode conversion (of lower-hybrid waves into hot-plasma modes) accounts for the lower-hybrid current-drive limit.

This work was supported by National Science Foundation Grant No. ECS-8414541.

---

[a] Present address: Western Research Corporation, San Diego, CA 92121.

[1] N. J. Fisch, Phys. Rev. Lett. **41**, 873 (1978).

[2] T. H. Stix, Phys. Rev. Lett. **15**, 878 (1965).

[3] T. Yamamoto *et al.*, Phys. Rev. Lett. **45**, 716 (1980).

[4] S. C. Luckhardt *et al.*, Phys. Rev. Lett. **48**, 152 (1982).

[5] S. Bernabei *et al.*, Phys. Rev. Lett. **49**, 1255 (1982).

[6] M. Nakamura *et al.*, J. Phys. Soc. Jpn. **51**, 3696 (1982); S. Tanaka *et al.*, in *Proceedings of the Tenth International Conference on Plasma Physics and Controlled Nuclear Fusion Research, London, 1984* (International Atomic Energy Agency, Vienna, 1985), Vol. 1, p. 623.

[7] M. Porkolab *et al.*, in *Proceedings of the Tenth International Conference on Plasma Physics and Controlled Nuclear Fusion Research, London, 1984* (International Atomic Energy Agency, Vienna, 1985), Vol. 1, p. 463.

[8] A. Santini, in Proceedings of the IAEA Technical Committee Meeting on Non-Inductive Current Drive in Tokamaks, Abington, Oxon, England, 1983, Culham Laboratory Report No. CLM-CD, 1983 (unpublished), p. 278; see also Table I in J.-G. Wegrowe and F. Engelmann, Comments Plasma Phys. Controlled Fusion **8**, 211 (1984).

[9] F. Alladio *et al.*, Nucl. Fusion **24**, 725 (1984).

[10] V. V. Alikkaev *et al.*, in Proceedings of the IAEA Technical Committee Meeting on Non-Inductive Current Drive in Tokamaks, Abington, Oxon, England, 1983, Culham Laboratory Report No. CLM-CD, 1983 (unpublished).

[11] C. Gormezano *et al.*, in Ref. 7, p. 503.

[12] K. Toi *et al.*, in Ref. 7, p. 523.

[13] L. Leuterer *et al.*, in Ref. 7, p. 597.

[14] M. Porkolab, IEEE Trans. Plasma Sci. **PS-12**, 107 (1984).

[15] M. Porkolab *et al.*, Phys. Rev. Lett. **53**, 450 (1984).

[16] M. J. Mayberry *et al.*, Phys. Rev. Lett. **55**, 829 (1985).

[17] M. Yoshikawa *et al.*, in Proceedings of the Eleventh International Conference on Plasma Physics and Controlled Nuclear Fusion Research, Kyoto, Japan, 1986 (to be published), paper A-I-1.

[18] F. Parlange *et al.*, in Ref. 7, p. 557.

[19] G. Tonon and D. Moulin, in Ref. 7, p. 557.

[20] Wegrowe and Engelmann, Ref. 8.

[21] V. Krapchev and A. Bers, Phys. Fluids **21**, 2123 (1978).

[22] P. Bonoli, IEEE Trans. Plasma Sci. **PS-12**, 95 (1984).

[23] S. Succi *et al.*, in Ref. 7, p. 549.

[24] E. Canobbio and R. Croci, in Ref. 7, p. 567.

[25] L. H. Sverdrup and P. M. Bellan, Bull. Am. Phys. Soc. **31**, 1578 (1986).

9 Summary and Conclusions

Launching lower hybrid waves in tokamak plasma to drive toroidal current is a complicated endeavor. There are numerous interesting aspects worthy of investigation, but only a few can be pursued. It is therefore no surprise that many questions have arisen during this undertaking, and that not all of them have been answered.

An example of what has been ignored includes the plasma structure. Encore plasma has a complicated structure of its own. The grill antenna is not simply butted against the smooth surface of homogeneous and isotropic plasma. There is turbulence and various modes such as drift waves. Ripples and "sausages" of plasma dance past the antenna. With high RF power, pondermotive forces push on the plasma near the mouths of the antenna waveguides. Whether by Doppler shifts, parametric decay or other processes, the launched LH waves generate new waves at other frequencies.

Despite the seeming chaos, relatively simple and appealing theories describe much of what takes place. The cold plasma dielectric tensor predicts the lower hybrid mode accessibility and propagation angle. The LH propagation angle depends simply on the toroidal magnetic field and this is observed. LH wave accessibility is simply related to a combination of the plasma density and magnetic field. This behavior is observed. The changes in plasma current seen are most dramatic at low plasma current where accessibility is best. Quadrature phasing does produce a directional spectrum of launched LH waves.

In order for the fast waves launched by the grill antenna to interact with the much slower thermal electrons, some LH wave power must dramatically "slow down" and increase in parallel refractive index ($N_{||}$). Theoretically this can occur through sufficient poloidal propagation but this may or may not be the dominant mechanism. No one has ever proved that LHCD was ineffective due to lack of a mechanism for slowing down LH waves. Virtually all reported experiments launch an $N_{||}$ spectrum that is too fast to damp on thermal electrons. Virtually all reported experiments also drive plasma current with efficiency on the order of amps per watt. This was not the experience on Encore.

When it became evident that the current drive efficiency on Encore was abnormally low, a plethora of questions arose. Did the antenna function properly? Was

RF power measured correctly? Was the end of the antenna close enough to the cutoff for the slow mode? Was the phasing of the antenna correct? Was the L/R time constant of the tokamak short enough to see a large RF driven current? All of these questions were answered in the affirmative.

The density limit phenomenon was well publicized, but not understood. It described a condition in which current drive efficiency would plummet. Difficult theories such as parametric decay were proposed to explain the phenomenon. Instead it was shown in chapter 8 that a very simple and appealing theory invoking the "warm" plasma dielectric tensor explained everything. Adding temperature to the cold dielectric tensor allows the description of plasma heating with lower hybrid waves. A key connection was realized. When LH waves dramatically slow down, they can, under some conditions, mode convert to an ion plasma wave and heat the plasma. If this occurs before the LH waves have slowed sufficiently to reach the tail of the electron distribution, current drive can be blocked. The conditions for the mode conversion to the ion plasma wave depend upon the plasma density, as well as many other variables. A mysterious phenomenon became simply explained by the algebra of the plasma dielectric tensor. If LHCD is incorporated into a future energy producing tokamak, attention will be directed to the location in parallel refractive index of the mode conversion to the ion plasma wave.

An equally mysterious phenomenon was encountered when low current ($\leq$ 160 amp) discharges were observed in Encore by application of RF with the grill antenna. Antenna phasing did not specify the direction of the current. Many factors were explored that also proved to play no role in the direction of the current, until the truth was stumbled upon.

The direction of the plasma current was obtained not by antenna phasing but rather by the unintentional spiraling of the toroidal magnetic field lines. When the electron acceleration is near the plasma periphery, the spiraling presents an asymmetry that favors one toroidal direction over the other. It is not known why the antenna phasing failed to produce significant asymmetry in the plasma current. The highly inhomogeneous nature of the unusual low current discharges may play a role.

Energetic electron tails produced by LHCD are less collisional than less energetic electrons. The increased mean free path of these energetic electrons allows them to spiral along the toroidal field lines for greater distances before suffering collisional redirection. They thus have more time to sample magnetic field errors. If an energy producing tokamak is ever built incorporating LHCD, significant attention will be paid to minimizing field errors.

With the use of a miniature electron source and a probe capable of scanning the minor cross section and detecting the electrons, the field errors in Encore were observed and quantified. The behavior of the hot electrons confirms the spiral nature of the toroidal field lines.

Encore has been operated in a purely RF mode without the use of an ohmic target plasma. Electrons with energies above 100eV were observed in these RF-sustained discharges. The beams of electrons are not confined in the conventional tokamak sense due to the low poloidal magnetic field. The vertical field plays an important role in the propagation of the low current beams.